

ACTA UNIVERSITATIS CAROLINAE

AUC GEOGRAPHICA



59
2/2024

AUC Geographica is licensed under a Creative Commons Attribution License (<http://creativecommons.org/licenses/by/4.0>), which permits unrestricted use, distribution, and reproduction in any medium, provided the original author and source are credited.

© Charles University, 2024
ISSN 0300-5402 (Print)
ISSN 2336-1980 (Online)

PREFACE

Lukáš Brodský^{1,*}, Irene Maria Bollati², Marcus Nüsser^{3,4}

¹ Charles University, Faculty of Science, Department of Applied Geoinformatics and Cartography, Czechia

² University of Milan, Earth Science Department, "A. Desio", Italy

³ Heidelberg University, South Asia Institute, Department of Geography, Germany

⁴ Heidelberg University, Heidelberg Center for the Environment, Germany

* Corresponding author: lukas.brodsky@natur.cuni.cz

We are pleased to present a themed issue of *AUC Geographica* 2/2024, which is dedicated to our multifaceted research conducted in the Alpine environment. This research and education activities were conducted within the framework of the 4EU+ cooperation initiative. The three universities participating in this project have collaborated in both research and education since 2021 and include Charles University (Czechia), University of Milan (Italy) and Heidelberg University (Germany) (Fig. 1). We are pleased to present the results of the first three-year collaboration in the combined study of the Belvedere Glacier (Italian Alps), an iconic debris-covered glacier, situated in the Monte Rosa Massif, the second-highest mountain of the European Alps. The site is well-known not only as

a popular tourist destination, but also because of natural hazards related to glacial and geomorphological processes, which are locally affecting hamlets and the tourist trail network.

The principal aim of this international collaboration has been to establish a research foundation for education, with a particular focus on PhD students, and to create an appropriate context for integrated research topics in physical geography, geomorphology and remote sensing. By employing modern methodologies, we seek to collect new data and develop new strategies for the research of glacier-related changes and its hazards during the global climate change. The collaboration started with the provision of university mini-grants, which facilitated the



Fig. 1 Our research group in the field in 2021.

Brodský, L., Bollati, I. M., Nüsser, M. (2024): Preface. *AUC Geographica* 59(2), 161–162

<https://doi.org/10.14712/23361980.2024.20>

© 2024 The Authors. This is an open-access article distributed under the terms of the Creative Commons Attribution License (<http://creativecommons.org/licenses/by/4.0>).



Fig. 2 Devastating flash flood from 2024 (Rio Tambach in the Staffa Village, part of Macugnaga), according Beba Schranz on www.nimbus.it.

organisation of several seminars, research exchanges, and fieldwork aimed at data collection and training for early career scientists and students. This has led to the preparation of several Master and PhD theses and their presentation during scientific congresses for young researchers in 2022 and 2023. Moreover, we have produced none research papers and intend to further develop our database for future fieldwork-based research on glacier changes and associated geo-hazards. The most recent natural hazards, such as a debris flow, which occurred on 27 August 2023, and the 29–30 June 2024 flash flood (Fig. 2), justify our continuing research in this area. These events have significantly impacted several locations in the Western Italian Alps and the Southern Swiss Alps, especially the Macugnaga watershed.

The Belvedere Glacier, a prominent feature of the Alps, has undergone notable changes in recent decades that have been affected by climatic fluctuations.

This debris covered glacier exhibits highly distinctive response patterns within the Alpine region. This special issue of the AUC Geographica (<https://karolinum.cz/en/journal/auc-geographica>) presents the research on the Belvedere Glacier (see Table of Content), with a particular focus on its dynamic responses to environmental changes. The articles included in this special issue employ a range of methodological approaches, including remote sensing and *in-situ* field observations, absolute and relative datings, monitoring and mapping. They provide a more comprehensive understanding of the glacier's current state since 1951 in comparison to long-term historical records (Fig. 3). The first article reviews previous research in this area by various Swiss and Italian researchers. The remaining articles analyse the current dynamics of glacier retreat and down-wasting through the application of innovative techniques, which yield new findings in glaciology and associated geo-environmental studies.

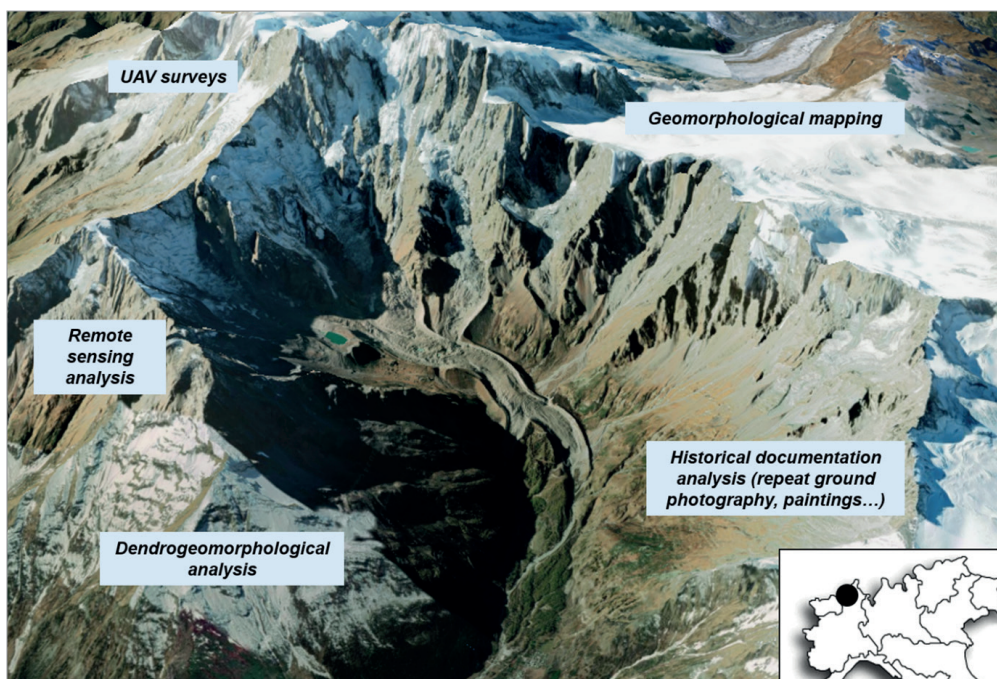


Fig. 3 The head of the Anzasca Valley, the valley of the Belvedere Glacier where we are currently used to work with our students for educational and research purposes.

Dynamics and related hazards of the Belvedere Glacier in the Italian Alps: a review

Jan Kropáček^{1,*}, Pragya Mehrishi¹, Irene Maria Bollati², Lukáš Brodský³, Manuela Pelfini², Roberto Azzoni², Susanne Schmidt⁴, Marcus Nüsser^{4,5}, Vít Vilímek¹

¹ Charles University, Faculty of Science, Department of Physical Geography and Geoecology, Czechia

² University of Milan, Earth Science Department, "A. Desio", Italy

³ Charles University, Faculty of Science, Department of Applied Geoinformatics and Cartography, Czechia

⁴ Heidelberg University, South Asia Institute, Department of Geography, Germany

⁵ Heidelberg University, Heidelberg Center for the Environment, Germany

* Corresponding author: kropacj@natur.cuni.cz

ABSTRACT

The Belvedere glacier is an intensively studied glacier in the Italian Alps on the east face of the Monte Rosa, which is currently undergoing a fast deglaciation connected to various slope failures and Glacial Lake Outburst Floods. Measurements of the terminus position have been carried out since the 1920s. Since 2000, more attention has been paid to this area due to the occurrence of large mass movements and a surge-type event. In this review, research articles and various reports dealing mainly with glacier dynamics, rock and ice avalanches, Glacial Lake Outburst Floods, and other hazardous processes were considered. Aerial photogrammetry, Unmanned Aerial Vehicles, satellite stereo-processing and several terrestrial approaches (laser scanning, geophysics, measurements of near-surface heat flow, ablation stakes and camera-lapse) provided a base for quantifying the ongoing processes. Despite efforts based on the comparison of Digital Elevation Models, this review shows that the evolution of the Belvedere glacier in terms of ice volume is still partially unknown due to the low temporal frequency of aerial surveys, technical limitations of the Unmanned Aerial Vehicles used, and the fact that most studies focus only on the lower part of the glacier. The hazardous supraglacial Effimero lake that appeared during the surge-type event has been well documented, and interventions to mitigate potential risks were put in place, but the trigger of the event and the evolution of the lake basin have not yet been clarified. Mass wasting and outburst floods are mainly documented in the grey literature. The degradation of permafrost was suggested to be the driver of rock and ice avalanches, including one of the largest ice avalanches in the Alps, which occurred in 2005. In summary, the Belvedere Glacier and the surrounding rock walls have experienced repeated slope failures, an incident of surge and several outburst floods. Despite regular monitoring, a clear picture of its behavior due to the changing climate is still unknown. This review is intended to pave the way for further integrative studies.

KEYWORDS

Belvedere Glacier; surge-type event; debris-covered glacier; glacier changes; natural hazards; climate change

Received: 8 June 2024

Accepted: 27 November 2024

Published: 12 December 2024

Kropáček, J., Mehrishi, P., Bollati, I. M., Brodský, L., Pelfini, M., Azzoni, R., Schmidt, S., Nüsser, M., Vilímek, V. (2024): Dynamics and related hazards of the Belvedere Glacier in the Italian Alps: a review. *AUC Geographica* 59(2), 163–183
<https://doi.org/10.14712/23361980.2024.21>

© 2024 The Authors. This is an open-access article distributed under the terms of the Creative Commons Attribution License (<http://creativecommons.org/licenses/by/4.0>).

1. Introduction

Mountain glaciers have been undergoing rapid and accelerating changes due to global warming (e.g. Bhat-tacharya et al. 2021; Neckel et al. 2014). Deglaciation was documented on a global scale with multiple consequences including sea level rise, modification of river discharge regimes (Huss and Hock 2018), natural hazards, impacts on hydropower generation, irrigation, and glacier tourism (Harrison et al. 2018; Zemp et al. 2019; Nüsser and Schmidt 2021; Bollati et al. 2023).

Mountain deglaciation is particularly severe in the Alps where glacier retreat since the end of the Little Ice Age (LIA), ~1850–1860 as documented by Ivy-Ochs et al. (2009), despite minor glacier advances at the beginning of the 20th Century and in the 1970s–1980s (e.g. Citterio et al. 2007). Glacier retreat and downwasting have recently accelerated by the rapid increase in air temperature during the last few decades (IPCC 2022; Davaze et al. 2020; Paul et al. 2020; Kropáček et al. 2014). For the Alps, Sommer et al. (2020) report a regional variable mean mass balance of -0.5 to -0.9 m a^{-1} in the period 2000–2014 while Davaze et al. (2020) reported a mean annual mass balance of -0.74 ± 0.20 m w.e. a^{-1} from 2000 to 2016. This massive glacier shrinkage in the Alps is accompanied by a progressive increase in supraglacial debris coverage (Azzoni et al. 2018) which contributes to the transformation from debris-free glaciers to partially or completely debris-covered ones. The climate change scenarios indicate that future volumes of alpine glaciers will further decrease as the mean mass balance predicted for the year 2050 was calculated as -1.3 m w.e. a^{-1} by Huss (2012). The mass loss of glaciers in the Alps will exceed 80% (RCP 8.5) by the end of the 21st century, compared to 2015 (Pörtner et al. 2019). In terms of glacier related hazards, deglaciation leads to slope instabilities developing along the glaciers via the process of debuitressing (Ballantyne 2002; McColl 2012; Spreafico et al. 2021). Glacial retreat increases also the susceptibility to GLOFs (e.g. Chowdhury 2021). In the Alps, landslides induced by debuitressing were described for instance at Aletschgletscher (Kääb 2002; Kos et al. 2016).

The rising air temperature also leads to the degradation of mountain permafrost (Haeberli and Beniston 1998; Harris et al. 2003; Gobiet et al. 2014; Jacquemart et al. 2024), which in turn favours rock-falls (Deline et al. 2015; McColl 2012), rock and ice avalanches and debris flows (Fischer et al. 2013; Kropáček et al. 2021)

The release of a large mass of ice from hanging glaciers resulting in ice avalanches can change into catastrophic mass flows, characterised by sudden onset, high velocity and long runout (Evans et al. 2021). Several recurrent ice avalanches threatening settlements and infrastructure were described in the Alps (e.g. Vincent et al. 2015; Faillettaz et al. 2016; Margreth 2017). A transition from cold to temperate glacier bed

can lead to the collapse of a whole glacier as Faillettaz et al. (2011) elucidated for the collapse of Aletschgletscher in September 1895 recognized as the largest known ice avalanche in the Alps. However, even relatively smaller ice avalanches can result in casualties as it occurred at Marmolada in the Italian Alps in July 2022 (Olivieri et al. 2023). In some cases, ice and snow avalanches are triggered not by permafrost thaw, but by earthquakes (Klimeš et al. 2009).

Due to glacier retreat, glacial lakes (e.g. proglacial lakes) develop, threatening downstream populations by Glacial Lake Outburst Floods (GLOFs) (Emmer et al. 2016; Harrison et al. 2018; Huggel et al. 2003; Viani et al. 2016; Pandey and Kropáček 2023; Bollati et al. 2023; Schmidt et al. 2020). A fast increase in the number of glacial lakes with regional variation has been described for the Alps in several studies, e.g. for the Aosta Valley (Viani et al. 2020), for the Austrian Alps (Buckel et al. 2018) and for the Swiss Alps (Mölg et al. 2021).

A continuous eight-fold increase in the number of glacial lakes since the LIA was reported for the Austrian Alps by Buckel et al. (2018). The development of glacial lakes was described in more detail in the Swiss Alps, where the annual increase in area and number was the highest in 1946–1973. It decreased towards the end of the 20th century, and increased again in 2006–2016 (Mölg et al. 2021). Similarly, in the Aosta Valley in the Western Italian Alps, the number of lakes doubled and their area increased by approximately 30% in the period 2006–2015 (Viani et al. 2020; 2022). In terms of timing, GLOFs in the Alps occur about two months earlier compared to the beginning of the 20th century, while the trend in extreme events has not changed (Veh et al. 2022; Veh et al. 2023). The occurrence of GLOFs is commonly related to global warming (e.g. Chiarle et al. 2021). However, the temporal pattern of GLOFs often does not match with climatic fluctuations (Harrison et al. 2018). Moreover, the analyses of the temporal pattern of GLOF frequency suffer from bias in reporting due to the more frequent reporting in the recent period (Veh et al. 2022).

Belvedere Glacier together with the east face of Monte Rosa has been a hotspot of processes, leading to GLOFs and large mass wasting events. The processes include the development of two glacier lakes and destabilisation of slopes, both of them connected to climate change-driven deglaciation. The area features a long record of research papers dealing with various aspects and timescales. However, many publications related to the occurrence of glacier hazards and mitigation strategies belong to the grey literature. This review is an effort to bring together the main findings in a synoptic overview, including information from largely neglected material.

1.1 Object and aim of the study

In this review, we focused on the debris-covered Belvedere Glacier located in the Italian Alps. This glacier

is anomalous in the Alps in terms of the extent of debris cover, large proportion of avalanche feeding and low altitude of the terminus. It also features a flow acceleration referred to as surge-type event, unique in the Alps. This glacier received a lot of attention over the last four decades, mainly due to the hazardous processes affecting the area and population, but it has been explored already since the end of the 18th century (Kropáček et al. 2024, in this issue). There is a long record of natural hazards associated with the Belvedere Glacier, mainly related to GLOFs, rock and ice avalanches and even a surge-type event in 2001–2002. The east face of Monte Rosa has been intensively discussed due to the fast deglaciation and related mass-wasting processes (e.g. Käab et al. 2004; Fischer et al. 2006; 2011).

This review study aims to assess the dynamics of the Belvedere Glacier and related natural hazards resulting from GLOFs and mass wasting in the surrounding rock slopes and lateral moraine based on available literature. It covers the changes and events starting at the beginning of the 20th century when systematic observations began. Earlier reports that are significant for the history of high mountain research, at least at the European scale, are briefly summarised (for further details see Kropáček et al. 2024, in this issue).

This review begins by presenting the methodological framework and study area (Sections 2 and 3). Next, it examines the remote sensing and in-situ methods used in the studies (Section 4). Sections 5 and 6 address glacier dynamics and related natural hazards, respectively. This is followed by a discussion that includes a critical assessment of the studies (Section 7) and concludes with insights into future research opportunities (Section 8).

2. Methodological framework

A search was conducted on the SCOPUS database for the articles using various combinations of keywords relevant to the study on Belvedere Glacier. The articles

were considered relevant if they dealt with the study of glacier dynamics and related natural hazards. The search was not filtered by years, or the techniques used (Tab. 1).

Tab. 1 Keywords used for literature search on SCOPUS and their outputs.

Keywords	Total documents	Relevant
'Belvedere' AND 'glacier'	24	17
'Monte Rosa east face'	7	3
'Monte Rosa' AND 'climate change'	18	15
Total	49	35
Total after removing duplicates		19

The search with different keywords yielded duplicate results as well, which were removed. In total 19 articles were observed to fulfil the criteria of the objective (Tab. 2). The selected studies and their temporal coverage are displayed in Fig. 1. Several historical texts in the Italian language with information on floods and glacier extent were also considered, including Stoppani (1876), Somigliana (1917) and Monterin (1922, 1926). Monterin's first article (Monterin 1922) represents the first glaciological study of Belvedere Glacier based on ground measurements. Furthermore, the comprehensive reports by VAW (1984, 1985 and 1986) also in the Italian language were considered. Belvedere Glacier has attracted considerable attention since the year 2000 especially due to the surge-type event. The studies and events are also reported in national and local papers and various blogs and websites such as the AGU Landslide blog (<https://eos.org/landslide-blog>) and Nimbus website (http://www.nimbus.it/ghiacciai/2002/020626belvedere_art.htm). They mainly focus on the specific events of rock falls from the Monte Rosa headwall, GLOFs and the formation of the temporary (ephemeral) supraglacial lake that accompanied the surge-type event. This type of grey literature has also been used to enrich the review and clarify the glacier's behaviour and events in recent history.

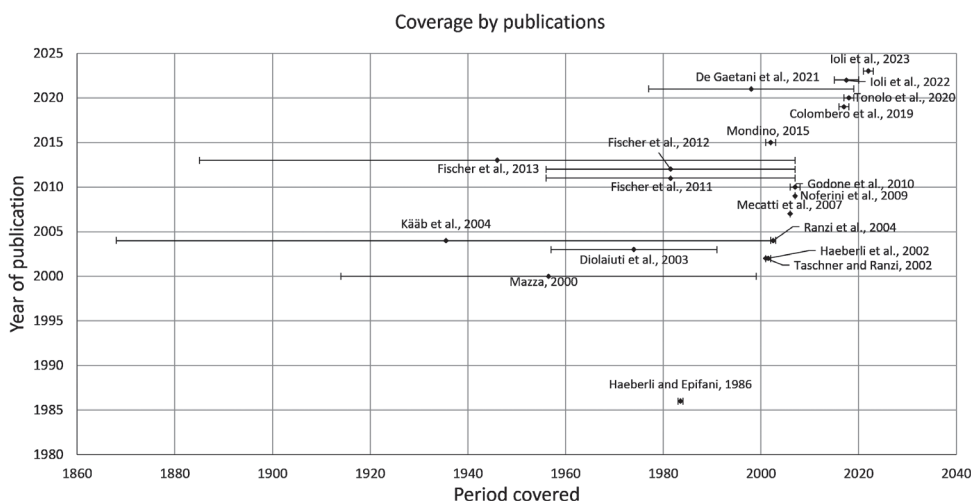


Fig. 1 Temporal coverage by the 19 research articles found by the SCOPUS search using the criteria defined in Tab.1 is shown as the time span of the study on the x-axis while the year of publication on the y-axis.

Tab. 2 Basic details of the articles found by the SCOPUS search.

No.	Study	Parameter	Location	Duration	Methodology
1	Haerberli and Epifani 1986	buried glacier ice	Lago delle Locce	1983–1984	geophysical soundings and drillings
2	Mazza 2000	glacier dynamics	Belvedere	1914–1999	compilation of results from various studies
3	Haerberli et al. 2002	surge	Belvedere and Monte Rosa	2001–2002	photographs and field visits
4	Taschner and Ranzi 2002	surface temperature	Belvedere	2001	satellite thermal measurements
5	Diolaiuti et al. 2003	thickness and volume	Belvedere	1957–1991	topographic maps
6	Fischer et al. 2003	permafrost thawing, slope instabilities	Monte Rosa (East face)	1885–2003	field photographs, permafrost models, aerial photographs
7	Ranzi et al. 2004	debris-covered glacier	Belvedere and Miage	2002–2003	field energy balance station, ASTER
8	Kääb et al. 2004	glacier hazards	Monte Rosa	1868–2003	review of studies
9	Mecatti et al. 2007	ice flow velocity	Belvedere	2006	ablation stakes, ground based SAR
10	Noferini et al. 2009	range velocity and elevation	Belvedere	2007	around based SAR interferometer
11	Godone et al. 2010	glacier ablation	Belvedere Glacier	2006–2008	ablatometric stakes
12	Fischer et al. 2011	topographic changes	Monte Rosa (East face)	1956–2007	aerial photogrammetry
13	Fischer et al. 2012	slope failure, erosion rate	Monte Rosa (East face)	1956–2007	aerial photogrammetry
14	Mondino 2015	map surface changes	Belvedere	2001–2003	aerial photogrammetry
15	Colombero et al. 2019	Ice thickness	terminal lobes	2016–2018	GPR
16	Tonolo et al. 2020	3D glacier mapping	Belvedere Glacier	2017–2019	stereo images
17	De Gaetani et al. 2021	elevation changes	Belvedere Glacier	1977–2019	aerial and UAV images
18	Ioli et al. 2022	glacier velocity and volume	Belvedere Glacier	2015–2020	UAVs
19	Ioli et al. 2023	terminus retreat	left lobe of the terminus	since 2021	time lapse cameras (stereo)

3. Study area

Belvedere Glacier is situated at the eastern side of Monte Rosa (4634 m a.s.l.), the second highest summit in the Alps on the border between Italy and Switzerland (Fig. 2). The glacier is located in the Anzasca Valley in the Piemonte region of Italy, close to the village of Macugnaga. Belvedere Glacier originates from the east face of Monte Rosa, which is a compact rock wall of metamorphic rocks forming the highest rock face in the Alps with a vertical span of about 2600 m (Diolaiuti et al. 2003). The glacier flows towards North-Northeast and terminates approximately 2 km west of Macugnaga. According to the Global Land Ice Measurements from Space (GLIMS) (Cogley et al. 2022), the glacier extends from 4487 m a.s.l. down to an elevation of about 1840 m a.s.l. In 1983, it covered an area of about 5.58 km² (WGMS 2023). Belvedere is an elevated sediment bed glacier (Monterin 1922; Mazza 2000). The ice of the snout, reaching several tens of metres in thickness, is superimposed on the sediment layer reaching a depth of 100–200 m (VAW 1985).

Belvedere is a humid-temperate glacier (Kääb et al. 2004; Haerberli et al. 2002). It has a limited accumulation basin and is mostly fed by snow and ice avalanches. In the 20th century the tributary Locce and Nordend glaciers separated from the Belvedere due to their retreat, which further reduced ice contribution. Rockfalls from the east face of Monte Rosa contribute

to its debris coverage (Haerberli et al. 2002; Diolaiuti et al. 2003). The upper part of the glacier is steep, and its geometry is heavily determined by the relief of the east face, covered by hanging glaciers and firns. The hanging glaciers undergo rapid changes in geometry and release ice avalanches, which accumulate on the glacier at the toe of the wall (Kääb et al. 2004; Fischer et al. 2006). The lower part of the glacier, which has an average slope of 10° (Godone et al. 2010), is heavily debris-covered. The thickness of the debris cover measured in 2000 was 4–5 cm and it reached 20–30 cm on the frontal lobes (Diolaiuti et al. 2003). The terminus of Belvedere Glacier reaches 1840 m a.s.l., which is much lower than the nearby glaciers in the Monte Rosa Massif (Lys: 2395 m a.s.l., Verra: 2770 m a.s.l. and Gornergletscher: 2207 m a.s.l.), mainly due to the debris-cover and low solar exposure.

The terminal portion of Belvedere Glacier is bilobate and reaches below the tree-line. The lobes are separated by a moraine complex. A surge-type movement was observed between the summer of 2001 and 2002 that uplifted the glacier surface in the lower part by 10–25 m (Haerberli et al. 2002; Truffer et al. 2021). After the surge, an ephemeral lake appeared near the foot of the Monte Rosa east face, posing a threat to the village of Macugnaga (Tamburini and Mortara 2005). Therefore, this lake was constantly monitored by Civil protection until its extinction. In August 2003, glacier thinning started on most parts of Belvedere Glacier (Truffer et al. 2021).

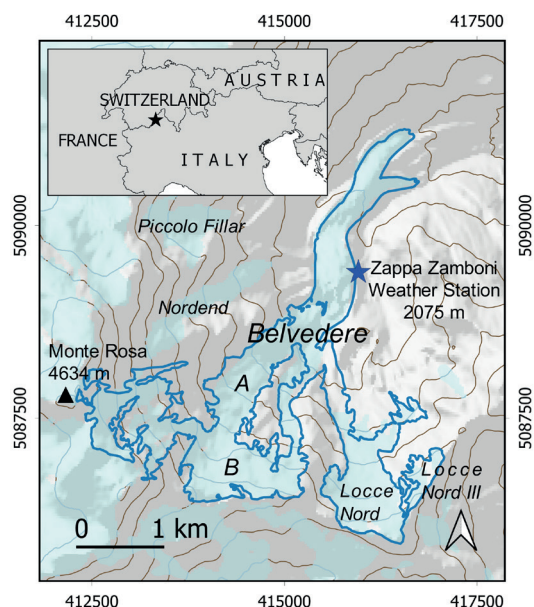


Fig. 2 The glaciers on the east face of Monte Rosa. The glacier limits and the toponyms refer to the New Italian Glacier Inventory (Paul et al. 2020). The background is a hillshade map obtained by the Digital Elevation Model (DEM) of Regione Piemonte. The glaciers not distinguished by the inventory as separate glaciers but mentioned in this text are marked by capital letters: A: Ghiacciaio del Monte Rosa and B: Ghiacciaio del Signal.

The climate data from Zappa Zamboni weather station (2075 m a.s.l.) located next to the lower part of the glacier indicates significant seasonal variations. January and February are cold and dry with average maximum air temperatures around $-0.4\text{ }^{\circ}\text{C}$ and mean monthly precipitation under 10 mm. Spring (March–May) sees rising temperatures and increasing precipitation, peaking in May at 206 mm. Summer (June–August) is warm, with average maximum temperatures between $13.3\text{ }^{\circ}\text{C}$ and $15.5\text{ }^{\circ}\text{C}$ and moderate precipitation. Autumn (September–November) features gradually cooling temperatures and substantial rainfall, particularly in October with 147 mm. December marks the onset of winter, with temperatures dropping and precipitation decreasing to 11 mm.

3.1 Historical explorations and name changes

Belvedere Glacier has received a lot of attention since the very beginning of scientific mountain explorations. As early as in 1780 the glacier was visited by Amoretti who described a glacier gate at one of the terminal lobes which was then the source of the Anza River (Amoretti 1817). The terminus of the glacier was crossed by De Saussure in 1787 who carried out a trigonometric measurement of the elevation of Monte Rosa. Temperature and pressure measurements were done by Zumstein during his ascent of one of the summits of Monte Rosa (Zumstein 1824). A map of Monte Rosa showing roughly the outlines of Belvedere Glacier was published by Welden who

visited Belvedere in 1823 (Welden 1824). Forbes (1845) noted that Belvedere was rather stagnant in contrast to Lys Glacier. A detailed study on the geology of the Monte Rosa massif was published by Schlagintweit (1853). The first topographic map of the area in 1 : 50,000 scale was published by the Kingdom of Piedmont-Sardinia in 1820–1821. Since the 1920s, systematic measurements of the position of glacier terminus have been carried out by the Italian Glaciological Committee. The first aerial photographs used in the studies about Belvedere Glacier originate from the 1950s, see more information on this in Kropáček et al. 2024, in this issue.

In the historical literature, the glacier was called Macugnaga Glacier (*Ghiacciaio di Macugnaga* in Italian) e.g. by Monterin (1922) and it encompassed the glacier tongue and a large part of the glacierized east face. This name was used in the annual glaciological surveys published by the Italian Glaciological Committee till the 1950s. Starting in 1953 the surveys have been using the name Belvedere Glacier (*Ghiacciaio del Belvedere*). However, the name Belvedere was related only to the lower, debris-covered part of the glacier. Most of the articles treated in this review stuck to this convention. The separate names for accumulation and ablation areas of a single glacier do not make sense from the glaciological point of view and results in confusion, especially if volume changes are calculated only for Belvedere Glacier i.e. the ablation part (as shown further in the text).

Interestingly, the Italian Glacier Inventory (CNR-CGI 1961) (http://repo.igg.cnr.it/ghiacciaiCGI/ghiacciai_new.html), the Belvedere Glacier includes all glaciers of the east face connected to the lower part at that time (*Ghiacciaio Nord delle Locce*, *Ghiacciaio del Signal*, *Ghiacciaio del Monte Rosa*, *Ghiacciaio della Nordend*). At present, some of these glaciers are already disconnected. Further on in this text we use the term ‘Belvedere Glacier’ as defined in the New Italian Glacier Inventory (Paul et al. 2020) including both its accumulation and ablation parts (Fig. 2).

4. Review of the used techniques

4.1 Remote sensing based studies

The analysed papers show that various techniques have been used to study the Belvedere Glacier. In-situ measurements to quantify changes in volume and mass balance are time-consuming, expensive, and require mountaineering expertise which makes them dangerous as well. To overcome all these limitations, photogrammetry, aerial photography, and remote sensing techniques prove to be extremely useful. Photogrammetry is used to generate DEMs of glaciers’ surface from overlapping image pairs. The images can be acquired from aerial platforms, terrestrial stations or satellites acquiring very high-resolution (VHR)

imagery and recently also from Unmanned Aerial Vehicles (UAVs).

Topographical maps based studies

Belvedere glacier was mapped using aerial surveys in various scales and for various purposes. The first map used for studies about the volume of Belvedere Glacier from 1957 was acquired in the framework of the International Geophysical Year (Tab. 3). The survey was carried out by the Italian Aerial Survey Agency (EIRA) in Florence for the Italian Glaciological Committee (Diolaiuti et al. 2003). Another map from 1977 was compiled by the Swisstopo, and the map from 1991 is a technical map of the Piedmont region.

Tab. 3 Topographical maps used in the studies on volume changes of Belvedere Glacier.

Year	Scale	Contour interval	Agency
1957	1 : 5,000	5 m	EIRA
1977	1 : 25,000	20 m	Swiss Topo
1983	1 : 2,000	2 m	–
1991	1 : 10,000	10 m	Technical map of Piedmont region

In a study about Belvedere Glacier for the municipality of Macugnaga (VAW 1985) compared the 1957, 1977 and 1983 maps (Tab. 3 and Tab. 4). They note that the glacier outlines especially in its debris-covered part may not be accurate due to the difficulty to distinguish between debris cover and surrounding terrain. Furthermore, they revealed a discrepancy of 12.5 ± 1.5 m in the zone of the glacier between the 1957 and 1983 maps which had to be accounted for (Tab. 3 and Tab. 4). In a study focused on volume changes of Belvedere Glacier by Diolaiuti et al. (2003), DEMs based on the 1957 and 1991 maps were compared. Both maps were converted to raster representation and overlaid. The drawback was the coverage of the 1957 map limited to the lower part of the glacier.

Tab. 4 Data sources used by various authors for the analysis of volume changes.

Authors	Topo maps	Aerial Photographs	UAV	LiDAR	VHR satellite
VAW 1985	1957, 1977, 1983	1983			
Diolaiuti et al. 2003	1957, 1991				
Kääb et al. 2004		1995, 1999			
Fischer et al. 2013		1956, 1988, 2001 (Swisstopo)		2005, 2007	
De Gaetani et al. 2021		1977, 1991, 2001, 2009, 2019			
Mondino 2015		2001, 2003			
Tonolo et al. 2020			2019		2017
Ioli et al. 2022			2015–2020		

Aerial photogrammetry based studies

Aerial photographs of the east face of Monte Rosa are available at the Italian Military Geographical Institute for the years 1951, 1954, 1968, 1970, 1988, 1992, 1996 and 2004. They can be obtained at several levels of scanning density. The frequency of the aerial surveys allowed for monitoring of glacier changes and anomalies on decadal time scales (Tab. 4). Additionally, aerial orthoimages from 2009–2011 are available for download, while images from 1980–1990, 2015, and 2018 can be accessed as Web Map Service (WMS) layers on the Piemonte region's information portal (Geoportale Piemonte).

Since 1954, the surveys have used black and white photography with the standard film format 23×23 cm at various flight heights resulting in scales ranging from 1 : 30,000 to 1 : 47,000. Only the 1950 survey by Santoni company, which was flown at an altitude of 5,000 m, used 13×18 cm glass plates at a scale of 1 : 26,000. The surveys were carried out for various purposes.

Mondino (2015) derived elevation changes over the lower part of the glacier based on two image pairs from 2001 and 2003. He applied a simultaneous multi-temporal aerial image bundle adjustment approach, shared ground control points (GCPs), which was compared against traditional strategies for aerial stereo-pair adjustment. The improved relative accuracy in height coordinates was quantified as 0.65 m compared to single bundle adjustment resulting in 2.63 m.

Another aerial survey was carried out by the Laboratory for Climate Change Monitoring of the *Politecnico di Torino* in 2019 employing a small aircraft with the medium format Phase One iXM-RS150F photogrammetric camera with 150 Mpx sensor and 50 mm focal length lens onboard. The altitude limit of the aircraft at 4,000 m and the payload weight prevented the coverage of the upper part of the glacier. A DEM based on the data was utilised by Tonolo et al. (2020) for the analysis of mass changes of the lower part of the Belvedere Glacier.

The development of digital photogrammetric cameras with high-quality sensors has eased the surveying of remote and orographically complex areas to be georeferenced with fewer GCPs which reduced the fieldwork. A digital multispectral camera was used for the aerial survey in 2009 carried out by a private company (*Compagnia Generale Ripresearee*). Resulting data together with scanned photographs of the surveys in 1977, 1991 and 2001 were used by De Gaetani et al. (2021) for derivation of DEMs, which in turn were used for the calculation of volume changes of the lower part of Belvedere Glacier.

In particular, Fischer et al. (2011) mapped topographic changes from a set of high-resolution (2 m) aerial stereo pairs with the root mean square error in vertical dimension ranging from 1.5 to 2.5 m.

Unmanned Aerial Vehicles (UAVs) based studies

Since 2015 unmanned aerial vehicles (UAV) have been used to monitor volume changes of Belvedere

Glacier. This approach is based on the availability of affordable carriers, low-cost sensors, Structure from Motion techniques (SfM), and Differential Global Positioning Systems (DGPS) for geometry control.

Starting in 2016, UAV campaigns using both fixed-wing and copter platforms were carried out by *Alta Scuola Politecnica (Politecnico di Torino e Milano)* in order to identify regions of ice gain and loss of Belvedere Glacier (Tonolo et al. 2020). Due to technical limitations, they could acquire data only for the lower part of the glacier in about three days. DEM based on UAV data was also used by De Gaetani et al. (2021). They carried out five UAV flights in July and August 2019 in conjunction with aerial photogrammetry for the derivation of volume changes of the lower part of Belvedere Glacier (Tab. 3). They used fixed-wing UAV Parrot Disco with low-cost HawkEye Firefly 8S camera with 12 Mpx CMOS sensor. The flight height of 120 m above the ground resulted in a ground resolution of the image data of 5 cm.

Furthermore, Ioli et al. (2022) accomplished an aerial survey using different UAV platforms including fixed-wing eBee drone carrying a compact camera Canon PowerShot S110, Parrot Disco FPV with HawkEye Firefly 8S lightweight camera and quadcopter DJI Phantom 4 Pro with DJI FC6310 camera. They acquired data each year in the period 2015–2020 with ground resolution ranging from 5 to 9 cm. Both De Gaetani et al. (2021) and Ioli et al. (2022) used UAVs in combination with aerial stereo pairs employing SfM and Multi-View Stereo algorithms to build photogrammetric models to study the elevation change of the glacier surface. They achieved accuracy on the scale of decimetres.

Lidar based studies

Lidar measurements were used for the analysis of topographic changes on the east face of Monte Rosa related to thaw of permafrost by Fischer et al. (2013). They used two DEMs based on Airborne Laser Scanning (ALS), one assembled from data acquisitions by an aeroplane in 2005, the other one by helicopter in September 2007.

Satellite data based studies

The technique for glacier monitoring which has no altitude limit and does not require fieldwork in a demanding mountain environment is satellite stereo-image acquisition by very-high resolution instruments. An archived in-track stereo-pair of Pléiades 1-A images from October 2019 were used for the generation of a DEM by Tonolo et al. (2020). They used Rational Function Model for the stereo-processing which resulted in an ortho-image and DEM to map and analyse surface elevation change of the lower part of the Belvedere Glacier. Pléiades 1-A satellite was launched under the French-Italian ORFEO Programme in October 2003. It acquires very-high resolution image data with ground sample distance

in nadir of 0.5 m in panchromatic mode and 2 m in multispectral mode, which includes three visible and one near-infrared spectral band (Gleyzes et al. 2012).

Thermal satellite data from Landsat and ASTER along with ground-based measurements were used by two studies to analyse the sensitivity of the temperature to the physical properties of the debris cover of Belvedere Glacier (Taschner and Ranzi 2002). Ranzi et al. (2004) were able to identify debris-covered glaciers using satellite-borne thermal radiometers where the debris layer was less than 40–50 cm as the surface temperature of the supraglacial debris was 4.5 °C colder, on average, than debris deposits near by the glacier.

4.2 In-situ measurements

Seismic methods and Ground Penetrating Radar (GPR)

On the occasion of the International Geophysical Year (1957), the Experimental Geophysical Observatory of Trieste carried out seismic prospecting for mapping of the glacier bed (Visintini 1957). The maximum depth was measured as about 225 m. This was followed in 1984 by a campaign of Ground Penetration Radar (GPR) measurements using the USGS Monopuls Radar of 1 to 5 MHz frequency (VAW 1985). The two approaches provided similar results in terms of ice depth with discrepancies generally within 5 to 10%. However, in the middle part of the glacier snout, the GPR measurements showed a layer of unknown origin about 50–100 m above the ice bottom detected by the seismic.

Further GPR campaigns, both by helicopter and from the glacier surface were carried out in 2002–2003 for the detection of the ice thickness below the Effimero Lake and along several transects downstream (Tamburini and Mortara 2005). Despite difficulties in the interpretation given by the debris cover and water present in the ice mass, they estimated the ice thickness below Effimero Lake as 120 m. Furthermore, Colombero et al. (2019) acquired GPR profiles and seismic measurements for the terminal lobes of Belvedere from 2016 to 2018, to estimate the ice thickness and reconstruct the bottom morphology. They detected a more than 40 m thick layer of subglacial deposits and they also indicated the presence of bedrock at 80 m depth in the frontal portion of the left lobe. Apart from the frontal lobes, only noisy measurements, not allowing any ice bottom detection, could be obtained.

Bottom temperatures of the winter snow cover (BTS)

A combination of geophysical soundings and drillings to study the buried glacier ice close to the Locce Lake was used by Haerberli and Epifani (1986). The geophysical soundings included indirect measurements of near-surface heat flow, geoelectrical resistivity, and seismic refraction. BTS approach was applied in February 1983 to map the distribution of the near-surface underground ice, using thermistor probes that

were lowered to the soil-snow interface. Fifteen electrical DC resistivity soundings were carried out in the summer of 1983 to investigate the extent of underground ice and to confirm if it was frozen ground or buried glacier ice. Furthermore, the BTS approach was applied on the lobes of Belvedere Glacier by VAW (1985). The application of this approach, which allows to reveal the presence of ice below a layer of debris, resulted in the detection of ice in the shadowed parts of the moraines of Belvedere.

Terrestrial Laser Scanner

A monitoring campaign using TLS was conducted by Godone and Godone (2012) in the summer and autumn of 2006 and 2007 carrying out measurements of the central/lower part of the glacier. Furthermore, measurements of the 2005 and 2007 landslides that affected the terminal moraine of the North Locce Glacier, a former tributary on the right side of the Belvedere Glacier, were carried out. The surface comparison gave an average measure of landslide movement of over 2 m with an average rate of 0.05 m/day. In addition, the total vertical shift of the landslide mass has been estimated as 36.62 m through manual measurement, since the trigger of the event. The difference in surfaces' elevation indicated the ablation ranging from 2 to 8 m in the period 2006–2007. In the summer 2006 and 2007 two ground-based Synthetic Aperture Radar (SAR) surveys were conducted at Belvedere Glacier to produce surface velocity maps (Mecatti et al. 2007; Pieraccini et al. 2008; Noferini et al. 2009).

Ablation stakes and camera-lapse

Moreover, a network of ablation stakes has been installed providing annual ablation and surface displacement velocity since 2009. The results are reported in the Annual Glaciological Survey of Italian Glaciers edited by the (Italian Glaciological Committee). Additionally, measurements on ablation stakes from 1983/84 are available (VAW 1985). Repeated photography was used extensively to document the mass wasting processes (Fischer et al. 2013; Tamburini et al. 2013) and changes in the geometry of the glaciers (VAW 1985). Recently, a pair of time lapse camera systems was installed by Ioli et al. (2023) to monitor the volume changes of the left lobe of the terminus.

5. Glacier dynamics

5.1 Changes in glacier area and frontal glacier position

There is a large uncertainty in the area of Belvedere Glacier in various sources. The glacier area provided in articles dealing with the lower part of the glacier depends on the placement of the arbitrary border in

the steep upper part of the glacier and is given in the range from 1.47 to 1.78 km² (De Gaetani et al. 2021; Diolaiuti et al. 2003). The total area of Belvedere Glacier also varies based on the source and is in the range from 4.4 to 5.58 km² (RGI, reports of the World Glacier Monitoring Service (WGMS), Global Glacier Change Bulletin). The variation is mainly due to the different number of hanging and tributary glaciers included rather than by real changes in extent (Fig. 2).

Area changes reported in two studies (VAW 1985 and Diolaiuti et al. 2003) are difficult to compare due to different observation periods and due to the difference in the delineation of the lower and upper part of the glacier (Tab. 5). The fluctuation of glacier front is a better indicator of changes in glacier extent because these changes occurred in the frontal zone. The glacier front fluctuation based on the field measurement of the left lobe organised by the Italian Glaciological Committee is shown in Fig. 3b. Apart from an advance at the end of the 1960s there were several years of minor advances (1986–1989, 1991, 1994) in the period 1986–2000 and several periods of retreat (1990, 1992–1993, 1995–2000), corresponding to the general trend recorded in the Italian Alps (Citterio et al. 2007). This was followed by a period of advance (50.5 metres) from 2001 to 2005 connected to the surge-type event while afterwards a strong retreat (2007–2022: –232 metres) was recorded (Italian Glaciological Committee reports). In the period 1974–1985, the measurements of the terminal positions are missing.

Tab. 5 Changes in areal extent of Belvedere Glacier reported by two studies.

Period	Areal change (km ²)	Mean yearly rate (km ² a ⁻¹)	Source
1957–1983	+0.06	+0.023	VAW 1985
1977–1983	+0.09	+0.015	VAW 1985
1957–1991	–0.017	–0.0005	Diolaiuti et al. 2003

5.2 Changes in ice volume

The records of ice volume change for Belvedere Glacier are mainly based on aerial photographs, UAV data and historical maps. Again, they cover different time spans which renders them difficult to compare. Furthermore, they are focused on the lower part of the glacier, apart from just one study. It is thus difficult to come up with a clear overview of the volume changes of Belvedere Glacier in time (Fig. 3c).

A study covering a large time span (1957–1991) was carried out by Diolaiuti et al. (2003) using a comparison of DEMs from topographical maps (Fig. 3c). The change in volume estimated for the lower part of the glacier was +22.7 × 10⁶ m³ which included the thickness of the supraglacial debris. The mean change in glacier thickness in the period 1957–1991 was assessed as +15 m, with annual increase of +0.44 m/year.

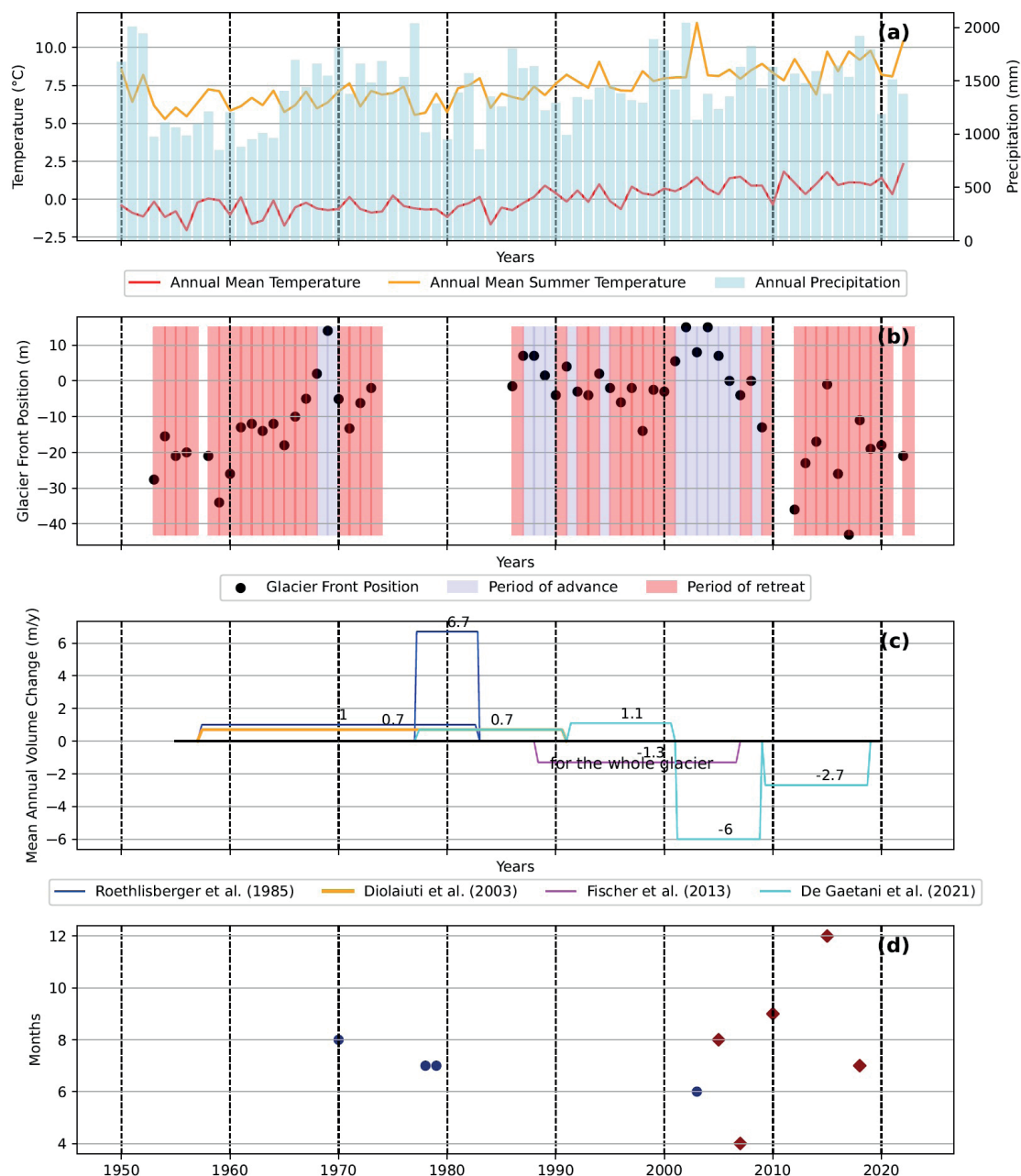


Fig. 3 The changes in climate, glacier geometry, GLOFs, and rock and ice avalanches since the 1950s shown with E-obs temperature and precipitation (E-obs gridded dataset 0.1×0.1 degree, Haylock et al. 2008) (a), record of glacier front fluctuations with respect to the previous year as published by the Italian Glaciological Committee (b), mean volume changes calculated using maps and DEMs. Except for Fischer et al. 2013, the figures refer only to the lower part of the glacier (c) and recorded GLOFs and rock and ice avalanches (d).

Negative change was recorded in the retreating frontal sector with the highest thickness change of -30 m. An increase in thickness between 10 – 20 m was registered for over 50% of the glacier while less than 5% of the surface experienced thinning.

A similar approach using topographical maps for the estimation of volume changes of the lower part of the glacier was conducted by (VAW 1985). In addition to the 1957 and 1983 topographical maps, the Swiss topographical map from 1977 was used. The calculated volume change of 26×10^6 m³ in the period 1957–1983 corresponds to a mean thickness increase of $+18.42$ m ($+0.71$ m/year) (Fig. 3c). The largest

volume increase occurred in the central portion of the lower part of the glacier where the thickness increase exceeded $+35$ m while the volume losses were located close to the terminus of the left lobe. In 1984 the surface of the glacier reached the level of the top of the LIA moraine.

A substantial part of the volume increase observed by VAW (1985) occurred in the period 1977–1983 (mean thickness increase of $+18.77$ m and $+3.31$ m/year). Interestingly, the comparison of the 1957 and the 1983 maps revealed a discrepancy in off-glacier areas of 15.5 ± 1.5 m which was accounted for by a respective correction of the volumetric and

thickness changes. A study published one decade later by Fischer et al. (2013) revealed a total volume loss of $-25 \times 10^6 \text{ m}^3$ for the entire glacier in the period 1988–2007 (Fig. 3c).

Another study using photogrammetry conducted by De Gaetani et al. (2021) focused on volume changes in the lower part of the glacier during the period 1977–2019 (Fig. 3c). It revealed a gain in volume of about $+20.66 \times 10^6 \text{ m}^3$ from 1977 to 2001. The rate of volume gain increased by about 50% during this period. This period was followed by a decline in the volume from 2001 to 2019. First, the average annual volume loss amounted to $-5.97 \times 10^6 \text{ m}^3/\text{year}$ from 2001 to 2009. The reduction was witnessed also in the next decade but with a lesser severity of $-2.72 \times 10^6 \text{ m}^3/\text{year}$. The total loss in volume of $-54.28 \times 10^6 \text{ m}^3$, over the 42 years covered by the study was marked by distinct nonlinearity (De Gaetani et al. 2021). The down-wasting observed in the period 2001–2009, almost totally compensated for the volume increase of the previous 20 years. The start of the thinning of the lower part of Belvedere was observed by Kääb et al. (2004) in summer 2003. Since the end of the surge-type movement, the retreat has been continuing, resulting in thickness reduced by tens of metres, as measured in the lower part of the glacier (De Gaetani et al. 2021).

The lower part of the glacier was also studied by Ioli et al. (2022) who derived annual volume changes

in the period 2015–2020 using UAV-based DEMs. The volume changes ranged between $-2 \times 10^6 \text{ m}^3$ and $-3.5 \times 10^6 \text{ m}^3$. The results are however biased by the fact that in the years 2015–2017, data from the beginning, and in 2018–2020 from the end of the ablation period were used.

In all but one case, the studies were focused on the lower part of the glacier. Older studies relied mainly on topographical maps while the newer ones on the evaluation of aerial photographs and UAV images. Despite mismatches of the results and difficulty in integrating the different time spans of the studies (Fig. 3c), it appeared that Belvedere Glacier experienced a transition from positive to negative volume change between the 1980s and the beginning of the 2000s.

5.3 Glacier flow velocity and surge-type event

The velocities measured on stakes ranged from 34.8 to 47.6 m/year in 1983/84. The surface velocity was estimated to be 30–40 m/year in the period 1995–1999, i.e. before the beginning of the surge-type event (Fischer et al. 2013). Glacier flow velocities speeded up to 110–200 m/year in the period 1999–2001 (Kääb et al. 2004; see details in paragraph 5.4). According to field measurements, the surface displacement velocity in 2020 was about 20 m/year in the upper part of

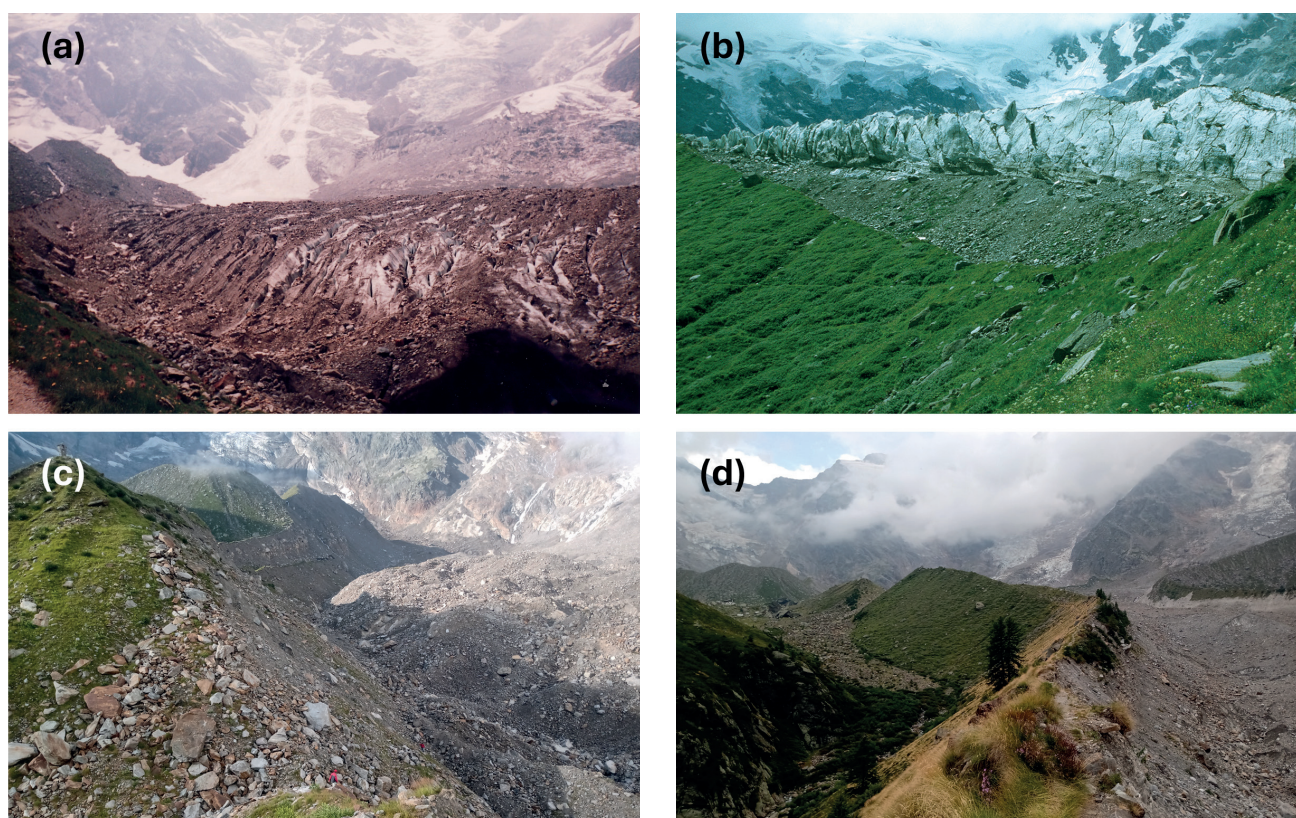


Fig. 4 Glacier volume changes documented by ground photographs detailing the place of the breach of the right moraine close to the Zappa-Zamboni Hut at the beginning of the 1990s by I. Bollati (a), during the surge-type event in 2001 by J. Eberle (b), in 2023 by J. Kropáček (c) and a more distant view along the moraine in 2022 by J. Kropáček (d).

the glacier tongue and 2–4 m/year at the glacier snout (Baroni et al. 2020).

At the beginning of the 2000s, the glacier underwent a flow speed up and marked changes in geometry described as a surge-type or surge-like event by several authors (Haeberli et al. 2002; Diolaiuti et al. 2003; Käab et al. 2004; Fischer et al. 2006). The first signs of the event were recognised in the summer of 2000 as the lower portion of the steep part of the glacier displayed extreme crevassing indicating acceleration in flow, which resulted in compression and deformations on the surface of the lower part of the glacier (Haeberli et al. 2002). Further observations of an unusual change in flow and geometry were carried out in spring of 2001 (Haeberli et al. 2002; Käab et al. 2004).

In the lower part, the glacier surface rose for up to 20 m reaching the level of the LIA moraine (Mortara et al. 2003). Debris-free and heavily crevassed ice was seen towering above the moraine at the place of the 1904 breach threatening the path to Zappa Zamboni Hut (Fig. 4) (Haeberli et al. 2002). Flow velocities of up to 110 m/year in the period 1999–2001 and 200 m/year in autumn 2001 were determined photogrammetrically (Käab et al. 2004). This is a significant increase compared to 1994–1999, in which the flow velocity was only 32–43 m/year (Käab et al. 2005). The accelerated flow was observed till the spring 2003 and since the summer 2003, the ice thickness of the lower part has been decreasing (Käab et al. 2004). Although the features related to the event such as crevassing appeared from 2000 to 2003, the duration of the event is usually given as 2001–2002.

An interesting insight into the dynamics of this event is provided by the maps of surface elevation changes of the lower part of the glacier generated by De Gaetani et al. (2021) despite a rather coarse temporal resolution. In the period 1977–1991, the surface elevation change was a rather uniform increase while the elevation difference image for the following period (1991–2001) shows a pattern marking the beginning of the surge-type event. This pattern consists of an intense elevation decrease on the transition to the steeper part of the glacier and at the same time an elevation increase in the lower portion of the glacier. This agrees with observations by Käab et al. (2004) who identified the ice thinning of about 20 m at the location of the depression in the period 1995–1999. The accelerated flow first involved the lower flat part of the glacier leading to a lack of support for its steeper part (Käab et al. 2004), while Haeberli (2002) reported the first signs of the acceleration in the lower portion of the steep part of the glacier, as observed in summer 2000.

The results of De Gaetani et al. (2021) further show a shift of the lowered part downstream due to the glacier movement in the period 2001–2009. In the lower part, the Effimero Lake developed during spring snowmelt in 2001 for the first time (Haeberli et al. 2002). There was also a marked thickening at both

lobes likely due to the surge-type event. This stage was followed by an overall strong surface lowering in the period 2009–2019 and an elevation increase on the transition to the steep part of the glacier (De Gaetani et al. 2021). This increase occurred almost exactly in the area of the initial lowering in the period 1991–2001. Despite these detailed observations, the exact mechanism of this event remains unclear (Mazza 2003; Truffer et al. 2021).

6. Natural hazards related to glacier dynamics

6.1 Slope failures

The observation of mass movement activity on the east face of Monte Rosa started in the 1990s (Käab et al. 2004; Fischer et al. 2013). After an initial period of reduced activity, an increase in events, including massive ice avalanches, rockfall, and debris flows, was reported for the period 1999–2001. In the central part of the rock face the total volume loss of approximately $25 \times 10^6 \text{ m}^3$ in the period 1988–2007 was observed by Fischer et al. (2013).

The east face of Monte Rosa witnessed four massive rock and ice avalanches which led to significant changes in its morphology. In August 2005, a major ice avalanche occurred due to a glacier detachment with a thickness of 40 m in the elevation zone between 3580 and 3820 m a.s.l. (Tamburini et al. 2013). With its volume of $1.2 \times 10^6 \text{ m}^3$, it was recognised as one of the largest ice avalanches documented in the European Alps (Fischer et al. 2013). The ice accumulation, which had an area of about 1.1 km², reached close to the Zamboni hut located more than 3 km downstream, but no casualty was recorded.

A large rock avalanche of 15–30 m thickness and $0.2 \times 10^6 \text{ m}^3$ volume occurred in April 2007 from the uppermost part of the face of Monte Rosa in the region of continuous permafrost at an elevation of 4000–4200 m a.s.l. The runout path and spreading area were almost the same as the previous ice avalanche event. The cause was linked to the exceptionally high temperatures recorded in April 2007 inducing permafrost degradation and thawing (Tamburini et al. 2013).

Two large rockfalls occurred below the summit of Punta Tre Amici (Fig. 5), in the upper basin of Northern Locce Glacier. The first one with a volume of $0.1 \times 10^6 \text{ m}^3$ happened in September 2010 (Fischer et al. 2013; Paranunzio et al. 2016). The second one ($0.2 \times 10^6 \text{ m}^3$) was triggered by a period of extreme warmth and low snowfall till mid of November and occurred on the night of 16 December 2015, at an altitude of approximately 3400 m a.s.l. Temperature reaching 7 °C was measured at the altitude of 3000 m a.s.l. by a radio-sonde above Milan in the neighbouring province four days prior the event (Chiarle et al. 2015). The accumulated material reached the southern

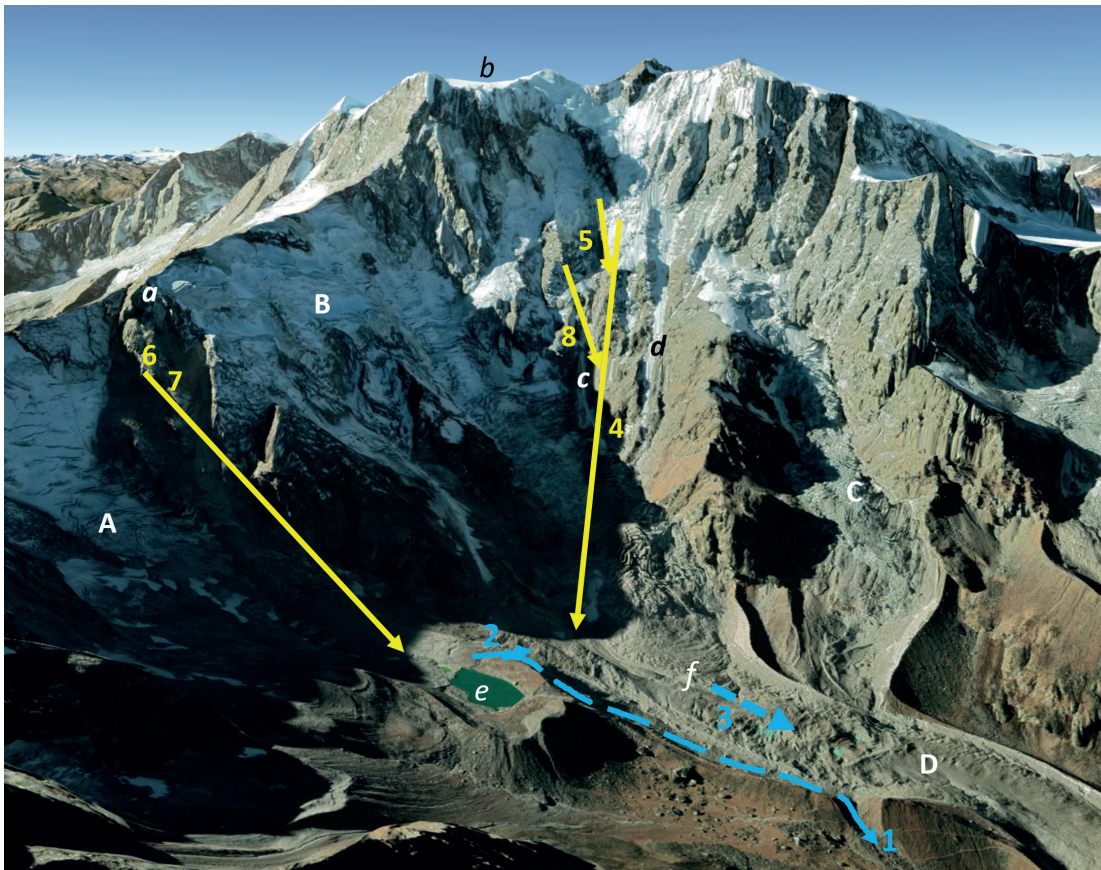


Fig. 5 Major rock and ice avalanches as well as GLOFs that have occurred at the east face of Monte Rosa and Belvedere Glacier (marked by numbers): 1: 1904, water pocket outburst (Somigliana 1917; Käab et al. 2004), 2: 1970, 1978, 1979 lake outburst (Käab et al. 2004), 3: 2003 lake outburst, 4: 2005 rock and ice avalanche (Fischer 2006), 5: 2007 rock avalanche (Tamburini 2013), 6 September 2010, rockfall (Fischer et al. 2013), 7: December 2015, rockfall (Chiarle et al. 2015), 8: 11 July 2018, rock-ice avalanche (I. Bollati's field observation), Glaciers: A: North Locce Gl., B: Signal Gl., C: Nordend Gl., D: Belvedere Gl., Other features: a: Punta Tre Amici, b: Colle Gnifetti, c: Imseng Channel, d: Marinelli Channel, e: Locce Lake, f: Position of Effimero Lake in 2002. (Source of the background image: Google Earth).

shore of Lake Locce at the altitude of 2300 m a.s.l. The slope instability was already noticed in August as a debris flow from the slope of Punta Tre Amici was observed after early snowfall at higher altitudes (Chiarle et al. 2015).

These large-scale events together with frequent minor rock and ice avalanches resulted in a significant change in morphology of the entire cirque. These changes were quantified for the central part of the Monte Rosa east face prior to the major rock and ice avalanches (1988–2001) by Fischer et al. (2013) who determined a reduction of the steep glaciers and bedrock for up to 115 m in perpendicular direction to the slope. Most of the detachment zones of the slope failures were observed to be located either at the boundary of the estimated permafrost distribution zones or were found to be characterised by changing permafrost conditions (Boeckli et al. 2012; Fischer et al. 2006; Tamburini et al. 2013).

6.2 Glacier lake outbursts

There is a rich history of GLOFs originating from the lakes and englacial pockets in the east part of the

Monte Rosa massif that threatened the downstream settlements. In total seven outburst floods from glacial lakes and water pockets were documented (Fig. 5, Fig. 6). The first one occurred in August 1868 caused by the burst of an englacial water pocket after prolonged rainfall led to a collapse of the lateral moraine close to the left terminus (Haeberli et al. 2002) and the accumulation of boulders over an area of about 1 km² in front of the glacier (Stoppiani 1876). Two older events were described in historical records, but it is not known whether they originated from a glacial lake: one in 1820, during which the moraine at 1585 m a.s.l. was breached, and another one was a large flood on 26–28 August 1834, which brought large pieces of ice some 15 km downstream (Bertamini 2005; Mortara and Tamburini 2009).

A similar event was reported by “La Voce” magazine in August 1896, where water cut two ways through the moraine and devastated meadows near Pecetto and Macugnaga. In 1904, another drainage of an englacial water pocket caused the collapse of the right lateral moraine (Somigliana 1917). In September 1922, following several days of rain, a large mass of water was expelled from the glacier, destroying

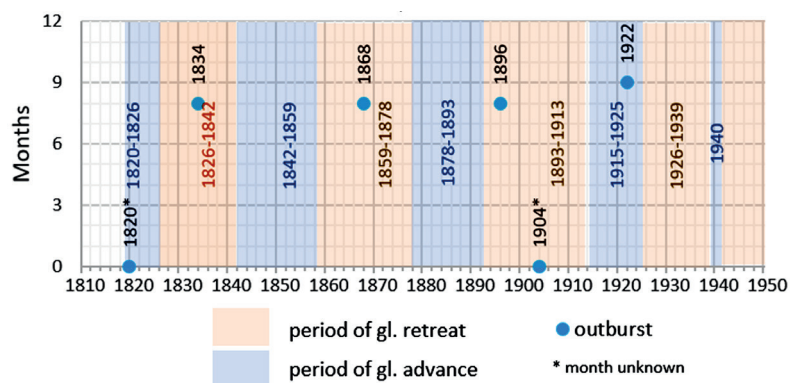


Fig. 6 The record of outbursts for the period 1820–1950 collected from various sources, superimposed by the periods of retreat and advance of Belvedere Glacier as listed in Monterin (1926).

a 100 m-long wall constructed to protect Macugnaga. Big ice blocks were carried over 6 km downstream (Monterin 1926).

A sequence of three outburst floods occurred in the 1970s: on 13 August 1970, 2 August 1978 and in July 1979 (Fig. 5). The floods issued from the Locce Lake, dammed by both moraine and ice. These floods progressively widened the breach through the right lateral moraine, which was initially cut in 1904. The 1979 event seriously damaged the Belvedere chair-lift and flooded the valley bottom over a length of 1 km and a mean width of 150 m, almost reaching the Pecetto hamlet near Macugnaga (Mazza 1998; Tropeano et al. 1999).

In the vicinity to Locce Lake, in the ablation seasons 2002 and 2003, the supraglacial Effimero Lake appeared in a depression caused by the surge event. During the heatwave of June 2002, the lake reached its maximum size of 0.15 km², a maximum depth of 57 m and a volume of about 3×10^6 m³ and threatened to burst (Tamburini and Mortara 2005; Truffer et al. 2021). To reduce the risk of a GLOF, a pumping system was installed by the Italian Civil Defense Department, and emergency evacuation planes were prepared for the downstream settlements. The lake level lowered as a combined effect of the pumping, cold weather and subglacial drainage. However, in spring 2003, due to rapid snow melt in May a fast increase of the lake level was observed resulting in an outburst flood between 18 and 20 June (Fig. 5). A water volume of 2.3×10^6 m³ was released without causing damage (Ranzi et al. 2004; Tamburini and Mortara 2005; Chiarle and Mortara 2008; Godone et al. 2010).

6.3 Erosion and collapse of moraines

Even if the destabilisation of the moraine started at the end of the LIA (Mortara et al. 2023), the powerful surge-type event caused morphological changes to the existing moraine system of the glacier. As Belvedere Glacier has been losing speed as well as thickness since the surge, the moraines have lost the support exerted by the glaciers and experienced erosion and partial collapse (Tamburini et al. 2019; Mortara et al. 2023). The right lateral moraine of the left glacier lobe

has shown instability in the form of subsidence on the inner side. The recent change was the appearance of a 180 m long crack in the moraine spur that separates the lobes of the glacier and hosts the chairlift station. It intercepts both sides of the moraine. The detached block partially collapsed before May 2022.

The partial collapse of the right lateral moraine causing severe problems to the hiking path towards the Zamboni-Zappa hut (Mortara et al. 2023), started in October 2016 with some minor collapses in October 2021 and April 2022 (www.meteoliveco.it). Several other events were reported by the local and regional press.

As the moraines will continuously lose their support by the shrinking glacier, further erosion and instabilities of the moraines can be expected. This is especially true for the moraines surrounding the lobes as very high rates of down-wasting were measured here. For instance, on the right lobe, a loss of 46 cm in thickness within 10 days was measured at the end of July 2019, in spite of being covered with a thick layer of debris protecting the underlying ice from solar radiation (Tamburini et al. 2019).

7. Discussion

The dynamics of Belvedere Glacier were recorded mainly as fluctuations of its left terminus. However, it has been shown in many studies that fluctuations of glacier fronts are in offset with respect to climate forcing (e.g. Zemp et al. 2007). Mass balance of Belvedere Glacier was calculated as averages over multi-year periods mainly only for its lower ablation part. Although Belvedere Glacier was included in the global assessments of glacier status by IAHS and UNESCO published within the period of five years since 1959 (Kasser 1973), it can hardly represent general behaviour of glaciers in this region.

7.1 Anomalous behaviour of Belvedere Glacier

In many respects Belvedere Glacier is rather anomalous which was recognized already in the 1920s by Monterin (1926). This is mainly due to the prevailing

avalanche feeding mechanism resulting in an extensive debris cover which modifies both the mass balance and its gradient compared to clean-ice glaciers (Rowan et al. 2015). Glaciers which are mainly avalanche-fed tend to be longer and reach lower altitudes. The insulating effect of the debris leads to lower ice losses (Nakawo et al. 1999), as the high avalanche activity leads to extensive debris cover (Laha et al. 2017). We assume that the insulating effect of debris cover at Belvedere plays this role mainly at the terminus as its thickness in the rest of the ablation zone has the below-critical thickness of 5–10 cm (Reznichenko 2010). The ice loss of debris-covered glaciers is more in terms of ice thickness rather than by retreat of their terminus (e.g. Kirkbride and Warren, 1999). In general, in contrast to clean-ice glaciers, debris-covered glaciers have a delayed reaction to climate drivers. In the Italian Alps, certain similarities can be found at Miage Glacier in the Mont Blanc area (e.g. Mihalcea et al. 2008). It is heavily debris-covered, its terminus reaches below the tree line and its tongue is divided into two separate lobes. According to Fischer et al. (2013), the debris coverage on glaciers will increase in the future due to further glacier down-wasting.

The surge-type event in the years 2001 and 2002 was almost unique in the Alps. According to the RGI there are only three other surging glaciers in the Alps, the Vernagtferner in the Austrian Alps, documented by Hoinkes (1969) and Chelen and Damma glaciers in the Swiss Alps discussed by Roethlisberger (1969). The Vernagtferner surge was different as it was recurrent with an average period of 82 years. Furthermore, Vernagtferner features distinctly different geometry having a large accumulation area and low debris cover. The possible surge events of Chelen and Damma glaciers were carbon-dated with the age falling between 1650 ± 80 B.P. and 2280 ± 120 B.P., respectively (Roethlisberger 1969).

During the 2001/2002 event, Belvedere Glacier had roughly twice higher flow velocity compared to the previous period. Surge events are typical with velocity increase for an order of magnitude. This event is thus referred to as a surge-type event, not a surge. The study by VAW (1985) revealed that there was another event of a large volume increase of the lower part of Belvedere Glacier which occurred in the period 1977–1984 for which a steep decrease in temperature in the nearby Sabione basin was reported by Giaccone et al. (2015). In this period the glacier thickness in the lower part increased on average for 18.77 m. This figure is close to the increase of about 20 m during the 2000/2001 event given by Käab et al. (2004). In the period 1977–1984, a general glacier retreat in the Alps following an advance in the 1970s was recorded. However, the exact timing and duration of this event is unknown. There are also no records of the flow velocity during this period. The IGC surveys noticed abundant cracking

of the glacier in 1978, the appearance of longitudinal crevasses in 1980. An increase in volume due to the inflow from the upper part (Monte Rosa Glacier) was reported in 1981 which was followed by stationarity or slight expansion in 1982. The IGC surveys were, however, mainly focused on measurements of variations of the left terminus and did not contain systematic information on changes in glacier volume or its quantification. It remains also unclear whether the volume increase reported in 1981 accounts for the whole volume change calculated by VAW (1985) for the period 1977–1984. In both cases, the volume of the lower part of the glacier increased considerably. Historical photographs revealed that the ice surface exceeded slightly the crests of the lateral LIA moraines. Despite the mentioned similarities to the event in 2000/2001, the notable volume increase in 1977–1984 was probably a delayed manifestation of the general advance of glaciers in the Alps in the 1970s. Debris covered glaciers typically react to climatic signals with a certain delay (Rowan et al. 2015). Brenva Glacier, another debris-covered glacier in the Italian Alps kept advancing even until 1991, Even Lys, which is a debris-free glacier close to Belvedere, advanced until 1985 (Diolaiuti et al. 2003). The mentioned increase in thickness of Belvedere Glacier was not exceptional as for instance the thickness increase of the debris-covered Miage glacier in the Italian Alps was about 40 m in its lower part (Diolaiuti et al. 2003).

7.2 Relationship between climate and occurrence of natural hazards

While climate change is pointed out as the driver of the increase in the number of various types of glacier related natural hazards, great care has to be taken before accepting this explanation for particular events. It has been generally recognized that the occurrence of natural hazards in glacial environment is affected by the retreat and down-wasting of glaciers (Emmer et al. 2016; Frey et al. 2010; Hartmeyer et al. 2020). Various mechanisms play their role in this relation such as debulking leading to slope failures, thawing of permafrost triggering rock and ice avalanches and glacier retreat giving rise to GLOF-prone lakes (Viani et al. 2016).

It appears that from the recorded outburst floods at Belvedere, four floods occurred during phases of glacier retreat, and two floods during advancing phases. For two outbreaks in the 1970s, the records on the glacier front position are missing. (Fig. 3b, Fig. 6). The timing of the surge-type event coincides with the period of glacier down-wasting. This was determined by Fischer et al. (2011) by means of DEM differencing for the period 1988–2007. The mean value of glacier thinning derived by this approach has, however, a low information value with respect to the concrete year in which the triggering of the event

occurred. The studies by De Gaetani et al. (2021) and Diolaiuti et al. (2003) seem to contradict the negative trend in volume but they were conducted only for the lower part of the glacier disregarding the accumulation areas which are by some sources regarded as separate glaciers as for instance the Signal Glacier (Fig. 5).

While comparing the 2001/02 surge-type event with temperature and precipitation (Fig. 3a), it is interesting to note that the event does not match the peak in summer mean surface temperature and minimum in precipitation in 2003 marking the anomalous heat wave in Europe. It occurred during rather normal years in terms of temperature (Fig. 3a) but it coincides with two precipitation extremes. In 2000 and 2002, Pecetto Station recorded annual precipitation totals that were 73% and 51% above the station's average, respectively.

The recorded rockfalls and rock/ice avalanches coincide with the period of decreasing ice volume. This is in line with the findings by Fischer et al. (2013) and Ravanel et al. (2010). However, most of the records on rock and ice avalanches are available for the period starting in 2000 as no older systematic observations exist. Their connection to the thawing of permafrost and the movement of the failure zone toward higher altitudes was explicitly mentioned by Fischer et al. (2013). The slope failures, especially the deep-seated ones, can however, be delayed with respect to climate warming even for millennia (Lebrout et al. 2013) due to the extremely slow heat diffusion into rocks.

The comparison of natural hazards occurrence with the periods of glacier retreat and down-wasting is hampered in the case of the east face of Monte Rosa by several difficulties. The record of the events is not homogeneous with smaller events further in the past being likely neglected. The record on glacier status is far from being complete. For the period until 1957, we have to rely on the information about the position of the left terminus measured annually in the field by operators of the Italian Glaciological Committee. The movements of the terminus, however, represent a delayed climate signal. The volume changes, that react sensitively to the climate signal, each year are available only as a mean for several years.

7.3 Critical assessment of the studies

Despite a number of research papers focused on glacier dynamics and related natural hazards in the study area, there are still many gaps in understanding major processes shaping the climate – glacier – natural hazards relations and their drivers.

Volumetric glacier changes are purely documented as only the lower part of the glacier, roughly corresponding to its ablation area, was mainly analysed. This was due to different interpretation of the glacier extent, described in the study area section, and

due to technical limitations, such as the limited flight height of the UAVs used (De Gaetani et al. 2021). The resulting volume changes do not represent the whole glacier and are difficult to compare with other studies. The comparison of the three studies dealing with volumetric changes is challenging also due to the only partial overlap of the study periods.

Mass wasting studies often do not systematically deal with the triggering mechanisms and predisposing processes. As thawing of mountain permafrost due to global warming is obviously predisposing slope failures, this was specifically mentioned only in studies by Fischer et al (2006; 2011; 2013). The mass wasting processes were mainly described in grey literature with only limited effort to analyse the events from a broader perspective.

Diolaiuti et al. (2003) found the debris cover on the lower part of the glacier in most of its area to be in the range of 5–10 cm. It's a widely accepted fact that debris cover affects the mass balance of glaciers (Mihalcea et al. 2008 and references therein). The lower albedo of a thin debris layer, compared to snow and ice, leads to augmented melting due to the increased absorption of short-wave radiation. On the contrary, a thick layer of debris decreases melting due to the insulation effect of the cover (Nicholson and Benn 2006; Östrem 1959; Stokes et al. 2007). The critical thickness is given as 5–10 cm by Stokes et al. (2007) which implies that only a small part of the Belvedere Glacier experiences the insulating effect of the debris cover.

Although the effect of thawing of mountain permafrost on mass wasting in steep rock faces has been described by various authors (e.g. Deline et al. 2015), it was recognized only by one of the treated studies. The study by Fischer et al. (2013) is focused on the dynamics of mountain permafrost at the east face of Monte Rosa as a driving factor of rock and ice avalanches. Changes in the status of permafrost have not been monitored systematically in the study area.

8. Conclusions

The Belvedere Glacier has a distinctly different geometry compared to other glaciers in the Monte Rosa massif and is also outstanding in the scale of the entire Alps, with few analogs (e.g. Miage glacier at the Mont Blanc massif). Due to the avalanche-feeding from the steep east face transporting products of intensive frost weathering, the lower part of the glacier is heavily debris-covered. The difference in glacier dynamics with respect to the nearby glaciers in the Monte Rosa Massif (e.g. Lys) was noticed already in the 1920s. Although much effort has been made to monitor the terminus position and changes in volume, there are still major gaps in understanding the volumetric changes of this glacier. The only volume change study that considers the whole Belvedere

Glacier including the upper steep part is based on two DEMs for the period 1988–2007, which is rather long to understand short-term variations in volume such as the surge-type event.

There is still potential for volumetric studies of the entire glacier including the steep upper part going back at least to the 1950s. Efforts based on UAV measurements had to omit the steep face as they encountered their technical limits. Detailed information on the volumetric changes of the Belvedere Glacier would be invaluable for comparing its dynamics with climate fluctuations.

The behaviour of the Belvedere Glacier during the cold spell in the 1970s, during which most of the glaciers in the Alps advanced and gained volume, remains little known. Quantitative conclusions are missing from many studies because their results are only displayed as maps and figures, i.e. providing no information on glacier volume change. The surge-type event in 2001–2002 was unique in the Alps and is a highly interesting process moreover linked to the development of the hazardous Effimero lake. Clarification of the triggering mechanism and driving factors of the surge-type event still remains a challenge. Although a delay of the glacier behaviour with respect to climate drivers can be expected for a debris-covered glacier, due to the missing information on volume changes, it is not possible to make a clear conclusion about whether this holds for Belvedere Glacier.

The east face of Monte Rosa saw a series of GLOFs, rock and ice avalanches and landslides, which were documented with different levels of detail and in different time scales. Many of the events considered in this study were documented in the grey literature. A detailed record of mass-wasting events due to glacier retreat and permafrost degradation in the east face exists for the period after the year 2000.

Although the review is based on a substantial body of valuable research, there are still opportunities to gain further insights into the dynamic processes, particularly in terms of high spatial, and temporal details, and potentially also new modelling techniques. Belvedere Glacier obviously deserves attention due to the concentration of processes and related hazards, otherwise rarely seen in the Alps.

Acknowledgements

The research was supported by the 4EU+ grant number 4EU+/23/F4/19 and by the Charles University Grant Agency project (GAUK project no. 208223) awarded to Pragma Mehrishi. We are grateful to Dr. Andrea De Zordi from Provincia del Verbano-Cusio-Ossola (Settore III – Assetto del Territorio Georisorse e Tutela Faunistica, Servizio Rete Natura 2000 e Forestazione) for his support to our field surveys.

References

- Amoretti, C. (1817): *Viaggio da Milano ai tre Laghi Maggiore, di Lugano e di Como e le monti che li Circondano*, Milano.
- Azzoni, R. S., Fugazza, D., Zerboni, A., Senese, A., D'Agata, C., Maragno, D., Carzaniga, A., Cernuschi, M., Diolaiuti, G. A. (2018): Evaluating high-resolution remote sensing data for reconstructing the recent evolution of supra glacial debris: A study in the Central Alps (Stelvio Park, Italy). *Progress in Physical Geography* 42(1), 3–23, <https://doi.org/10.1177/0309133317749434>.
- Baroni, C., Bondesan, A., Carturan, L., Chiarle, M. (2020): Editors. *Annual Glaciological Survey of Italian Glaciers*. *Geografia Fisica e Dinamica Quaternaria* 43(2), 221–313, <https://doi.org/10.4461/GFDQ.2020.43.10>.
- Ballantyne, C. K. (2002): Paraglacial geomorphology. *Quaternary Science Reviews* 21(18–19), 1935–2017, [https://doi.org/10.1016/S0277-3791\(02\)00005-7](https://doi.org/10.1016/S0277-3791(02)00005-7).
- Bertamini, T. (2005): *Storia di Macugnaga*. Parrocchia di Macugnaga, Macugnaga.
- Bhattacharya, A., Bolch, T., Mukherjee, K., King, O., Menounos, B., Kapitsa, V., Neckel, N., Yang, W., Yao, T. (2021): High Mountain Asian glacier response to climate revealed by multi-temporal satellite observations since the 1960s. *Nature Communications* 12(1), 1–13, <https://doi.org/10.1038/s41467-021-24180-y>.
- Boeckli, L., Brenning, A., Gruber, S., Noetzli, J. (2012): Permafrost distribution in the European Alps: Calculation and evaluation of an index map and summary statistics. *Cryosphere* 6(4), 807–820, <https://doi.org/10.5194/tc-6-807-2012>.
- Bollati, I., Leonelli, G., Vezzola, L., Pelfini, M. (2015): The role of ecological value in geomorphosite assessment for the debris-covered Miage glacier (Western Italian Alps) based on a review of 2.5 centuries of scientific study. *Geoh Heritage* 7, 119–135, <https://doi.org/10.1007/s12371-014-0111-2>.
- Bollati, I. M., Viani, C., Masseroli, A., Mortara, G., Testa, B., Tronti, G., Pelfini M., Reynard, E. (2023): Geodiversity of proglacial areas and implications for geosystem services: A review. *Geomorphology* 421: 108517, <https://doi.org/10.1016/j.geomorph.2022.108517>.
- Buckel, J., Otto, J. C., Prasicek, G., Keuschnig, M. (2018): Glacial lakes in Austria-Distribution and formation since the Little Ice Age. *Global and Planetary Change* 164, 39–51, <https://doi.org/10.1016/j.gloplacha.2018.03.003>.
- Caccianiga, M., Andreis, C., Diolaiuti, G., D'Agata, C., Mihalcea, C., Smiraglia, C. (2011): Alpine debris-covered glaciers as a habitat for plant life. *The Holocene* 21(6), 1011–1020, <https://doi.org/10.1177/0959683611400219>.
- Chiarle, M., Mortara, G. (2008): Geomorphological impact of climate change on alpine glacial and periglacial areas. *Interpraevent* 2008, 2, 111–122.
- Chiarle, M., Mortara, G., Tamburini, A., Martelli, D., Sergio, L., Berro, D. C. (2015): The Collapse of 16–17 December 2015 at Punta Tre Amici (Macugnaga, Monte Rosa), Nimbus, http://www.nimbus.it/ghiacciai/2016/160119_CrolloTreAmici.htm.
- Chiarle, M., Geertsema, M., Mortara, G., Clague, J. J. (2021): Relations between climate change and mass movement: Perspectives from the Canadian Cordillera and the European Alps. *Global and Planetary*

- Change 202: 103499, <https://doi.org/10.1016/j.gloplacha.2021.103499>.
- Chowdhury, A., Kroczyk, T., Kumar, De S., Vilímek, V., Chand Sharma, M., Debnath, M. (2021): Glacial Lake Evolution (1962–2018) and Outburst Susceptibility of Gurudongmar Lake Complex in the Tista basin, Sikkim Himalaya (India). *Water* 13(24): 3565, <https://doi.org/10.3390/w13243565>.
- Citterio, M., Diolaiuti, G., Smiraglia, C., D'Agata, C., Carnielli, T., Stella, G., Siletto, G. B. (2007): The fluctuations of Italian glaciers during the last century: a contribution to knowledge about Alpine glacier changes. *Geografiska Annaler: Series A, Physical Geography* 89(3), 167–184, <https://doi.org/10.1111/j.1468-0459.2007.00316.x>.
- Cogley, G. (submitter); Braun, M. (analyst) (2022): GLIMS Glacier Database. Boulder, CO., National Snow and Ice Data Center, <http://dx.doi.org/10.7265/N5V98602>.
- Colombero, C., Comina, C., Toma, E. De, Franco, D., Godio, A. (2019): Ice Thickness Estimation from Geophysical Investigations on the Terminal Lobes of Belvedere Glacier (NW Italian Alps). *Remote Sensing* 11(7): 805, <https://doi.org/10.3390/rs11070805>.
- Davaze, L., Rabatel, A., Dufour, A., Hugonnet, R., Arnaud, Y. (2020): Region-Wide Annual Glacier Surface Mass Balance for the European Alps From 2000 to 2016. *Frontiers in Earth Science* 8, 1–14, <https://doi.org/10.3389/feart.2020.00149>.
- De Gaetani, C. I., Ioli, F., Pinto, L. (2021): Aerial and UAV images for photogrammetric analysis of Belvedere Glacier evolution in the period 1977–2019. *Remote Sensing*, 13(18): 3787, <https://doi.org/10.3390/rs13183787>.
- Deline, P., Gruber, S., Delaloye, R., Fisher, L., Geertsema, M., Giardino, M., Hasler, A., Kirkbride, M., Krautblatter, M., Magnin, F., McColl, S.T., Ravanel, L., Schoeneich, P. (2015): Ice loss and slope stability in high-mountain regions. In: W Haeblerli, C Whiteman, eds. *Snow and Ice-Related Hazards, Risks, and Disasters*. Elsevier, Amsterdam, pp. 521–561, <https://doi.org/10.1016/B978-0-12-394849-6.00015-9>.
- Diolaiuti, G., D'Agata, C., Smiraglia, C. (2003): Belvedere Glacier, Monte Rosa, Italian Alps: Tongue Thickness and Volume Variations in the Second Half of the 20th Century. *Arctic, tarctic, and Alpine Research* 35(2), 255–263, [https://doi.org/10.1657/1523-0430\(2003\)035\[0255:BGMRIA\]2.0.CO;2](https://doi.org/10.1657/1523-0430(2003)035[0255:BGMRIA]2.0.CO;2).
- Emmer, A., Klimeš, J., Mergili, M., Vilímek, V., Cochachin, A. (2016): 882 lakes of the Cordillera Blanca: An inventory, classification, evolution and assessment of susceptibility to outburst floods. *Catena* 147, 269–279, <https://doi.org/10.1016/j.catena.2016.07.032>.
- Evans, S. G., Delaney, K. B., Rana, N. M. (2021): The occurrence and mechanism of catastrophic mass flows in the mountain cryosphere. In *Snow and ice-related hazards, risks, and disasters*, 541–596. Elsevier, <https://doi.org/10.1016/B978-0-12-817129-5.00004-4>.
- Faillietaz, J., Funk, M., Vagliasindi, M. (2016): Time forecast of a break-off event from a hanging glacier. *The Cryosphere* 10(3), 1191–1200, <https://doi.org/10.5194/tc-10-1191-2016>.
- Fischer, L., Käab, A., Huggel, C., Noetzi, J. (2006): Geology, glacier retreat and permafrost degradation as controlling factors of slope instabilities in a high-mountain rock wall: the Monte Rosa east face. *Natural Hazards and Earth System Sciences* 6(5), 761–772, <https://doi.org/10.5194/nhess-6-761-2006>.
- Fischer, L., Eisenbeiss, H., Käab, A., Huggel, C., Haeblerli, W. (2011): Monitoring topographic changes in a periglacial high-mountain face using high-resolution DTMs, Monte Rosa East Face, Italian Alps. *Permafrost and Periglacial Processes* 22(2), 140–152, <https://doi.org/10.1002/ppp.717>.
- Fischer, L., Huggel, C., Käab, A., Haeblerli, W. (2013): Slope failures and erosion rates on a glacierized high-mountain face under climatic changes. *Earth Surface Processes and Landforms* 38(8), 836–846, <https://doi.org/10.1002/esp.3355>.
- Forbes, J. D. (1845): *Reisen in den Savoyer Alpen und in anderen Theilen der Penninen-Kette nebst Beobachtungen über die Gletscher*, Stuttgart.
- Frey, H., Haeblerli, W., Linsbauer, A., Huggel, C., Paul, F. (2010): A multi-level strategy for anticipating future glacier lake formation and associated hazard potentials. *Natural Hazards and Earth System Science* 10(2), 339–352, <https://doi.org/10.5194/nhess-10-339-2010>.
- Giaccone, E., Colombo, N., Acquotta, F., Paro, L., Fratianni, S. (2015): Climate variations in a high altitude Alpine basin and their effects on a glacial environment (Italian Western Alps). *Atmosfera* 28(2), 117–128, <https://doi.org/10.20937/ATM.2015.28.02.04>.
- Gleyzes, M. A., Perret, L., Kubik, P. (2012): Pleiades system architecture and main performances. *The International Archives of the Photogrammetry, Remote Sensing and Spatial Information Sciences* 39, 537–542, <https://doi.org/10.5194/isprsarchives-XXXIX-B1-537-2012>.
- Gobiet, A., Kotlarski, S., Beniston, M., Heinrich, G., Rajczak, J., Stoffel, M. (2014): 21st century climate change in the European Alps – A review. *Science of the Total Environment*, 493, 1138–1151, <https://doi.org/10.1016/j.scitotenv.2013.07.050>.
- Godone, D., Godone, F., Tamburini, A., Leonardo, V. (2010): Belvedere Glacier monitoring: A multidisciplinary approach. *International Symposium on Geo-information for Disaster Management (Gi4DM) 2010 Turin*, February 2–4, 2010.
- Godone, D., Godone, F. (2012): The Support of Geomatics in Glacier Monitoring: The Contribution of Terrestrial Laser Scanner. *Laser Scanner Technology*, <https://doi.org/10.5772/33463>.
- Haeblerli, W., Beniston, M. (1998): Climate change and its impacts on glaciers and permafrost in the Alps. *Ambio* 27(4), 258–265, <https://doi.org/10.2307/4314732>.
- Haeblerli, W., Epifani, F. (1986): Mapping the Distribution of Buried Glacier Ice – An Example from Lago Delle Locce, Monte Rosa, Italian Alps. *Annals of Glaciology* 8, 78–81, <https://doi.org/10.1017/s02603055000118x>.
- Haeblerli, W., Käab, A., Paul, F., Chiarle, M., Mortara, G., Mazza, A., Deline, P., Richardson, S. (2002): A surge-type movement at Ghiacciaio del Belvedere and a developing slope instability in the east face of Monte Rosa, Macugnaga, Italian Alps. *Norsk Geografisk Tidsskrift* 56(2), 104–111, <https://doi.org/10.1080/002919502760056422>.
- Harris, C., Mühl, D. V., Isaksen, K., Haeblerli, W., Sollid, J. L., King, L., Holmlund, P., Dramis, F., Guglielmin, M., Palacios, D. (2003): Warming permafrost in European mountains.

- Global and Planetary Change 39(3–4), 215–225, <https://doi.org/10.1016/j.gloplacha.2003.04.001>.
- Harrison, S., Kargel, J. S., Huggel, C., Reynolds, J., Shugar, D. H., Betts, R. A., Emmer, A., Glasser, N., Haritashya, U. K., Klimeš, J., Reinhardt, L., Schaub, Y., Wiltshire, A., Regmi, D., Vilímek, V. (2018): Climate change and the global pattern of moraine-dammed glacial lake outburst floods. *Cryosphere* 12(4), 1195–1209, <https://doi.org/10.5194/tc-12-1195-2018>.
- Hartmeyer, I., Delleske, R., Keuschnig, M., Krautblatter, M., Lang, A., Christoph Otto, J., Schrott, L. (2020): Current glacier recession causes significant rockfall increase: The immediate paraglacial response of deglaciating cirque walls. *Earth Surface Dynamics* 8(3), 729–751, <https://doi.org/10.5194/esurf-8-729-2020>.
- Haylock, M. R., Hofstra, N., Klein Tank, A. M. G., Klok, E. J., Jones, P. D., New, M. (2008): A European daily high-resolution gridded data set of surface temperature and precipitation for 1950–2006. *Journal of Geophysical Research: Atmospheres* 113(D20), 148–227, <https://doi.org/10.1029/2008JD010201>.
- Hoinkes, H. C. (1969): Surges of the Vernagtferner in the Ötztal Alps since 1599. *Canadian Journal of Earth Sciences* 6(4), 853–861, <https://doi.org/10.1139/e69-086>.
- Huggel, C., Kääb, A., Haeberli, W., Krummenacher, B. (2003): Regional-scale GIS models for assessment of hazards from glacier lake outburst: evaluation and application in the Swiss Alps. *Natural Hazards and Earth System Sciences* 3(6), 647–662, <https://doi.org/10.5194/nhess-3-647-2003>.
- Huss, M. (2012): Extrapolating glacier mass balance to the mountain-range scale: The European Alps 1900–2100. *Cryosphere* 6(4), 713–727, <https://doi.org/10.5194/tc-6-713-2012>.
- Huss, M., Hock, R. (2018): Global-scale hydrological response to future glacier mass loss. *Nature Climate Change* 8(2), 135–140, <https://doi.org/10.1038/s41558-017-0049-x>.
- Ioli, F., Bianchi, A., Cina, A., De Michele, C., Maschio, P., Passoni, D., Pinto, L. (2022): Mid-term monitoring of glacier's variations with UAVs: The example of the Belvedere Glacier. *Remote Sensing* 14(1), 1–19, <https://doi.org/10.3390/rs14010028>.
- Ioli, F., Bruno, E., Calzolari, D., Galbiati, M., Mannocchi, A., Manzoni, P., Martini, M., Bianchi, A., Cina, A., De Michele, C., Pinto, L. (2023): A replicable open-source multi-camera system for low-cost 4D glacier monitoring. *International Archives of the Photogrammetry, Remote Sensing and Spatial Information Sciences (ISPRS Archives)*, XLVIII-M-1-2023, 137–144, <https://doi.org/10.5194/isprs-archives-XLVIII-M-1-2023-137-2023>.
- IPCC (2022): Sixth Assessment Report of the Intergovernmental Panel on Climate Change, Cambridge University Press, Cambridge, UK and New York, NY, USA, <https://doi.org/10.1017/9781009325844>.
- Italian Glaciological Committee. Available online: <https://www.glaciologia.it/i-ghiacciai-italiani/le-campagne-glaciologiche/> (accessed on 21. 5. 2024).
- Ivy-Ochs, S., Kerschner, H., Maisch, M., Christl, M., Kubik, P. W., Schlüchter, C. (2009): Latest Pleistocene and Holocene glacier variations in the European Alps. *Quaternary Science Reviews* 28 (21–22), 2137–2149, <https://doi.org/10.1016/j.quascirev.2009.03.009>.
- Jacquemart, M., Weber, S., Chiarle, M., Chmiel, M., Cicoira, A., Corona, C., Eckert, N., Gaume, J., Giacona, F., Hirschberg, J., Kaitna, R., Magnin, F., Mayer, S., Moos, Ch., van Herwijnen, A., Stoffel, M. (2024): Detecting the impact of climate change on alpine mass movements in observational records from the European Alps. *Earth-Science Reviews* 258: 104886, <https://doi.org/10.1016/j.earscirev.2024.104886>.
- Kääb, A. (2002): Monitoring high-mountain terrain deformation from repeated air-and spaceborne optical data: examples using digital aerial imagery and ASTER data. *ISPRS Journal of Photogrammetry and Remote Sensing* 57(1–2), 39–52, [https://doi.org/10.1016/S0924-2716\(02\)00114-4](https://doi.org/10.1016/S0924-2716(02)00114-4).
- Kääb, A., Huggel, C., Barbero, S., Chiarle, M., Cordola, M., Epifani, F., Haeberli, W., Mortara, G., Semino, P., Tamburini, A., Viazzo, G. (2004): Glacier hazards at Belvedere Glacier and the Monte Rosa East Face, Italian Alps: processes and mitigation 1, 67–78.
- Kääb, A., Huggel, C., Fischer, L., Guex, S., Paul, F., Roer, I., Salzmann, N., Schlaefli, S., Schmutz, K., Schneider, D., Strozzi, T., Weidmann, Y. (2005): Remote sensing of glacier- and permafrost-related hazards in high mountains: An overview. *Natural Hazards and Earth System Science* 5(4), 527–554, <https://doi.org/10.5194/nhess-5-527-2005>.
- Kasser, P. (1973): *Fluctuations of Glaciers 1965–1970*, IAHS UNESCO, Paris.
- Kirkbride, M. P., Warren, C. R. (1999): Tasman Glacier, New Zealand: 20th-century thinning and predicted calving retreat. *Global and Planetary Change* 22(1–4), 11–28, [https://doi.org/10.1016/S0921-8181\(99\)00021-1](https://doi.org/10.1016/S0921-8181(99)00021-1).
- Klimeš, J., Vilímek, V., Omelka, M. (2009): Implications of geomorphological research for recent and prehistoric avalanches and related hazards at Huascarán, Peru. *Natural Hazards* 50, 193–209, <https://doi.org/10.1007/s11069-008-9330-7>.
- Kos, A., Amann, F., Strozzi, T., Delaloye, R., von Ruetten, J., Springman, S. (2016): Contemporary glacier retreat triggers a rapid landslide response, Great Aletsch Glacier, Switzerland. *Geophysical Research Letters* 43(24), 12466–12474, <https://doi.org/10.1002/2016GL071708>.
- Kropáček, J., Neckel, N., Bauder, A. (2014): Estimation of mass balance of the grosser Aletschgletscher, Swiss Alps, from ICESat laser altimetry data and digital elevation models. *Remote Sensing* 6(6), 5614–5632, <https://doi.org/10.3390/rs6065614>.
- Kropáček, J., Vilímek, V., Mehrishi, P. (2021): A preliminary assessment of the Chamoli rock and ice avalanche in the Indian Himalayas by remote sensing. *Landslides* 18(10), 3489–3497, <https://doi.org/10.1007/s10346-021-01742-1>.
- Laha, S., Kumari, R., Singh, S., Mishra, A., Sharma, T., Banerjee, A., Nainwal, H. C., Shankar, R. (2017): Evaluating the contribution of avalanching to the mass balance of Himalayan glaciers. *Annals of Glaciology* 58(75), 110–118, <https://doi.org/10.1017/aog.2017.27>.
- Margreth, S., Funk, M., Tobler, D., Dalban, P., Meier, L., Lauper, J. (2017): Analysis of the hazard caused by ice avalanches from the hanging glacier on the Eiger west face. *Cold Regions Science and Technology* 144, 63–72, <https://doi.org/10.1016/j.coldregions.2017.05.012>.
- Mazza, A. (1998): Evolution and dynamics of Ghiacciaio Nord delle Locce (Valle Anzasca, Western Alps) from

- 1854 to the present. *Geografia Fisica e Dinamica Quaternaria* 21(2), 233–243.
- Mazza, A. (2000): Some results of recent investigations on Ghiacciaio del Belvedere (Anzasca valley, western Alps) taking into account the glacier mechanics. *Geografia Fisica e Dinamica Quaternaria* 23(7), 59–71.
- Mazza, A. (2003): The kinematics wave theory: a possible application to “Ghiacciaio del Belvedere” (Valle Anzasca, Italian Alps). Preliminary hypothesis. *Terra glacialis* 6, 23–36.
- McCull, S. T. (2012): Paraglacial rock-slope stability. *Geomorphology* 153, 1–16, <https://doi.org/10.1016/j.geomorph.2012.02.015>
- Mecatti, D., Noferini, L., Macaluso, G., Pieraccini, M., Luzi, G., Atzeni, C. (2007): Remote sensing of glaciers by ground-based radar interferometry. *IEEE International Geoscience and Remote Sensing Symposium, Barcelona, Spain*, 4501–4504, <https://doi.org/10.1109/IGARSS.2007.4423856>.
- Mihalcea, C., Brock, B. W., Diolaiuti, G., D’Agata, C., Citterio, M., Kirkbride, M. P., Cutler E.M.J., Smiraglia, C. (2008): Using ASTER satellite and ground-based surface temperature measurements to derive supraglacial debris cover and thickness patterns on Miage Glacier (Mont Blanc Massif, Italy). *Cold Regions Science and Technology* 52(3), 341–354, <https://doi.org/10.1016/j.coldregions.2007.03.004>.
- Mölg, N., Huggel, C., Herold, T., Storck, F., Allen, S., Haeberli, W., Schaub, Y., Odermatt, D. (2021): Inventory and evolution of glacial lakes since the Little Ice Age: Lessons from the case of Switzerland. *Earth Surface Processes and Landforms* 46(13), 2551–2564, <https://doi.org/10.1002/esp.5193>.
- Mondino, E. B. (2015): Multi-temporal image co-registration improvement for a better representation and quantification of risky situations: the Belvedere Glacier case study. *Geomatics, Natural Hazards and Risk* 6(5–7), 362–378, <https://doi.org/10.1080/19475705.2014.927804>.
- Monterin, U. (1922): Il Ghiacciaio di Macugnaga dal 1870 al 1922. *Bolletino Del Comitato Glaciologico Italiano* 5, 12–40.
- Monterin, U. (1926): La fine della fase progressiva e l’inizio della nuova fase di ritiro dei ghiacciai italiani nel Monte Rosa 1922–1925. *Zeitschrift für Gletscherkunde* 15(1), 31–54.
- Mortara, G., Chiarle, M., Tamburini, A. (2003): The Emergency Caused by the “Effimero” Lake on the Belvedere Glacier (Macugnaga, Monte Rosa Group, Italian Alps). In: D. Richard and M. Gay (Editors). *EVG1 2000 00512*.
- Mortara, G., Tamburini, A. (2009): Il ghiacciaio del Belvedere e l’emergenza del Lago Effimero. *Regione Piemonte*.
- Mortara, G., Chiarle, M., Tamburini, A., Mercalli, L., Cat Berro, D. (2023): a vent’anni dal Lago Effimero (Ghiacciaio del Belvedere, Monte Rosa): eredità di un evento emblematico per le Alpi. *Nimbus* 90, 26–41.
- Nakawo, M., Yabuki, H., Sakai, A. (1999): Characteristics of Khumbu Glacier, Nepal Himalaya: Recent change in the debris-covered area. *Annals of Glaciology* 28, 118–122, <https://doi.org/10.3189/172756499781821788>.
- Neckel, N., Kropáček, J., Bolch, T., Hochschild, V. (2014): Glacier mass changes on the Tibetan Plateau 2003–2009 derived from ICESat laser altimetry measurements. *Environmental Research Letters* 9(1): 014009, <https://doi.org/10.1088/1748-9326/9/1/014009>.
- Nicholson, L., Benn, D. I. (2006): Calculating ice melt beneath a debris layer using meteorological data. *Journal of Glaciology* 52(178), 463–470, <https://doi.org/10.3189/172756506781828584>.
- Noferini, L., Mecatti, D., Macaluso, G., Pieraccini, M., Atzeni, C. (2009): Monitoring of Belvedere Glacier using a wide angle GB-SAR interferometer. *Journal of Applied Geophysics* 68(2), 289–293, <https://doi.org/10.1016/j.jappgeo.2009.02.004>.
- Nüsser, M., Schmidt S (2021): Glacier changes on the Nanga Parbat 1856–2020: A multi-source retrospective analysis. *Science of The Total Environment* 785: 147321, <https://doi.org/10.1016/j.scitotenv.2021.147321>.
- Östrem, G. (1959): Ice Melting under a Thin Layer of Moraine, and the Existence of Ice Cores in Moraine Ridges. *Geografiska Annaler* 41(4), 228–230, <https://doi.org/10.1080/20014422.1959.11907953>.
- Pandey, A., Kropáček, J. (2023): Rapid formation and drainage of a new glacial lake in the Monte Rosa Massif, Swiss Alps, as observed on Sentinel-2 imagery. *Annals of Glaciology* 64(92), 156–158, <https://doi.org/10.1017/aog.2023.19>.
- Paranunzio, R., Laio, F., Chiarle, M., Nigrelli, G., Guzzetti, F. (2016): Climate anomalies associated with the occurrence of rockfalls at high-elevation in the Italian Alps. *Natural Hazards and Earth System Sciences* 16(9), 2085–2106, <https://doi.org/10.5194/nhess-16-2085-2016>.
- Paul, F., Rastner, P., Azzoni, R. S., Diolaiuti, G., Fugazza, D., Bris, R. Le, Nemeč, J., Rabatel, A., Ramusovic, M., Schwaizer, G., Smiraglia, C. (2020): Glacier shrinkage in the Alps continues unabated as revealed by a new glacier inventory from Sentinel-2. *Earth System Science Data* 12(3), 1805–1821, <https://doi.org/10.5194/essd-12-1805-2020>.
- Pieraccini, M., Noferini, L., Mecatti, D., Macaluso, G., Luzi, G., Atzeni, C. (2008): Digital elevation models by a GBSAR interferometer for monitoring glaciers: the case study of Belvedere Glacier. *IEEE International Geoscience and Remote Sensing Symposium, Boston, MA, USA*, pp. IV-1061–IV-1064, <https://doi.org/10.1109/IGARSS.2008.4779909>.
- Pörtner, H. O., Roberts, D. C., Masson-Delmotte, V., Zhai, P., Tignor, M., Poloczanska, E., Weyer, N. M. (2019): The ocean and cryosphere in a changing climate. IPCC special report on the ocean and cryosphere in a changing climate. Cambridge University Press, Cambridge, UK and New York, NY, USA, <https://doi.org/10.1017/9781009157964>.
- Ranzi, R., Grossi, G., Iacovelli, L., Taschner, S. (2004): Use of multispectral ASTER images for mapping debris-covered glaciers within the GLIMS Project. *IEEE International Geoscience and Remote Sensing Symposium, Anchorage, AK, USA*, 1144–1147, <https://doi.org/10.1109/IGARSS.2004.1368616>.
- Ravello, L., Allignol, F., Deline, P., Gruber, S., Ravello, M. (2010): Rock falls in the Mont Blanc Massif in 2007 and 2008. *Landslides* 7(4), 493–501, <https://doi.org/10.1007/s10346-010-0206-z>.
- Reznichenko, N., Davies, T., Shulmeister, J., McSaveney, M. (2010): Effects of debris on ice-surface melting rates:

- an experimental study. *Journal of Glaciology* 56(197), 384–394.
- Röthlisberger, H. (1969): Evidence for an ancient glacier surge in the Swiss Alps. *Canadian Journal of Earth Sciences* 6(4), 863–865, <https://doi.org/10.1139/e69-087>.
- Rowan, A. V., Egholm, D. L., Quincey, D. J., Glasser, N. F. (2015): Modelling the feedbacks between mass balance, ice flow and debris transport to predict the response to climate change of debris-covered glaciers in the Himalaya. *Earth and Planetary Science Letters* 430, 427–438, <https://doi.org/10.1016/j.epsl.2015.09.004>.
- Schlagintweit, A. (1853): Über die orographische und geologische Struktur der Gruppe des Monte Rosa 6. Weigel, Leipzig.
- Schmidt, S., Nüsser, M., Baghel, R., Dame, J. (2020): Cryosphere hazards in Ladakh: the 2014 Gya glacial lake outburst flood and its implications for risk assessment. *Natural Hazards* 104, 2071–2095, <https://doi.org/10.1007/s11069-020-04262-8>
- Somigliana, C. (1917): Primi rilievi del Ghiacciaio di Macugnaga. *Rivista Club Alpino Italiano*, 65–67.
- Sommer, C., Malz, P., Seehaus, T. C., Lippl, S., Zemp, M., Braun, M. H. (2020): Rapid glacier retreat and downwasting throughout the European Alps in the early 21st century. *Nature Communications* 11: 3209, <https://doi.org/10.1038/s41467-020-16818-0>.
- Spreafico, M. C., Sternai, P., Agliardi, F. (2021): Paraglacial rock-slope deformations: sudden or delayed response? Insights from an integrated numerical modelling approach. *Landslides* 18(4), 1311–1326, <https://doi.org/10.1007/s10346-020-01560-x>.
- Stokes, C. R., Popovnin, V., Aleynikov, A., Gurney, S. D., Shahgedanova, M. (2007): Recent glacier retreat in the Caucasus Mountains, Russia, and associated increase in supraglacial debris cover and supra-/proglacial lake development. *Annals of Glaciology* 46, 195–203, <https://doi.org/10.3189/172756407782871468>.
- Stoppani, A. (1876): Il Bel Paese. Ed. Agnelli, Milano.
- Tamburini, A., Mortara, G. (2005): The case of the “Effimero” lake at Monte Rosa (Italian Western Alps): studies, field surveys, monitoring. In F. Maraga, M. Arattano (Eds.), 10th Conference of the Euromediterranean Network of Experimental and Representative Basins (ERB) 77, 179–184. International Hydrological Programme.
- Tamburini, A., Villa, F., Fischer, L., Hungr, O., Chiarle, M., Mortara, G. (2013): Slope instabilities in high-mountain rock walls. Recent events on the Monte Rosa east face (Macugnaga, NW Italy). *Landslide Science and Practice: Spatial Analysis and Modelling* 3, 327–332, https://doi.org/10.1007/978-3-642-31310-3_44.
- Tamburini, A., Chiarle, M., Mortara, G. (2019): The collapse of the moraine of the Belvedere Glacier (Monte Rosa, Ossola). *Nimbus Web*. http://www.nimbus.it/ghiacciai/2019/190816_BelvedereCollassoMorene.htm.
- Taschner, S., Ranzi, R. (2002): Comparing the Opportunities of LANDSAT-TM and ASTER Data for Monitoring a Debris Covered Glacier in the Italian Alps within the GLIMS Project. *IEEE International Geoscience and Remote Sensing Symposium* 2(C), 1044–1046, <https://doi.org/10.1109/IGARSS.2002.1025770>.
- Tonolo, F. G., Cina, A., Manzino, A., Fronteddu, M. (2020): 3D glacier mapping by means of satellite stereo images: the Belvedere Glacier case study in Italian Alps. *The International Archives of the Photogrammetry, Remote Sensing and Spatial Information Sciences XLIII*, 1073–1079, <https://doi.org/10.5194/isprs-archives-XLIII-B2-2020-1073-2020>.
- Tropeano, D., Govi, M., Mortara, G., Turitto, O., Sorzana, P., Negrini, G., Arattano, M. (1999): Eventi alluvionali e frane nell’Italia settentrionale Periodo 1975–1981. Truffer, M., Kääb, A., Harisson, W. D., Osipova, G. B., Nosenko, G. A., Espizua, L., Gilbert, A., Fischer, L., Huggel, C., Craw Burns, P. A. (2021): Glacier surges. In: Haeberli, W., Whiteman, C. A., Shroder, J. F. (Eds.) (2021): *Snow and Ice-Related Hazards, Risks, and Disasters* 10. Amsterdam, The Netherlands: Elsevier, 417–466, <https://doi.org/10.1016/B978-0-12-817129-5.00003-2>.
- VAW (Versuchsanstalt für Wasserbau, Hydrologie und Glaziologie, ETH Zürich) (1984): Ricerche glaciologiche al Lago delle Locce, Macugnaga, Italia. Versuchsanstalt für Wasserbau, Hydrologie und Glaziologie ETH Zürich 97 (2), 100.
- VAW (1985): Studi sul comportamento del Ghiacciaio del Belvedere, Macugnaga, Italia. Versuchsanstalt für Wasserbau, Hydrologie und Glaziologie ETH Zürich 97 (3), 157.
- VAW (1986): Valutazione dei Rischi Glaciali nella Regione Macugnaga/Monte Rosa Macugnaga, Italia. Versuchsanstalt für Wasserbau, Hydrologie und Glaziologie ETH Zürich 97 (4), 153.
- Viani, C., Giardino, M., Huggel, C., Perotti, L., Mortara, G. (2016): An overview of glacier lakes in the Western Italian Alps from 1927 to 2014 based on multiple data sources (historical maps, orthophotos and reports of the glaciological surveys). *Geografia Fisica e Dinamica Quaternaria*, 39(2), 203–214, <https://doi.org/10.5167/uzh-136706>
- Viani, C., Machguth, H., Huggel, C., Godio, A., Franco, D., Perotti, L., Giardino, M. (2020): Potential future lakes from continued glacier shrinkage in the Aosta Valley Region (Western Alps, Italy). *Geomorphology* 355: 107068, <https://doi.org/10.1016/j.geomorph.2020.107068>.
- Viani, C., Colombo, N., Bollati, I. M., Mortara, G., Perotti, L., Giardino, M. (2022): Socio-environmental value of glacier lakes: assessment in the Aosta Valley (Western Italian Alps). *Regional Environmental Change* 22(1): 7, <https://doi.org/10.1007/s10113-021-01860-5>.
- Vincent, C., Thibert, E., Harter, M., Soruco, A., Gilbert, A. (2015): Volume and frequency of ice avalanches from Tacconnaz hanging glacier, French Alps. *Annals of Glaciology* 56(70), 17–25, <https://doi.org/10.3189/2015AoG70A017>.
- Visintini, G. (1957): Rilevamenti di ghiacciai e studi glaciologici in occasione dell’anno geofisico (Ghiacciaio del Belvedere, Ghiacciaio del Calderone). *Bollettino del Comitato Glaciologico Italiano* 10/II, 33–70.
- Welden, L. (1824): Der Monte Rosa. Eine topographische und naturhistorische Skizze, Carl Gerold, Wien. <https://www.abebooks.com/book-search/title/zumstein/first-edition/book/>.
- WGMS (2023): Fluctuations of Glaciers Database. World Glacier Monitoring Service (WGMS), Zurich, Switzerland, <https://doi.org/10.5904/wgms-fog-2023-09>.
- Zemp, M., Huss, M., Thibert, E., Eckert, N., McNabb, R., Huber, J., Barandun, M., Machguth, H., Nussbaumer, S. U., Gärtner-Roer, I., Thomson, L., Paul, F., Maussion, F., Kutuzov, S., Cogley, J. G. (2019): Global glacier mass

changes and their contributions to sea-level rise from 1961 to 2016. *Nature* 568, 382–386, <https://doi.org/10.1038/s41586-019-1071-0>.

Zemp, M., Paul, F., Hoelzle, M., Haeberli, W. (2007): 11 Glacier Fluctuations in the European Alps 1850–2000: an overview and a spatiotemporal analysis of available data. *Darkening Peaks: Glacier Retreat, Science, and Society*, edited by Orlove, B., Wiegandt, E., Luckman, B. H.,

Berkeley: University of California Press, 152–167, <https://doi.org/10.1525/9780520934245-012>.

Zumstein, I. (1824): Beschreibung der fünf Reisen auf die Spitzen des Monte Rosa nebst einem Anhang der von Herrn Zumstein gemachten Reisen zur Ersteigung seiner Gipfel in Welden, L., *Der Monte Rosa. Eine topographische und naturhistorische Skizze*, Carl Gerold, Wien.

The Belvedere Glacier elevation change between 1951 and 2023

Lukáš Brodský^{1,*}, Shruti Pancholi¹, Susanne Schmidt², Marcus Nüsser^{2,3}, Roberto Sergio Azzoni⁴, Gianluca Tronti⁴

¹ Charles University, Faculty of Science, Department of Applied Geoinformatics and Cartography, Czechia

² Heidelberg University, Department of Geography, South Asia Institute, Germany

³ Heidelberg University, Heidelberg Center for the Environment, Germany

⁴ University of Milan, Earth Science Department, "A. Desio", Italy

* Correspondence author: lukas.brodsky@natur.cuni.cz

ABSTRACT

This study describes and analyses elevation changes in the debris-covered tongue of the surge-type Belvedere Glacier (Western Italian Alps) between 1951 and 2023 using remote sensing data, including historical aerial photographs, Lidar and drone acquisitions. High-resolution digital surface models from 1951, 2009 and 2023 enabled detailed observation of the spatially heterogeneous patterns of change caused by debris cover, avalanches, a surge-type event, supraglacial meltwater, and glacial lake outburst floods in the context of global warming. In the period of 1951–2009, the mean rate of downwasting was quantified as 0.24 metres per year (14 metres in total), ranging from –83.5 to 32.2 metres. During the second observation period from 2009 to 2023, the mean downwasting rate was estimated to be 1.8 metres per year (25 metres in total), varying from –73.9 to 26.9 metres. The 2001–2002 surge-type event, meltwater streams and supraglacial lakes are considered to be the main drivers forcing elevation changes and shaping its spatial variation and surface structures. In general, the changes in the glacier have accelerated between 2009 and 2023. This paper demonstrates the high potential of differenced digital surface models with high spatial resolution to detect the processes of glacier dynamics in high detail.

KEYWORDS

glacier; remote sensing; elevation change; glacier melt

Received: 17 April 2024

Accepted: 11 November 2024

Published online: 17 December 2024

Brodský, L., Pancholi, S., Schmidt, S., Nüsser, M., Azzoni, R. S., Tronti, G. (2024): The Belvedere Glacier elevation change between 1951 and 2023. *AUC Geographica* 59(2), 184–202

<https://doi.org/10.14712/23361980.2024.22>

© 2024 The Authors. This is an open-access article distributed under the terms of the Creative Commons Attribution License (<http://creativecommons.org/licenses/by/4.0>).

1. Introduction

Glaciers are considered as important indicators of climate change since they react sensitively to climatic conditions (Lemke et al. 2007; Oerlemans et al. 2000; Jóhannesson et al. 1989). An accelerated mass loss of glaciers over recent decades can be observed in all mountain regions (Hugonnet et al. 2021; Zemp et al. 2019). As a result of glacier downwasting, englacial debris accumulates at the surface and leads to an expansion of supraglacial debris cover (Fleischer et al. 2021; Schmidt and Nüsser 2009; Thakuri et al. 2014; Azzoni et al. 2018). In addition, the extent and thickness of supraglacial debris cover also depend on debris supply from surrounding rock walls and glacial transport from the upper reaches (Kirkbride and Deline 2013). Thus, the relative debris coverage and the number of debris-covered glaciers will further increase due to ongoing glacier decrease resulting from climate change (Jouvet and Huss 2019, Racoviteanu et al. 2022). On a global scale, the relative debris coverage amounts to 4.4% of the glacierized area (excluding Greenland and Antarctica) with huge variations from less than 1% in the Canadian and Arctic Region to about 26% in the Caucasus and Middle East. In Central Europe, the percentage of debris-covered glacierized areas amounts to 10.4% (Scherler et al. 2018). The extent and thickness of debris cover influence the ablation rates. While the melting rates beneath thin debris layers (less than 3 cm) are higher than for clean ice, the ablation rates under thick layers of 1–2 m, become negligible (Hewitt 2005; Mattson et al. 1993). Supraglacial lakes and ice cliffs, which are regularly formed on debris-covered glaciers, mainly due to reduced glacier velocity and gentle slope angles in the ablation zone, can both increase ablation rates (Bhambri et al. 2023; Brun et al. 2016; Huo et al. 2021; Pellicciotti et al. 2015; Salerno et al. 2017). As a consequence, mass loss rates can be higher in the middle parts of the glacier than in the debris-covered terminus (Benn et al. 2012). In contrast, other studies from the Himalayas showed that the lowering rates of debris-covered glaciers are the same or even higher than for clean-ice glaciers (Kääb et al. 2012). Thus, the impact of debris cover on glacier mass balances is still under discussion (Hock et al. 2019; Muhammad, et al. 2020). Compared to a large number of studies on the impact of debris cover on glacier mass loss in the Himalayan region (Maurer et al. 2019), only a few debris-covered glaciers were so far investigated in the European Alps (Fleischer et al. 2021; Fugazza et al. 2023; Fyffe et al. 2019).

Debris-covered glacier surfaces are subject to extensive and rapid climate-induced geomorphological changes (Westoby et al. 2020). Several evolution patterns are described in detail: localised debris thinning across ice cliff faces, except those which were decaying, where debris thickened; pervasive debris thinning across larger, back-wasting slopes, including those bordered by supraglacial streams, as well as ingestion

of debris by a newly exposed englacial conduit. These findings highlight a fast evolution of the morphology of debris-covered glacier leading to effects not only in ice melting magnitude and distribution but also inhibits across-glacier meltwater flow, both supra- and sub glacially (Mölg et al. 2020; Racoviteanu et al. 2022). Consequently, the investigation of the evolution pattern of the debris-covered glacier surface with remote-sensing data is needed (Westoby et al. 2020).

Ground measurements (Huss and Bauder 2009; Zemp et al. 2009; Fujita and Nuimara 2011; Yao et al. 2012), remote-sensing observations (Rignot et al. 2003; Bolch et al. 2012; Kääb et al. 2012; Maurer et al. 2019), and modelling studies (Radić and Hock 2006; Huss et al. 2008; Immerzeel et al. 2013) have all contributed to the documentation of volumetric glacier changes.

In recent years, geodetic methods based on remote sensing data are commonly used for estimating mass balance (Fischer et al. 2015; Kääb et al. 2012; Nuimura et al. 2017; Pellicciotti et al. 2015). Elevation changes contribute to the estimation of volume and mass changes of glaciers, as their mass loss or gain can be calculated using two digital elevation models (DEM) acquired at different times and an estimate of ice or snow density (Chandrasekharan and Ramsankaran 2023; Berthier et al. 2007; Paul et al. 2015; Bolch et al. 2008; Bolch et al. 2011; Bhambri et al. 2023; Nüsser and Schmidt 2021). This technique has been applied on elevation models derived from laser altimetry, and aerial stereo photographs, recently also on satellite optical stereo images, and radar data, but also on Unmanned Aerial Vehicle-acquired data (UAV, also known as drone). Each of them undertakes different procedures to retrieve elevation data. Laser altimetry is very precise but often has poor spatial coverage. Radar provides the best spatial coverage but can suffer from elevation errors due to the penetration of the radar signal into low-density snow and firn (Brenner et al. 2007; Berthier et al. 2016). Stereoscopic imagery frequently exhibits excellent spatial coverage, yet typically demonstrates lower temporal sampling and requires sufficient radiometric quality. UAV makes data capture of stereo images more affordable and provides the possibility to choose better contrast conditions and to decide the time intervals of multi-temporal monitoring, keeping the advantage of proximal surveys with high resolution (Haubek and Prinz 2013).

Retrieving quantitative characteristics of the glaciers requires dedicated processing workflows. Paul et al. (2015) provided a comprehensive overview of suitable algorithms for data processing and improvement of error characteristics. Glacier elevation changes from DEM differencing allow local or region-wide mass balance to be determined. They state that the spatial representativeness of elevation changes measurements and the density of the material gained or lost are the most critical assumptions for the task (Huss 2013; Paul et al. 2015). They mention that “elevation and volume change measurements are free

from related hypotheses and can therefore be independently converted to mass changes later using a density scenario of choice”.

Several studies have already analysed elevation changes of the ablation zone of Belvedere Glacier using DSM differencing to analyse surface changes (Mondino 2015; Tonolo et al. 2020; Ioli et al. 2022; De Gaetani et al. 2021). However, these studies are based on stereo pairs over shorter periods, 2001–2003 (Mondino 2015), 2017–2019 (Tonolo et al. 2020), and 2015–2020 (Ioli et al. 2022). Only De Gaetani et al. (2021) applied the elevation change analysis for a longer period, between 1977 and 2019. The period since 1951 has not yet been analysed.

Our study aims to analyse elevation changes of the debris-covered Belvedere Glacier part between 1951 and 2023 and to estimate glacier volume changes over a 72-year period using historical stereo aerial images and recently acquired UAV imagery and Lidar data from 2009.

2. Study area

Belvedere Glacier (Fig. 1) is located on the east face of Monte Rosa (4634 m a.s.l.), a prominent peak in the Western Italian Alps on the border between Italy and Switzerland. It is one of the largest debris-covered

glaciers of the Alps covering 4.51 km² (Mortara et al. 2009; Smiraglia et al. 2015). The debris-covered tongue reaches from about 2250 m a.s.l. to its lowest level at about 1800 m a.s.l., where it splits into two separate lobes. This tongue covers 1.8 km², with a length of 3 km and a maximum width of around 0.5 km. It is mostly elongated in a South-North direction. In 2001–2002 the glacier experienced a surge-type event (Kääb et al. 2004). The detailed study area description can be found in Kropáček et al. (2024).

3. Data sources

A combination of stereoscopic optical aerial images, UAV remote sensing imagery, and Lidar data (Geoportale Piemonte 2024) was used. Firstly, 16 grayscale analogue aerial images from 1951, were acquired from the IGM-Italian Military Geographic Institute. Secondly, 2198 digital UAV (DJI Mavic 2) images of the main ablation area and moraines from 2023, were acquired by the authors. The UAV acquisition covers only the ablation part of the Belvedere Glacier system given the limits of the UAV. Thirdly, the 5 m resolution Lidar Digital Surface Model and 0.4 m resolution orthophoto, were acquired from Geoportale Piemonte in 2024.

The quality of grayscale aerial historical images from 1951 can be characterised as generally

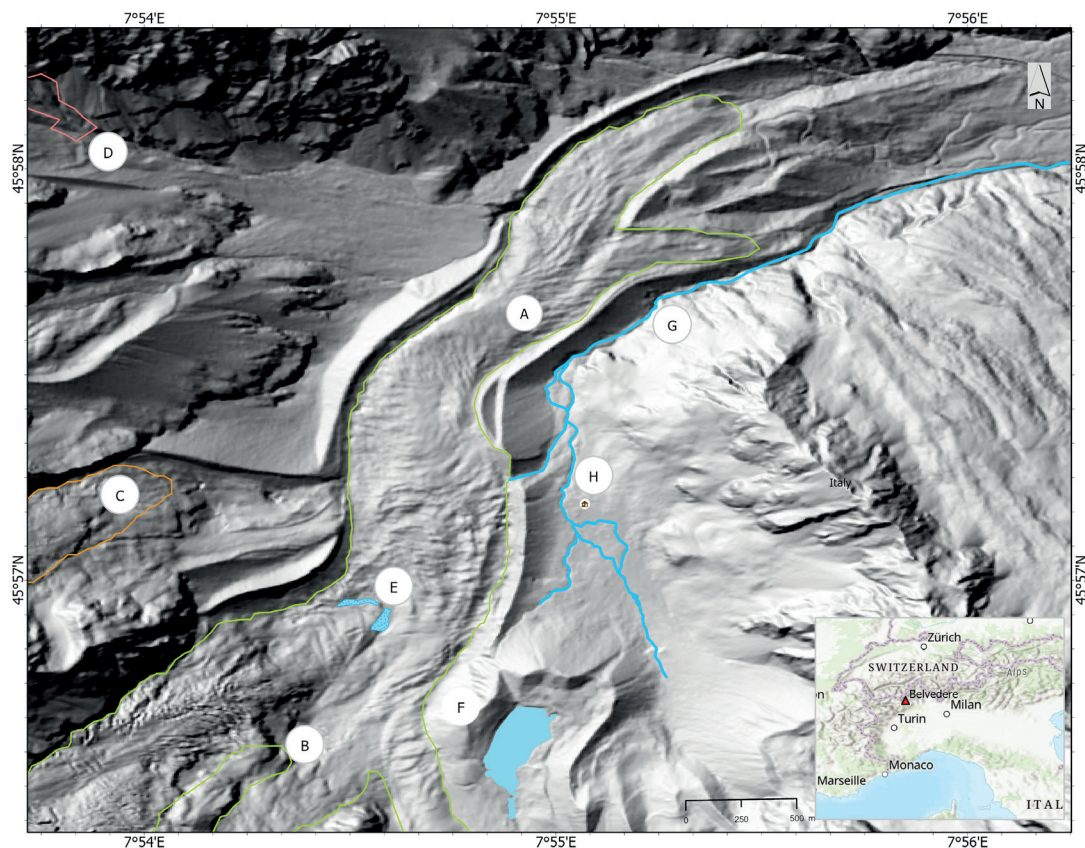


Fig. 1 A – Belvedere Glacier in green, 7°55'E, 45°57'N, B – Monte Rosa East face, C – Nordend Glacier (brown), D – Castelfranco Glacier (pink), E – Effimero Lake, F – Lago delle Locce, G – Torrent Pedriola creek, H – Zamboni-Zappa hut. Data source: DSM hillshade (Geoportale Piemonte 2024), Glacier boundaries Azzoni et al. (2024, in this issue), OpenStreetMap 2017.

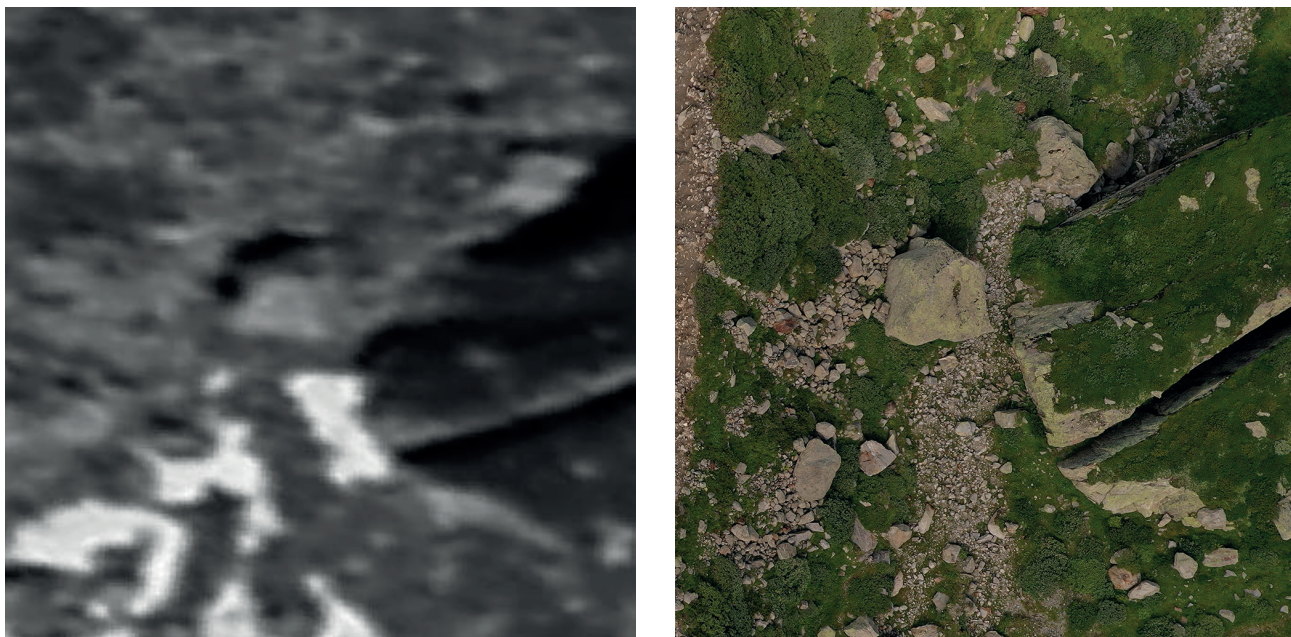


Fig. 2 Sample of historical aerial imagery in 1951 and a sample of UAV image in 2023 from the orographic-right moraine of Belvedere Glacier.

acceptable for 3D reconstruction but limited in spatial resolution (Fig. 2). The images were scanned at 10 μm/px resolution by Epson Expression 12000 XL scanner by the Istituto Geografico Militare. These cover the Belvedere main body and the two main lobes, allowing the recognition of main important features such as fractures and particular rocks on and near the moraines. The comparison between historical and modern data should consider the different spatial resolutions, such as the 3 cm resolution of UAV images. However, given the high

geomorphological dynamics of the area, and the corresponding displacements of features, this comparison is possible.

The 2023 consecutive strips of digital RGB images acquired by UAV (Fig. 3) are well distributed over the debris-covered Belvedere Glacier and moraines with 70% frontal as well as side overlap. The survey was mainly concentrated on the glacier part with the ephemeral lake. It was not possible to cover the entire western moraine area due to the large size and the weather conditions during the surveys.

Tab. 1 Cameras characteristics.

Date	Aircraft	Camera	Sensor	Focal length (mm)	Image size (px)
1951/08/24	N/A	Santoni	Analog, (glass 13 × 18)	195	~12800 × 17700
2023/08/02	DJI Mavic 2	Hasselblad	RGB CMOS 1/2.3"	28	4000 × 3000

DSM realised through airborne Lidar surveys 2009, 5-metre spatial resolution, is considered as a reference model in this study. The associated 0.4-meter resolution orthophoto was received from the same survey.

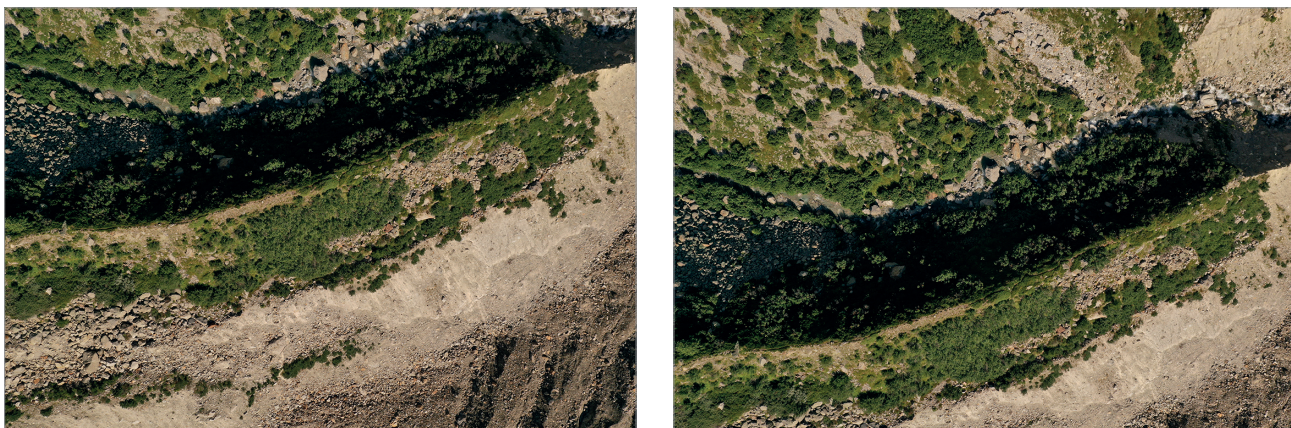


Fig. 3 Sample of raw UAV images with an overlap of 70% (Date: 2023/08/02).

4. Methods

The process of analysing the volume changes from the multi-temporal dataset began with the processing of historical stereo images to generate a DSM for change detection.

4.1 Ground Control Points collection

The ground control points (GCP) and control points (CP) were used for the purposes of referencing and correcting the models and orthophotos. A total of 24 GCPs and CPs were used for the historical orthophotos from 1951, while 26 GCPs and CPs were employed for the 2023 surveys.

The GCPs (and CPs) for the 1951 image processing were partly (13) measured in-situ on natural features and partly (11) identified on the 0.4 m orthophoto.

The in-situ measured GCPs were collected using Trimble R12i GNSS System with differential signal from RTX. Notable and recognisable flat features, such as large rocks, were selected. The coordinates and elevations of these GCPs were collected in-situ with the associated accuracy, the initial threshold accuracy for the coordinates collection was set to 0.1 m. These natural GCPs are marked with the starting letter “N” and a number in Fig. 4. The additional 21 GSPs identified on the 0.4 m orthophoto used the original Lidar Digital Surface Model received from Geoportale Piemonte in 2024.

The GCPs (and CPs) for the 2023 image processing were partly (16) measured in-situ (Trimble R12i GNSS System) on natural features and partly (10) provided by the Politecnico di Milano (De Gaetani et al. 2021; Ioli et al. 2022). There were 27 50 × 50 cm polypropylene markers identified as fixed points on the stable deposits and measured with a high-quality Global Navigation Satellite System (GNSS). Field measurements were made using a dual-frequency (L1/L2) geodetic quality GNSS receiver Leica GS14 (De Gaetani et al. 2021). In the upper part of the glacier, a real-time kinematic RTK correction was applied (~10 min time sampling, 1 Hz sampling rate). For the rest of the markers, a post-processing approach was adopted using a local master station (Leica GPS1200). The official European reference system ETRF2000 was used, resulting in a coordinate accuracy of 1.5 cm in planimetry and 3 cm in elevation, in terms of root mean square error (RMSE) (De Gaetani et al. 2021). However, only seven of the high-quality GCPs could be utilised for the 2023 data processing (Fig. 4, marks starting with “D”), and three CPs allocated for validation purposes. The high-quality points only covered the lower part of the glacier.

4.2 Historical aerial stereo image processing

The 16 grayscale aerial photographs from 1951 were processed to generate DSM surfaces for reconstructing morphometric changes. The generation of stereo models was performed with the SfM

(Structure-from-Motion) Agisoft Metashape Professional v. 1.7.5 (Agisoft 2024). The inner and outer orientations of the scanned images were calibrated by Agisoft to obtain a stereo model. Manual camera protocol or camera orientation parameters were not applied before the SfM process as they were not available.

The tie points were automatically generated for the orientation of the scenes by the software.

To acquire the six parameters of interior and exterior orientation, a bundle block adjustment method was used in Agisoft. 15 GCPs and 9 CPs were utilised for the bundle block adjustment process. A measured accuracy of the natural GCPs were utilized for reference weighting. Taking into account the data density, the final DSM grids were generated with a ground resolution of 0.1 m. The root mean square error (RMSE) was used as evaluation metrics:

$$RMSE = \sqrt{\frac{\sum_{i=1}^n (x_i - y_i)^2}{n}},$$

where x_i and y_i are the coordinates of the GCPs or CPs, and n is the number of points.

4.3 UAV stereo image processing

The workflow for UAV stereo image processing follows in principle the process as presented in chapter 4.1. The model generation was performed with the SfM running the same software.

The UAV flight elevation was fixed at 100 m above ground level from the starting point, providing a theoretical ground sampling distance of 3.2 cm. The mission planner Pix4Dcapture v.4.11.0 (Pix4D 2024) was used to parametrize the image capture in a single grid, a camera angle 90°. In total, 2198 images were acquired over the main part of the debris-covered glacier and side moraines.

26 targets spread along the glacier were used as CPs and selected in each image, 17 GCPs for the alignment process and 9 CPs for the error estimation. The accuracy of the individual GCP markers was set based on the in-situ measurements using the Trimble R12i instrument and 0.03 m for the Politecnico di Milano GCPs.

The 3D reconstruction starts with the automatic recognition of Tie and Key points through *Scale Invariant Feature Transform-SIFT* algorithms and the alignment process through *SfM* algorithms, obtaining the *Sparse Cloud* and the Camera orientation.

The 3D reconstruction process continues through Multi-View Stereo algorithms, applied to obtain the *Dense Cloud*. The last phase consists of the DSM generation, using the depth maps generated through the previous process, obtaining a 0.1 m raster DSM.

4.4 Change analysis

The change analysis involves comparing two or more DSMs acquired at different time points to identify and

quantify changes in the terrain's elevation. The measurement of changes in glacier elevation by differencing is a widely used method for estimating changes in glacier volume and mass at local and regional scales (Sommer et al. 2020; Bhambri et al. 2023).

Before making a relative DSM comparison, it was assured that the DSMs from different time points are co-registered. This step is critical for accurate differencing. The datasets were resampled to the common 1 m spatial resolution prior to the co-registration as a compromise between the 0.5 m resolution from the historical and UAV data processing and the 5 m resolution from the 2009 elevation model.

The co-registration procedure is based on the method proposed by Knuth et al. (2023). They introduced a multi-stage co-registration method, which involved a point cloud alignment method followed by the slope and aspect dependent method by Nuut and Kääb (2011). An iterative co-registration approach is used, which means that the co-registration process is performed in several iterations to progressively refine the alignment. The point clouds of the terrain models for the years 1951 and 2023 were finely co-registered with the 2009 Lidar point cloud (Geoportale Piemonte 2024) as the reference. The point

pair picking alignment tool of CloudCompare software was used for this process. Specific masking (glacier boundaries: Azzoni et al. 2024, in this issue) was used to perform co-registration outside the glacier. The co-registration process involves minimising the sum of squares of the distances between corresponding points in the DSMs. This is a common optimization approach to achieve the best alignment. The outputs are aligned DSMs and the co-registration parameters, which refer to the transformation parameters applied to one or more DSMs to align them with the reference.

The quantified elevation change of the glacier is the input information for the following step, the estimation of the volume of ice gained and lost. An estimation of the changes in glacier elevation across two intervals is performed, using a well-established process called DSM differencing. The two differenced DSMs enable to estimate the volume changes between 1951 and 2023. They are used to estimate the spatial variation of volume changes corresponding to the mean, minimum, and maximum differences for the periods 1951–2009, 2009–2023, and 1951–2023. The volume change is calculated over a constant area of the glacier and surrounding region. The UAV-derived DSM in 2023 was used to delineate the glacier boundary. The DSMs (1951 and 2009) were clipped by the extent of the 2023 DSM and later by the glacier boundary shapefile. The study area is approximately $1.6 \times 10^6 \text{ m}^2$ in size. To calculate the mass change of the Belvedere Glacier, the density of ice was assumed to be $850 \pm 60 \text{ kg m}^{-3}$ following Huss (2013).

5. Results

The combination of GNSS measurements and manually selected GCPs allowed the generation of high-resolution DSMs of the complex terrain of Belvedere Glacier and its orthophotos (Tab. 2, Fig. 5). The accuracy of the 1951 DSM in the vertical dimension amounts to -0.68 m on CPs. Some problems in the 1951 DSM can be detected in the southern part of the glacier, where visible outliers create high-frequency texture patterns. They are also partially visible in the northern terminus of the main tongue. This area also suffers from some erratic points, and local errors in the 1951 DSM due to imprecise image matching and low image quality, but these artefacts do not affect the main trends in the topographic changes analysed in this study. The UAV-derived DSM 2023 resulted in a much higher accuracy of -0.08 m compared to the historical 1951 DSM processing (Tab. 2). The precision of the natural GCPs, determined through the utilisation of the Trimble R12i GNSS with RTX differential data enhancement, exhibited a mean value of 0.017 m in Easting, 0.094 m in Northing, and 0.045 m in elevation.

Fig. 5 illustrates the DSM related orthophotos as part of the photogrammetric process. The 1951

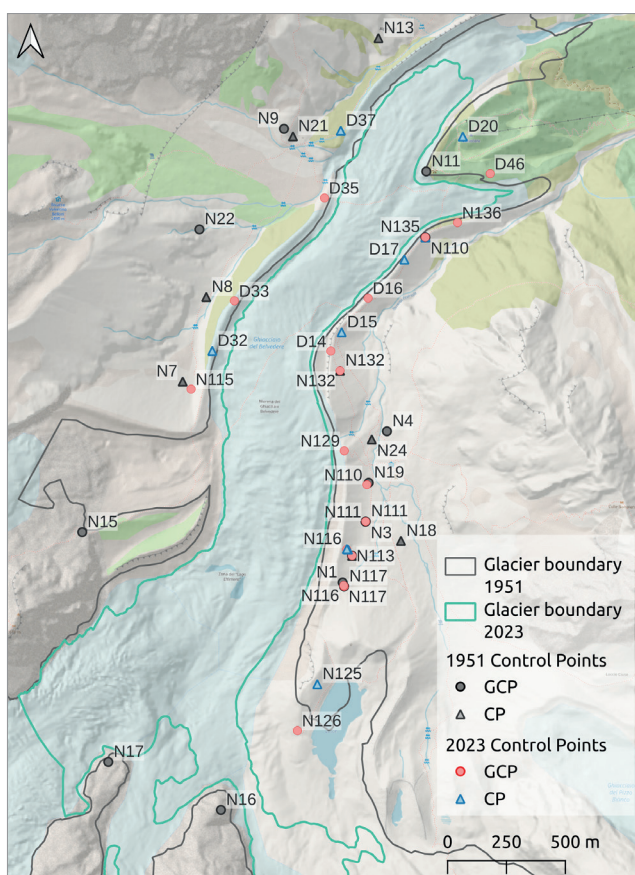


Fig. 4 Location of the Control Points used for the photogrammetric models, background: OpenStreetMap data (OpenStreetMap 2017) and the 2009 hill-shade derived from Lidar DSM 2009 (Geoportale Piemonte 2024)

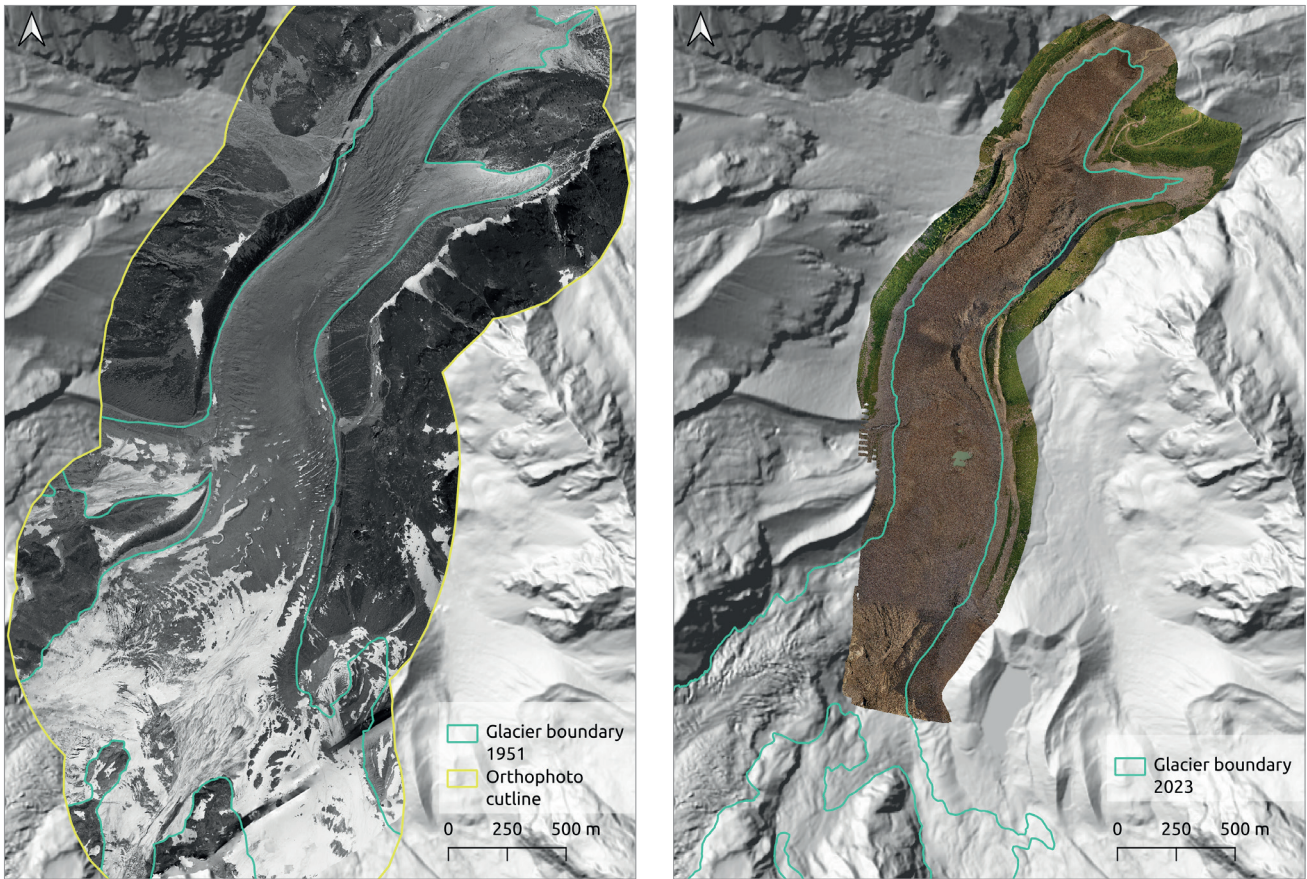


Fig. 5 Belvedere Glacier orthophotos from aerial 1951 and UAV 2023 images and hill-shade derived from Lidar DSM 2009 (Geoportale Piemonte 2024).

Tab. 2 RMSE computed on CPs for each photogrammetric model.

DSM	E (m)	N (m)	h (m)
1951	-0.25	-0.04	-0.68
2023	0.39	0.06	-0.08

E, N, h – ground coordinates Easting, Northing, and elevation

grayscale orthophoto appears compact over the entire area of the glacier and its surroundings, although there are some irregular outliers. The 2023 orthophoto (Fig. 5, right) shows a number of cloud shadows (radiometric variability) along the debris-covered glacier. The changing weather conditions partly affected the accuracy of the image matching, which propagated into the DSM quality.

Although the accuracy of the retrieved 1951 and 2023 DSMs is relatively high, the aim was to compare the independently processed models. The

comparison preceded the co-registration process. The accuracy assessment of the relative DSMs after co-registration is presented in Tab. 3. It presents an evaluation of how well the DSMs align with a common reference model 2009. The Tab. 3 shows key parameters after the co-registration, the mean values are well near zero, however, the spread of the points reveals variations.

Tab. 3 DSM post-co-registration statistics.

DSM compared to 2009 reference	Mean (m)	Median (m)	RMSE (m)
1951	0.386	-0.051	0.91
2023	-0.394	0.0712	0.71

Note: the glacier was masked a priori of the co-registration process with outliers defined as mean ± 3 sigma of the DSM differences outside of glacier.

Tab. 4 Elevation and volume changes of the Belvedere Glacier tongue (excluding the Monte Rosa east face).

	Mean Elevation Change	Total Volume Change [$\text{m}^3 \times 10^6$]	Volume Change [$\text{m}^3 \times 10^6 \text{ yr}^{-1}$]	Mass Change [Mt]	Mass/unit area [kg/m^2]	Mass balance [m w.e.]	Annual mass change [m w.e. yr^{-1}]
1951–2009	-14.01	-15.73	-0.27	-13.37 \pm 0.27	-11899.41	-11.89	-0.21
2009–2023	-24.82	-27.95	-1.99	-23.71 \pm 1.67	-21105.92	-21.14	-1.51
1951–2023	-38.34	-43.61	-0.61	-37.07 \pm 2.61	-33002.22	-33.01	-0.46

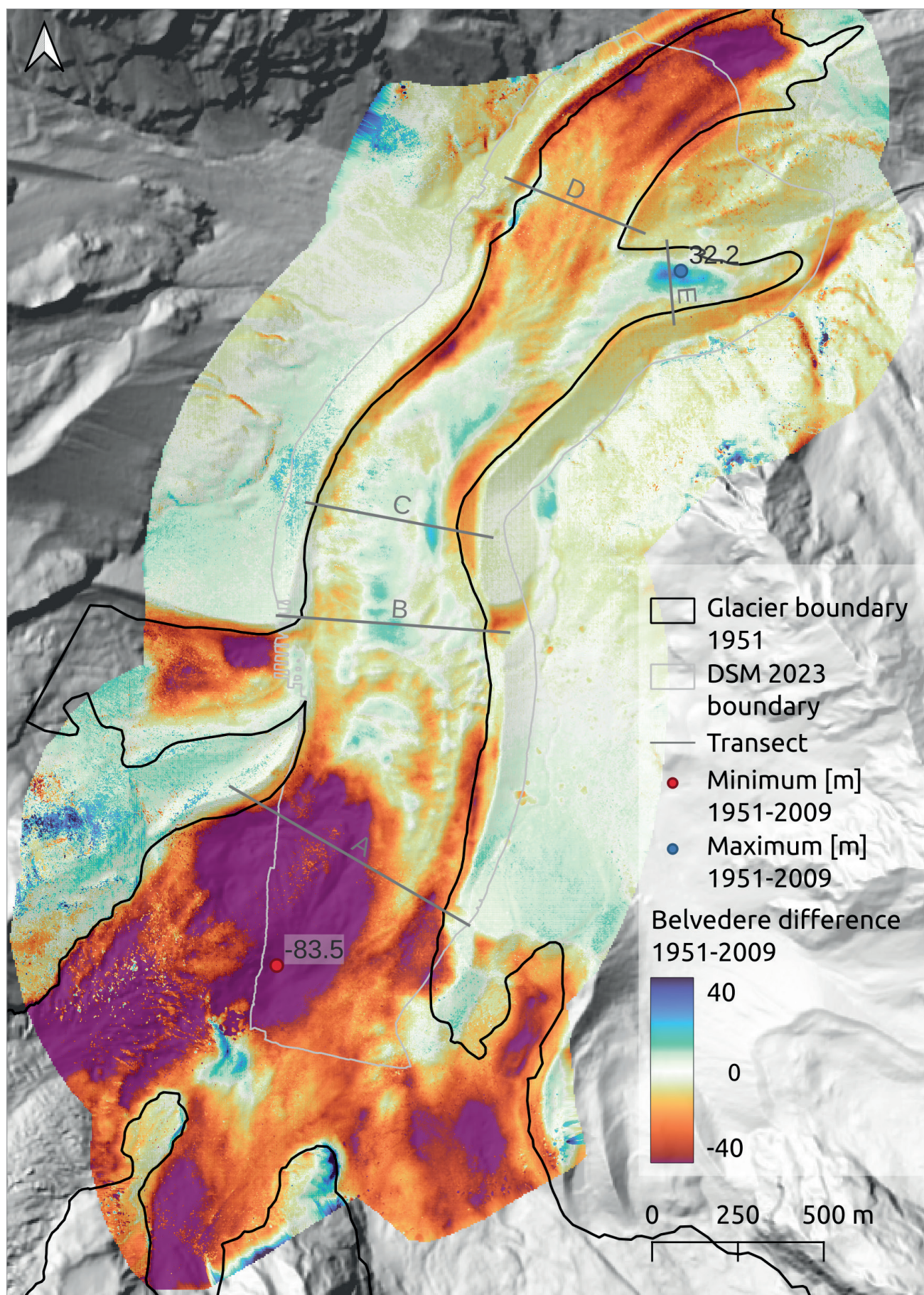


Fig. 6 Glacier elevation change between 1951 and 2009 illustrated with dichromatic colour ramp centred around 0, glacier outlines 1951 (Azzoni et al. 2024, in this issue).

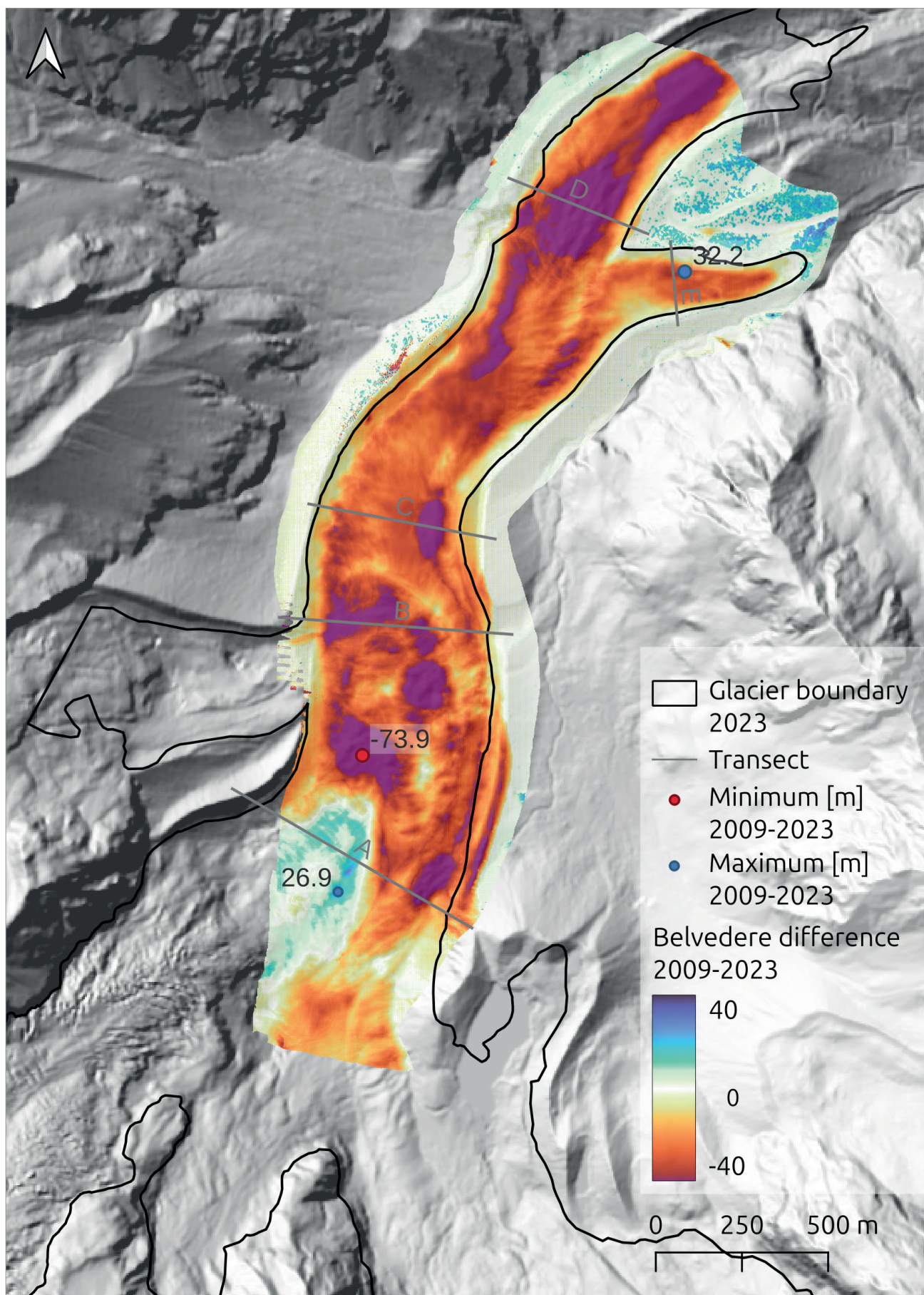
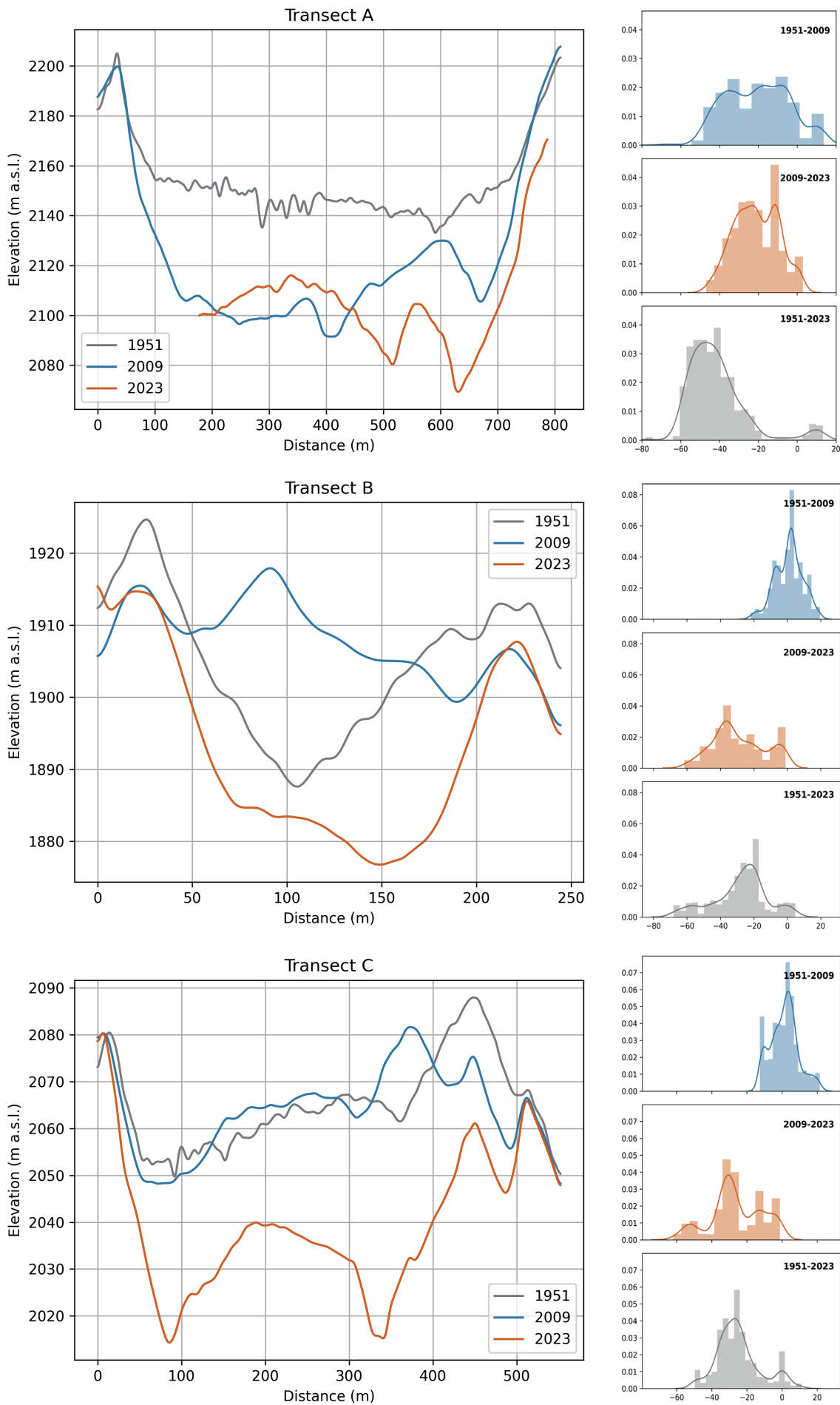


Fig. 7 Glacier elevation change between 2009 and 2023 illustrated with dichromatic colour ramp centred around 0, glacier limit 2023 (Azzoni et al 2024, in this issue).



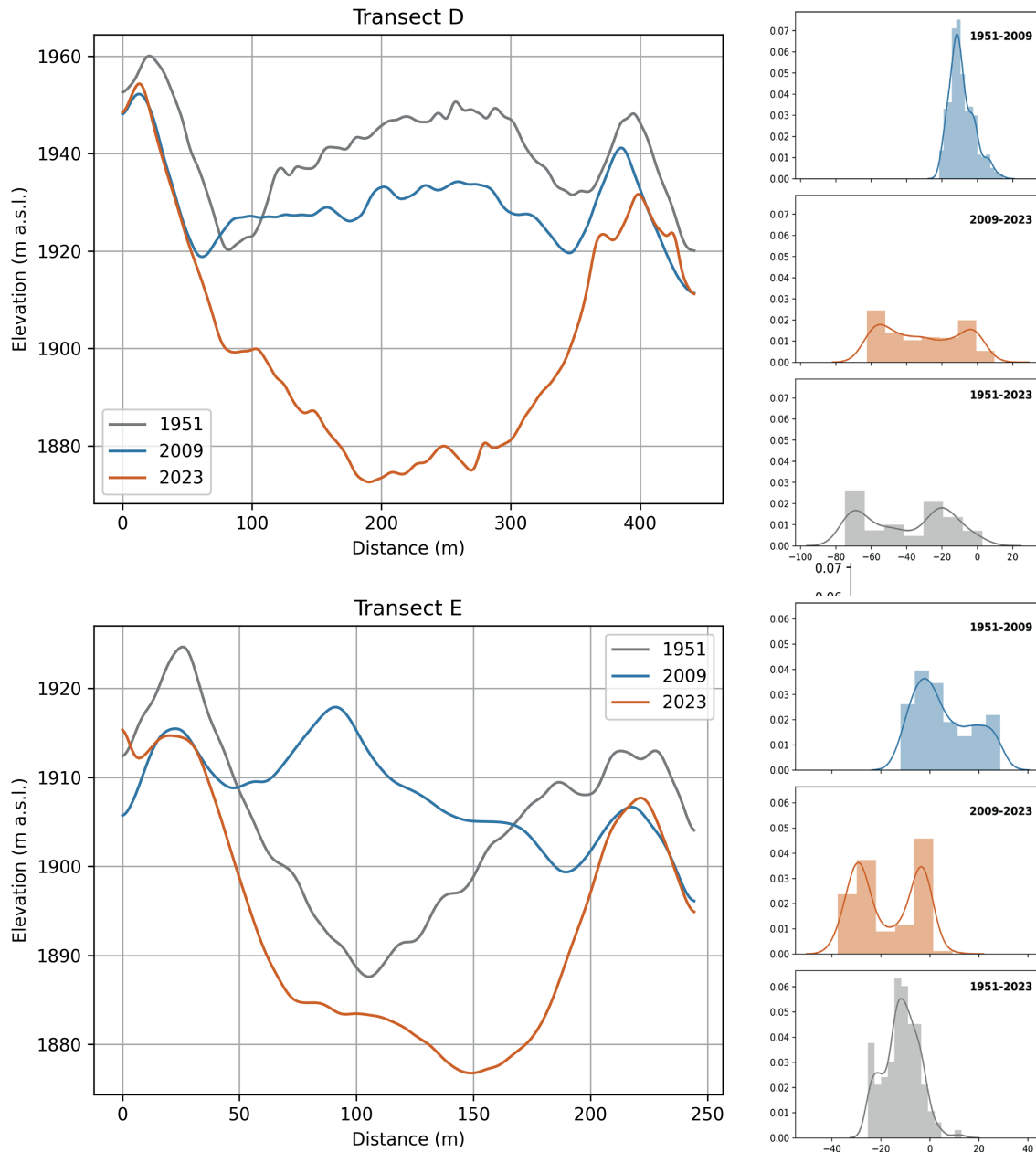


Fig. 8 Five transect profiles of the Belvedere Glacier (Fig. 6 and Fig. 7) illustrate the surface in 1951, 2009, and 2023 and the elevation changes. Transect A: transition area receiving avalanches from the Monte Rosa east face; Transect B: central part of the debris-covered glacier near the glacio-fluvial stream of Nordend Glacier and the moraine breach. Transect C: central part of Belvedere Glacier with the double moraine formation on the eastern and two water channels on both sides of the glacier. Transects D and E: the two lobes of the glacier tongue.

The differenced DSMs 1951–2009 and 1951–2023 show some changes in the vicinity of the glacier, in particular tree growth close to the terminal moraine. Other changes in the stable ground are caused by noise, which is often unavoidable when processing historical data.

Based on the differenced DSMs, significant elevation changes of the Belvedere Glacier were detected over the entire observation period 1951–2023, which amounted to a mean elevation change of -38.3 m (-0.53 m yr^{-1}) (Tab. 4). The average downwasting amounted to -0.24 m yr^{-1} between 1951 and 2009 (-14.0 m in total), equating to a specific mass change

rate of -0.2 m w.e. yr^{-1} . In the second observation period 2009–2023, the ice loss was more than seven-fold higher at -1.77 m yr^{-1} (-24.8 m in total), equating to -1.51 m w.e. yr^{-1} . The increasing trend in the annual mean temperature is also documented in the supplement (Appendix 1). These downwasting rates of the glacier tongue (excluding the Monte Rosa east face) are equivalent to a mass loss of 13.4 ± 0.27 Mt (Megatonnes) from 1951–2009 and a further loss of 23.7 ± 1.67 Mt in the period 2009–2023.

In addition to the acceleration of the glacier thinning rates, large differences in the spatial pattern of elevation changes become apparent between the two

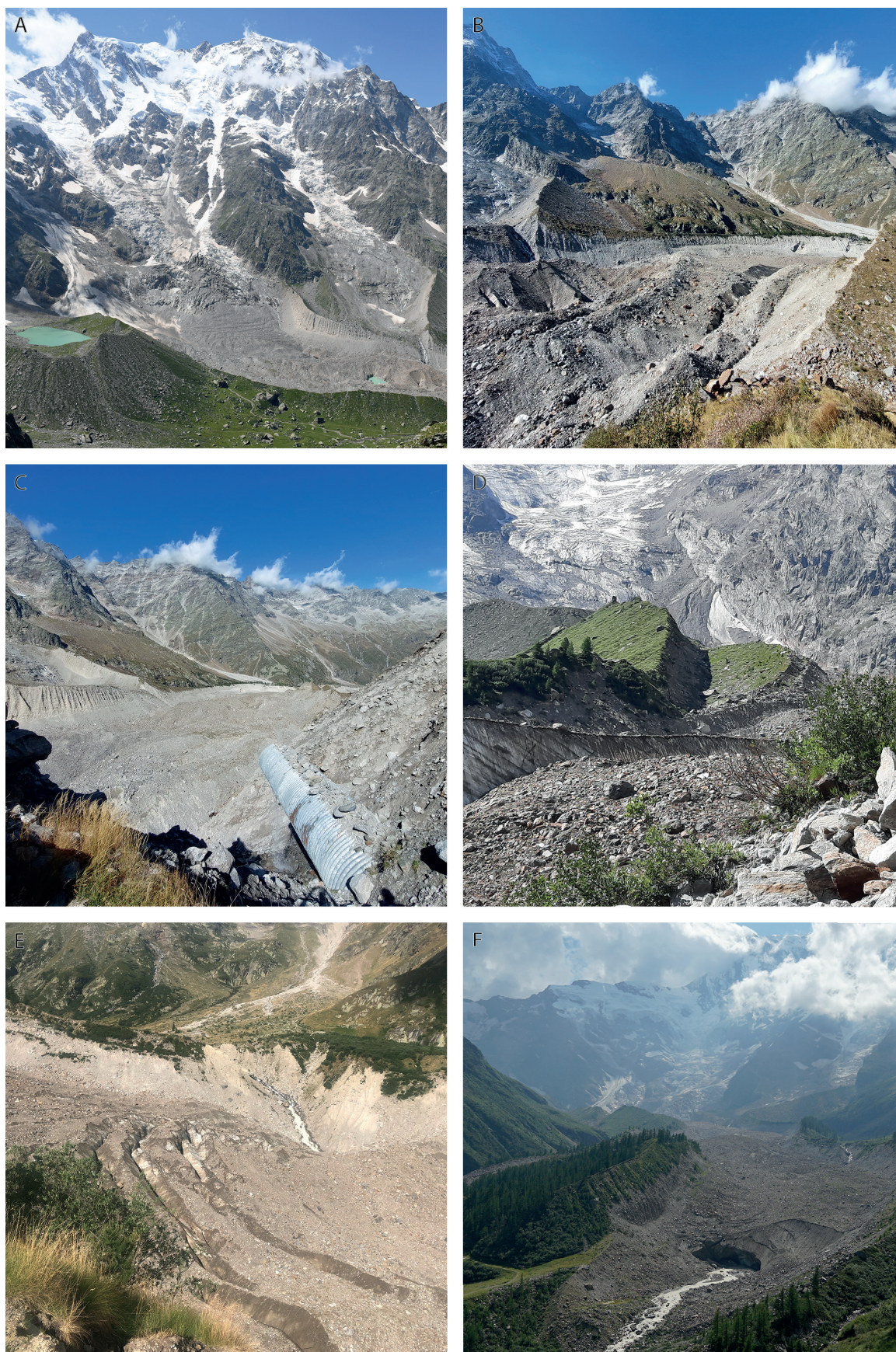


Fig. 9 Terrestrial photographs of Belvedere Glacier with distinctive geomorphological features; A: Monte Rosa east face and transition zone of Belvedere Glacier (2021/08/11); B: debris-covered tongue modulated by meltwater streams and ice-marginal channels (2023/09/30); C: drainage pipe of Lago delle Locce and collapse of the moraine (2023/09/30); D: double moraine from the North with Monte Rosa east face at background (2023/08/02); E: ice cliffs and meltwater stream from Castelfranco Glacier on the Belvedere Glacier (2022/08/09); F: Glacier terminus of the debris-covered primary lobe (2021/08/12).

observation periods (Fig. 6–8, Transect A–D). Along the central part of the glacier tongue, the surface lowering amounted to less than -10 m (Fig. 8, Transect B and Transect C) with some small parts with mass gain. The highest mass gain of up to 32.2 m can be identified at the secondary lobe, despite the fact that the frontal position of the glacier retreated by about 70 m (Fig. 8, Transect E). Some spots with a much higher surface lowering can be identified along the glacier tongue with a maximum of 83.5 m in the transition zone at the foot of Monte Rosa east face. In this part, the depression of the Effimero Lake was formed in 2002 and completely drained in 2003 (Transect A). Furthermore, the retreat of the primary lobe (Transect D) by about 170 m (Azzoni et al. 2024, in this issue) and of the Nordend Glacier by about 755 m (in the timeframe 1951–2021 since the UAV orthophoto is not available for this area) become evident by high mass losses.

In contrast to the first period, the entire glacier tongue is characterised by massive downwasting during the second observation period 2009–2023. Thus, in all transects the glacier surface is lower than in 1953. Some areas of more pronounced downwasting up to -73.9 m can be identified (Fig. 6), which appear as a series of depressions distributed along the entire glacier tongue. Some of these depressions are at least temporarily filled with water (Fig. 7) and one of them (Fig. 8, Transect B) is connected to the glacio-fluvial stream of Nordend Glacier, flowing to the Belvedere Glacier and visible as a small line in the differenced DSM. Furthermore, along the eastern margin of the tongue, two linear structures with accelerated mass loss are visible, connected to the outlet of Lago delle Locce. Compared to the former period, both glacier lobes showed drastic downwasting with a decrease of about -70 m and -25 m at the primary and secondary lobe, respectively. In addition to the thinning of the glacier, the collapse of the lateral moraine becomes visible as a characteristic double structure in the differenced DSMs (Fig. 8, Transect C). Only in the southern part of the tongue, the transition zone to the Monte Rosa east face (Transect A), a maximum increase of 26.9 m can be observed (Fig. 7).

In addition to the accelerated thinning of the glacier, there are also notable changes in certain geomorphological features (Fig. 6–8), such as the widespread collapse of lateral moraines amounting up to 40 m due to debuitressing and the breach (width 80 m) in the eastern lateral moraine caused by the surge-type event in 2001–2002 as well as downwasting (up to 60 m) due to meltwater from the tributary Castelfranco Glacier and from Lake Locce (up to 55 m). Furthermore, the formation of a double-crested moraine is dislocated by up to 60 m on the eastern lateral moraine and is highlighted in Profile C of Fig. 8. Moreover, the moraine in the vicinity of Lake Locce decreased by about 40 m, as indicated by transect A.

6. Discussion

The multitemporal change analysis of Belvedere Glacier provides valuable insights into the dynamics over the period 1951–2023. The combination of historical, UAV, and aerial data, along with the DSM difference approach, contributes to a comprehensive understanding of recent changes of debris-covered glaciers in the region.

6.1 Elevation data

The DSM from 1951 has been processed for the first time. Although there are some visible outliers (probably caused by mass movements and vegetation growth), the digitization of the historical data allowed the creation of a digital representation of the historical glacier surface with a high spatial resolution, enabling the detection of long-term elevation changes. The accuracy of the retrieved DSM from 1951 is comparable to the accuracy of the DSM from 1977 processed by De Gaetani et al. (2021), except in the vertical dimension (RMSE 0.43 m compared to 0.91 m).

The accuracy of the 2023 DSM is comparable to UAV data processing 2020 by Ioli et al. (2022) in the upper part of the Belvedere Glacier. However, they also achieved accuracies below 0.1 m RMSE in other years.

6.2 Glacier elevation changes

The analysis of the two differenced high spatial resolution DSMs enables the detection of the complex processes and related changes of the surge-type and debris-covered Belvedere Glacier since 1951. The Belvedere Glacier belongs to the few glaciers in the Alps with positive mass balances during the second half of the 20th century. According to Diolaiuti et al. (2003), the glacier tongue has already retreated in the early 1990s, while De Gaetani et al. (2021) observed ice volume gains until the 1990s. Due to the duration of the first observation period lasting from 1951 to 2009, the period of mass gain and the reverse trend is not captured by the differenced DSMs used in the present study. However, the long observation period indicates a massive mass loss, as the glacier surface in 2023 is on average 38 m below that of 1951 (mean annual thinning rate -0.5 m per year), which is in line with the increasing trend of mean annual temperature trend since 1987, Appendix 1, statistically confirmed by Mann-Kendall test with p-value of 5.75×10^{-14} . During 2009–2023 an elevation thinning with 1.7 m per year can be observed (mass change rate of -1.5 m w.e. per year), that is much higher than for the Italian Alps, which amounted to -0.5 m per year (mass change rate of 0.6 m w.e. per year) during 2000–2014 (Sommer et al. 2020; Hugonnet et al. 2021). This comparatively high thinning rate might be caused by the exclusion of the headwall,

which forms the accumulation zone of the Belvedere Glacier. The present study examined glacier elevation changes of the debris-covered ablation zone using reference Lidar elevation points (2009) and very high-resolution images (2023 UAV ground sampling distance 3.2 cm), which resulted in elevation models with sub-meter accuracy. It can be assumed that the discrepancy between the studies can be attributed to the fact that the accumulation area was not examined in the present study. Until now, no other study has yet processed elevation changes in very high spatial resolution with sub-meter accuracy for the entire Belvedere Glacier.

It can also be assumed that the surge-type event 2001–2002 (Kääb et al. 2004) has a long-term impact on mass balances. Like in the case of the Vernagtferner, one of the few surge-type glaciers in the Alps showing higher mass losses after surging events (Charalampidis et al. 2018). In contrast, on the regional scale no significant differences of mass losses were observed between surge-type and non-surge glaciers in the Karakoram (Farinotti et al. 2020; Gardelle et al. 2013). However, it becomes obvious from the differenced DSM 2009–2023, that the surge-induced surface thickening of about 30 m in the upper part of the glacier tongue (from near Locce Lake to Rifugio Zamboni) (Truffer et al. 2021), completely melted. The surge movement, which probably originated from the foot of the Monte Rosa east face (Kääb et al. 2004; Truffer et al. 2021) is detectable in the differenced DSM 1953–2009 as the large depression in the transition zone near the temporary Effimero Lake, which bursted in June 2003 (Truffer et al. 2021). According to Kääb et al. (2004), the ice loss amounted to 20 m at this spot during 1995–1999 and a further ice loss occurred due to the surge movement. During 2009–2023, the lower part of the headwall shows positive elevation changes, which might be a response to the rapid ice loss in the vicinity of Effimero Lake or due to the accumulation of large avalanches in 2005 and 2010, quantified by Fischer et al. (2013) and Tamburini et al. (2013). Due to the steep headwall of the Monte Rosa east face, the transition zone is characterised by frequent ice avalanches, similar to the case of the Karakoram and Nanga Parbat glaciers (Hewitt 2014; Bhambri et al. 2017; Nüsser and Schmidt 2021).

Due to the high spatial resolution of the differenced DSMs, also the accelerated ablation along water bodies can be detected. The linear features of accelerated ablation indicate ice-marginal channels and meltwater streams, such as those from the Nordend Glacier and Locce Lake and from the Castelfranco Glacier, which flow partly on the Belvedere Glacier. These streams are often connected to large depressions, some of them were formed by supraglacial lakes (Brodský et al. 2024, in this issue), others by roof collapses of englacial water bodies (Gulley and

Benn 1997). To which degree this can also be related to the subglacial outburst of Effimero lake (Truffer et al. 2021) remains an open question.

Furthermore, the impact of ice cliffs, which are often connected to supraglacial lakes and increase mass loss (Bhambri et al. 2023; Brun et al. 2016; Pellicciotti et al. 2015; Salerno et al. 2017), needs to be analysed in more detail. Especially, as the typical inversion of the ablation gradient along debris-covered glaciers as shown for the debris-covered glaciers in the Khumbu region, Himalaya (Benn et al. 2012) does not exist. In contrast, the lowermost part and the transition zone of the Belvedere Glacier both showed a more pronounced thinning than the central part. The higher ablation rates along the left lobe might be caused by ice-cliffs or by a changed flow direction as it seems that the surge event fed only the smaller right lobe. As the right lobe is characterised by a thick supraglacial debris-cover, the ice loss is less pronounced compared to the left lobe. However, velocity measurements, which were carried out by Ioli et al. (2022) since 2015, showed that both lobes probably consist of stagnant ice. In the upper part, the high ablation rates might be caused by the occurrence of supraglacial lakes as well as the more patchy debris coverage.

As in other studies (De Gaetani et al. 2021; Diolaiuti et al. 2003), the Monte Rosa east face was excluded from the calculations of changes. However, headwalls of ice and avalanche-fed debris-covered glaciers are important for an improved understanding of mass balances (Hewitt 2014; Nüsser and Schmidt 2021), often neglected in long-term models (Laha et al. 2017). Furthermore, they are important sources for the debris supply to the glaciers (Racoviteanu et al. 2022). Especially in the case of the Belvedere Glacier this is of utmost importance, where an increase of the debris-covered area can be observed since the end of the 19th century (Kropáček et al. 2024, in this issue) as Monte Rosa east face slope failures started in 1990, while several large rock and ice avalanches occurred in the 2000s (Fischer et al. 2013). The mass loss at the Monte Rosa east face was quantified, while its impact on the Belvedere Glacier is unknown.

6.3 Consequences on glacier geomorphology

In addition to the glacier changes, the differenced DSM also highlights some geomorphological changes occurred in surrounding areas. The formation of a breach in the lateral moraine caused by the surge event in 2001–2002 becomes evident with a strong erosion of the outer side of the moraine and the accumulation of the eroded material further downstream. A similar breach is evident at the base of the debris flow cone of the Castelfranco Glacier. Here, during more intense rainfall events, the debris flow channel cuts through the moraine reaching the glacier.

This action leads to a progressive enlargement of the moraine.

The significant reduction in ice thickness has led to widespread slipping of the inner margin of the moraines due to debuttressing phenomena (Azzoni et al. 2023). This is particularly evident on the left bank upstream of the breccia caused by the melting water of Castelfranco Glacier, on the left bank just downstream of Lago delle Locce (Fig. 6) and on the right side of the main lobe. Here, although the main ridge of the moraine is stable, the large loss of thickness has led to the formation of double-crested moraine as highlighted also in the profiles of Fig. 7. The displacement rate of this sliding, calculated with dendro-geomorphological analysis, is 1.87 metres per year for the 2018–2023 timeframe (Bollati et al. 2024, in this issue).

From the comparison of the DSMs, an evolution of the Belvedere Glacier moraine near Lago delle Locce is also observable. Here, also an anthropogenic impact on the geomorphology of the area is evident. In fact, following the erosion of this sector of the moraine and the alarm for a possible sudden draining of the lake, in 1979 a series of interventions were carried out that altered the shape of the moraine. Excavating a deep trench in the moraine and installing a drainage pipe diverting water to the inner side of the moraine led to significant changes in this area. The effect of this operation is still ongoing as the discharge of water pipe on the moraine's flank promotes localised erosion.

7. Conclusion and outlook

The processing of the 1951 historical data into a DSM for the first time is an important step in understanding the dynamic processes that have taken place on Belvedere Glacier over the last 72 years. The high spatial resolution of the DSMs allows detailed observation and deciphering of the spatially heterogeneous downwash pattern caused by complex processes such as debris cover, avalanches, surge, supraglacial meltwater and GLOFs, and their relationship to global warming. These high spatial resolution data are necessary for a better understanding of the response of glaciers to global warming. Downwasting of Belvedere Glacier has accelerated, as documented by the massive elevation changes between our latest observation period (2009–2023). The massive mass loss in the long term observation period is in line with the increasing trend of mean annual temperature since 1987, also statistically confirmed. While our data does not directly identify the surge-type event, the impacts are unmistakable when examined in the context of the analysed data sets. The 2001–2002 surge event, meltwater streams and supraglacial lakes are considered to be the main drivers forcing elevation changes and shaping its spatial variation and surface structures.

The compared DSMs also reveal geomorphological changes, including breaches in lateral moraines caused by glacier surges and debris flows, leading to erosion and downstream material accumulation, with similar processes observed at the Castelfranco Glacier during heavy rainfall. Also, the significant reduction in ice thickness caused widespread moraine slipping due to debuttressing, particularly near Castelfranco Glacier and Lago delle Locce.

For future work, it will be beneficial to increase the temporal resolution of DSMs to analyse glacier dynamics and associated geohazards in more detail. The area to be analysed shall include the Monte Rosa east face as well.

Acknowledgements

This research was funded by the 4EU+ project Remote Sensing of the Cryosphere Dynamics under the Influence of Climate Change, grant number 4EU+/23/F4/19. Disk space to store remote sensing images was supplied by the project “e-Infrastruttura CZ” (e-INFRA CZ LM2018140) supported by the Ministry of Education, Youth and Sports of the Czech Republic. This research was also partly funded by University of Milan through the Sostegno alla ricerca Project 2022 (Evoluzione dei processi geomorfologici e degli impatti sul ciclo idrologico in contesti sensibili al cambiamento climatico).

The Authors would like to thank the Province of Verbano-Cusio-Ossola for the permit of UAV (dr. Andrea De Zordi, Settore III – Assetto del Territorio Georisorse e Tutela Faunistica, Servizio Rete Natura 2000 e Forestazione). The Authors would also like to thank Francesco Ioli and Livio Pinto from the Department of Civil and Environmental Engineering, Politecnico di Milano, for kindly sharing the coordinates of the GCPs on Belvedere Glacier.

We also acknowledge the E-OBS dataset from the EU-FP6 project UERRA (<http://www.uerra.eu>) and the Copernicus Climate Change Service, and the data providers in the ECAandD project (<https://www.ecad.eu>).

References

- Agisoft Metashape. (2024). Available online: <https://www.agisoft.com> (accessed on 25 January 2024).
- Azzoni, R. S., Fugazza, D., Zerboni, A., Senese, A., D'Agata, C., Maragno, D., Carzaniga, A., Cernuschi, M., Diolaiuti, G. A. (2018): Evaluating high-resolution remote sensing data for reconstructing the recent evolution of supra glacial debris: A study in the Central Alps (Stelvio Park, Italy). *Progress in Physical Geography: Earth and Environment* 42(1), 3–23, <https://doi.org/10.1177/0309133317749434>.
- Azzoni, R. S., Pelfini, M., Zerboni, A. (2023): Estimating the Evolution of a Post-Little Ice Age Deglaciated Alpine Valley through the DEM of Difference (DoD). *Remote*

- Sensing 15(12): 3190, <https://doi.org/10.3390/rs15123190>.
- Benn, D. I., Bolch, T., Hands, K., Gulley, J., Luckman, A., Nicholson, L. I., Quincey, D., Thompson, S., Toumi, R., Wiseman, S. (2012): Response of debris-covered glaciers in the Mount Everest region to recent warming, and implications for outburst flood hazards. *Earth-Science Reviews* 114, 156–174, <https://doi.org/10.1016/j.earscirev.2012.03.008>.
- Berthier, E., Arnaud, Y., Kumar, R., Ahmad, S., Wagnon, P., Chevallier, P. (2007): Remote sensing estimates of glacier mass balances in the Himachal Pradesh (Western Himalaya, India). *Remote Sensing of Environment* 108(3), 327–338, <https://doi.org/10.1016/J.RSE.2006.11.017>.
- Berthier, E., Cabot, V., Vincent, C., Six, D. (2016). Decadal region-wide and glacier-wide mass balances derived from multi-temporal aster satellite digital elevation models. Validation over the mont-blanc area. *Frontiers in Earth Science* 4: 194833, <https://doi.org/10.3389/feart.2016.00063>.
- Bhambri, R., Hewitt, K., Kawishwar, P., Pratap, B. (2017): Surge-type and surge-modified glaciers in the Karakoram. *Scientific Reports* 7: 15391, <https://doi.org/10.1038/s41598-017-15473-8>.
- Bhambri, R., Schmidt, S., Chand, P., Nüsser, M., Haritashya, U., Sain, K., Tiwari, S. K., Yadav, J. S. (2023): Heterogeneity in glacier thinning and slowdown of ice movement in the Garhwal Himalaya, India. *Science of The Total Environment* 875: 162625, <https://doi.org/10.1016/j.scitotenv.2023.162625>.
- Bolch, T., Buchroithner, M., Pieczonka, T., Kunert, A. (2008): Planimetric and volumetric glacier changes in the Khumbu Himal, Nepal, since 1962 using Corona, Landsat TM and ASTER data. *Journal of Glaciology* 54(187), 592–600, <https://doi.org/10.3189/002214308786570782>.
- Bolch, T., Pieczonka, T., Benn, D. I. (2011): Multi-decadal mass loss of glaciers in the Everest area (Nepal Himalaya) derived from stereo imagery. *The Cryosphere* 5, 349–358, <https://doi.org/10.5194/tc-5-349-2011>.
- Bolch, T., Kulkarni, A. V., Käab, A., Huggel, C., Paul, F., Cogley, J. G., Frey, H., Kargel, J. S., Fujita, K., Scheel, M., Bajracharya, S. R., Stoffel, M. (2012): The State and Fate of Himalayan Glaciers. *Science* 336, 310–314, <https://doi.org/10.1126/science.1215828>.
- Brenner, A. C., DiMarzio, J. P., Zwally, H. J. (2007): Precision and accuracy of satellite radar and laser altimeter data over the continental ice sheets, *IEEE Transactions on Geoscience and Remote Sensing* 45(2), 321–331, <https://doi.org/10.1109/TGRS.2006.887172>.
- Brodský, L., Rusnák, S., Schmidt, S., Vilímek, V., Azzoni, R. S., Nüsser, M., Tronti, G., Kropáček, J., Pandey, A. (2024): Interannual spatio-temporal evolution of the supraglacial lakes on the Belvedere Glacier between 2000 and 2023. *AUC Geographica* 59(2), 214–228, <https://doi.org/10.14712/23361980.2024.24>.
- Brun, F., Buri, P., Miles, E. S., Wagnon, P., Steiner, J., Berthier, E., Ragetti, S., Kraaijenbrink, P. D. A., Immerzeel, W. W., Pellicciotti, F. (2016): Quantifying volume loss from ice cliffs on debris-covered glaciers using high-resolution terrestrial and aerial photogrammetry. *Journal of Glaciology* 62, 684–695, <https://doi.org/10.1017/jog.2016.54>.
- Chandrasekharan, A., Ramsankaran, R. (2023): Reconstructing 32 years (1989–2020) of annual glacier surface mass balance in Chandra Basin, Western Himalayas, India. *Regional Environmental Change* 23: 118, <https://doi.org/10.1007/s10113-023-02112-4>.
- Charalampidis, C., Fischer, A., Kuhn, M., Lambrecht, A., Mayer, C., Thomaidis, K., Weber, M. (2018): Mass-Budget Anomalies and Geometry Signals of Three Austrian Glaciers. *Frontiers in Earth Science* 6: 218, <https://doi.org/10.3389/feart.2018.00218>.
- Cornes, R., van der Schrier, G., van den Besselaar, E. J. M., Jones, P.D. (2018): An Ensemble Version of the E-OBS Temperature and Precipitation Datasets, *Journal of Geophysical Research: Atmospheres* 123(17), 9391–9409, <https://doi.org/10.1029/2017JD028200>.
- OpenStreetMap contributors (2017): Available online: <https://planet.osm.org>, url: <https://www.openstreetmap.org> (accessed on 10.3.2024).
- De Gaetani, C. I., Ioli, F., Pinto, L. (2021): Aerial and UAV Images for Photogrammetric Analysis of Belvedere Glacier Evolution in the Period 1977–2019. *Remote Sensing* 13: 3787, <https://doi.org/10.3390/rs13183787>.
- Farinotti, D., Immerzeel, W. W., de Kok, R. J., Quincey, D. J., Dehecq, A. (2020): Manifestations and mechanisms of the Karakoram glacier Anomaly. *Nature Geoscience* 13, 8–16, <https://doi.org/10.1038/s41561-019-0513-5>.
- Fischer, L., Huggel, C., Käab, A., Haeberli, W. (2013): Slope failures and erosion rates on a glacierized high-mountain face under climatic changes. *Earth Surface Processes and Landforms* 38(8), 836–846, <https://doi.org/10.1002/esp.3355>.
- Fischer, M., Huss, M., Hoelzle, M. (2015): Surface elevation and mass changes of all Swiss glaciers 1980–2010. *The Cryosphere* 9(2), 525–540, <https://doi.org/10.5194/tc-9-525-2015>.
- Fleischer, F., Otto, J., Junker, R. R., Hölbling, D. (2021): Evolution of debris cover on glaciers of the Eastern Alps, Austria, between 1996 and 2015. *Earth Surface Processes and Landforms* 46(9), 1673–1691, <https://doi.org/10.1002/esp.5065>.
- Fugazza, D., Valle, B., Caccianiga, M. S., Gobbi, M., Traversa, G., Tognetti, M., Diolaiuti, G. A., Senese, A. (2023): Glaciological and meteorological investigations of an Alpine debris-covered glacier: the case study of Amola Glacier (Italy). *Cold Region Science Technology* 216: 104008, <https://doi.org/10.1016/j.coldregions.2023.104008>.
- Fujita, K., Nuimura, T. (2011): Spatially heterogeneous wastage of Himalayan glaciers. *Proceedings of the National Academy of Sciences of the United States of America* 108(34), 14011–14014, <https://doi.org/10.1073/pnas.1106242108>.
- Fyffe, C. L., Brock, B. W., Kirkbride, M. P., Mair, D. W. F., Arnold, N. S., Smiraglia, C., Diolaiuti, G., Diotri, F. (2019): Do debris-covered glaciers demonstrate distinctive hydrological behaviour compared to clean glaciers? *Journal of Hydrology* 570, 584–597, <https://doi.org/10.1016/j.jhydrol.2018.12.069>.
- Gardelle, J., Berthier, E., Arnaud, Y., Käab, A. (2013): Region-wide glacier mass balances over the Pamir-Karakoram-Himalaya during 1999–2011. *The Cryosphere* 7(4), 1263–1286, <https://doi.org/10.5194/tc-7-1263-2013>.

- Geoportale Piemonte (2014). Available online: <http://www.geoportale.piemonte.it> (accessed on 15. 1. 2024).
- Gulley, J., Benn, D. I. (1997): Structural control of englacial drainage systems in Himalayan debris-covered glaciers. *Journal of Glaciology* 53(182), 399–412, <https://doi.org/10.3189/002214307783258378>.
- Haubeck, K., Prinz, T. (2013): A UAV-Based Low-Cost Stereo Camera System for Archaeological Surveys – Experiences from Doliche (Turkey), *International Archives of the Photogrammetry, Remote Sensing and Spatial Information Sciences XL-1/W2*, 195–200, <https://doi.org/10.5194/isprsarchives-XL-1-W2-195-2013>.
- Hewitt, K. (2005): The Karakoram anomaly? Glacier expansion and the “elevation effect”, *Karakoram Himalaya. Mountain Research and Development* 25(4), 332–340, [https://doi.org/10.1659/0276-4741\(2005\)025\[0332:TKAGEA\]2.0.CO;2](https://doi.org/10.1659/0276-4741(2005)025[0332:TKAGEA]2.0.CO;2).
- Hewitt, K. (2014): *Glaciers of the Karakoram Himalaya: Glacial Environments, Processes, Hazards and Resources. Advances in Asian Human-Environmental Research.* Springer, <https://doi.org/10.1007/978-94-007-6311-1>.
- Hock, R., Rasul, G., Adler, C., Cáceres, B., Gruber, S., Hirabayashi, Y., Jackson, M., Kääb, A., Kang, S., Kutuzov, S., Milner, A., Molau, U., Morin, S., Orlove, B., Steltzer, H. (2019): High Mountain Areas, IPCC Special Report on the Ocean and Cryosphere in a Changing Climate, 131–202, https://www.ipcc.ch/site/assets/uploads/sites/3/2019/11/06_SROCC_Ch02_FINAL.pdf.
- Hugonnet, R., McNabb, R., Berthier, E., Menounos, B., Nuth, C., Girod, L., Farinotti, D., Huss, M., Dussaillant, I., Brun, F., Kääb, A. (2021): Accelerated global glacier mass loss in the early twenty-first century. *Nature* 592, 726–731, <https://doi.org/10.1038/s41586-021-03436-z>.
- Huo, D., Bishop, M. P., Bush, A. B. G. (2021): Understanding Complex Debris-Covered Glaciers: Concepts, Issues, and Research Directions. *Frontiers in Earth Science* 9: 652279, <https://doi.org/10.3389/feart.2021.652279>.
- Huss, M. (2013): Density assumptions for converting geodetic glacier volume change to mass change. *The Cryosphere* 7(3), 877–887, <https://doi.org/10.5194/tc-7-877-2013>.
- Huss, M., Bauder, A., Funk, M., Hock, R. (2008): Determination of the seasonal mass balance of four Alpine glaciers since 1865. *Journal of Geophysical Research* 113(1): F01015, <https://doi.org/10.1029/2007jf000803>.
- Huss, M., Bauder, A. (2009): 20th-century climate change inferred from four long-term point observations of seasonal mass balance. *Annals of Glaciology* 50(50): 207–214, <https://doi.org/10.3189/172756409787769645>.
- Immerzeel, W., Pellicciotti, F., Bierkens, M. (2013): Rising river flows throughout the twenty-first century in two Himalayan glacierized watersheds. *Nature Geoscience* 6, 742–745, <https://doi.org/10.1038/ngeo1896>.
- Ioli, F., Bianchi, A., Cina, A., De Michele, C., Maschio, P., Passoni, D., Pinto, L. (2022): Mid-Term Monitoring of Glacier’s Variations with UAVs: The Example of the Belvedere Glacier. *Remote Sensing* 14: 28, <https://doi.org/10.3390/rs14010028>.
- Jóhannesson, T., Raymond, C., Waddington, E. (1989): Time-Scale for Adjustment of Glaciers to Changes in Mass Balance. *Journal of Glaciology* 35(121), 355–369, <https://doi.org/10.3189/S00221430000928X>.
- Jouvet, G., Huss, M. (2019): Future retreat of Great Aletsch Glacier. *Journal of Glaciology* 65, 869–872, <https://doi.org/10.1017/jog.2019.52>.
- Kääb, A., Huggel, C., Barbero, S., Chiarle, M., Cordola, M., Epifani, F., Haeblerli, W., Mortara, G., Semino, P., Tamburini, A., Viazzo, G. (2004): Glacier hazards at Belvedere Glacier and the Monte Rosa East Face, Italian Alps: Processes and Mitigation. *Internationales Symposium Interpraevent 2004 – Riva/Trient*. https://www.researchgate.net/publication/242231211_Glacier_hazards_at_Belvedere_glacier_and_the_Monte_Rosa_east_face_Italian_Alps_Processes_and_mitigation.
- Kääb, A., Berthier, E., Nuth, C., Gardelle, J., Arnaud, Y. (2012): Contrasting patterns of early twenty-first-century glacier mass change in the Himalayas. *Nature* 488, 495–498, <https://doi.org/10.1038/nature11324>.
- Kendall, M. G. (1957). Review of Rank Correlation Methods. *Biometrika*, 44(1/2), 298–298, <https://doi.org/10.2307/2333282>.
- Knuth, F., Shean, D., Bhushan, S., Schwat, E., Alexandrov, O., McNeil, C., Dehecq, A., Florentine, C., O’Neel, S. (2023): Historical Structure from Motion (HSfM): Automated processing of historical aerial photographs for long-term topographic change analysis. *Remote Sensing of Environment* 285: 113379, <https://doi.org/10.1016/j.rse.2022.113379>.
- Kirkbride, M. P., Deline, P. (2013): The formation of supraglacial debris covers by primary dispersal from transverse englacial debris bands. *Earth Surface Processes and Landforms* 38(15), 1779–1792, <https://doi.org/10.1002/ESP.3416>.
- Kropáček, J., Mehrishi, P., Bollati, I. M., Brodský, L., Pelfini, M., Azzoni, R., Schmidt, S., Nüsser, M., Vilfmek, V. (2024): Dynamics and related natural hazards of Belvedere Glacier in the Italian Alps: a review. *AUC Geographica* 59(2), 163–183, <https://doi.org/10.14712/23361980.2024.21>.
- Laha, S., Kumari, R., Singh, S., Mishra, A., Sharma, T., Banerjee, A., Nainwal, H. C., Shankar, R. (2017). Evaluating the contribution of avalanching to the mass balance of Himalayan glaciers. *Annals of Glaciology* 58(75pt2), 110–118, <https://doi.org/10.1017/aog.2017.27>.
- Lemke, P., Ren, J., Alley, R. B., Allison, I., Carrasco, J., Flato, G., Fujii, Y., Kaser, G., Mote, P., Thomas, R. H., Zhang, T. (2007): Observations: Changes in Snow, Ice and Frozen Ground. *Climate Change: The Physical Science Basis. Contribution of Working Group I to the Fourth Assessment Report of the Intergovernmental Panel on Climate Change* [Solomon, S., Qin, D., Manning, M., Chen, Z., Marquis, M., Averyt, K. B., Tignor, M., Miller, H. L. (eds.)]. Cambridge University Press, Cambridge, United Kingdom and New York, NY, USA, <https://www.ipcc.ch/site/assets/uploads/2018/02/ar4-wg1-chapter4-1.pdf>.
- Mattson, L. E., Gardner, J. S., Young, G. J. (1993): Ablation on debris covered glaciers: an example from the Rakhiot Glacier, Punjab, Himalaya. *Snow and Glacier Hydrology. IAHS Publication* 218, 289–294.
- Maurer, J. M., Schaefer, J. M., Rupper, S., Corley, A. (2019): Acceleration of ice loss across the Himalayas over the past 40 years. *Science Advances* 5(6): eaav7266, <https://doi.org/10.1126/sciadv.aav7266>.
- Mölg, N., Ferguson, J., Bolch, T., Vieli, A. (2020): On the influence of debris cover on glacier morphology: How

- high-relief structures evolve from smooth surfaces. *Geomorphology* 357: 107092, <https://doi.org/10.1016/j.geomorph.2020.107092>.
- Mondino, E. B. (2015): Multi-temporal image co-registration improvement for a better representation and quantification of risky situations: the Belvedere Glacier case study. *Geomatics, Natural Hazards and Risk* 6(5–7), 362–378, <https://doi.org/10.1080/19475705.2014.927804>.
- Mortara, G., Tamburini, A., Ercole, G., Semino, P., Chiarle, M., Godone, F., Guiliano, M., Haerberli, W., Käab, A., Huggel, Ch., Fischer, L., Cordola, M., Barbero, S., Salandin, A., Rabuffetti, D., Mercalli, L., Cat Berro, D., Carton, A., Mazza, A., Godone, D., Federici, P., Viazzo, G., Epifani, F., Valsesia, T. (2009): Il ghiacciaio del Belvedere e l'emergenza del Lago Effimero. Regione Piemonte. Bussoleno: Societa' Meteorologica Subalpina.
- Muhammad, S., Tian, L., Ali, S., Latif, Y., Wazir, M. A., Goheer, M. A., Saifullah, M., Hussain, I., Shiyin, L. (2020): Thin debris layers do not enhance melting of the Karakoram glaciers. *Science of The Total Environment* 746: 141119, <https://doi.org/10.1016/J.SCITOTENV.2020.141119>.
- Nüsser, M., Schmidt, S. (2021): Glacier changes on the Nanga Parbat 1856–2020: A multi-source retrospective analysis. *Science of The Total Environment* 785: 147321, <https://doi.org/10.1016/j.scitotenv.2021.147321>.
- Nuimura, T., Fujita, K., Yamaguchi, S., Sharma, R. R. (2012): Elevation changes of glaciers revealed by multitemporal digital elevation models calibrated by GPS survey in the Khumbu region, Nepal Himalaya, 1992–2008. *Journal of Glaciology* 58(210), 648–656, <https://doi.org/10.3189/2012JG11J061>.
- Nuimura, T., Fujita, K., Sakai, A. (2017). Downwasting of the debris-covered area of Lirung Glacier in Langtang Valley, Nepal Himalaya, from 1974 to 2010. *Quaternary International* 455, 93–101, <https://doi.org/10.1016/j.quaint.2017.06.066>.
- Nuth, C. Käab, A. (2011): Co-registration and bias corrections of satellite elevation data sets for quantifying glacier thickness change. *The Cryosphere* 5(1), 271–290, <https://doi.org/doi:10.5194/tc-5-271-2011>.
- Oerlemans, J., Reichert B.K. (2000): Relating glacier mass balance to meteorological data by using a seasonal sensitivity characteristic. *Journal of Glaciology* 46(152), 1–6, <https://doi.org/10.3189/172756500781833269>.
- Paul, F., Bolch, T., Käab, A., Nagler, T., Nuth, C., Scharer, K., Shepherd, A., Strozzi, T., Ticconi, F., Bhambri, R., Berthier, E., Bevan, S., Gourmelen, N., Heid, T., Jeong, S., Kunz, M., Lauknes, T. R., Luckman, A., Merryman Boncori, J. P., Moholdt, G., Muir, A., Neelmeijer, J., Rankl, M., VanLooy, J., Van Niel, T. (2015): The glaciers climate change initiative: Methods for creating glacier area, elevation change and velocity products. *Remote Sensing of the Environment* 162, 408–426, <https://doi.org/10.1016/j.rse.2013.07.043>.
- Pellicciotti, F., Stephan, C., Miles, E., Herreid, S., Immerzeel, W. W., Bolch, T. (2015): Mass-balance changes of the debris-covered glaciers in the Langtang Himal, Nepal, from 1974 to 1999. *Journal of Glaciology* 61(226), 373–386, <https://doi.org/10.3189/2015JG13J237>.
- Pix4D (2024). Pix4Dcapture software available online: <https://www.pix4d.com/product/pix4dcapture/> (accessed on 25 January 2024).
- Racoviteanu, A. E., Nicholson, L., Glasser, N. F., Miles, E., Harrison, S., Reynolds, J. M. (2022): Debris-covered glacier systems and associated glacial lake outburst flood hazards: challenges and prospects. *Journal of the Geological Society* 179: jgs2021-084, <https://doi.org/10.1144/jgs2021-084>.
- Radić, V., Hock, R. (2006): Modeling future glacier mass balance and volume changes using ERA-40 reanalysis and climate models: A sensitivity study at Storglaciären, Sweden. *Journal of Geophysical Research: Earth Surface* 111(F3): 3003, <https://doi.org/10.1029/2005JF000440>.
- Rignot, E., Rivera, A., Casassa, G. (2003): Contribution of the Patagonia Icefields of South America to Sea Level Rise. *Science* 302(5644), 434–437, <https://doi.org/10.1126/science.1087393>.
- Salerno, F., Thakuri, S., Tartari, G., Nuimura, T., Sunako, S., Sakai, A., Fujita, K. (2017): Debris-covered glacier anomaly? Morphological factors controlling changes in the mass balance, surface area, terminus position, and snow line altitude of Himalayan glaciers. *Earth Planetary Science Letters* 471, 19–31, <https://doi.org/10.1016/j.epsl.2017.04.039>.
- Scherler, D., Wulf, H., Gorelick, N. (2018): Global Assessment of Supraglacial Debris-Cover Extents. *Geophysical Research Letters* 45(21), 11798–11805, <https://doi.org/10.1029/2018GL080158>.
- Schmidt, S., Nüsser, M. (2009): Fluctuations of Raikot Glacier during the past 70 years: a case study from the Nanga Parbat massif, northern Pakistan. *Journal of Glaciology* 55(194), 949–959, <https://doi.org/10.3189/002214309790794878>.
- Smiraglia, C., Azzoni, R. S., D'Agata, C. A. R. L. O., Maragno, D., Fugazza, D., Diolaiuti, G. A. (2015): The evolution of the Italian glaciers from the previous database to the New Italian Inventory. Preliminary considerations and results. *Geografia Fisica e Dinamica Quaternaria* 38(1), 79–87.
- Sommer, C., Malz, P., Seehaus, T. C., Lippl, S., Zemp, M., Braun, M. H. (2020): Rapid glacier retreat and downwasting throughout the European Alps in the early 21st century. *Nature Communications* 11: 3209, <https://doi.org/10.1038/s41467-020-16818-0>.
- Tamburini, A., Villa, F., Fischer, L., Hungr, O., Chiarle, M., Mortara, G. (2013): Slope Instabilities in High-Mountain Rock Walls. Recent Events on the Monte Rosa East Face (Macugnaga, NW Italy). In: Margottini, C., Canuti, P., Sassa, K. (eds.): *Landslide Science and Practice*. Springer Berlin Heidelberg, Berlin, Heidelberg, https://doi.org/10.1007/978-3-642-31310-3_44.
- Thakuri, S., Salerno, F., Smiraglia, C., Bolch, T., D'Agata, C., Viviano, G., Tartari, G. (2014): Tracing glacier changes since the 1960s on the south slope of Mt. Everest (central Southern Himalaya) using optical satellite imagery. *The Cryosphere* 8(4), 1297–1315, <https://doi.org/10.5194/tc-8-1297-2014>.
- Tonolo, F. G., Cina, A., Manzano, A., and Fronteddu, M. (2020): 3D Glacier Mapping by Means of Satellite Stereo Images: The Belvedere Glacier Case Study in the Italian Alps. *The International Archives of the Photogrammetry, Remote Sensing and Spatial Information Sciences*, XLIII-B2-2020, 1073–1079, <https://doi.org/10.5194/isprs-archives-XLIII-B2-2020-1073-2020>.
- Truffer, M., Käab, A., Harrison, W. D., Osipova, G. B., Nosenko, G. A., Espizua, L., Gilbert, A., Fischer, L., Huggel, C., Craw

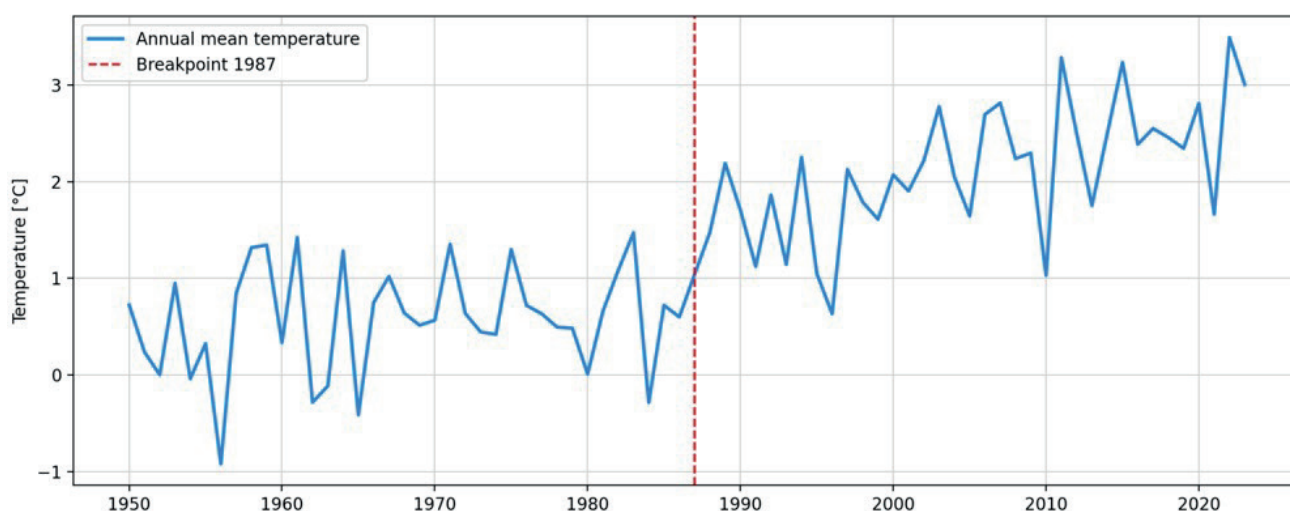
- Burns, P. A., Lai, A. W. (2021): Glacier surges, in: *Snow and Ice-Related Hazards, Risks, and Disasters*. Elsevier, 417–466, <https://doi.org/10.1016/B978-0-12-817129-5.00003-2>.
- Westoby, M. J., Rounce, D. R., Shaw, T. E., Fyffe, C. L., Moore, P. L., Stewart, R. L., Brock, B. W. (2020): Geomorphological evolution of a debris-covered glacier surface. *Earth Surface Processes and Landforms* 45(14), 3431–3448, <https://doi.org/10.1002/esp.4973>.
- Yao, T., Thompson, L., Yang, W., Yu, W., Gao, Y., Guo, X., Yang, X., Duan, K., Zhao, H., Xu, B., Pu, J., Lu, A., Xiang, Y., Kattel, D. B., Joswiak, D. (2012): Different glacier status with atmospheric circulations in Tibetan Plateau and surroundings. *Nature Climate Change* 2, 663–667, <https://doi.org/10.1038/nclimate1580>.
- Zemp, M., Huss, M., Thibert, E., Eckert, N., McNabb, R., Huber, J., Barandun, M., Machguth, H., Nussbaumer, S. U., Gärtner-Roer, I., Thomson, L., Paul, F., Maussion, F., Kutuzov, S., Cogley, J. G. (2019): Global glacier mass changes and their contributions to sea-level rise from 1961 to 2016. *Nature* 568, 382–386, <https://doi.org/10.1038/s41586-019-1071-0>.
- Zeileis, A., Leisch, F., Hornik, K., and Kleiber, C. (2002). *Strucchange: An R package for testing for structural change in linear regression models*. *Journal of Statistical Software* 7(2), 1–38, <https://doi.org/10.18637/jss.v007.i02>.
- Zemp, M., Hoelzle, M., Haeberli, W. (2009): Six decades of glacier mass-balance observations: a review of the worldwide monitoring network. *Annals of Glaciology* 50(50), 101–111, <https://doi.org/10.3189/172756409787769591>.
- WGMS (2024): *Fluctuations of Glaciers Database*. World Glacier Monitoring Service (WGMS), Zurich, Switzerland, <https://doi.org/10.5904/wgms-fog-2024-01>.

Appendix

This supplement offers a supplementary analysis of temperature time series data (Appendix 1) for the location of Belvedere Glacier. The supplementary data and analysis facilitate comprehension of the long-term trends pertinent to the article's primary focus: the intricate, spatially heterogeneous patterns of glacier elevation change resulting from debris cover, avalanches, surge-type events, supraglacial meltwater, and glacial lake outburst floods in the context of global warming.

The data were obtained from the E-OBS dataset, which was generated as part of the EU-FP6 UERRA

project (<http://www.uerra.eu>), and from the Copernicus Climate Change Service. The initial 0.1-degree grid data for daily mean temperature were aggregated to yield annual mean temperature data. A Mann-Kendall test (Kendall 1957) was conducted to identify any potential trends in temperature. The test yielded a p-value of 5.75×10^{-14} , indicating a statistically significant increasing trend. Furthermore, the break dates algorithm, as developed by Zeileis et al. (2002), was used. The analysis identified a breakpoint in 1987 based on the annual mean temperature time series.



Appendix 1 Annual mean temperature time-series for Belvedere Glacier with breakpoint analysis.

Long-term (1951–2023) surface changes of the Belvedere Glacier observed through aerial and UAV orthophotos

Roberto Sergio Azzoni^{1,*}, Irene Maria Bollati¹, Manuela Pelfini¹, Stefano Valzasina¹, Lukáš Brodský²

¹ University of Milan, Earth Science Department, “A. Desio”, Italy

² Charles University, Faculty of Science, Department of Applied Geoinformatics and Cartography, Czechia

* Corresponding author: robertosergio.azzoni@unimi.it

ABSTRACT

Glacier retreat is a key indicator of climate change, with significant implications for geomorphological hazards and ecosystem stability. This article focuses on the surface evolution of the Belvedere Glacier from 1951 to 2023. Using high-resolution orthophotos and manual mapping, we tracked changes in the glacier’s area and shape over time. The results show three significant phases of change: the separation of the Nordend Glacier from the Belvedere Glacier (1951–1991), the partial separation of the central accumulation basin from the debris-covered tongue (2006–2015), and the separation of the Locce Nord Glacier (2018–2021). These changes, combined with a surge event from 1999 to 2002, have significantly altered the glacier’s dynamics and accelerated its retreat. Manual mapping was accurate in areas with scarce debris cover but faced challenges in debris-covered areas due to limited image resolution, snow cover, and debris characteristics. Despite these difficulties, we observed that the glacier remained stable until the late 1990s, when it began a rapid retreat. This recent retreat is consistent with rates observed in the early 20th century. The study highlights the importance of surface mapping to quantify the areal loss and to understand broader changes in glacier structure and mass flow that drive its retreat. Our results provide key data for future studies and highlight the need for continued monitoring of Alpine glaciers in the context of accelerating climate change.

KEYWORDS

glacier mapping; frontal variation; remote-sensing; orthophoto; Belvedere Glacier

Received: 1 November 2024

Accepted: 27 November 2024

Published online: 18 December 2024

Azzoni, R. S., Bollati, I. M., Pelfini, M., Valzasina, S., Brodský, L. (2024): Long-term (1951–2023) surface changes of the Belvedere Glacier observed through aerial and UAV orthophotos. *AUC Geographica* 59(2), 203–213

<https://doi.org/10.14712/23361980.2024.23>

© 2024 The Authors. This is an open-access article distributed under the terms of the Creative Commons Attribution License (<http://creativecommons.org/licenses/by/4.0>).

1. Introduction

Glacier studies are crucial in the context of climate change, as glaciers serve as sensitive indicators of regional and global environmental transformations (Hock and Huss 2021). The accelerated retreat of glaciers worldwide is among the most visible and impactful consequences of rising global temperatures, with significant implications for water resources, sea-level rise, ecosystems services in glacierized and proglacial systems, geoheritage and tourism activities (Garavaglia et al. 2010; D'Agata et al. 2020; Paul et al. 2020; Azzoni et al. 2023; IPCC 2023; Bollati et al. 2023; Fice-tola et al. 2024). Climate-driven glacier retreat reduces glaciers size and triggers several geomorphological hazards like glacier collapse, Glacial Lake Outburst Floods (GLOFs), and debris flow (Racoviteanu et al. 2022). As glaciers melt and retreat, meltwater accumulates in depressions, forming proglacial lakes (Viani et al. 2020). Unstable moraines or ice often dam these lakes, increasing the risk of outburst floods when natural barriers fail and release water downstream (Car-rivick and Tweed 2016). Several GLOFs have devastated communities and infrastructure in regions such as the Himalayas, Andes, and European Alps (Haerberli et al. 2017). Rising temperatures and glaciers thinning heighten the risk of ice and rock avalanches (see e.g. Kropacek et al. 2021). Glacier instability, steep terrain, and melting permafrost drive large-scale collapses, such as the 2002 Kolka Glacier collapse in the Caucasus Mountains (Huggel et al. 2005). Thus, climate change impacts glaciers through both gradual retreat and sudden, catastrophic events, posing serious risks to landscapes and human settlements. Long-term monitoring of glaciers using remote sensing methods

provides essential information to track changes in glacier area, volume, and mass balance, and helps to produce climate models and adaptation strategies (Zekol-lari et al. 2020; Sommer et al. 2021). This monitoring is essential also for debris-covered glaciers, which present a series of unique and complex challenges to those investigating climate-glacier dynamics and their role in downstream impacts (Huo et al. 2021).

Mapping debris-covered glaciers is difficult due to their lack of clear surface features. Indeed, unlike clean ice glaciers, debris-covered glacier surface is similar with surrounding landscape, complicating boundary identification (Bolch et al. 2007). Layers of rock fragments and fine sediments cover these glaciers, obscuring ice margins and internal structures. This debris complicates manual mapping with traditional methods (Bolch et al. 2008). Additionally, factors such as debris thickness, surface slope, and seasonal variations affect mapping accuracy (Bhardwaj et al. 2014). Recent advancements in remote sensing, like combining satellite multispectral imagery with Digital Elevation Models (DEMs), have greatly improved the ability to map debris-covered glaciers automatically (Racoviteanu et al. 2022). This approach detects glacier boundaries more accurately under debris cover (Mitkari et al. 2022). Machine learning algorithms also enhance mapping precision, as shown in the Hunza Basin study by Khan et al. (2020). Deep learning convolutional neural networks (LeCun et al. 2015) now outperform traditional machine learning, especially in spatially complex tasks like glacier boundary mapping (Xie et al. 2020). SAR interferometry coherence has also proven effective in accurately mapping ablation areas (Lippl et al. 2018; Ahmad and Fugazza 2023). Despite these innovative semi-automated

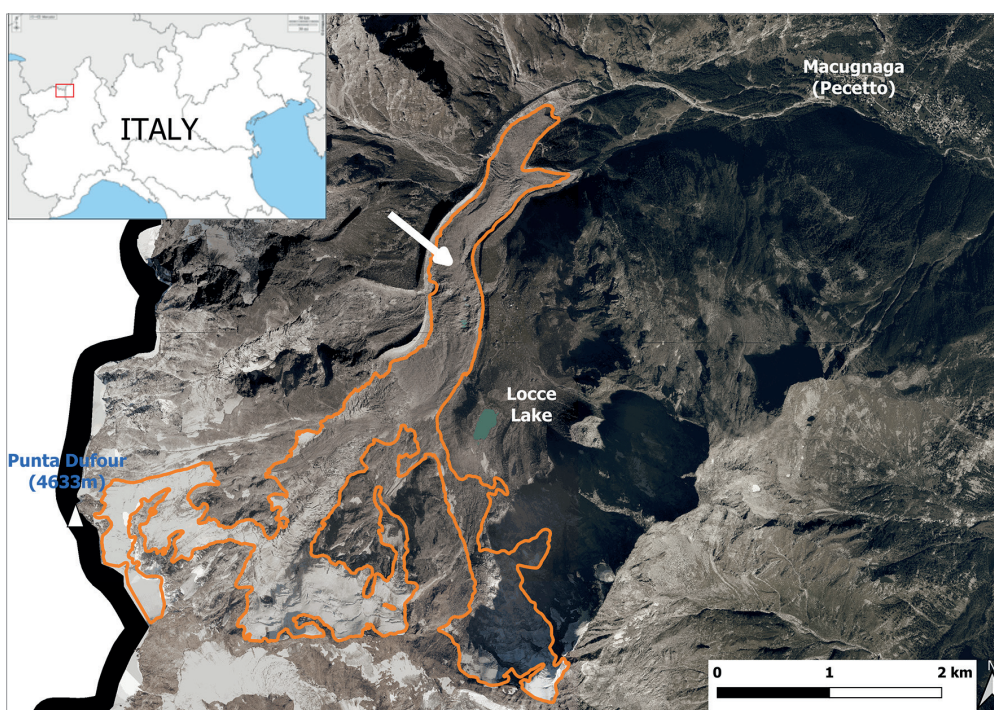


Fig. 1 Belvedere Glacier location map. The background image refers to the 2018 aerial orthophoto (0.3 m resolution) available on the Piemonte Region Web GIS. The glacier perimeter (in orange) was produced by the authors based on the same orthophoto. The debris-cover tongue is indicated by the white arrow.

methods, orthophoto analysis and manual mapping remain highly accurate for small-scale analysis. These methods provide a reliable temporal record for tracking changes in glacier extent and debris cover over time (Azzoni et al. 2018).

The Belvedere Glacier, on the eastern slope of Monte Rosa in the Italian Alps, represents a unique case in the Alpine region. Classified as a debris-covered glacier, it exemplifies hazards linked to deglaciation. Rockfalls, icefalls, GLOFs, glacier surges, and debris flows have marked its history reported in several studies conducted over the past 50 years as reviewed by Kropáček et al. (2024) in this issue. To better understand the evolution of this significant glacier, this study analyses the Belvedere Glacier evolution by manually identifying glacier boundaries using high-resolution orthophotos from 1951 to 2023. In detail this study aims to track changes in the glacier's area and to examine glacier-related hazards in a broader context. It also explores the role of paraglacial processes (*sensu* Ballantyne 2002), which are featuring the deglaciation stage due to global warming.

1.1 Study area

The Belvedere Glacier lies on the eastern slope of Monte Rosa (4634 m a.s.l.), a prominent peak in the western Italian Alps along the Italian-Swiss border. As one of the largest debris-covered glaciers in the Alps, covers 4.51 km² (Mortara et al. 2009; Smiraglia et al. 2015). The debris-covered tongue extends from approximately 2250 m a.s.l. to its lowest point at around 1800 m a.s.l., where it divides into two distinct lobes. This tongue covers an area of 1.8 km², measuring 3 km in length and reaching a maximum width of about 0.5 km. In 1999–2002, the glacier underwent a surge-type event (Kääb et al. 2004), whose effects are still recorded in the dynamics of lateral moraines (Bollati et al. 2024, in this issue). Numerous studies have focused on the Belvedere Glacier in recent years. For a detailed list, please refer to the review by Kropáček et al. (2024).

2. Material and methods

High-resolution orthophotos served as the main source of information for the Belvedere Glacier area. In order to delineate the glacier boundaries and calculate the areas, historical greyscale, and recent colour orthophotos were analysed, as shown in Tab. 1. The orthophotos are derived from high-resolution aerial photographs and are characterised by low or no cloud cover. They were mostly acquired at the end of summer when the glaciers have minimal snow cover, making their boundaries clearer and easier to detect. The orthophotos were used as a base layer in QGIS Desktop 3.36 for detecting and mapping glacier boundaries, enabling surface area calculations.

Tab. 1 Details of the images used for the mapping of the Belvedere Glacier.

Year	Type	Source	Resolution (m)
1951	orthophoto	IGM	0.5
1991	orthophoto	Piedmont Region – WMS	1.0
1994	orthophoto	MASE – WMS	1.0
2000	orthophoto	MASE – WMS	0.5
2006	orthophoto	MASE – WMS	0.5
2015	orthophoto	AGEA – WMS	0.5
2018	orthophoto	AGEA – WMS	0.3
2021	orthophoto	AGEA – WMS	0.2
2023	orthophoto	UAV flight (authors)	0.1

Notes: IGM: Italian Military Geographic Institute, MASE: Ministry of Environment and Energy Security, AGEA: National Agency for Agriculture; WMS: Web Map Service. Detailed information about 1951 orthophoto processing and 2023 UAV survey are available on Brodský et al. (2024).

To identify the glacier boundaries across different years, we performed manual mapping based on the interpretation of the glacier boundaries. Mapping proved to be easier in debris-free areas but posed challenges on the debris-covered ablation tongue. To ensure accurate and consistent mapping, enhancing the understanding of glacier changes over time, we applied specific guidelines:

Following clear geomorphological features: we identified and traced stable, visible glacier contours, such as ridge or moraines, and used distinctive signs like crevasses, edges, and color or texture changes to trace the glacier's structure.

Avoiding seasonal snow: we distinguished between permanent glacier ice and seasonal or temporary snow cover to maintain mapping precision.

Simplifying lines where appropriate: we avoided adding unnecessary details. Simpler lines are often more effective for representing the actual glacier boundaries, especially if minor details do not affect the overall representation.

Digitizing consistently at an appropriate zoom level: we chose a zoom level that allowed clear visualization of necessary details without excessive precision, which could lead to overlay complex traces.

Accounting for shadows and terrain: shadows and natural terrain features were considered, as they can alter the perception of glacier boundaries. We used images taken in optimal lighting to minimize misinterpretation.

Using multiple layers for comparison: by overlaying images from different periods or seasons we compared changes over time, even if lower resolution. This helps verify mapping accuracy and distinguish permanent areas from those subject to seasonal variations.

Operator experience was crucial for interpreting surface features accurately, as verified by comparing the 2023 drone image mapping with field observations from the same year. Orthophotos, available only

in RGB format and accessed via WMS, limited our ability to apply automatic or semi-automatic mapping methods, such as band combinations and filters, suggested by Paul et al. (2017). To enhance data accuracy, we conducted multiple digitization experiments following Paul et al. (2017). For each year, we digitized the boundaries three times independently and calculated the mean area and standard deviation. Accuracy was expressed as the percentage ratio between the standard deviation and the mean glacier area for each year. We excluded 1951 and 2023 from error assessment due to incomplete orthophoto coverage of the glacier area.

In addition to mapping glacier boundaries from orthophotos, we analyzed frontal variations measured over the past century and published in the Bulletins of the Glaciological Committee and later Open Access in the journal *Geografia Fisica e Dinamica Quaternaria* (<https://www.gfdq.glaciologia.it/index.php/GFDQ>). These *in situ* measurements provide precise records of frontal changes, allowing for direct comparison with variations derived from orthophoto analysis.

3. Results

Tab. 2 shows the surface area evolution of the Belvedere Glacier from 1951 to 2023, with incomplete data for 1951 and 2023 due to the lack of complete orthophotos. For the other years (1991, 1994, 2000, 2006, 2015, 2018, and 2021), four manual mapping attempts were made to evaluate the accuracy of this method (Paul et al. 2017). The 2021 data represents the aggregate surface area of the Belvedere Glacier and the Locce Glacier to preserve comparability with the previous years. The results show that the mapped areas slightly vary between the attempts made for that year. For example, in 2006, the standard deviation is significantly higher (0.259 km^2) than in the other years, indicating greater variability in the attempts.

Regarding the method's accuracy, the calculated percentage error varies between years. For example,

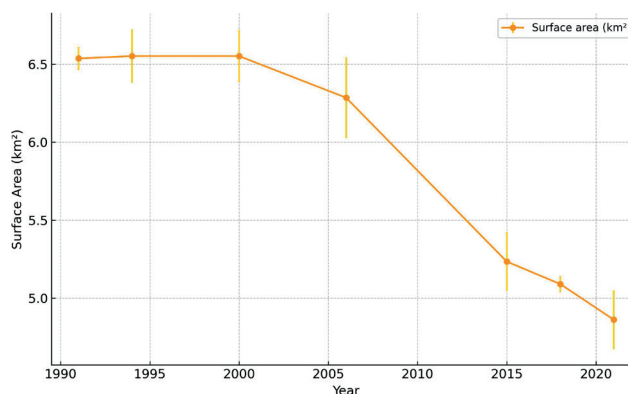


Fig. 2 The evolution of the surface area of the Belvedere Glacier from 1991 to 2021 is reported. Error bars represent the standard deviation for each year based on four manual mapping attempts (Tab. 2).

the error in 2018 is as low as 1.0%, indicating high precision in mapping that year, while in 2006, the error reaches over 4.1%, reflecting greater variability and thus reduced precision. This variation in error suggests that the manual mapping method performs with higher accuracy in some years than others, potentially influenced by factors such as image quality, seasonal snow cover, and shadow effects. Overall, the accuracy of the method averages between 1-4%, which aligns with acceptable standards for manual glacier boundary mapping in long-term studies (Paul et al. 2017), though it underscores the importance of multiple mapping attempts to minimize errors.

Fig. 2 illustrates the changing surface area of the Belvedere Glacier between 1991 and 2021, considering only the years with a complete mapping (i.e., 1991, 1994, 2000, 2006, 2015, 2018, 2021), revealing two distinct phases in its evolution. The first phase, spanning from 1991 until approximately 2000, indicates a relatively stable glacier surface area, even exhibiting a slight increase. This subtle growth may be linked to the early stages of the surge event whose acme was observed in 2001–2002, a phenomenon wherein a glacier experiences rapid advance due to the build-up and subsequent release of subglacial meltwater

Tab. 2 Surface area measurements (in km^2) of the Belvedere Glacier from 1951 to 2023, based on manual mapping attempts and related Standard Deviation (SD) and Accuracy. Only partial data are available for 1951 and 2023 due to the lack of complete orthophotos. The 2021 data represents the aggregate surface area of the Belvedere Glacier and the Locce Glacier.

Year	Surface (km^2)	Surface (km^2) Attempt 2	Surface (km^2) Attempt 3	Surface (km^2) Attempt 4	Surface (km^2) Mean	SD (km^2)	Accuracy
1951	2.691*						
1991	6.537	6.708	6.676	6.652	6.643	0.074	1.1%
1994	6.551	6.291	6.662	6.642	6.536	0.171	2.6%
2000	6.552	6.783	6.742	6.422	6.625	0.169	2.6%
2006	6.285	6.495	5.975	6.545	6.325	0.259	4.1%
2015	5.234	5.444	5.075	5.480	5.308	0.190	3.6%
2018	5.090	5.181	5.201	5.197	5.168	0.052	1.0%
2021	4.861	4.709	4.681	5.091	4.836	0.188	3.9%
2023	1.091*						

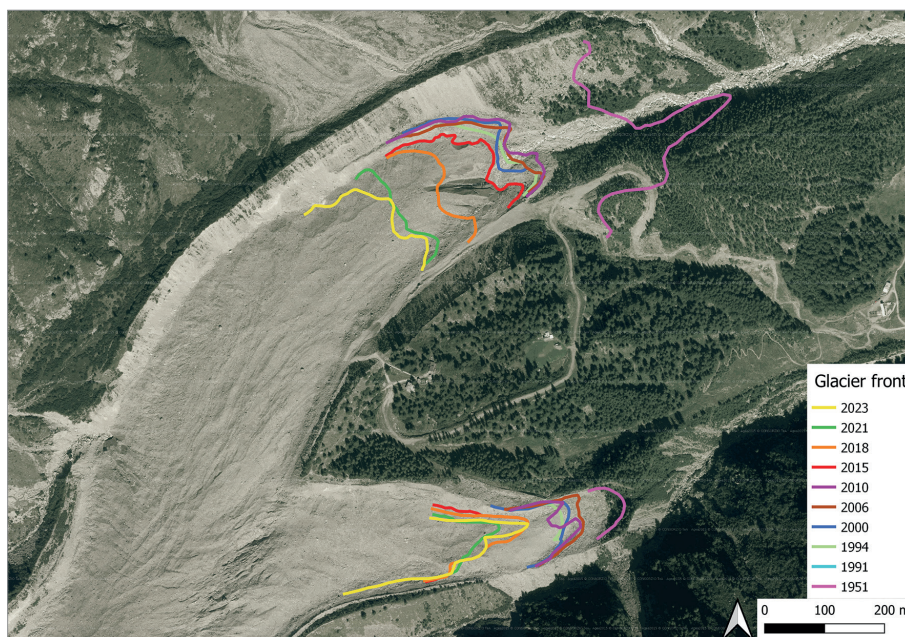


Fig. 3 The position of the front of the two lobes of the Belvedere Glacier during the period 1951–2023. The orthophoto in the background is from 2015 (WMS by AGEA; Tab. 1).

or internal ice dynamics. This period of stability, and slight expansion, could reflect also conditions favourable to glacier thickening, such as sustained winter snowfall or cooler summer temperatures, which would have counterbalanced typical ablation (i.e., ice loss) rates.

The second phase, which begins post-2000 (after the surge exhaustion, 2002–2003) and extends to 2021, shows a marked shift to an extreme negative trend in the glacier’s surface area (Fig. 2). This sharp decline from about 6.5 km² down to below 5.5 km² after 2013 year indicates accelerated ice loss, likely intensified by rapid retreat following surge events that reduce support from lateral moraines. Additionally, increased warming trends contribute to this process. The continued surface area reduction aligns with regional observations of glacier mass loss driven by rising temperatures, which increase melt rates,

reduce glacier thickness, and can fragment the glacier structure.

The analysis of orthophotos highlights the evolution of the front position of the two lobes from 1951 to 2023, as shown in Figure 3. The north-western lobe shows a significant retreat from 1951 to 1991. From 1991 to 2015, glacier front variation decreases (about 25 m). During this period, the 2006 front is notably more advanced than in 1991, 1994, and 2001, with the latter two being almost identical. This suggests that effects of the 1999–2002 surge are visible even four years later. The substantial ice mass transfer to lower elevations led to pronounced retreat in the following years, especially from 2015 to 2021, where some areas retreated by 200 meters within six years.

In contrast, the south-eastern lobe displays less dynamic movement (Fig. 3). Frontal changes are smaller (160 m versus more than 400 m in 1951–2023-time

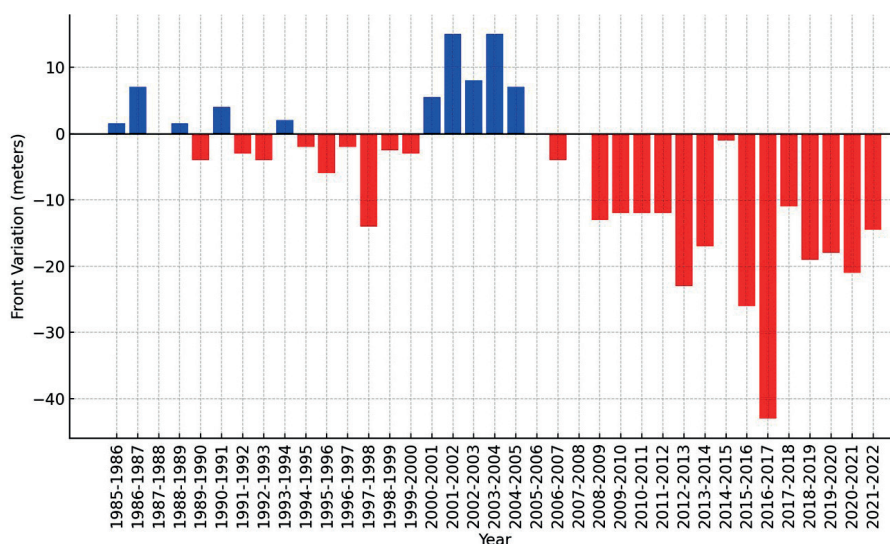


Fig. 4 Annual frontal variation of the Belvedere Glacier (north-western lobe) in the period 1985–2022. Source: Annual Glaciological Survey of Italian Glaciers reported in the “*Bollettino del Comitato Glaciologico Italiano*” (Baroni et al. 2022).

span), revealing three distinct phases. The first phase is a significant retreat from 1951 to 1991. The second phase, from 1991 to 2010, shows relative stability and includes the surge event, which remains visible. The third phase, marked by a notable retreat, spans 2015 to 2021, with the front position remaining largely stable. This reduced glacial activity in the south-eastern lobe has contributed to greater frontal stability in this part of the glacier.

Data from the Bulletin of the Italian Glaciological Committee from 1985 to 2021 (Baroni et al. 2022) enable a detailed analysis of changes in the glacier's frontal position. These annual data specifically track the north-western lobe of the glacier. Figure 4 shows several notable trends. From 1985 to 2000, the glacier front remained relatively stable, with a slow progression (+10 m) followed by slight retreat (−35 m). This pattern aligns with the behaviour of Alpine glaciers, where a rapid but strong positive glacial pulse concluded in the late 1980s (Diolaiuti et al. 2003). Between 2000 and 2006, the glacier advanced by over 50 meters due to a surge. After three years of stability following the surge, the glacier front began a prolonged and intense retreat, peaking in 2017 with a 43-meter reduction. The latest data on frontal variation (2022) show a retreat of 14.5 meters, close to the 17.8 meter retreat reported by Ioli et al. (2024).

To extend the record of glacier front variation and compare measured data with observations from the 1951 orthophoto, we also considered data from the Report of the glaciological survey of 1985 (Armando et al. 1986), which provides cumulative glacier variation data since 1922 (Fig. 5). Although the temporal resolution is lower (only four data points over 63 years), this period reveals a significant glacier retreat from the start of measurements until the mid-1970s, when colder conditions led to front stability. Data from 1957 align with observations from the orthophoto. The graph slope indicates that the retreat rate over the past decade matches rates recorded in the early 1900s.

4. Discussion

To better define the evolution of the Belvedere Glacier, we analysed the rate of glacier surface change. Fig. 6 shows this rate from 1991 to 2021, with each bar representing the rate of glacier surface area change between consecutive measurements. We calculated this rate as the difference in surface area divided by the years elapsed. Error bars indicate uncertainty, based on the standard deviation of manual mapping attempts (Tab. 2).

The graph reveals a consistent decreasing trend of surface area reduction, particularly in the latter half of the interval. In the first two periods, the glacier remains nearly stable, showing no significant area changes. Around 2000, despite the surge event, a clear increase in the rate of area reduction emerges, intensifying in more recent periods. The negative peak between 2007 and 2015 likely reflects the surge, which transported a large ice mass to lower elevations where it then melted rapidly. Unfortunately, the orthophoto timing doesn't allow for exact mapping of the surge's advance. A detailed analysis of the surge dynamics lies beyond this study's scope and has been covered in previous works (e.g., Mortara et al. 2009), including analyses using satellite imagery (Landsat data; Haeberli et al. 2002).

Mapping debris-covered glaciers presents considerable challenges and uncertainties (Paul et al. 2017). In this study, we applied manual mapping and assessed the accuracy of this approach through four mapping attempts. Results show accuracy rates ranging from 1.0% in 2018 to 4.1% in 2006.

Several factors influence this variability: image resolution, snow cover, and the timing of orthophoto acquisition. The highest accuracy (1.0%) was achieved in 2018 with high-resolution orthophotos (0.3 m/pixel) and no snow cover, allowing for simpler and more precise mapping. The 2021 orthophoto, though offering the highest resolution (0.2 m/pixel), produced an accuracy of 3.6% due to snow cover over accumulation basins. In contrast, the 1991 orthophoto, despite lower

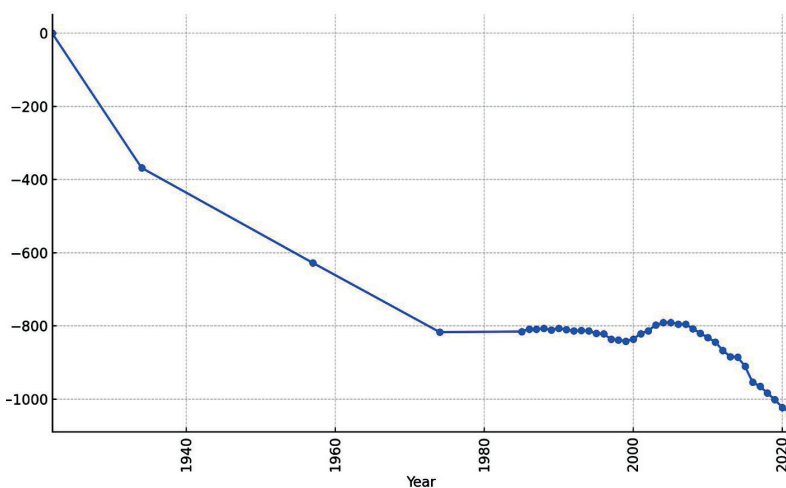


Fig. 5 Frontal variation of the Belvedere Glacier from 1922 to 2021.

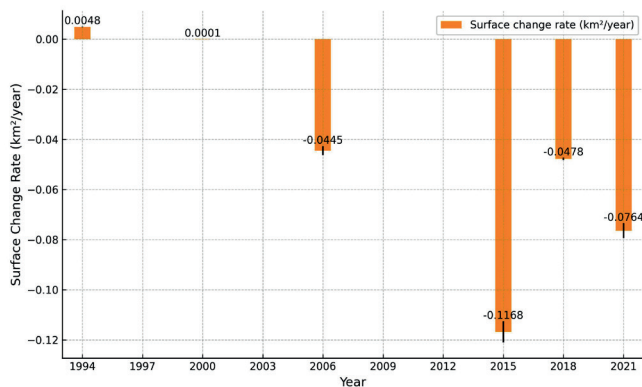


Fig. 6 Bar chart showing the surface change rate of the Belvedere Glacier from 1991 to 2021, with error bars representing the uncertainty in manual mapping attempts. Labels above each bar indicate the calculated surface change rate in km²/year.

resolution (1.0 m/pixel) and being black and white, achieved excellent accuracy due to minimal snow cover.

The 2006 orthophoto represents a unique case, showing the lowest accuracy (4.1%). Although the resolution was good (0.5 m/pixel) with minimal snow cover, overexposure reduced perimeter accuracy. Using WMS data (Tab. 1) prevented adjustments to exposure, which could have improved data quality.

The glacier perimeter mapping and multitemporal orthophoto analysis enabled quantification of areal variation and front position evolution. This approach also revealed general dynamics in the morphology of the Belvedere Glacier and its interactions with tributary glaciers, significantly impacting the recent evolution of the glacier tongue. Three key phases were identified between 1951 and 2023:

- The rupture of the connection between the Nordend Glacier and the Belvedere Glacier between 1951 and 1991.
- The partial interruption of the connection between the central accumulation basin of the Belvedere and the debris-covered tongue between 2006 and 2015.

- The rupture of the connection between the Locce Nord accumulation basin and the Belvedere Glacier between 2018 and 2021.

The glacier’s retreat led to a significant event impacting the evolution of the Belvedere Glacier’s ablation tongue. The separation of the Nordend Glacier from the Belvedere Glacier, visible in the comparison between the 1951 orthophoto (Fig. 7A) and the 1991 orthophoto (Fig. 7B), severed the connection to an important accumulation basin for the Belvedere Glacier. The Nordend Glacier covered approximately 0.63 km² in 1957 and 0.57 km² in 2010, maintaining a maximum elevation above 3500 meters a.s.l. (Smiraglia et al. 2015). Until the 1950s, it provided a significant mass input to the debris-covered tongue of the Belvedere Glacier.

Two other changes in the glacier morphology have had a significant impact on the evolution of the ablation tongue (Fig. 8). The central part of the accumulation basin was connected to the main debris-covered tongue by two large icefalls, which gradually decreased in size over time. Between 2010 (Fig. 8a) and 2015 (Fig. 8b), one of these two connecting icefalls was severed, directing the entire glacial flow through the main icefall. The last and most significant change in the glacier shape was the separation of Locce Nord Glacier from the Belvedere Glacier, which occurred between 2018 (Fig. 8C) and 2021 (Fig. 8D). Field observations confirmed this separation. In 2021, Tab. 2 reports a total glacier area of 4.86 km², the result of combining the Belvedere and the Locce glaciers that had already separated. This is incorrect from a glaciological perspective: indeed the Locce Glacier (0.98 km²) should be considered as a glacial body, dynamically separated from the Belvedere Glacier (3.88 km²). This type of fragmentation observed on the Belvedere Glacier is a typical situation for many Alpine glaciers in the current context of climate change (Smiraglia et al. 2015).

The effects of these two separations are evident in the glacier’s evolution and will become increasingly

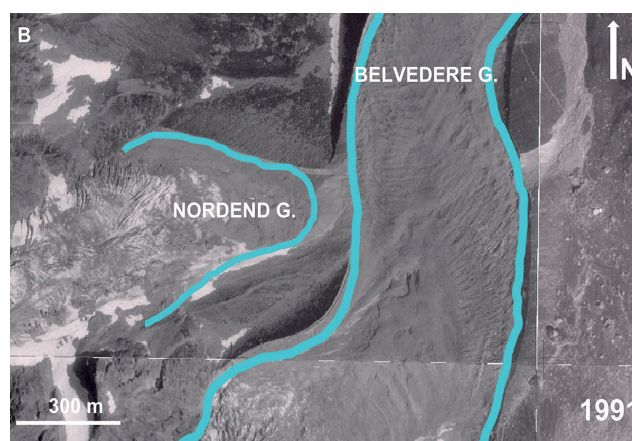
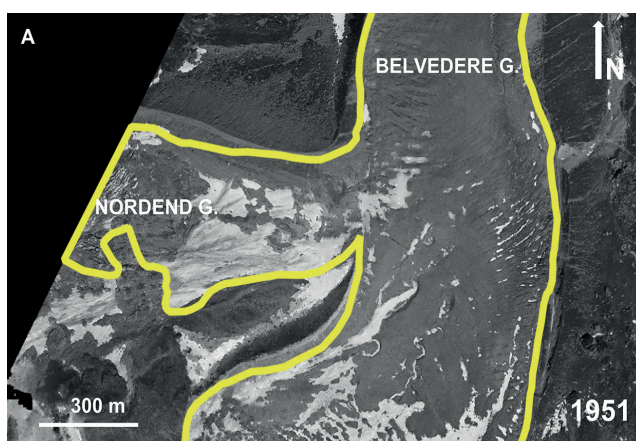


Fig. 7 Comparison between 1951 (a) and 1991 (b), where the interruption of the connection between the Nordend Glacier and the Belvedere Glacier is clearly evident.

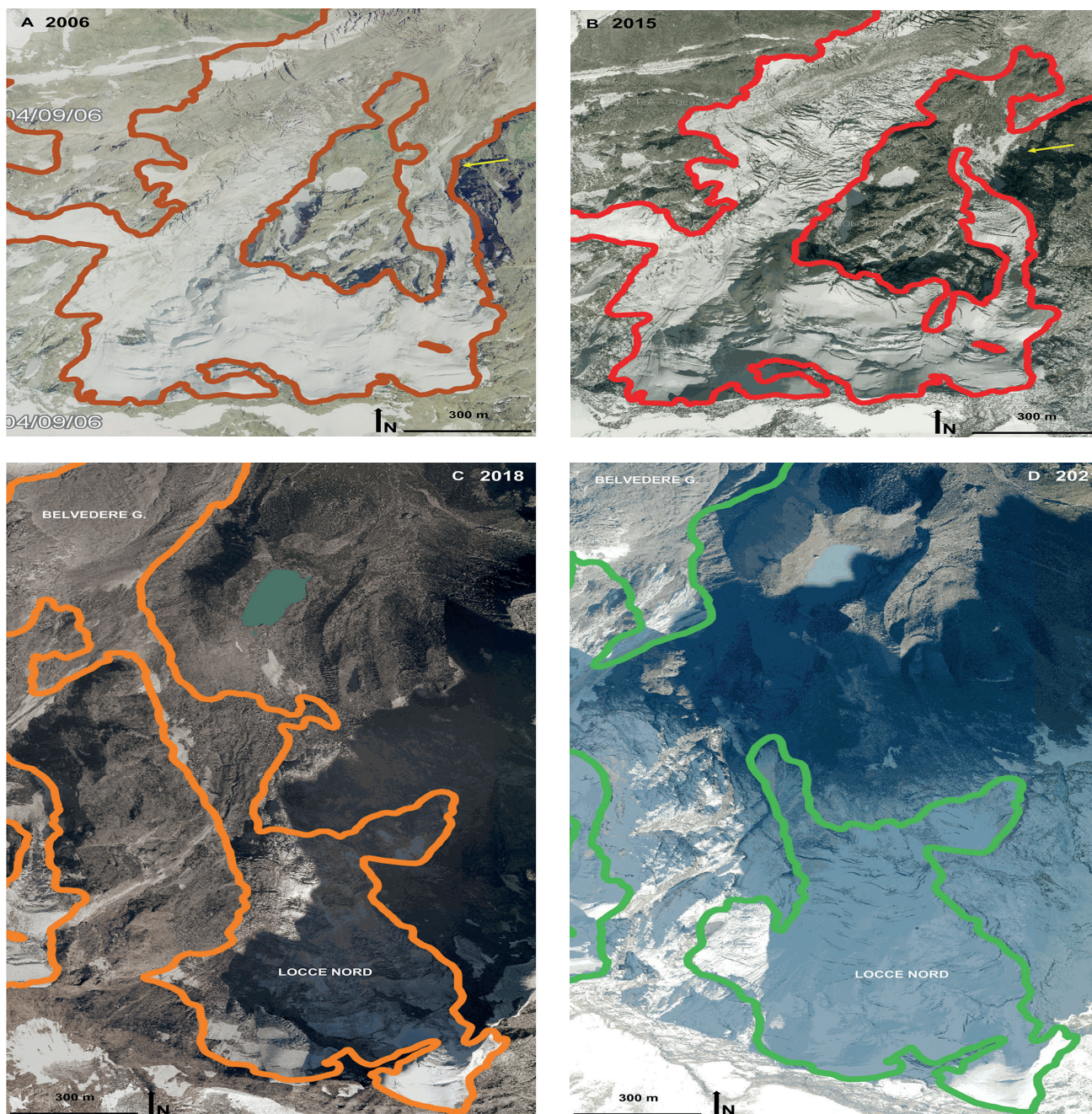


Fig. 8 Fragmentation of the central accumulation basin of the Belvedere Glacier occurred between 2006 (A) and 2015 (B), and the detachment of the Locce Glacier from the main body of the Belvedere Glacier occurred between 2018 (C) and 2021 (D).

pronounced. The absence of glacial flow from the Locce Glacier, which ceased only a few years ago, will further impact the main glacier tongue. Reduced mass transfer leads to localized surface lowering and a decrease in downglacier surface gradient. This, in turn, lowers driving stress and glacier velocity, causing the lower ablation zones to become increasingly stagnant (Benn et al. 2012; Nuimura et al. 2017). As downwasting progresses in the future, formerly efficient supraglacial and englacial drainage networks will break up, and supraglacial lakes will probably form in surface depressions. Ablation rates around these lakes are typically one or two orders of

magnitude higher than sub-debris melt rates, meaning that extensive lake formation accelerates overall ice loss. This process drastically alters surface topography and debris cover, leading to a rapid decline in glacier volume.

5. Conclusions

The analysis of the Belvedere Glacier highlights the critical role of surface mapping, not only for obtaining numerical data but also in assessing glacier morphological evolution. Changes observed in the

glacier surface and frontal dynamics provide valuable insights into the broader processes governing ice flow and retreat. Between 1951 and 2023, significant morphological transformations occurred, notably the disconnection of tributary glaciers (Nordend and Locce), which greatly impacted the glacier's mass flow and retreat dynamics.

The mapping approach used in this study, combining orthophotos analysis and manual delineation of glacier boundaries, demonstrated both the challenges and benefits of studying debris-covered glaciers. Although the manual mapping method showed acceptable accuracy, the debris cover presented complexities, especially in areas where thick debris layers obscured ice boundaries. Despite these challenges, the results presented a clear picture of the glacier's evolution, showing periods of stability and retreat, with a surge event at the beginning of the 2000s, temporarily affecting glacier dynamics.

The study confirms that the recent retreat rate mirrors patterns observed in the early 20th century, indicating a return to high rates of ice loss. The disconnection of the tongue from two accumulation basins have accelerated retreat and downwasting processes, which could lead to a completely new dynamic for the glacier, not observed in the past century.

In conclusion, mapping of glacier surfaces, especially for debris-covered glaciers like the Belvedere, is essential for tracking areal changes and understanding the evolving dynamics of ice flow, mass balance and the associated geomorphological hazards, especially link with paraglacial-type processes featuring deglaciation stages. As glaciers continue to respond to climate change, ongoing monitoring and high-resolution mapping will be crucial for predicting future trends and mitigating risks.

Data availability

The orthophotos used in this work are available through the WMS service of the Ministry of Environment and Energy Security (<https://gn.mase.gov.it/portale/servizio-di-consultazione-wms>) and the Piedmont Region (<https://www.geoportale.piemonte.it>). The 1951 and 2023 orthophotos and the glacier outlines are available on Zenodo (Brodsky et al. 2024b; Azzoni et al. 2024).

Acknowledgements

This research was funded by the 4EU+ project Remote Sensing of the Cryosphere Dynamics under the Influence of Climate Change, grant number 4EU+/23/F4/19. Disk space to store remote sensing images was supplied by the project “e-Infrastruttura CZ” (e-INFRA CZ LM2018140) supported by the Ministry of Education, Youth and Sports of the Czech Republic.

This research was also partly funded by University of Milan through the Sostegno alla ricerca Project 2022 (Evoluzione dei processi geomorfologici e degli impatti sul ciclo idrologico in contesti sensibili al cambiamento climatico) and supported by GEOTRes (Geoheritage threatening and resilience: mapping the impact of geomorphic and human processes in sensitive morphoclimatic environments) project financed by the Italian Ministry of University and Research (MUR), grant PRIN202223RAZZO_01 (P.I. R.S. Azzoni). The Authors would like to thank the Province of Verbano-Cusio-Ossola for the permit of UAV (dr. Andrea De Zordi, Settore III – Assetto del Territorio Georisorse e Tutela Faunistica, Servizio Rete Natura 2000 e Forestazione).

References

- Ahmad, A., Fugazza, D. (2023): Fusion of Sentinel-1 Interferometric Coherence and Sentinel-2 MSI for Debris-Covered Glacier Boundary Delineation: Case Study of Batura, Passu, Ghulkin, and Gulmit Glaciers, Pakistan. *Geografia Fisica e Dinamica Quaternaria* 46(1–2), 229–240.
- Armando, E., Smiraglia, C., Zanon G. (1986): Report of the glaciological survey of 1985. *Geografia Fisica e Dinamica Quaternaria* 9(2), 81–136.
- Azzoni, R. S., Fugazza, D., Zerboni, A., Senese, A., D'Agata, C., Maragno, D., Carzaniga, A., Cernuschi, M., Diolaiuti, G. A. (2018): Evaluating high-resolution remote sensing data for reconstructing the recent evolution of supra glacial debris: A study in the Central Alps (Stelvio Park, Italy). *Progress in Physical Geography: Earth and Environment* 42(1), 3–23, <https://doi.org/10.1177/0309133317749434>.
- Azzoni, R. S., Pelfini, M., Zerboni, A. (2023): Estimating the Evolution of a Post-Little Ice Age Deglaciated Alpine Valley through the DEM of Difference (DoD). *Remote Sensing* 15(12): 3190, <https://doi.org/10.3390/rs15123190>.
- Azzoni R. S., Bollati I. M., Pelfini M., Valzasina S. Brodsky L. (2024): Surface Evolution of the Belvedere Glacier from aerial and UAV orthophotos from 1951 to 2023 – glacier outlines dataset, <https://doi.org/10.5281/zenodo.14059745>.
- Ballantyne, C. K. (2002): Paraglacial geomorphology. *Quaternary Science Reviews* 21(18–19), 1935–2017, [https://doi.org/10.1016/S0277-3791\(02\)00005-7](https://doi.org/10.1016/S0277-3791(02)00005-7).
- Baroni, C., Bondesan, A., Carturan, L., Chiarle, M., Scotti, R. (2022): Annual Glaciological Survey of Italian Glaciers (2021). *Geografia Fisica e Dinamica Quaternaria* 45(1), 69–167.
- Bhardwaj, A., Joshi, P. K., Singh, M. K., Sam, L., Gupta, R. D. (2014): Mapping debris-covered glaciers and identifying factors affecting the accuracy. *Cold Regions Science and Technology* 106–107, 161–174, <https://doi.org/10.1016/j.coldregions.2014.07.006>.
- Benn, D. I., Bolch, T., Hands, K., Gulley, J., Luckman, A., Nicholson, L. I., Quincey, D., Thompson, S., Toumi, R., Wiseman, S. (2012): Response of debris-covered glaciers in the Mount Everest region to recent warming, and

- implications for outburst flood hazards. *Earth-Science Reviews* 114(1–2), 156–174, <https://doi.org/10.1016/j.earscirev.2012.03.008>.
- Bolch, T., Buchroithner, M. F., Kunert, A., Kamp, U. (2007, June): Automated delineation of debris-covered glaciers based on ASTER data. In *Geoinformation in Europe. proceedings of the 27th EARSeL Symposium* (pp. 4–6).
- Bolch, T., Buchroithner, M. F., Pieczonka, T., Kunert, A. (2008): Planimetric and volumetric glacier changes in the Khumbu Himal, Nepal, since 1962 using Corona, Landsat TM and ASTER data. *Journal of Glaciology* 54(187), 592–600, <https://doi.org/10.3189/002214308786570782>.
- Bollati, I. M., Viani, C., Masseroli, A., Mortara, G., Testa, B., Tronti, G., Pelfini M., Reynard, E. (2023): Geodiversity of proglacial areas and implications for geosystem services: A review. *Geomorphology* 421: 108517, <https://doi.org/10.1016/j.geomorph.2022.108517>.
- Bollati, I. M., Azzoni, R. S., Tagliaferri, A., Tronti, G., Pelfini, M., Vilmeck, V., Brodsky, L. (2024): What do trees reveal about the sliding of the lateral moraine of the Belvedere Glacier (western Italian Alps)? *AUC Geographica* 59(2), 255–271, <https://doi.org/10.14712/23361980.2024.14>.
- Brodsky, L., Pancholi, S., Schmidt, S., Nusser, M., Azzoni, R. S., Tronti, G. (2024): Belvedere Glacier elevation change between 1951 and 2023. *AUC Geographica* 59(2), 184–202, <https://doi.org/10.14712/23361980.2024.22>.
- Brodsky, L., Pancholi, S., Schmidt, S., Nusser, M., Azzoni, R., Tronti, G. (2024b): Belvedere Glacier 1951 and 2023 datasets. Zenodo, <https://doi.org/10.5281/zenodo.14063811>.
- Carrivick, J. L., Tweed, F. S. (2016): A global assessment of the societal impacts of glacier outburst floods. *Global and Planetary Change* 144, 1–16, <https://doi.org/10.1016/j.gloplacha.2016.07.001>.
- D'Agata, C., Diolaiuti, G., Maragno, D., Smiraglia, C., Pelfini, M. (2020): Climate change effects on landscape and environment in glacierized Alpine areas: retreating glaciers and enlarging forelands in the Bernina group (Italy) in the period 1954–2007. *Geology, Ecology, and Landscapes* 4(1), 71–86, <https://doi.org/10.1080/24749508.2019.1585658>.
- Diolaiuti, G., D'Agata, C., Smiraglia, C. (2003): Belvedere Glacier, Monte Rosa, Italian Alps: tongue thickness and volume variations in the second half of the 20th century. *Arctic, Antarctic, and Alpine Research* 35(2), 255–263, [https://doi.org/10.1657/1523-0430\(2003\)035\[0255:BGMRIA\]2.0.CO;2](https://doi.org/10.1657/1523-0430(2003)035[0255:BGMRIA]2.0.CO;2).
- Garavaglia, V., Pelfini, M., Bollati, I. (2010): The influence of climate change on glacier geomorphosites: the case of two Italian glaciers (Miage Glacier, Forni Glacier) investigated through dendrochronology. *Geomorphologie: Relief, Processus, Environnement* 16(2), 153–164, <https://doi.org/10.4000/geomorphologie.7895>.
- Haeberli, W., Kääb, A., Paul, F., Chiarle, M., Mortara, G., Mazza, A., Deline, P., Richardson, S. (2002): A surge-type movement at Ghiacciaio del Belvedere and a developing slope instability in the east face of Monte Rosa, Macugnaga, Italian Alps. *Norsk Geografisk Tidsskrift-Norwegian Journal of Geography* 56(2), 104–111, <https://doi.org/10.1080/002919502760056422>.
- Haeberli, W., Schaub, Y., Huggel, C. (2017): Increasing risks related to landslides from degrading permafrost into new lakes in de-glaciating mountain ranges. *Geomorphology* 293, 405–417, <https://doi.org/10.1016/j.geomorph.2016.02.009>.
- Hock, R., Huss, M. (2021): Glaciers and climate change. In *Climate change*, 157–176. Elsevier, <https://doi.org/10.1016/B978-0-12-821575-3.00009-8>.
- Huggel, C., Zraggen-Oswald, S., Haeberli, W., K. A., Polkvoj, A., Galushkin, I., Evans, S. G. (2005): The 2002 rock/ice avalanche at Kolka/Karmadon, Russian Caucasus: assessment of extraordinary avalanche formation and mobility, and application of QuickBird satellite imagery. *Natural Hazards and Earth System Sciences* 5(2), 173–187, <https://doi.org/10.5194/nhess-5-173-2005>.
- Huo, D., Bishop, M. P., Bush, A. B. (2021): Understanding complex debris-covered glaciers: Concepts, issues, and research directions. *Frontiers in Earth Science* 9: 652279, <https://doi.org/10.3389/feart.2021.652279>.
- Ioli, F., Dematteis, N., Giordan, D., Nex, F., Pinto, L. (2024): Deep Learning Low-cost Photogrammetry for 4D Short-term Glacier Dynamics Monitoring. *PFJ Journal of Photogrammetry, Remote Sensing and Geoinformation Science*, 1–22, <https://doi.org/10.1007/s41064-023-00272-w>.
- IPCC (2023): Climate Change 2023: Synthesis Report. Contribution of Working Groups I, II and III to the Sixth Assessment Report of the Intergovernmental Panel on Climate Change [Core Writing Team, H. Lee and J. Romero (eds.)]. IPCC, Geneva, Switzerland, 35–115.
- Ficetola, G. F., Marta, S., Guerrieri, A., Cantera, I., Bonin, A., Cauvy-Frauni, S. et al. (2024): The development of terrestrial ecosystems emerging after glacier retreat. *Nature* 632, 336–342, <https://doi.org/10.1038/s41586-024-07778-2>.
- Kääb, A., Huggel, C., Barbero, S., Chiarle, M., Cordola, M., Epifani, F., Haeberli, W., Mortara, G., Semino, P., Tamburini, A., Viazzo, G. (2004): Glacier hazards at Belvedere Glacier and the Monte Rosa East Face, Italian Alps: Processes and Mitigation. *Internationales Symposium Interpraevent 2004 – Riva/Trient*. <https://api.semanticscholar.org/CorpusID:51803664>.
- Khan, A. A., Jamil, A., Hussain, D., Taj, M., Jabeen, G., Malik, M. K. (2020) Machine-Learning Algorithms for Mapping Debris-Covered Glaciers: The Hunza Basin Case Study. *IEEE Access* 8, 12725–12734, <https://doi.org/10.1109/ACCESS.2020.2965768>.
- Kropacek, J., Vilimek, V., Mehrishi, P. (2021): A preliminary assessment of Chamoli ice and rock fall in Indian Himalayas by remote sensing. *Landslides*, 18, 8, 3489–3497.
- Kropáček, J., Mehrishi, P., Bollati, I. M., Brodsky, L., Pelfini, M., Azzoni, R. S., Schmidt, S., Nusser, M., Mortara, G., Tamburini, A., Vilmeck, V. (2024): Dynamics and related hazards of Belvedere Glacier in the Italian Alps: a review. *AUC Geographica* 59(2), 163–183, <https://doi.org/10.14712/23361980.2024.21>.
- LeCun, Y., Bengio, Y., Hinton, G. (2015): Deep learning. *Nature* 521, 436–444, <https://doi.org/10.1038/nature14539>.
- Lipll, S., Vijay, S., Braun, M. (2018): Automatic delineation of debris-covered glaciers using InSAR coherence derived from X-, C- and L-band radar data: a case study of Yazgyl Glacier. *Journal of Glaciology* 64(247), 811–821, <https://doi.org/10.1017/jog.2018.70>.

- Mortara, G., Tamburini, A., Ercole, G., Semino, P., Chiarle, M., Godone, F., Guiliano, M., Haerberli, W., Kaab, A., Huggel, C., Fischer, L., Cordola, M., Barbero, S., Salandin, A., Rabuffetti, D., Mercalli, L., Cat Berro, D., Carton, A., Mazza, A., Godone, D., Federici, P., Viazzo, G., Epifani, F., Valsesia, T. (2009): Il ghiacciaio del Belvedere e l'emergenza del Lago Effimero. Regione Piemonte. Bussoleno: Societa' Meteorologica Subalpina.
- Mitkari, K. V., Arora, M. K., Tiwari, R. K., Sofat, S., Gusain, H. S., Tiwari, S. P. (2022): Large-scale debris cover glacier mapping using multisource object-based image analysis approach. *Remote Sensing* 14(13): 3202, <https://doi.org/10.3390/rs14133202>.
- Nuimura, T., Fujita, K., Sakai, A. (2017): Downwasting of the debris-covered area of Lirung Glacier in Langtang Valley, Nepal Himalaya, from 1974 to 2010. *Quaternary International* 455, 93–101, <https://doi.org/10.1016/j.quaint.2017.06.066>.
- Paul, F., Bolch, T., Briggs, K., Kaab, A., McMillan, M., McNabb, R., Nagler, T., Nuth, C., Rastner P., Strozzi, T., Wuite, J. (2017): Error sources and guidelines for quality assessment of glacier area, elevation change, and velocity products derived from satellite data in the Glaciers_cci project. *Remote Sensing of Environment* 203, 256–275, <https://doi.org/10.1016/j.rse.2017.08.038>.
- Paul, F., Rastner, P., Azzoni, R. S., Diolaiuti, G., Fugazza, D., Le Bris, R., Nemeč, J., Rabatel, A., Ramusovic, M., Schwaizer, G., Smiraglia, C. (2020): Glacier shrinkage in the Alps continues unabated as revealed by a new glacier inventory from Sentinel-2. *Earth System Science Data* 12: 1805–1821, <https://doi.org/10.5194/essd-12-1805-2020>.
- Racoviteanu, A. E., Nicholson, L., Glasser, N. F., Miles, E., Harrison, S., Reynolds, J. M. (2022): Debris-covered glacier systems and associated glacial lake outburst flood hazards: challenges and prospects. *Journal of the Geological Society* 179(3), 2021–2084, <https://doi.org/10.1144/jgs2021-084>.
- Sommer, C., Malz, P., Seehaus, T. C., Lippl, S., Zemp, M., Braun, M. H. (2020): Rapid glacier retreat and downwasting throughout the European Alps in the early 21st century. *Nature Communications* 11(1): 3209, <https://doi.org/10.1038/s41467-020-16818-0>.
- Smiraglia, C., Azzoni, R. S., D'Agata, C., Maragno, D., Fugazza, D., Diolaiuti, G. A. (2015): The evolution of the Italian glaciers from the previous data base to the New Italian Inventory. Preliminary considerations and results. *Geografia Fisica e Dinamica Quaternaria* 38(1), 79–88.
- Viani, C., Machguth, H., Huggel, C., Godio, A., Franco, D., Perotti, L., Giardino, M. (2020): Potential future lakes from continued glacier shrinkage in the Aosta Valley Region (Western Alps, Italy). *Geomorphology* 355: 107068, <https://doi.org/10.1016/j.geomorph.2020.107068>.
- Westoby, M. J., Rounce, D. R., Shaw, T. E., Fyffe, C. L., Moore, P. L., Stewart, R. L., Brock, B. W. (2020): Geomorphological evolution of a debris-covered glacier surface. *Earth Surface Processes and Landforms* 45(14), 3431–3448, <https://doi.org/10.1002/esp.4973>.
- Zekollari, H., Huss, M., Farinotti, D. (2020): On the imbalance and response time of glaciers in the European Alps. *Geophysical Research Letters* 47(2): e2019GL085578, <https://doi.org/10.1029/2019GL085578>.
- Xie, Z., Haritashya, U. K., Asari, V. K., Young, B. W., Bishop, M. P., Kargel, J. S. (2020): GlacierNet: A Deep-Learning Approach for Debris-Covered Glacier Mapping. *IEEE Access* 8, 83495–83510, <https://doi.org/10.1109/ACCESS.2020.2991187>.

Interannual spatio-temporal evolution of the supraglacial lakes on the Belvedere Glacier between 2000 and 2023

Lukáš Brodský^{1,*}, Samo Rusnák¹, Susanne Schmidt², Vít Vilímek³, Roberto Sergio Azzoni⁴, Marcus Nüsser^{2,5}, Gianluca Tronti⁴, Jan Kropáček³, Aayushi Pandey³

¹ Charles University, Faculty of Science, Department of Applied Geoinformatics and Cartography, Czechia

² Heidelberg University, South Asia Institute, Department of Geography, Germany

³ Charles University, Faculty of Science, Department of Physical Geography and Geoecology, Czechia

⁴ University of Milan, Earth Science Department, "A. Desio", Italy

⁵ Heidelberg University, Heidelberg Center for the Environment, Germany

* Corresponding author: lukas.brodsky@natur.cuni.cz

ABSTRACT

Understanding of the formation and evolution of supraglacial lakes in high mountain regions is crucial for accurately assessing their impact on glacier behaviour, hydrology, and potential hazards such as outburst floods. This article examines the annual spatio-temporal evolution of supraglacial lakes on the Belvedere Glacier between 2000 and 2023. Very high-resolution aerial photography and high-resolution satellite imagery were used to identify supraglacial lakes as small as 37 m² and narrow bands of ice-marginal lakes. The mapping revealed that the well-known Lake Effimero is stable in its position but unstable in size, with variations from 428 m² to 99.7 × 10³ m². These changes are potentially due to snowmelt or glacier dynamics. In 2002, the area of Effimero was at its largest extent observed during the study period. The first appearance of the Lake Effimero was revealed by the Landsat imagery on 27 May 2001, which differed from the findings of other studies. New lakes were observed to form in a manner independent of Effimero formation, exhibiting a consistent annual occurrence with nearly linear area growth up to 9.7 × 10³ m² in 2023. The formation of the lakes is shown to be influenced by their morphological characteristics.

KEYWORDS

supraglacial lake; glaciers; remote sensing; spatio-temporal dynamics

Received: 18 July 2024

Accepted: 28 November 2024

Published online: 18 December 2024

Brodský, L., Rusnák, S., Schmidt, S., Vilímek, V., Azzoni, R. S., Nüsser, M., Tronti, G., Kropáček, J., Pandey, A. (2024):

Interannual spatio-temporal evolution of the supraglacial lakes on the Belvedere Glacier between 2000 and 2023.

AUC Geographica 59(2), 214–228

<https://doi.org/10.14712/23361980.2024.24>

© 2024 The Authors. This is an open-access article distributed under the terms of the Creative Commons Attribution License (<http://creativecommons.org/licenses/by/4.0>).

1. Introduction

Spatio-temporal dynamics of supraglacial lakes (SGLs) have become a prominent research topic in the context of glacier downwasting (Miles et al. 2022) and glacial lake outburst floods (GLOFs) (e.g. Kropáček et al. 2015; Bollati et al. 2023). The evolution of SGLs due to climate warming can result in the transition to proglacial lakes, which present a significant threat to downstream areas. One such example is the Imja Lake in the Eastern Himalayas, where several SGLs were gradually transformed into a proglacial lake between 1976 and 1984 (e.g. Somos-Valenzuela et al. 2014).

Only a few studies analysed the spatio-temporal dynamics of supraglacial lakes. Wendleder et al. (2018) highlight the seasonal formation and evolution of supraglacial lakes on the Baltoro Glacier using multi-sensor time series data. They found that lakes generally form in early summer due to increased meltwater and precipitation, reaching peak levels before gradually draining towards the end of the summer. Watson et al. (2016) detect and analyse annual dynamics of SGLs in the Khumbu region. A net increase in the lake area was observed for six of nine studied glaciers between 2000 and 2015. Zeller et al. (2024) noted that lake stability varies widely in the Khumbu region, with some lakes being ephemeral and others persisting over multiple seasons or years.

A review by Bařka (2016) provides a summary of the factors involved in the formation and distribution of SGLs. Among the various factors, the first most significant is likely the impermeable glacier surface, which is determined by the density and fracturing of the ice. The critical value is reported to vary between 0.8 and 0.83 g/cm³ (Barnola et al. 1991) and 0.780–0.855 g/cm³ (Gregory et al. 2014). Another factor related to permeability is the occurrence of crevasses and their frequency.

A second factor is the availability of water. The highest position of the zero isotherm during the melt season defines the upper maximum level of SGLs occurrence (Benn et al. 2012; Sakai 2012). To consider the influence of debris cover, it is necessary to acknowledge that a thick cover prevents ice melting, and that the lower boundary of occurrence may be shifted to higher altitudes (Miles et al. 2017). SGLs exert an influence on the melting rates of glaciers. For instance, according to Miles et al. (2018; 2020), lakes may be responsible for 1/8 of the total ice loss observed in the Langtang Valley, Nepal. Furthermore, the debris covered Gangotri Glacier experienced twice as much thinning between 2000 and 2015 compared to neighbouring clean glaciers, due to the high density of ice cliffs and SGLs (Bhambri et al. 2023).

The third factor is the position of the lake in relation to the longitudinal valley profile. Most SGLs are formed on surface glacier tongues with gradients below 2° (Salerno et al. 2012; Reynolds 2000). However, higher values (up to 10°) are possible for smaller lakes (see

Bařka 2016) or lakes which tend to be transient due to the opening and closing of crevasses (Reynolds 2000). The mechanism of SGL appearance can be an obstruction of englacial and subglacial conduits (Richardson and Reynolds 2000). The material causing the obstruction can source for instance from debris cover.

The remote sensing-based monitoring of SGLs is a commonly employed method for determining the location, area, depth, and volume of lakes. A multitude of studies have demonstrated the high accuracy of SGL detection and tracking (Box and Ski 2007; Liang et al. 2012; Dirscherl et al. 2020). The limitations of optical data are typically related to spatial resolution in relation to the size of SGLs and cloud frequency in mountainous regions. Recently, studies have been published that also utilise SAR imagery (Schröder et al. 2020; Wendleder et al. 2021) to enhance temporal resolution during periods of dense cloud cover. Nevertheless, a direct comparison of the accuracy of SAR detection with that of optical data has yet to be conducted. One limitation of SAR is that the backscatter decreases in summer due to ice melt, which may negatively affect the separability of ice and water bodies. Additionally, the aforementioned studies are typically applied to Greenland, where the size of the SGLs is considerably larger, which is conducive to SAR data processing (Pope et al. 2016).

In the context of hazard assessment of glacial lakes, the volume of the lake is a crucial input parameter (Cook and Quincey 2015). The most reliable and, at the same time, most costly information on volume is based on bathymetry measurements by shipboard echo sounding (Gao 2009). A number of empirical formulas based on area-volume scaling have been proposed to provide an approximate estimate of the volume of SGLs (Cook and Quincey 2015; Watson et al. 2018). The estimation of volume can be also based on optical data and a physical model (Pope et al. 2016; Williamson et al. 2017). However, the method is limited to glaciers without debris cover, as the presence of suspended particles has a negative effect on the retrieval procedure (Brodský et al. 2022) and can effectively prevent the estimation of the lake depth.

SGLs are studied in many regions around the world; however, there are very few studies that describe this type of lake in the Alps. Very few cases of SGLs are reported by Viani et al. (2016), who identified them only on debris-covered glaciers in the Western Alps (Miage, Belvedere, and Schiantala Glacier), and they do not exceed 2% of the total number of glacial lakes. Buckel et al. (2018) investigated the Austrian glacial lakes, but no details are presented on SGLs. More recently, Ma et al. (2021) mapped all glacial lakes in the Alps using Google Earth Engine (GEE), revealing that during the period considered (2000–2019), SGLs experienced a 47% increase in area. Certainly, much more common in the Alps are glacier-marginal lakes, which often pose significant hazards (Diolaiuti et al. 2006).

Lake Effimero on the Belvedere Glacier is one of the most interesting SGL in terms of origin, evolution, and threat to the downstream area. During its brief lifespan, a comprehensive civil defence operation was initiated, encompassing pumping and the preparation of evacuation plans, geophysical and limnological measurements, and the mobilisation of the research community. The formation of Lake Effimero (Lago Effimero in Italian) was associated with a surge-like event that occurred primarily between 2001 and 2002 (Kääb et al. 2005). A 20 m deep ice depression had already formed at the lake's later location in the period 1995–1999 (Truffer et al. 2021). The depression was filled with clear meltwater in summer 2001 (Mortara and Mercalli 2002; Haeberli et al. 2002). During the melt season of 2002, the lake was filled with an abundance of meltwater from snow and ice due to a heat wave. As the lake level rose at a rate of 1 m per day (Truffer et al. 2021), it became evident that it constituted a significant risk to the downstream settlements and infrastructure. The area of the Effimero was initially estimated by Haeberli et al. (2002) to be 2,500 m² in 2001 based on ASTER satellite image acquired on 24 August 2001 and a “special airphoto” (most likely acquired on 11 October 2001). Another measurement using Differential Global Positioning System (DGPS) was carried out by Tamburini and Mortara (2005). They reported a lake area of over 150,000 m² on 8 July 2002, just a few days after the maximum lake level was reached on 26/27 June 2002 (Tamburini and Mortara 2005).

A sudden outburst occurred between 18 and 20 June 2003, resulting in the development of natural

englacial and partially supraglacial outflow channels, which released 2.3×10^6 m³ of water. Despite the large amount of released water, no serious damage occurred downstream due to already installed protection (Tamburini and Mortara 2005). Therefore, a better understanding of the interaction between SGL-forming factors and glacier dynamics is of utmost importance.

The objective of this study is to analyse the spatio-temporal evolution of SGLs on Belvedere Glacier from 2000 to 2023, with a particular focus on the evolution of Effimero Lake. A time series of twenty-four years of high-resolution and very high-resolution imagery is analysed. The study also aims to determine whether the dynamic supraglacial lake formation observed between 2016 and 2023 is a relic of Effimero Lake.

2. Study area

Belvedere Glacier (Fig. 1) is situated on the eastern face of Monte Rosa (4634 m a.s.l.), a prominent peak in the Western Italian Alps, situated on the border between Italy and Switzerland. Fig. 2 illustrates the supraglacial lakes as depicted by ground-based and unmanned aerial vehicle (UAV) photographs. The glacier is situated in the Anzasca Valley in the Piemonte region of Italy, less than two kilometres from the front rises the hamlet of Pecetto in the municipality of Macugnaga. Although the population of Pecetto is relatively small, the area is home to numerous hotels and service buildings for the existing ski area,

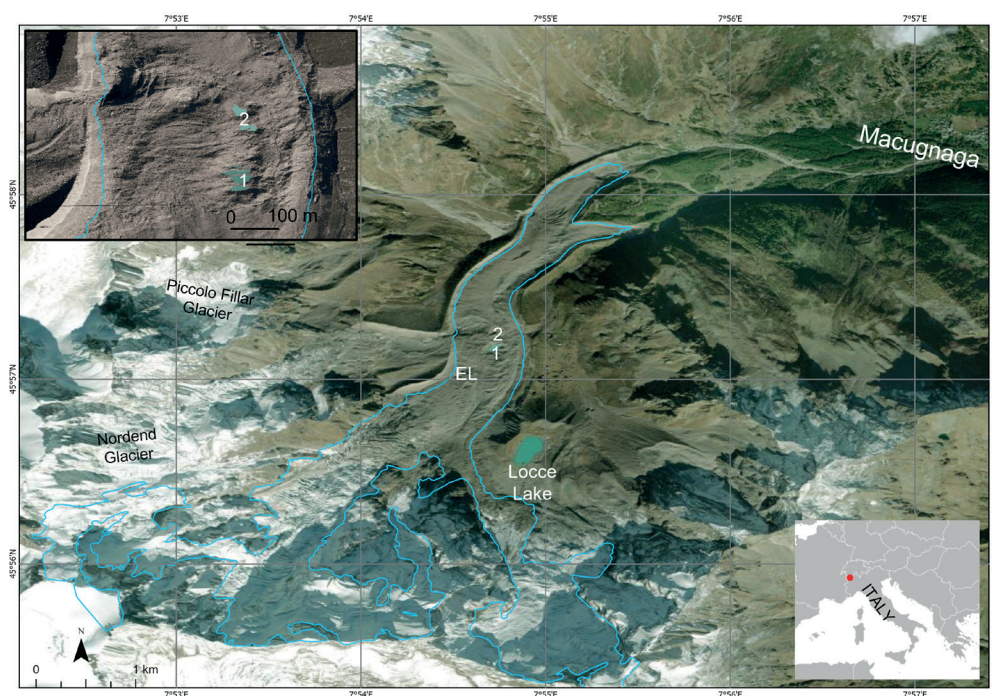


Fig. 1 Overview of the study area. Belvedere Glacier boundaries (from 2021 data) are reported in light blue. The positions of three SGLs are represented (EL = Effimero Lake; 1 = supraglacial lake 1; 2 = supraglacial lake 2). The location of Macugnaga settlement is reported in North Eastern sector of the images. Background: 2018 orthophoto (Geoportale Piemonte 2024).

which occupy the area between the glacier and the settlements.

3. Data sources

In order to analyse the inter-annual dynamics of the SGLs between 2000 and 2023, optical imagery with different sensors was utilised (Tab. 1). The objective was to obtain as many very high and high-resolution images (around 1 m and 20 m, respectively) as

possible within the sequence. Images devoid of cloud cover were selected, with a particular focus on the early summer season. Furthermore, the maximum area of the lakes was also considered. The aforementioned rules were applied to the RGB aerial images sourced from the local agencies and multispectral images retrieved from the RapidEye, and PlanetScope archives. Furthermore, SPOT (Satellite Pour l’Observation de la Terre) images were modified to fill temporal gaps.

The resulting dataset, which encompasses the entire observation period from 2000 to 2023, is



Fig. 2 Terrestrial photographs of the SGL from the north-east from 11 August 2021 (a), 10 August 2022 (b), 3 August 2023 (c), and UAV image from 3 August 2023 (d).

Tab. 1 Temporal and sensor coverage of the imagery used in this study.

Sensor	Spectral Bands	Spatial resolution (m)	Date
SPOT 4	RGB, NIR	20.0	2000/07/28, 2006/09/01
AEO orthophoto	RGB	0.4	2001/10/01, 2002/07/19
SPOT 5	PAN	20.0	2003/08/03
SPOT 5	RGB, NIR	20.0	2004/08/01, 2005/07/20, 2009/09/1
SPOT 2	B, R, NIR	20.0	2007/07/22, 2008/07/15
RapidEye	RGB, RE, NIR	5.0	2010/07/03, 2011/07/03, 2012/09/05, 2013/08/20, 2014/09/13, 2015/07/04, 2016/06/20
PlanetScope	RGB, NIR	3.0	2017/06/07, 2018/06/14, 2019/06/30, 2020/06/22, 2021/06/06, 2022/05/12, 2023/05/26

Note: AEO = aerial earth observation images; RGB = red, green, and blue; NIR = near-infrared; PAN = panchromatic; B = blue; R = red; RE = Red-Edge bands

heterogeneous in nature. It comprises two aerial orthophotos, seven RapidEye images, seven PlanetScope images (Planet Labs PBC, 2018), and six SPOT images. Furthermore, auxiliary data were used for visual interpretation guidance consisting of glacier outlines (Azzoni et al. 2024, in this issue) and an elevation model with a hill shade product (Geoportale Piemonte 2024).

4. Methods

The three principal stages of the data analysis process were the data preparation, the SGLs classification, and the GIS (Geographic Information System) analysis – the spatio-temporal SGLs evolution experiment, and visualisation. The data preparation stage entailed the co-registration of images from 2012, 2014, and 2015, as well as the orthorectification of RGB aerial images from 2001 and 2002. The co-registration was conducted using a first-order affine transformation in the ArcGIS Pro environment (version 3.2.0.), with the use of manually identified control points between the targeted image and the image from the year 2011. The 2009 AEO (Orthophoto from Piemonte Geoportal 2024) with a resolution of 0.4 m was used as a reference. Images from 2001 and 2002 were subjected to orthorectification in the Agisoft environment (version 1.7.5) utilising aerial survey photographs and manually selected ground control points (GCP).

The SGLs on the Belvedere Glacier were visually interpreted and digitised manually on twenty-four occasions (Tab. 1). This technique was selected for a number of reasons. Firstly, the number of lakes to be classified is limited. Secondly, the input images are highly heterogeneous in the sense of spectral (sensors) resolution, but also spatial and acquisition dates during the melt season. Thirdly, the automated model would require a minimal amount of training data, which could roughly equal the number of monitored years. A computer-assisted photointerpretation (CAPI) process was conducted in a timely manner, based on general land cover classification rules (e.g. Büttner and Kosztra 2017). Given the varying spatial resolution of the input images, it was not possible to set a minimal mapping unit. The smallest identified and digitised pond had a surface area of 37 m². The lake boundaries were delineated to encompass only the water area, excluding the visible ice cliffs (Fig. 2) and potential ice islands, given that it was not possible to ascertain from the images whether these are merely floating ice floes (Fig. 2) or complex glacier ice structures. The impact of seasonal fluctuations was not considered, as only one image per year was analysed.

In the case of the 2003 panchromatic image, the position and shape of the lake had already been checked in the years before and after this year. In this case, however, since 2002 was identified as the peak

area of Lake Effimero, only 2004 was found to be useful for understanding the spatio-temporal context of the image. Subsequently, temporal dependency logic was employed to verify the evolution of the manually edited lakes' boundaries. This entailed an examination of the sequence preceding and following the year when the edits were made. In other words, the classification procedure was not temporally independent. Temporal dependence in image analysis refers to the necessity of utilising multiple images acquired over time to comprehend the changes and dynamics observed in the appearance of the lake as it moves on the glacier at a speed comparable to that of the glacier itself, while also undergoing a change in size. This dependence on temporal information is of paramount importance for the monitoring and analysis of this dynamic phenomenon. See for instance Lhermitte et al. (2011) providing a quantitative evaluation of the time series similarity measures for the change detection ecosystem dynamics. The spatial pattern, size, and position of the SGLs are all subject to change over time. The methodological verification process was then applied to the entire time series, which enabled us to gain insight into the evolution of the lakes over the past twenty-four years. The reported areas represent the intersection of the two edited polygons.

Furthermore, the Jaccard score (NOAA 2024), also known as the Jaccard similarity coefficient, a statistic used for quantifying the similarity and diversity of sample sets, was employed to assess the accuracy of the SGLs editing.

$$J(A, B) = \frac{|A \cap B|}{|A \cup B|}$$

where the sets of edited polygons of the SGLs, designated as A and B as produced by different independent interpreters, respectively, are the subject of this study. The Jaccard score is a measure of similarity for the pairwise comparison of two spatial segments. Furthermore, it is assumed that the pixel size of the edited polygons is uncertain by 0.5 pixels. To account for the uncertainty associated with the spatial resolution of the images, the buffer zone was calculated to be 0.5 pixels in size. The validated SGL polygons were subjected to GIS analysis in the spatio-temporal SGL evolution experiment. The experiment included several standard vector/raster analyses to assess the density of SGLs over the monitored period, their changing spatial positions over time, their area and slope within the glacier system.

Lakes classification in this study:

Effimero Lake is a notable SGL that formed on the upper part of the ablation area of the Belvedere Glacier. The name “Effimero” translates to “ephemeral” in Italian, reflecting the transient nature of the lake, which can form and disappear within a single melt season.

Supraglacial lakes at sites 1 and 2 are those that consistently appear on the Belvedere Glacier between the Nordend Glacier entrance position and the lateral moraine breach near the Zamboni Zappa hut since 2012.

Other small supraglacial lakes are smaller lakes that abruptly appear around the two main distinct SGL locations, with an area ranging from 37 to 500 m².

Ice-marginal lakes (IML) are defined as bodies of water that form adjacent to a glacier. These lakes are distinct from the SGLs, which form on the surface of glaciers, and the subglacial lakes, which form beneath glaciers.

Additionally, a DEM-derived Topographic Wetness Index (TWI) (Boehner et al. 2002; Boehner and Selige 2006) was calculated to gain insight into the potential areas of lake formation. The TWI was derived utilising the SAGA GIS tool, namely the Topographic Wetness Index (One Step) (Conrad et al. 2015), to assess the topographic inclination for supraglacial water accumulation. The 1951, 2009, and 2023 digital surface models (DSM) were used to run the TWI and longitudinal profile analysis. The 2009 DSM from the Piemonte Geoportale (2024) was used in the study, while the 1951 and 2023 DSMs were processed in the study by Brodský et al. (2024, in this issue). A longitudinal profile of the glacier was constructed for the three specified periods. The accompanying slopes were calculated based on the convex hull of the elevation profile (i.e., the surface shape with the smallest convex envelope) due to the high variability of the slopes in the original DSM spatial sampling, as well as in the 5 m resolution.

Furthermore, the volume of the supraglacial lake site 1 was quantified in situ on 2 August 2023. A hand-held sonar LX-i from MarCum Technologies was used in conjunction with GPS measurements, which were made using a GPSMAP device from Garmin. The sonar enables one-handed measurements through the boat's hull or directly in the water adjacent to it,

with a maximum reach of 91 m and an accuracy of ± 0.9 m (MarCum Technologies technical documentation). The measurement beam is defined by a cone angle of 12°. A total of 33 depth measurements were taken from the deck of a small inflatable canoe. Subsequently, the individual readings from each device were integrated in the post-processing phase. The calculated depth was then compared with volume estimates derived from empirical area-volume formula developed for SGLs by Watson et al. (2018), based on Cook and Quincey (2015), but using a larger dataset on lakes:

$$V = 0.1535 \times A^{1.39},$$

where V is the volume and A is the area of the lake.

5. Results

Although the spectral, spatial, and radiometric resolution of the acquired 24 images varies considerably, it was possible to detect and map the lakes, as they are mostly spectrally distinct from their surrounding glacier surface. The only challenge for the CAPI was posed by the panchromatic image that was available in 2003. In the spatio-temporal SGLs evolution experiment, a quantitative analysis was conducted to assess the consistency of the lake boundaries, which had been edited by two independent interpreters. The twenty-three-year validation is presented in Fig. 3. The Jaccard score, as defined by the equation 1, indicates a high degree of consistency in the cross-comparison of the two independent interpreters. The local database of spatio-temporal SGL evolution is then used in the subsequent quantitative analysis.

The evolution of the lake between 2000 and 2023 demonstrates the high variability of the SGLs (Fig. 4). The largest SGL is Effimero, which reached a maximum size of 15.6×10^3 m² at an elevation of 2107 m a.s.l. after the 2001 surge event. In 2002, the lake reached its maximum size of 99.7×10^3 m².

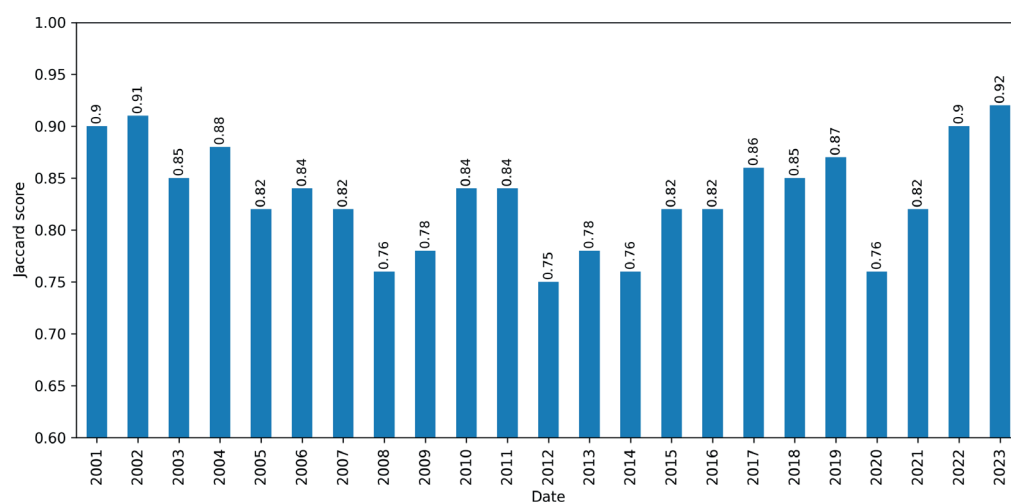


Fig. 3 Validation Jaccard's scores of the SGLs delineation.

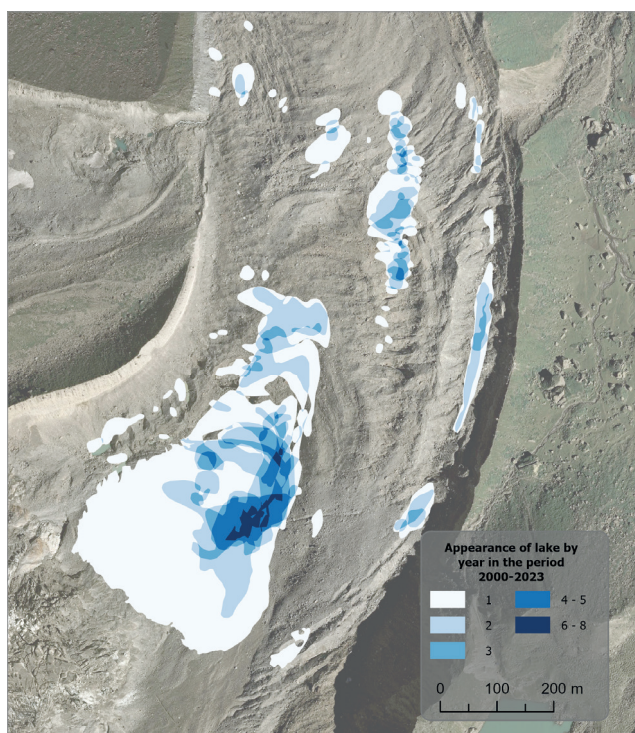


Fig. 4 Number of appearances of SGL in the annual time series of the mapped SGLs for the period 2000–2023 (stack of vectors), Background: orthophoto 2009 (Geoportale Piedmont 2009).

In 2003, the same supraglacial depression was refilled with water, but it reached a much smaller area of $7.7 \times 10^3 \text{ m}^2$ compared to the previous year.

In 2012 lakes sites 1 and 2 appeared and steadily grew, reaching their maximum area of 9718 m^2 in 2023. Furthermore, ice marginal lakes are particularly prevalent along the right margin of the central part of the glacier. The dimensions of IML exhibit a considerable range, spanning from 349 to $9.7 \times 10^3 \text{ m}^2$. Fig. 4 presents the number and size of occurrences of lakes in the multi-annual stack of all edited vectors. It is evident that there are two fundamental locations (1 and 2) predisposed for SGLs formation.

The temporal evolution of the position of Effimero Lake and supraglacial lake sites 1 and 2 from 2001–2023 and 2012–2023, respectively, is illustrated in a series of vectors representing annual maximum extent (Fig. 5 and Fig. 6). The SGLs are depicted as redrawn polygons, which indicate their movement with the glacier. The temporal evolution of SGLs encompasses a series of stages, from their formation to potential drainage or disappearance. The seasonal changes are not captured in this study, as only yearly data are used. Nevertheless, the analysis demonstrates the evolution of SGL and IML over a period of 23 years.

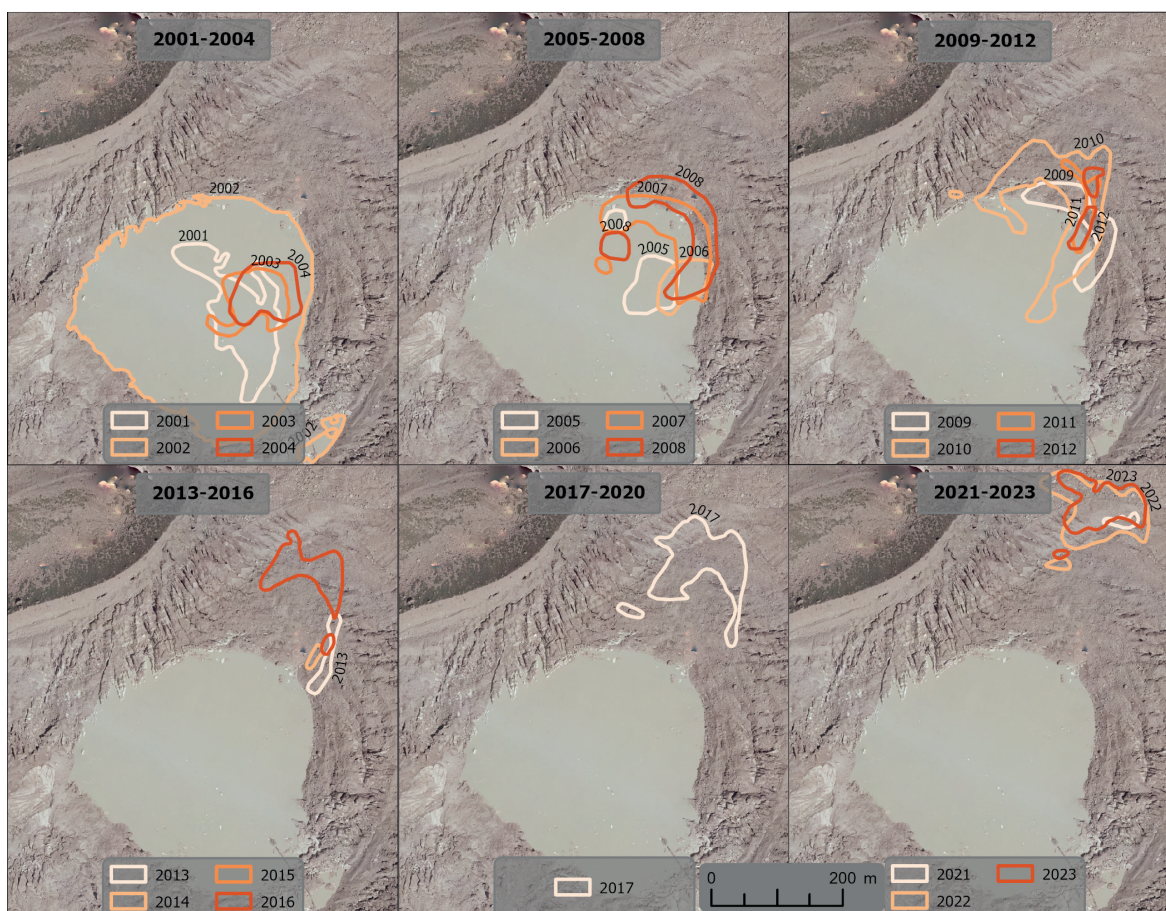


Fig. 5 The evolution of Lake Effimero between 2001 and 2023 is grouped into 4-year periods. For clarity, they are shown in separate sub-images. Background: orthophoto 2002 (orthorectified by the authors, data: CGR S.p.A.).



Fig. 6 Evolution of Supraglacial lakes site 1 and 2 in the period 2012–2023. Lake outlines per year in two 6-years periods over 2023 PlanetScope image (False colours combination: NIR, Red, Green). Image © 2023 Planet Labs PBC.

Lake Effimero exhibited a displacement of approximately 400 m over a period of 22 years. The supraglacial lakes at sites 1 and 2 exhibited a displacement of approximately 300 m over a period of 11 years. The study captures the formation and initial stages of both the Effimero and supraglacial lakes 1 and 2. The location of Effimero Lake appearance is clearly disconnected from the new formations at site 1 and 2 (Fig. 4) and the new SGLs formed between 2016 and 2023 are no relics of Effimero Lake.

The spatio-temporal evolution of the lakes is presented in Fig. 7, divided according to the classification introduced in the methods section. The area of Effimero 2002 ($99.7 \times 10^3 \text{ m}^2$) represents the largest extent observed during the study period. The area of Effimero exhibited a high degree of fluctuation. It appears to have disappeared by 2015, but then the basin of

Effimero was refilled with water, particularly at the beginning of the summer season (June). This refilling occurred again in 2016, 2017, 2022 and 2023. There was no water in the Effimero between 2018 and 2020 (Fig. 5).

In addition to the analysis of the spatio-temporal dynamics of the supraglacial lakes in a set of static maps (and animation in the appendix), we plot the longitudinal profile of the digital surface models (DSMs) from 1951, 2009 and 2023 DSMs to identify potential locations of SGLs, see Fig. 9 for the position of the profile and Fig. 10 the plotted elevation data.

The upper part of the longitudinal profile offers suitable positions for the development of the SGLs (distance 2000–3000 m), which exhibits an inclination of 0.6° in 2009 and 3.0° in 2023 (Fig. 10), while 4.2° in 1951. This part also exhibits considerable variability

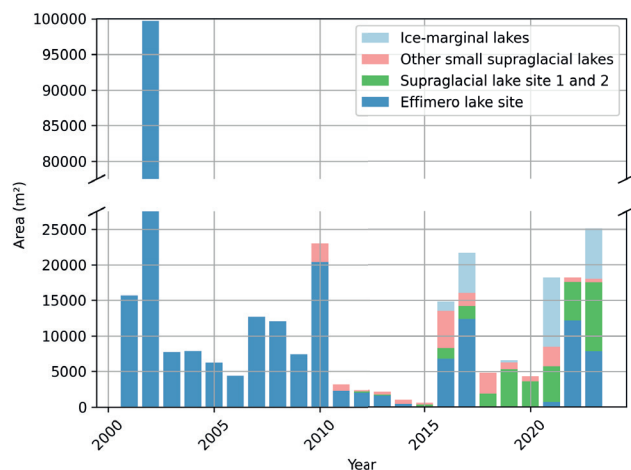


Fig. 7 Belvedere’s SGLs area evolution, in m^2 , in the period 2000–2023 per location.

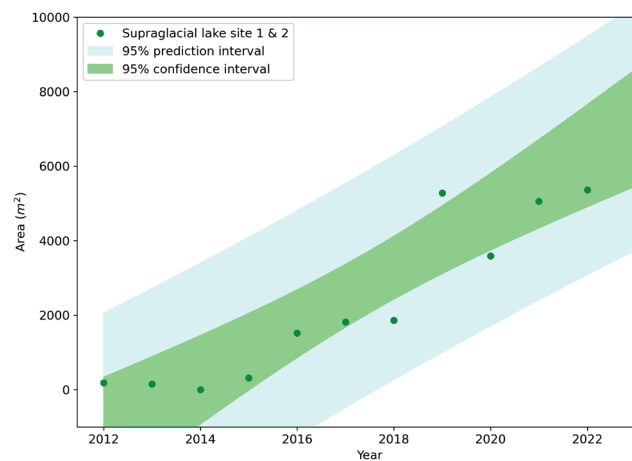


Fig. 8 Supraglacial lake site 1 and 2 temporal evolution in the period 2012–2023 and 95% confidence and prediction intervals of the linear model.

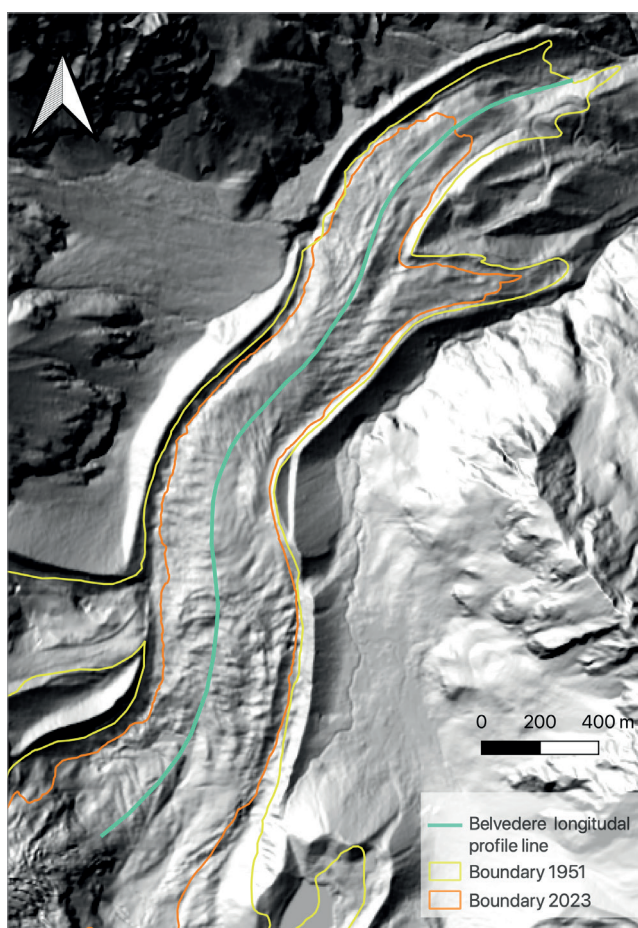


Fig. 9 Map of Belvedere glacier with longitudinal profile, background: hill shade 2009 DSM, glacier boundary (Azzoni et al. 2024, in this issue).

in slope inclination. The central portion (distance 1000–2000 m) and the lower portion (0–1000 m) of the glacier, where no SGLs can be observed, the inclination amounts around 6° and 10°, respectively, which is not well suitable for the lakes formation.

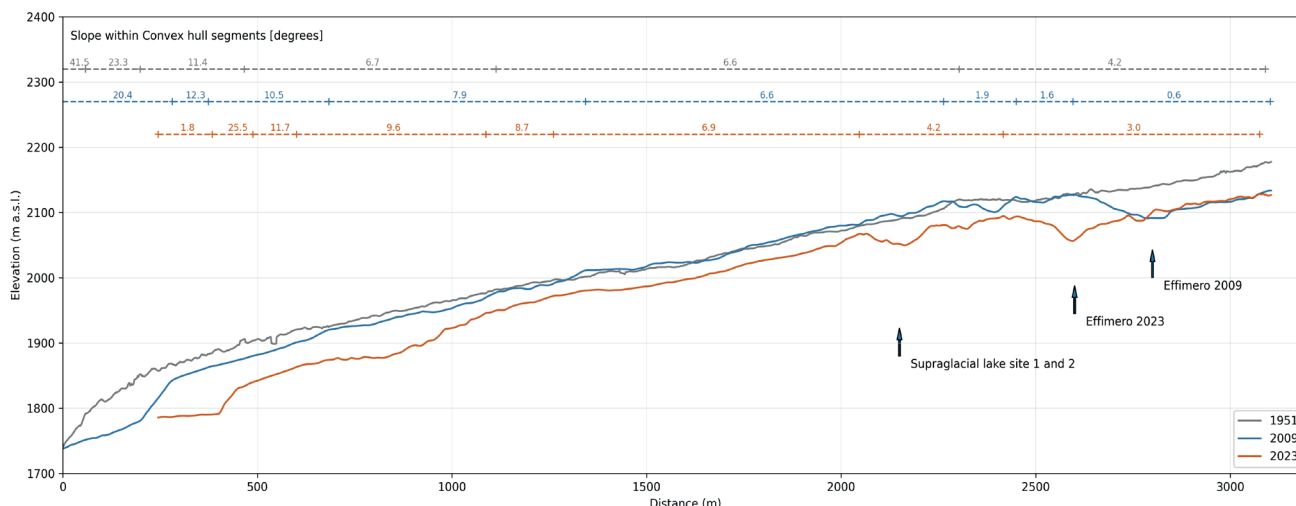


Fig. 10 Longitudinal profile and mean slope within the convex hull segments (horizontal lines) of Belvedere Glacier in 1951, 2009, 2023 (input data Brodsky et al. 2024 – in review).

The potential locations of SGLs on Belvedere Glacier are then examined using the TWI (Fig. 11). The formation of SGL is contingent upon the presence of suitable climatic and topographic conditions, which are particularly prevalent in specific regions of glaciers. The TWI illustrates the potential for water accumulation zones and their spatial variations due to morphometric features. To facilitate a comparison of the evolution of the glacier's morphometric features, the series of relative TWI values has been adjusted for the years 1951, 2009 and 2023. The high TWI values in the 2009 and 2023 TWI maps (approximately 20) correspond to the position of Effimero Lake, the lake sites 1 and 2 and the IMLs in the south-eastern glacier margin (Fig. 11).

The initial appearance of Lake Effimero is now dated to 27 May 2001 based on a sequence of Landsat 7 imagery captured between spring and autumn of 2001 (Fig. 12). It is evident that the lake area was significantly larger in the second half of June than in September or October. The intra-annual sequence of images indicates that the lake was formed during the May 2001 melt season. The first three images (27 May, 5 June and 12 June) demonstrate the presence of melting snow up to the residual snow observed on 21 June 2021.

Furthermore, the depth of the lake at site 1 was measured in situ with a bathymetric instrument to compare the volume of new lake formation with Effimero 2002. Of the 33 depth measurements, only ten had a valid GPS position; while the GPS position remained unchanged for the remaining points, that was not observed during the campaign. This phenomenon occurred primarily in points situated near the shoreline. It is postulated that this may have been due to reflections of the GPS signal on the steep shorelines, which in some instances were formed by vertical ice cliffs several metres in height. The ten valid points could not be used to interpolate the bathymetry of

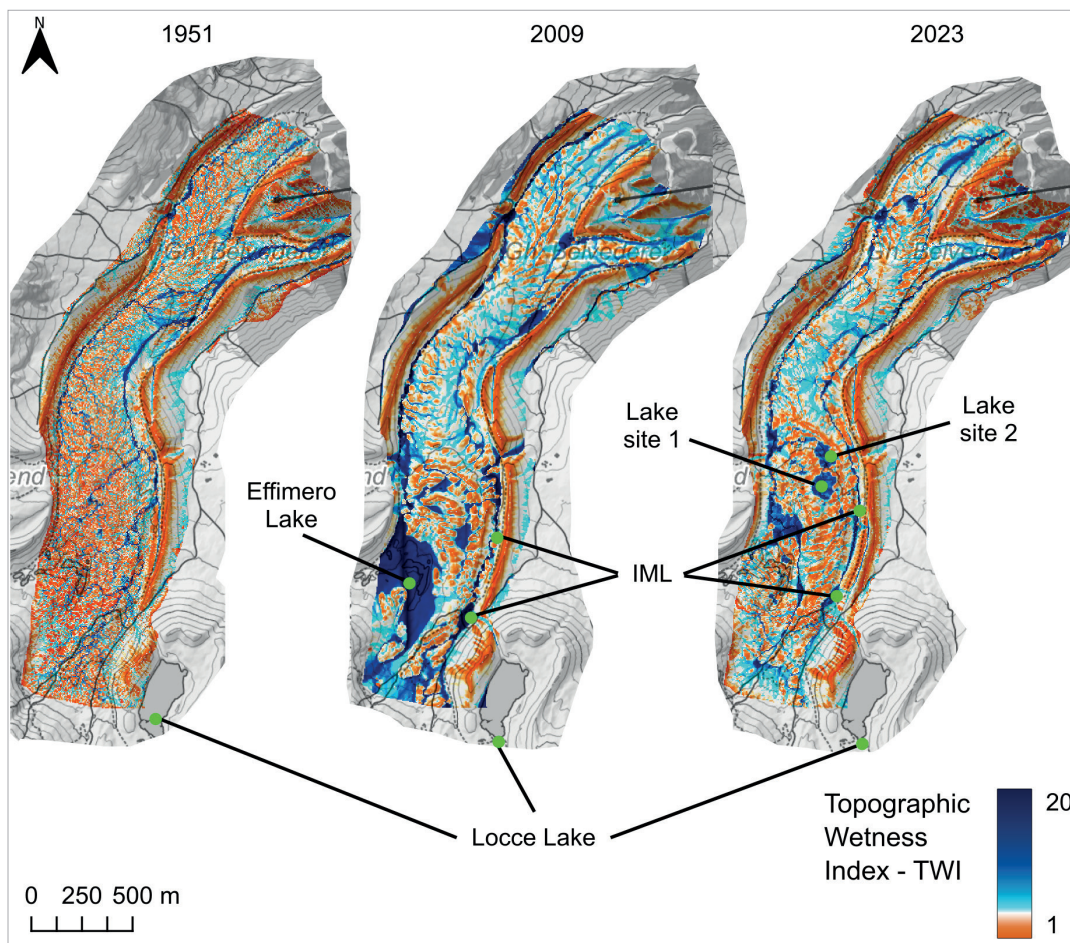


Fig. 11 Topographic Wetness Index variation among the years 1951, 2009 and 2023.

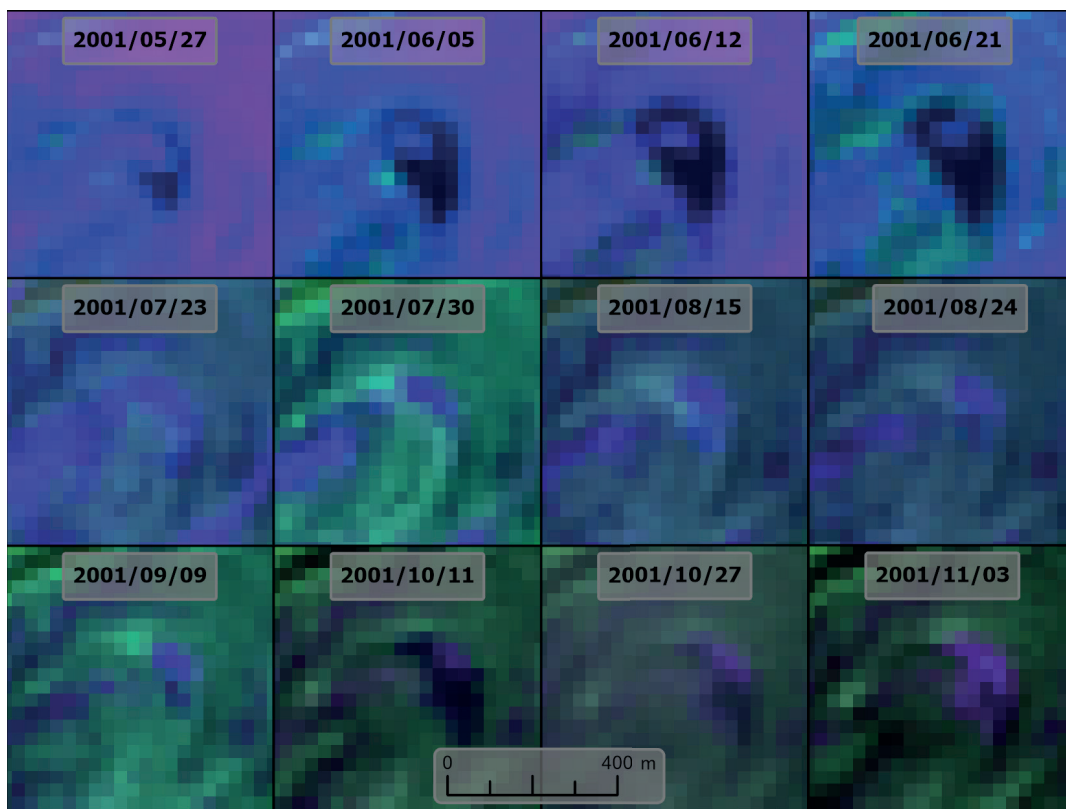


Fig. 12 Supraglacial lake formation in the Effimero Lake location in the year 2001. The snow appears in magenta colour and the lake in black in the false-colour synthesis. Image source: Landsat 7, Bands: NIR-SWIR-RED (Near-InfraRed, Short-Wave InfraRed, Red).

the entire lake, as they are concentrated around the centre, leaving the remainder without depth information. Consequently, all 33 depth measurements were employed to calculate the mean depth, which was multiplied by the lake area derived from the 2023 orthophoto, to provide an estimate of the lake volume.

The lake area was quantified by vectorising the lake shore in the 2023 orthoimage. As the lake area was calculated using very-high-resolution data, the error in calculating the volume is not considered. The mean lake depth is 9.8 m. As the lake depths do not follow a normal distribution, the volume error was derived using the Monte Carlo method, as described by Watson et al. (2018). A Monte Carlo simulation of 1,000 lake depth scenarios yielded a standard error of the mean depth of 1.4 m. The error in volume was then calculated by multiplying the area by the error in depth, resulting in a volume estimate of $50.6 \pm 7.2 \times 10^3 \text{ m}^3$. For comparison, the volume of the supraglacial lake was estimated using the empirical formula (Watson et al. 2018; Cook and Quincey 2015). The resulting volume was found to be $22.3 \times 10^3 \text{ m}^3$, which is less than half of the volume calculated based on the depth measurements. This suggests that the lake is considerably deeper than is typical for SGLs.

5. Discussion

The spatio-temporal evolution of supraglacial lakes on Belvedere Glacier is studied on an annual basis for the period 2000 to 2023. This is achieved primarily through the utilisation of very high and high-resolution satellite and AEO imagery. The high spatial resolution allows the detection of lakes as small as 37 m^2 , small strips of ice-marginal lakes with widths of 1–2 m, the delineation of lake boundaries in high detail, and the investigation of the spatio-temporal evolution of the lakes. Analyses of this nature are not feasible with pure Landsat images, which have a pixel size of 30 m (a minimal mapping unit of 3600 m^2 , assuming that four pixels are required to map an object of a lake). Kaushik et al. (2022), Hu et al. (2024), Ma et al. (2021), and Sharma et al. (2024) employed automated mapping and inventory of glacial lakes across the globe using high-resolution images, such as Landsat. The spatial resolution of Landsat represents a limit to the minimal mapping unit. However, the principal advantage of such data sets is their multi-decadal temporal coverage, which offers considerable potential for linking the detected changes to climate-induced glacier variations.

The quantitative results of the mapping validation indicate that there were no significant discrepancies between the two interpreters in their visual interpretation and manual editing of the lake boundary. The mean Jaccard score was 0.83, with a minimum of 0.75

and a maximum score of 0.92. Given the disparate nature of the sensors in the study, the spectral resolution varies considerably, encompassing panchromatic, multispectral, and true-colour RGB images, it was proved that the spectral resolution does not present a significant obstacle to the identification of the supraglacial lakes.

The secondary objective of the quantitative analysis was to provide a foundation for future evaluations of automated algorithms, specifically deep learning segmentation with Convolutional Neural Networks (CNN). The Jaccard score metric is a commonly used metric for the comparison of two or more image segmentations. The Jaccard score achieved in our study can be compared to the study by Wu et al. (2018). They evaluated the semantic segmentation of very-high-resolution remote sensing images using a fully convolutional network with an adaptive threshold for the number of land cover classes, including standing water. The Jaccard scores for the water varied between 0.71 and 0.83. In a study by Liu et al. (2022), a dense block was introduced into a convolutional neural network (CNN) architecture for the purpose of water body segmentation. The results exhibited a range of values between 0.72 and 0.76. Consequently, even minor discrepancies between two spatial delineations are penalised in the score, in contrast to the approach employed in classical remote sensing, where overall accuracy or F1-score is calculated based on e.g. random or stratified samples.

The annual evolution of supraglacial lakes on the Belvedere Glacier was studied, providing insights into their dynamics, possible formations, and implications for glacial processes. The first discovery of Effimero Lake on Belvedere Glacier was made by scientists engaged in monitoring the glacier. In 2002, Haerberli et al. employed ASTER satellite imagery and aerial photography to discern the emergence of a sizable supraglacial lake. This observation was made in the autumn of 2001. Fischer et al. (2006) propose that the formation of Lake Effimero was the consequence of elevated englacial water pressure or other processes associated with surge-like movement. The first appearance of the lake was dated by Fischer et al. (2006) to September 2001. However, our study proved that the first appearance of Lake Effimero occurred on 27 May 2001.

Also, the initial area of the Effimero Lake estimated by Haerberli et al. (2002) amounted to 2500 m^2 in the year 2001 and increased to $150,000 \text{ m}^2$ in June 2002 (Tamburini and Mortara 2005). Our results indicate that the maximum area of Effimero Lake fluctuated between $15,661 \text{ m}^2$ in October 2001, $99,700 \text{ m}^2$ in July 2002, and 7734 m^2 in August 2003, based on AEO orthophotos and SPOT 5 imagery. The highest level of the Effimero area was recorded in 2002.

The area of the SGLs at sites 1 and 2 fluctuate due to the availability of surface meltwater as also observed for SGLs in the Himalayan and Karakoram

region (Wendleder et al. 2021; Zeller et al. 2024). However, both sites are characterised by an almost linear increase.

The location of the lakes is situated in the area of the highest glacier velocity (approximately 20 m yr^{-1}), as presented in Ioli et al. (2022), which was measured between 2015 and 2020. It is challenging to assess the glacier velocity flow at the location of Lake Effimero, as it is situated at the periphery of the data presented in Ioli et al. (2022).

However, the shift in position of Effimero Lake with approximately 400 m over a period of 22 years is less pronounced than that observed at Lake site 1 and 2 which amounted to 300 m over a period of 11 years. Thus, it can be assumed that the position of the Effimero Lake is more stable due to its location in a flatter area of the glacier, as evidenced by the slope profile (Fig. 10). This can be attributed to the lower slope angle ($< 3^\circ$) in the upper part of the glacier. This is consistent with the findings of Reynolds (2000), who suggested that lakes can occur in slopes up to 10° . Salerno et al. (2012) established a threshold for the glacier tongue gradient of less than 2° .

The spatio-temporal analysis of the images also serves to reinforce the distinctive process of the Belvedere Glacier in relation to the presence and dynamics of SGLs. The documented cases of SGLs in the Alps are extremely rare (Viani et al. 2016), and none of them exhibit the scientific significance or relevance to risk prevention that those on the Belvedere Glacier do. The Belvedere Glacier is further distinguished by its status as one of the few debris-covered glaciers in the Alps, along with the Miage Glacier. However, detailed descriptions of the evolution of SGLs on the Miage Glacier are lacking, except for the ice-contact lake (Diolaiuti et al. 2006). Consequently, the dynamics of the supraglacial lakes on the Belvedere Glacier are more akin to those observed on large debris-covered glaciers in the Karakoram and Himalaya regions. The increase in supraglacial debris cover resulting from glacier collapse (Azzoni et al. 2018), coupled with the rise in the number of glacial lakes *sensu lato*, may lead to a future increase in supraglacial lakes on other Alpine glacier systems. This trend may have significant implications for risk management, especially as the lakes on the Belvedere Glacier are in avalanche and rockfall prone areas.

The present study shows annual observations of SGLs. While these observations provide valuable data, they are not without limitations. The annual observations may fail to identify seasonal critical changes, which could result in the generation of incomplete insights into the dynamics of the lakes (Zeller et al. 2024), such as rapid drainage or refilling events. The increase in temporal resolution can be addressed by utilising a full time series of Landsat, SPOT, and Sentinel-2, PlanetScope imagery. Such comprehensive time series could be employed to investigate the relationship between lake evolution and inter-annual climate

variability, as well as the processes of formation and behaviour from one year to the next as conducted for the Khumbu Himal (Zeller et al. 2024) or Baltoro Glacier (Wendleder et al. 2021). Furthermore, the utilisation of full time series would permit the analysis of melting processes, the potential integration with hydrological data and glaciological models, and the generation of new insights. Furthermore, risk management, in particular regarding potential GLOFs such as in 2003 (Tamburini and Mortara 2005), necessitates continuous and more frequent monitoring.

Nevertheless, an analysis of the full time series would result in a loss of spatial detail, from the 0.5 and 3.0 m analysis currently used to a spatial resolution of 10 and 30 m. Consequently, the analysis would fail to encompass 107 out of 126 lakes (85%). This loss would represent 26% of the lakes total area. Such a request presents a challenge in the analysis of high temporal resolution and integrated multi-source data. One may consider multimodal deep learning models (e.g., Benedetti et al. 2018) or spectral unmixing models (Racovitenau et al. 2021). The objective of this study was to analyse the interannual spatio-temporal evolution, utilising the highest spatial resolution of the input images to the greatest extent possible. This study presents, for the first time, the long-term spatial evolution of the supraglacial lakes on the Belvedere Glacier. To date, only a few studies have presented data on the lakes in a context spanning one or two years.

In addition to the spatio-temporal monitoring of the SGL dynamics, the depth of the lake at location 1 was measured in the summer of 2023 in order to calculate the volume of the lake. The calculated volume of the new formation based on bathymetric measurements in August 2023 was $50.6 \pm 7.2 \times 10^3 \text{ m}^3$, while the Watson et al. (2018) formula yielded $22.3 \times 10^3 \text{ m}^3$, representing an underestimate of 56%. In contrast, Lake Effimero reached its maximum extent of $99.7 \times 10^3 \text{ m}^3$ (our result) and volume of $3 \times 10^6 \text{ m}^3$ (Tamburini and Mortara 2003) at the end of June 2002. The corresponding volume resulting from the empirical formula of Watson et al. (2018) is $1.2 \times 10^6 \text{ m}^3$, which represents a similar underestimate of 60%. This indicates that both lakes have a comparable area to volume ratio, although both emerge from different origins. Ranzi et al. (2004) constructed a model of Lake Effimero, which they commenced on 1 April 2003 and continued until its sudden emptying on 18 June 2003. The volume of the lake was estimated to be approximately $2.7 \times 10^6 \text{ m}^3$. The sudden release of water was attributed to the formation of a subglacial channel system on the north side of the lake. For the period between 1 April and 30 June 2002, the simulated cumulative inflow is $3.4 \times 10^6 \text{ m}^3$, a value that is also consistent with the estimates of the civil protection authorities, who at that time initiated the artificial emptying of the lake through pumping stations.

6. Conclusion and future work

Understanding the formation and evolution of SGLs in high mountain regions is critical for assessing their impact on glacier behaviour, hydrology, and potential hazards such as GLOFs. This study examines the spatio-temporal evolution of SGLs on Belvedere Glacier on an annual basis for the period 2000 to 2023 using very-high-resolution AEO and satellite imagery, amended with several SPOT images. Such a dataset allowed the detection and monitoring of small SGLs and strips of ice-marginal lakes, their temporal evolution, their formation, and expansion

The spatio-temporal mapping of the lakes showed that Effimero can be assumed more stable in its the position but unstable in size, with anomalies possibly due to snowmelt or glacier changes (avalanches). The link to the snowmelt mechanism shall be demonstrated in a future study using time series of satellite imagery together with a climatic dataset.

The newly formed lakes at sites 1 and 2 are smaller, flow faster with the glacier, are more stable in their annual occurrence, and increase steadily (almost linearly) in size. They were formed independently of Effimero, as shown by the sequence of longitudinal profiles and the sequence of boundary mapping. The main factor in the formation of the lakes is the morphological feature documented by the TWI maps. The intra-annual variability of the lakes remains undiscovered in the study. Both Effimero and Lakes 1 and 2 correspond to the theoretically expected locations supported by the TWI maps, although the slope values are slightly higher in 2023.

Overall, the inter-annual evolution of supraglacial lakes on Belvedere Glacier highlights the importance of ongoing research and monitoring to better understand these processes and their implications. In future work, manual editing of lake boundaries shall be replaced by automatic semantic segmentation after image radiometric harmonisation using full time series of remote sensing imagery to also capture intra-annual snow variations and snowmelt rates.

Acknowledgements

This research was funded by the 4EU+ project Remote Sensing of the Cryosphere Dynamics under the Influence of Climate Change, grant number: 4EU+/23/F4/19.

This research was also partly funded by University of Milan through the Sostegno alla ricerca Project 2021 (Indicatori geomorfologici e geopedologici per ricostruire l'evoluzione delle aree di recente deglaciazione) and 2022 (Evoluzione dei processi geomorfologici e degli impatti sul ciclo idrologico in contesti sensibili al cambiamento climatico).

The authors also thank Planet Labs and CNES SPOT for access to their imagery.

Aerial images: Piemonte region of Italy, CGR S.p.A.

References

- Azzoni, R. S., Fugazza, D., Zerboni, A., Senese, A., D'Agata, C., Maragno, D., Carzaniga, A., Cernuschi, M., Diolaiuti, G. A. (2018): Evaluating high-resolution remote sensing data for reconstructing the recent evolution of supra glacial debris: A study in the Central Alps (Stelvio Park, Italy). *Progress in Physical Geography: Earth and Environment* 42(1), 3–23, <https://doi.org/10.1177/0309133317749434>.
- Azzoni, R. S., Bollati, I. M., Pelfini, M., Valzasina, S., Brodský, L. (2024): Long-term (1951–2023) surface changes of the Belvedere Glacier observed through aerial and UAV orthophotos. *AUC Geographica* 59(2), 203–213, <https://doi.org/10.14712/23361980.2024.23>.
- Barnola, J. M., Pimienta, P., Raynaud, D., Korotkevich, Y. S. (1991): CO₂-climate relationship as deduced from the Vostok ice core: a re-examination based on new measurements and on re-evaluation of the air dating. *Tellus B* 43(2), 83–90, <https://doi.org/10.1034/j.1600-0889.1991.t01-1-00002.x>.
- Bařka, J. (2016): Factors of formation and development of supraglacial lakes and their quantification: a review. *AUC Geographica* 51(2), 205–216, <https://doi.org/10.14712/23361980.2016.17>.
- Benedetti, P., Ienco, D., Gaetano, R., Osé, K., Pensa, R., Dupuy, S. (2018): M3Fusion: A Deep Learning Architecture for Multiscale Multimodal Multitemporal Satellite Data Fusion. *IEEE Journal of Selected Topics in Applied Earth Observations and Remote Sensing* 11(12), 4939–4949, <https://doi.org/10.1109/JSTARS.2018.2876357>.
- Benn, D. I., Bolch, T., Hands, K., Gulley, J., Luckman, A., Nicholson, L. I., Quincey, D. J., Thompson, S., Toumi, R., Wiseman, S. (2012): Response of debris-covered glaciers in the Mount Everest region to recent warming, and implications for outburst flood hazards. *Earth-Science Reviews* 114(1–2), 156–174, <https://doi.org/10.1016/j.earscirev.2012.03.008>.
- Bhambri, R., Schmidt, S., Chand, P., Nüsser, M., Haritashya, U., Sain, K., Tiwari, S. K., Yadav, J. S. (2023): Heterogeneity in glacier thinning and slowdown of ice movement in the Garhwal Himalaya, India. *Science of The Total Environment* 875:162625, <https://doi.org/10.1016/j.scitotenv.2023.162625>.
- Boehner, J., Koethe, R., Conrad, O., Gross, J., Ringeler, A., Selige, T. (2002): Soil Regionalisation by Means of Terrain Analysis and Process Parameterisation. *Soil Classification* 2001, 213–222.
- Boehner, J., Selige, T. (2006): Spatial prediction of soil attributes using terrain analysis and climate regionalisation. *Gottinger Geographische Abhandlungen* 115, 13–28.
- Bollati, I. M., Viani, C., Masseroli, A., Mortara, G., Testa, B., Tronti, G., Pelfini, M., Reynard, E. (2023): Geodiversity of proglacial areas and implications for geosystem services: A review. *Geomorphology* 421: 108517, <https://doi.org/10.1016/j.geomorph.2022.108517>.
- Box, J., Ski, K. (2017): Remote sounding of Greenland supraglacial melt lakes: Implications for subglacial hydraulics. *Journal of Glaciology* 53(181), 257–265, <https://doi.org/10.3189/172756507782202883>.
- Brodský, L., Vilímek, V., Šobr, M., Kroczeck, T. (2022): The Effect of Suspended Particulate Matter on the Supraglacial Lake Depth Retrieval from Optical Data.

- Remote Sensing 14(23): 5988, <https://doi.org/10.3390/rs14235988>.
- Buckel, J., Otto, J. C., Prasicek, G., Keuschnig, M. (2018): Glacial lakes in Austria-Distribution and formation since the Little Ice Age. *Global and Planetary Change* 164, 39–51, <https://doi.org/10.1016/j.gloplacha.2018.03.003>.
- Büttner, G., Kosztra, B. (2017): CLC2018 Technical Guidelines. European Environment Agency Technical report No 17/2007. Available online: https://www.eea.europa.eu/publications/technical_report_2007_17/download (accessed on 18. 5. 2024)
- Conrad, O., Bechtel, B., Bock, M., Dietrich, H., Fischer, E., Gerlitz, L., Wehberg, J., Wichmann, V., Böhner, J. (2015): System for Automated Geoscientific Analyses (SAGA) v. 2.1.4. *Geoscientific Model Development* 8(7), 1991–2007, <https://doi.org/10.5194/gmd-8-1991-2015>.
- Cook, S. J., Quincey, D. J. (2015): Estimating the volume of Alpine glacial lakes. *Earth Surface Dynamics* 3(4), 559–575, <https://doi.org/10.5194/esurf-3-559-2015>.
- Diolaiuti, G., Citterio, M., Carnielli, T., D'Agata, C., Kirkbride, M., Smiraglia, C. (2006): Rates, processes and morphology of freshwater calving at Miage Glacier (Italian Alps). *Hydrological Processes: An International Journal* 20(10), 2233–2244, <https://doi.org/10.1002/hyp.6198>.
- Dirscherl, M., Dietz, A. J., Kneisel, C., Kuenzer, C. (2020): Automated Mapping of Antarctic Supraglacial Lakes Using a Machine Learning Approach. *Remote Sensing* 12(7): 1203, <https://doi.org/10.3390/rs12071203>.
- Fischer, L., Käab, A., Huggel, C., Noetzi, J. (2006): Geology, glacier retreat and permafrost degradation as controlling factors of slope instabilities in a high-mountain rock wall: the Monte Rosa east face, *Natural Hazards and Earth System Sciences* 6(5), 761–772, <https://doi.org/10.5194/nhess-6-761-2006>.
- Gao, J. (2009): Bathymetric mapping by means of remote sensing: methods, accuracy and limitations. *Progress in Physical Geography* 33(1), 103–116, <https://doi.org/10.1177/0309133309105657>.
- Geoportale Piemonte (2024). Available online: <http://www.geoportale.piemonte.it> (accessed on 15. 1. 2024).
- Gregory, S. A., Albert, M. R., Baker, I. (2014): Impact of physical properties and accumulation rate on pore close off in layered firn. *The Cryosphere* 8(1), 91–105, <https://doi.org/10.5194/tc-8-91-2014>.
- Haerberli, W., Käab, A., Paul, F., Chiarle, M., Mortara, G., Mazza, A., Deline, P., Richardson, S. (2002): A surge-type movement at Ghiacciaio del Belvedere and developing slope instability in the east face of Monte Rosa, Macugnaga, Italian Alps. *Norsk Geografisk Tidsskrift – Norwegian Journal of Geography* 56(2), 104–111, <https://doi.org/10.1080/002919502760056422>.
- Hu, J., Zhang, T., Zhou, X., Yi, G., Bie, X., Li, J., Chen, Y., Lai, P. (2024): A Glacial Lake Mapping Framework in High Mountain Areas: A Case Study of the Southeastern Tibetan Plateau. *IEEE Transactions on Geoscience and Remote Sensing* 62, 1–12, <https://doi.org/10.1109/TGRS.2023.3349281>.
- Ioli, F., Bianchi, A., Cina, A., De Michele, C.; Maschio, P.; Passoni, D.; Pinto, L. (2022): Mid-Term Monitoring of Glacier's Variations with UAVs: The Example of the Belvedere Glacier. *Remote Sensing* 14(1): 28, <https://doi.org/10.3390/rs14010028>.
- Käab, A., Huggel, C., Fischer, L., Guex, S., Paul, F., Roer, I., Salzmann, N., Schlaefli, S., Schmutz, K., Schneider, D., Strozzi, T., Weidmann, Y. (2005): Remote sensing of glacier- and permafrost-related hazards in high mountains: An overview. *Natural Hazards and Earth System Science* 5(4), 527–554, <https://doi.org/10.5194/nhess-5-527-2005>.
- Kaushik, S., Singh, T., Joshi, P. K., Dietz, J. A. (2022): Automated mapping of glacial lakes using multisource remote sensing data and deep convolutional neural network. *International Journal of Applied Earth Observation and Geoinformation* 115: 103085, <https://doi.org/10.1016/j.jag.2022.103085>.
- Kropáček, J., Neckel, N., Tyrna, B., Holzer, N., Hovden, A., Gourmelen, N., Schneider, C., Buchroithner, M., Hochschild, V. (2015): Repeated glacial lake outburst flood threatening the oldest Buddhist monastery in north-western Nepal. *Natural Hazards and Earth System Sciences* 15(10), 2425–2437, <https://doi.org/10.5194/nhess-15-2425-2015>.
- Lhermitte, S., Verbesselt, J., Verstraeten, W. W., Coppin, P. (2011): A comparison of time series similarity measures for classification and change detection of ecosystem dynamics. *Remote Sensing of Environment* 115(12), 3129–3152, <https://doi.org/10.1016/j.rse.2011.06.020>.
- Liang, Y.-L., Colgan, W., Lv, Q., Steffen, K., Abdalati, W., Stroeve, J., Gallaher, D., Bayou, N. (2012): A decadal investigation of supraglacial lakes in West Greenland using a fully automatic detection and tracking algorithm. *Remote Sensing of Environment* 123, 127–138, <https://doi.org/10.1016/j.rse.2012.03.020>.
- Liu, Z., Chen, X., Zhou, S., Yu, H., Guo, J., Liu, Y. (2022): DUPnet: Water Body Segmentation with Dense Block and Multi-Scale Spatial Pyramid Pooling for Remote Sensing Images. *Remote Sensing* 14(21): 5567, <https://doi.org/10.3390/rs14215567>.
- Ma, J., Song, C., Wang, Y. (2021): Spatially and Temporally Resolved Monitoring of Glacial Lake Changes in Alps During the Recent Two Decades. *Frontiers in Earth Science* 9: 723386, <https://doi.org/10.3389/feart.2021.723386>.
- Miles, K. E., Hubbard, B., Irvine-Fynn, T. D. L., Miles, E. S., Quincey, D. J., Rowan, A. V. (2017): Review article: The hydrology of debris-covered glaciers – state of the science and future research directions. *The Cryosphere Discuss.* [preprint], <https://doi.org/10.5194/tc-2017-210>.
- Miles, K. E., Hubbard, B., Irvine-Fynn, T. D. L., Miles, E. S., Quincey, D. J., Rowan, A. V. (2020): Hydrology of Debris-Covered Glaciers in High Mountain Asia. *Earth-Science Reviews* 207: 103212, <https://doi.org/10.1016/j.earscirev.2020.103212>.
- Miles, E.S., Steiner, J.F., Buri, P., Immerzeel, W.W., Pellicciotti, F., (2022): Controls on the Relative Melt Rates of Debris-Covered Glacier Surfaces. *Environmental Research Letters* 17: 064004, <https://doi.org/10.1088/1748-9326/ac6966>.
- Miles, E. S., Willis, I., Buri, P., Steiner, J. F., Arnold, N. S., Pellicciotti, F. (2018): Surface Pond Energy Absorption across Four Himalayan Glaciers Accounts for 1/8 of Total Catchment Ice Loss. *Geophysical Research Letters* 45(19), 10464–10473, <https://doi.org/10.1029/2018GL079678>.
- Mortara, G., Mercalli, L. (2002): Il lago epiglaciale «Effimero» sul ghiacciaio del Belvedere, Macugnaga, Monte Rosa. *Nimbus* 7(23–24), 10–17.

- NOAA (2024): Forecast Verification Glossary. Available online: <https://www.swpc.noaa.gov/sites/default/files/images/u30/Forecast%20Verification%20Glossary.pdf> (accessed on 1. 2. 2024).
- Planet Labs PBC (2018): Planet Application Program Interface: In Space for Life on Earth. Available online: <https://api.planet.com> (accessed on 2. 2. 2024).
- Pope, A., Scambos, T. A., Moussavi, M., Tedesco, M., Willis, M., Shean, D., Grigsby, S. (2016): Estimating supraglacial lake depth in West Greenland using Landsat 8 and comparison with other multispectral methods. *The Cryosphere* 10(1), 15–27, <https://doi.org/10.5194/tc-10-15-2016>.
- Racoviteanu, A. E., Nicholson, L., Glasser, N. F. (2021): Surface composition of debris-covered glaciers across the Himalaya using linear spectral unmixing of Landsat 8 OLI imagery. *The Cryosphere* 15(9), 4557–458, <https://doi.org/10.5194/tc-15-4557-2021>.
- Ranzi, R., Grossi, G., Iacovelli, L., Taschner, S. (2004): Use of multispectral ASTER images for mapping debris-covered glaciers within the GLIMS Project. *IEEE International Geoscience and Remote Sensing Symposium*, 1144–1147, <https://doi.org/10.1109/IGARSS.2004.1368616>.
- Reynolds, J. M. (2000): On the formation of supraglacial lakes on debris-covered glaciers. *IAHS-AISH Publication* 264: 153–161.
- Richardson, S. D., Reynolds, J. M. (2000): An overview of glacial hazards in the Himalayas. *Quaternary International* 65–66, 31–47, [https://doi.org/10.1016/S1040-6182\(99\)00035-X](https://doi.org/10.1016/S1040-6182(99)00035-X).
- Sakai, A. (2012): Glacial Lakes in the Himalayas: A Review on Formation and Expansion Processes. *Global Environmental Research* 16, 23–30.
- Salerno, F., Thakuri, S., D'Agata, C., Smiraglia, C., Manfredi, E. C., Viviano, G., Tartari, G. (2012): Glacial lake distribution in the Mount Everest region: Uncertainty of measurement and conditions of formation. *Global and Planetary Change* 92–93, 30–39, <https://doi.org/10.1016/j.gloplacha.2012.04.001>.
- Schröder, L., Neckel, N., Zindler, R., Humbert, A. (2020): Perennial Supraglacial Lakes in Northeast Greenland Observed by Polarimetric SAR. *Remote Sensing* 12(17): 2798, <https://doi.org/10.3390/rs12172798>.
- Sharma, A., Thakur, V., Prakash, C., Sharma, A., Sharma, R. (2024): Deep Learning-Based Glacial Lakes Extraction and Mapping in the Chandra–Bhaga Basin. *Journal of the Indian Society of Remote Sensing* 52, 435–447, <https://doi.org/10.1007/s12524-024-01829-x>.
- Somos-Valenzuela, M. A., McKinney, D. C., Rounce, D. R., Byers, A. C. (2014): Changes in Imja Tsho in the Mount Everest region of Nepal. *The Cryosphere* 8(5), 1661–1671, <https://doi.org/10.5194/tc-8-1661-2014>.
- Tamburini, A., Mortara, G. (2005): The case of the “Effimero” lake at Monte Rosa (Italian western Alps): studies, field surveys, monitoring. *10th Conference of the Euromediterranean Network of Experimental and Representative Basins (ERB)* 77, 179–184.
- Truffer, M., Kääh, A., Harrison, W. D., Osipova, G. B., Nosenko, G. A., Espizua, L., Gilbert, A., Fischer, L., Huggel, C., Craw Burns, P. A., Lai, A. W. (2021): Chapter 13 – Glacier surges. In: Haerberli, W., Whiteman, C. (ed.): *Snow and ice-related hazards, risks, and disasters*; Elsevier, 2021, 417–466, <https://doi.org/10.1016/B978-0-12-817129-5.00003-2>.
- Viani, C., Giardino, M., HuGGel, C., Perotti, L., Mortara, G. (2016): An overview of glacier lakes in the Western Italian Alps from 1927 to 2014 based on multiple data sources (historical maps, orthophotos and reports of the glaciological surveys). *Geografia Fisica e Dinamica Quaternaria* 39(2), 203–214, <https://doi.org/10.4461/GFDQ.2016.39.19>.
- Watson, C. S., Quincey, D. J., Carrivick, J. L., Smith, M. W. (2016): The dynamics of supraglacial ponds in the Everest region, central Himalaya. *Global and Planetary Change* 142, 14–27, <https://doi.org/10.1016/j.gloplacha.2016.04.008>.
- Watson, C. S., Quincey, D. J., Carrivick, J. L., Smith, M. W., Rowan, A. V., Richardson, R. (2018): Heterogeneous water storage and thermal regime of supraglacial ponds on debris-covered glaciers. *Earth Surface Processes and Landforms* 43(1), 229–241, <https://doi.org/10.1002/esp.4236>.
- Wendleder, A., Friedl, P., Mayer, C. (2018): Impacts of Climate and Supraglacial Lakes on the Surface Velocity of Baltoro Glacier from 1992 to 2017. *Remote Sensing* 10(11): 1681, <https://doi.org/10.3390/rs10111681>.
- Wendleder, A., Schmitt, A., Erbertseder, T., D'Angelo, P., Mayer, C., Braun, M. H. (2021): Seasonal evolution of supraglacial lakes on Baltoro Glacier from 2016 to 2020. *Frontiers in Earth Science* 9: 725394, <https://doi.org/10.3389/feart.2021.725394>.
- Williamson, A. G., Neil, S. A., Alison, F. B., Ian, C., Willis, A. (2017): Fully Automated Supraglacial lake area and volume Tracking (“FAST”) algorithm: Development and application using MODIS imagery of West Greenland. *Remote Sensing of Environment* 196, 113–133, <https://doi.org/10.1016/j.rse.2017.04.032>.
- Wu, Z., Gao, Y., Li, L., Xue, J., Li, Y. (2018): Semantic segmentation of high-resolution remote sensing images using fully convolutional network with adaptive threshold. *Connection Science* 31(2), 169–184, <https://doi.org/10.1080/09540091.2018.1510902>.
- Zeller, L., McGrath, D., McCoy, S. W., Jacquet, J. (2024): Seasonal to decadal dynamics of supraglacial lakes on debris-covered glaciers in the Khumbu region, Nepal. *The Cryosphere* 18(2), 525–541, <https://doi.org/10.5194/tc-18-525-2024>.

Dynamics of equilibrium line altitude in glaciers of the Monte Rosa massif in the Alps derived from Sentinel-2 satellite images

Jan Kropáček^{1,*}, Pragma Mehrishi¹

¹ Charles University, Faculty of Science, Department of Physical Geography and Geoecology, Czechia

* Corresponding author: kropacja@natur.cuni.cz

ABSTRACT

The equilibrium line altitude (ELA) is an immediate indicator of the mass balance of glaciers. The evolution of the ELA of four major glaciers in the Monte Rosa (European Alps) massif was investigated in this study. We used Sentinel-2 satellite images to derive the end-of-summer snowline altitude (SLA) as an approximation of ELA considering the fluctuations in the snowline at the end of the ablation season (from August to mid-October in 2016–2023). SLA was estimated as a percentile of the histogram of the DEM of each glacier with the applied snow-mask, based on the normalised difference snow index (NDSI). ELA was determined as the maximum snowline elevation reached in the season. We found the mean ELA for the studied period as 3560, 3230, 3430 and 3570 m above the sea level for Gornergletscher, Belvedere Glacier, Grenzgletscher, and Lys Glacier respectively. These differences are likely due to the variation in slope orientation and amount of snow accumulation. An increase in ELA was found for all the glaciers in the studied period amounting to 22.7, 8.3, 33.1 and 27.0 m/y respectively. The pattern of temporal behaviour was similar for all the glaciers, although we expected a different behaviour of the Belvedere Glacier, which is characterized by various local effects, such as frequent avalanching and rough topography.

KEYWORDS

snowline; equilibrium line altitude; Monte Rosa massif; mountain glaciers; cryosphere

Received: 23 February 2024

Accepted: 10 October 2024

Published online: 27 November 2024

Kropáček, J., Mehrishi, P. (2024): Dynamics of equilibrium line altitude in glaciers of the Monte Rosa massif in the Alps derived from Sentinel-2 satellite images. *AUC Geographica* 59(2), 229–239

<https://doi.org/10.14712/23361980.2024.17>

© 2024 The Authors. This is an open-access article distributed under the terms of the Creative Commons Attribution License (<http://creativecommons.org/licenses/by/4.0>).

1. Introduction

In recent decades, mountain glaciers have been significantly losing volume on a global scale (e.g. Hugonnet et al. 2021; Brun et al. 2017; Neckel et al. 2014). One of the effective ways to quantify the response of glaciers to the changing climate is equilibrium line altitude (ELA) as it is a direct, undelayed response (Zemp et al. 2007; Žebre et al. 2021) compared to the retreat of terminus which provides a delayed signal, especially in the case of debris-covered glaciers such as Belvedere (Zemp et al. 2007). ELA is widely used in paleoclimatic reconstructions (Benn and Lehmkuhl 2000; Kerschner and Ivy-Ochs 2008; Spagnolo et al. 2019; Lukas and Bradwell 2010). In general, an equilibrium line is a position on the glacier in which the ablation is equal to the accumulation over a period of one year (Benn and Lehmkuhl 2000).

Its position is climate-driven, especially by temperature and precipitation (Benn and Lehmkuhl 2000). The interannual changes in ELA are mostly influenced by the summer temperature and anomalies in winter accumulation (Rabatel et al. 2013; Six and Vincent 2014). Monitoring of fluctuations in ELA over a long period can be thus used as an indicator of the regional-scale impact of climate change (Racoviteanu et al. 2019).

ELA in the Alps has undergone significant changes since the Little Ice Age (LIA). The mean vertical shift of ELA in the Swiss Alps since the LIA (in the period 1890–1973) was +90 m (Maisch 2000), which corresponds to its mean rise of 0.6 m/y. An increase in ELA in the western Alps by about 170 m in the period 1984–2010 was reported by Rabatel et al. (2013) based on remote sensing measurements on 43 glaciers, which is on average, 6.5 m/y. Based on a modelling effort relying on an approximation of the P/T relationship by a quadratic function, an increase in the ELA of the Alps by 114 m in the period 1971–2000 was determined by Žebre et al. (2021) which corresponds to an average rise of 3.8 m/y.

However, ELA is also influenced by local factors such as snow accumulation on convex surfaces, wind accumulation, topographic shading and debris cover (Benn and Lehmkuhl 2000). Furthermore, the position and evolution of ELA of an individual glacier are modulated by shading, avalanching and snow-drift (Securo et al. 2024). To reflect these effects, the term 'effective ELA' is used for single glaciers while the 'environmental ELA' is the ELA cleaned off of the local effects. Environmental ELA is defined as the regional altitude of zero mass balance averaged over a long period and can be used to characterise a region (Žebre et al. 2021). Effective ELA on a small glacier can be shifted hundreds of metres lower compared to the regional environmental ELA (Securo et al. 2024). Snow line rises in years of high snow accumulation or little snow melt, and can reach the topmost parts of glaciers in the years with exceptionally hot summers

(Østrem 1975) as it happened at Monte Rosa for instance in summer 2023 (Bloomberg 2023).

The distribution of snow on glaciers attracted attention at the early stages of glacier research. The idea that snow accumulation equals ablation at the firn line dates to the 19th century and has evolved into the modern concept of the equilibrium line altitude (ELA) in glaciology (Zeller 1893; Hoinkes 1970). Early methods for estimating the firn line laid the groundwork for understanding glacier dynamics, with pioneers like Richter (1885) and Brückner (1886) proposing accumulation-area ratios that are still relevant today (Meier 1962; Gross et al. 1977; Braithwaite and Raper 2009). Relationships between precipitation, temperature, and ELA have been established (Ahlmann 1924; Loewe 1971; Braithwaite 1985; Pellitiero et al. 2015), enabling the estimation of ELA with known meteorological parameters. With the advent of satellite data, methods for computing glacier volume changes and ELA shifts have advanced (Echelmeyer et al. 1996; Berthier et al. 2004; Gardelle et al. 2012; Rabatel et al. 2005, 2008, 2012a).

The ELA can be approximated by end-of-summer snow line altitude (SLA), facilitating long-term reconstructions (Lliboutry 1965; Rabatel et al. 2005; Barcaza et al. 2009). SLA can be identified on remote sensing images as the lower limit of last winter's snow (Østrem 1975). The end-of-summer SLA can be derived from multispectral satellite images in combination with a digital elevation model (DEM) with a high accuracy compared to ground measurements and it can also be derived on the glaciers with no ground data (Rabatel et al. 2005).

The major challenges are to distinguish between snow cover, exposed ice and clouds to convert the often curvy and insular snow limit to a single elevation and to account for the changing glacier surface elevation while using a DEM. Various approaches have been developed in recent decades but no standardised solution has been accepted yet (Racoviteanu et al. 2019).

Rabatel (2005, 2008, 2012) identified snow line manually in an RGB synthesis and advocated using the central part of the glacier for the estimation of ELA to avoid the effects of shadowing, additional snow inputs by avalanches and snow drift. Rastner et al. (2019) used Otsu thresholding of Landsat's near-infrared band for snow on glacier mapping and bins in the histogram of altitude with >50% of snow cover as an estimate of SLA. Racoviteanu et al. (2019) developed an automated approach based on band ratios using Landsat imagery and SRTM DEM. Loibl et al. (2022) mapped ELA from Landsat data for the entire High Asia for the period 1986–2021 using three spectral indices including the NDSI and median of the two lowest altitude range percentiles of the snow-covered part of the glaciers.

The methods of ELA derivation including distributed mass balance modelling and remote sensing,

allow for comprehensive studies of the climate-glacier relationship at various spatial scales (Demuth and Pietroniro 1999; Mathieu et al. 2009; Rabatel et al. 2013). Glaciers of Monte Rosa massif represent various settings in terms of orientation, longitudinal profile, type of feeding mechanisms and ice thermal state. Thus, they provide an opportunity to study the glacier-climate interactions at a detailed scale.

The objective of this study is to derive the recent changes in the ELA of four glaciers in the Monte Rosa massif. A further objective is to compare the trends of ELA for the four glaciers and to understand whether the Belvedere glacier has anomalous behaviour due to its distinctly different properties.

2. Study area

Monte Rosa is a highly glaciated mountain massif in the Western (Pennine) Alps. Its glaciation has been studied by scientists and explorers since the end of the 18th century. Monte Rosa massif formed as a nappe, is composed of high-pressure metamorphic gneiss (Froitzheim 2001). Its summits exceed 4000 m a.s.l. and the ice plateaus at Colle Gnifetti and Colle de Lys were used for the drilling of ice cores which probably cover the longest records in the Alps (Smiraglia et al. 2000).

There are four major glaciers at the Monte Rosa massif (Fig. 1). Gornergletscher is oriented towards the west and drains to the Matter Valley in Valais Canton, Switzerland. According to the Randolph Glacier Inventory (RGI) (RGI 7.0 Consortium 2023), it encompasses several glaciers, from which some have already detached such as Theodulgletscher, Breithorn-gletscher and Schwarzegletscher. As we are interested in the variation of ELA in the area, we treated detached glaciers separately (Fig. 1). The main trunk is actually formed by Grenz-gletscher from which Gornergletscher has detached recently (Rettig et al. 2023). An ephemeral lake developed at the place of the former confluence of the glaciers in the spring of 2022 (Pandey and Kropáček 2023). Gornergletscher was one of the focused glaciers by a mass balance study based on time-lapse photography by Huss et al. (2013). Grenz-gletscher is a polythermal glacier with typical persistent meltwater streams, in which the cold ice is located along the central flowline (Ryser et al. 2013). The former tributary glaciers including Gornergletscher are dominated by temperate ice. Before 2011, Gornier Lake periodically appeared at the ice margin on the confluence of Gornergletscher and Grenz-gletscher and drained sub-glacially later in the season (Huss et al. 2007).

Lys Glacier is located on the Italian side of the massif; it is oriented to the south and drains towards Gressoney Valley. This is probably the most monitored glacier in the Italian Alps. It has been retreating in the last decades, leaving behind a proglacial lake

(Diolaiuti et al. 2016). The retreat was alternated by a short period of advance between 1976 and 1985. The accumulation of persistent organic pollutants and pesticides has been intensively studied on the glacier (Villa et al. 2006; Rizzi et al. 2019). Lastly, Belvedere Glacier is a heavily debris-covered glacier and to large extent avalanche-fed with an elevated bed (Diolaiuti et al. 2016). It experienced a surge-like flow acceleration in the period 2001–2002 (Kääb et al. 2004; Truffer et al. 2021). The terminus of Belvedere is bi-lobate which reaches below the tree line. Several other smaller glaciers drain the massif for instance Piode, Nordend, Sesia and Nord delle Locce, but they are not part of this study (Fig. 1).

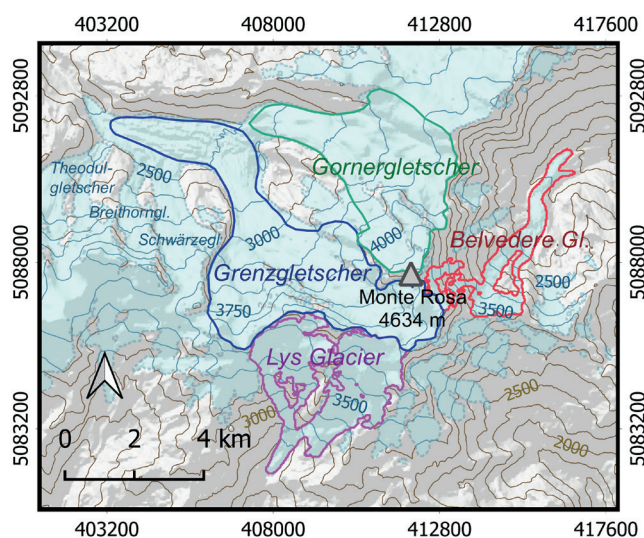


Fig. 1 The studied glaciers in the Monte Rosa massif represent various environmental settings. The contours with an interval of 250 m were derived from the Copernicus Digital Elevation Model with a 30 m cell size. The background map is based on Open Street Map (OSM) data. The coordinate system is UTM zone 32 North (EPGS 32632).

The massif hosts several interesting glacial lakes such as Locce Lake which appeared at the terminus of Nord delle Locce Glacier in the 1940s. It was the source of three glacier lake outburst floods in 1970, 1978 and 1979. A supraglacial lake called Effimero appeared in connection to the surge-like event in 2001–2002 in a depression on Belvedere Glacier at the transition between its steep and flatter part of the glacier.

The area features a harsh climate. Winter is relatively dry whereas there is more precipitation in Spring and Summer with minimum and maximum precipitation in February and May respectively. One of the summits of Monte Rosa (Punta Gnifetti) hosts the highest weather station in Europe located at Margherita Hut (4560 m a.s.l., the mean annual temperature -12.4°C) which started operation in 1904. During heat waves, the temperature can exceed 0°C for instance at the end of June 2019.

3. Methods

For the detection of SLA, we used Sentinel-2 data for the whole period of operation 2015–2023. Sentinel-2 is a constellation of two identical satellites Sentinel-2A and Sentinel-2B, launched in frames of the Copernicus programme of the European Commission (Drusch et al. 2012). Sentinel-2A was launched in 2015 and Sentinel-2B in 2017 which resulted in rather sparse data availability for the first two years of the operation. The year 2015 was omitted as only one relevant image was found.

The satellites carry the Multispectral Instrument (MSI) which is a broad-band optical sensor with 13 spectral bands in visible, near-infrared and short-wave infrared ranges of spectrum. The instrument operates with resolutions of 10, 20 and 60 metres. The constellation of the two satellites has a high temporal resolution with a revisit period of five days on the equator. The latitude of 45.9° overlap of neighbouring swaths covering the study area results in a revisit of three days which is unfortunately largely reduced by frontal and orographic cloudiness.

Tab. 1 List of Sentinel-2 images used in the analysis.

Date	Count	Dates
2016	4	03-Aug, 13-Aug, 23-Aug, 09-Sep
2017	9	05-Aug, 15-Aug, 25-Aug, 07-Sep, 20-Sep, 20-Aug, 23-Aug, 12-Sep, 22-Sep
2018	10	20-Aug, 30-Aug, 19-Sep, 22-Sep, 29-Sep, 12-Oct, 28-Aug, 04-Sep, 24-Sep, 27-Sep
2019	5	25-Aug, 17-Sep, 30-Aug, 09-Sep, 12-Sep
2020	8	01-Sep, 18-Sep, 28-Sep, 08-Oct, 27-Aug, 03-Sep, 13-Sep, 16-Sep
2021	7	06-Sep, 13-Sep, 06-Oct, 13-Oct, 29-Aug, 01-Sep, 11-Sep
2022	4	11-Sep, 18-Sep, 24-Aug, 16-Sep
2023	12	07-Aug, 24-Aug, 06-Sep, 26-Sep, 03-Oct, 12-Aug, 19-Aug, 22-Aug, 11-Sep, 01-Oct, 08-Oct, 11-Oct

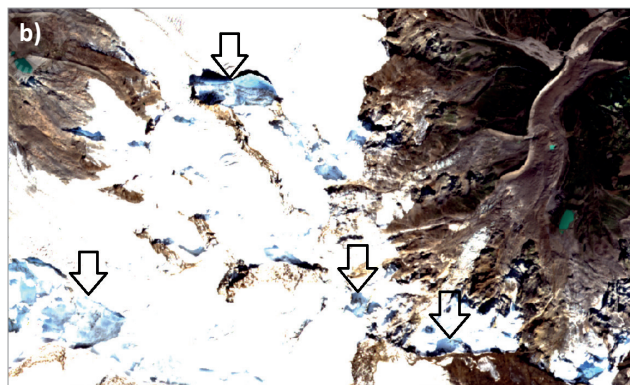


Fig. 3 Artefacts introduced by the topographic corrections in the L2A version of Sentinel-2 image showing the summit part of Monte Rosa and Belvedere glacier (b) compared to the same image processed without topographic corrections as applied in this study (a). The artefacts in the areas of shadows are marked by arrows. The image was acquired on 11 October 2023.

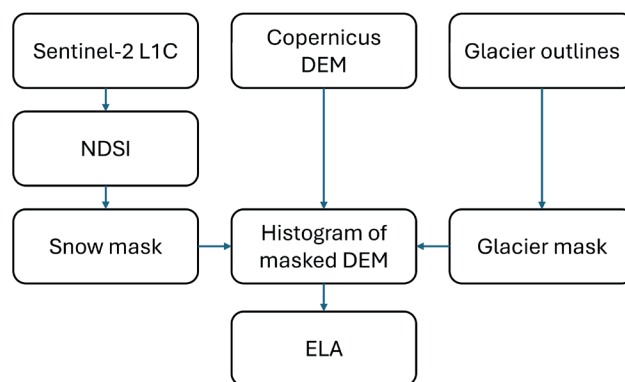


Fig. 2 Flow chart of ELA estimation based on Sentinel-2 image, Copernicus DEM and glacier outlines.

The further processing steps are shown in Fig. 2. We obtained Sentinel-2 images from Copernicus Browser and applied the filter of maximum cloudiness < 30%. As only the data for the end of ablation season are relevant for ELA estimation using end-of-summer snowline, Sentinel-2 images for the period of 1 August to 15 October from 2016 to 2023 were used. In the next step, the images were visually screened and the ones with extensive snow cover were removed from the selection (Tab. 1). To ensure consistency in ELA estimates, atmospheric correction was applied to the L1C product using Sen2Cor (Main-Knorn et al. 2017). The resulting L2A product differs from the one available via Copernicus Browser which contains the atmospheric corrections as well as corrections for topography. The topographic corrections which are efficient in moderate terrain, introduced some artefacts to the images in steep terrain, especially in the shadows. Examples of such artefacts are shown in (Fig. 3).

Randolph Glacier Inventory (RGI) version 7, which is a global shapefile of glacier borders, was used for the delineation of glaciers in this study (RGI 7.0 Consortium 2023). The RGI glacier outlines were used for Belvedere and Lys glaciers while some modifications were made in the case of Gornergletscher as

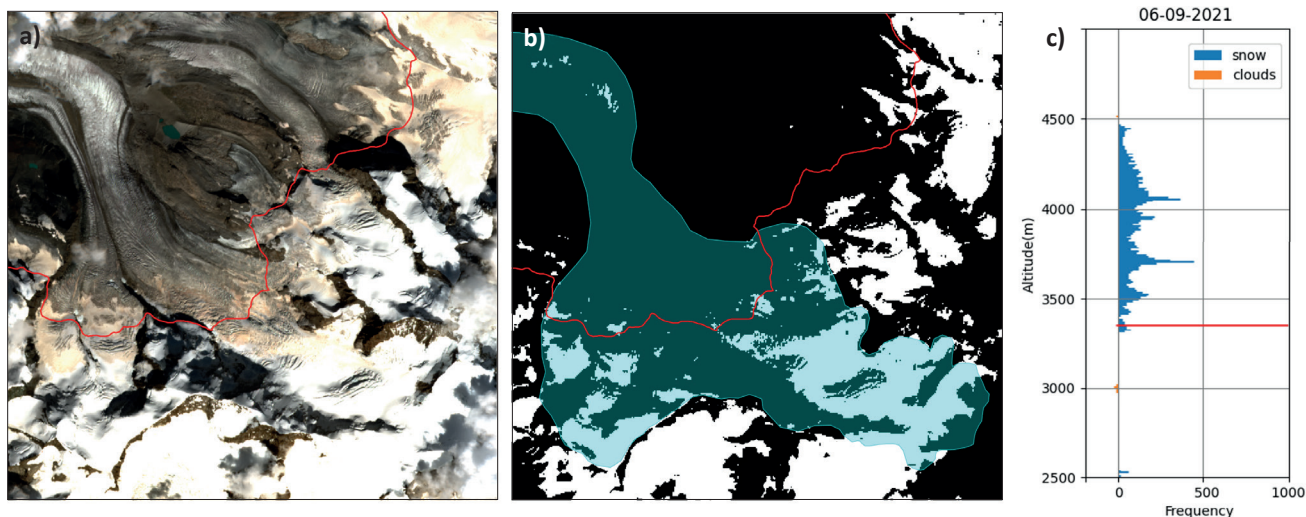


Fig. 4 Derived snow line (marked in red) on Grenzgletscher shown on Sentinel-2 image from 6 September 2021 as a contour 3350 m a.s.l. (a), on snow mask using NDSI threshold of 0.7 (b) and a histogram of Copernicus DEM under the mask of snow on glacier with SLA marked in red (c).

described in the section Study area. This way more homogeneous areas were obtained for snowline mapping in terms of slope and orientation.

$$NDSI = \frac{B3(G) - B11(SWIR)}{B3 + B11}$$

The Normalised Difference Snow Index (NDSI) (Valovcin 1976; Hall and Riggs 2010) with threshold 0.7 was used for mapping snow cover on the glaciers. This appeared to be effective for the distinction of snow from clouds. The images were checked again for cloud cover, as the cloudiness of higher altitudes can differ from the cloudiness given for the whole image and the threshold for maximum cloud percentage was applied only to the glacier area. The masks of opaque and cirrus clouds available in the used S2A product were used in this step. To derive the SLA, we used an approach based on thresholding of the histogram. For each glacier, a histogram of the DEM, under a mask resulting as a combination of snow mask based on the NDSI and glacier mask, was calculated. Then, the SLA for each image was calculated as the 3rd percentile of the histogram (Fig. 4). This reduced the impact of the outlying values in the histogram which could induce a bias in the results. The outlying values can be attributed to the noise or leftover snow caused by topography. The minimum value of the histogram of 2500 m a.s.l. was introduced to avoid the influence of blank ice on the lower part of Grenzgletscher. In the next step, histograms of snow on the glacier were plotted together with histograms of clouds on the glacier. Then the histograms were manually checked for the influence of clouds, especially in the zone of minimal altitude corresponding to the snow line. In the next step, ELA was determined as the maximum SLA in the period of 1 August to 15 October for each year.

To validate the automatized extraction of ELA, manual delineation of SLA was done for the Grenzgletscher

and Belvedere glaciers. The same dates of L2A images were used for the purpose and the bands were visualised as false colour RGB composite employing bands 8, 4 and 3 which enhanced the visibility of the snow line. Three points were identified along the snow line in places with good distinction of the snow-ice transition avoiding snow patches, trying to cover the whole width of the glacier. The elevation of the points was extracted from Copernicus DEM and the mean was calculated.

The weather parameters were obtained from the E-OBS dataset and Passo Del Monte Moro station, located 11 km from the main summit of Monte Rosa and 5 km from Belvedere Glacier to the north-east. E-OBS is an ensemble gridded dataset of 0.1-degree resolution (Cornes et al. 2018). The European Climate Assessment & Dataset project maintains and updates the dataset. The daily mean, minimum and maximum temperature and daily precipitation were extracted for the study area and used for plotting them to understand the scenario during our studied period. The same parameters were also extracted and plotted from the data from the Passo del Monte Moro Station operated by the *Agenzia regionale per la protezione ambientale Piemonte* for the same period.

4. Results

The processing of Sentinel-2 images resulted in a time series of SLA values for the four glaciers. The changes in SLA at the end of the ablation season in the period 2016–2023 are shown in Fig. 5. The relatively monotonous evolution of intra-annual values of SLA are interrupted by sudden fluctuations towards low altitudes. These fluctuations are due to the snowfall events. The four glaciers have a similar pattern of temporal variation in SLA. This is indeed due to their

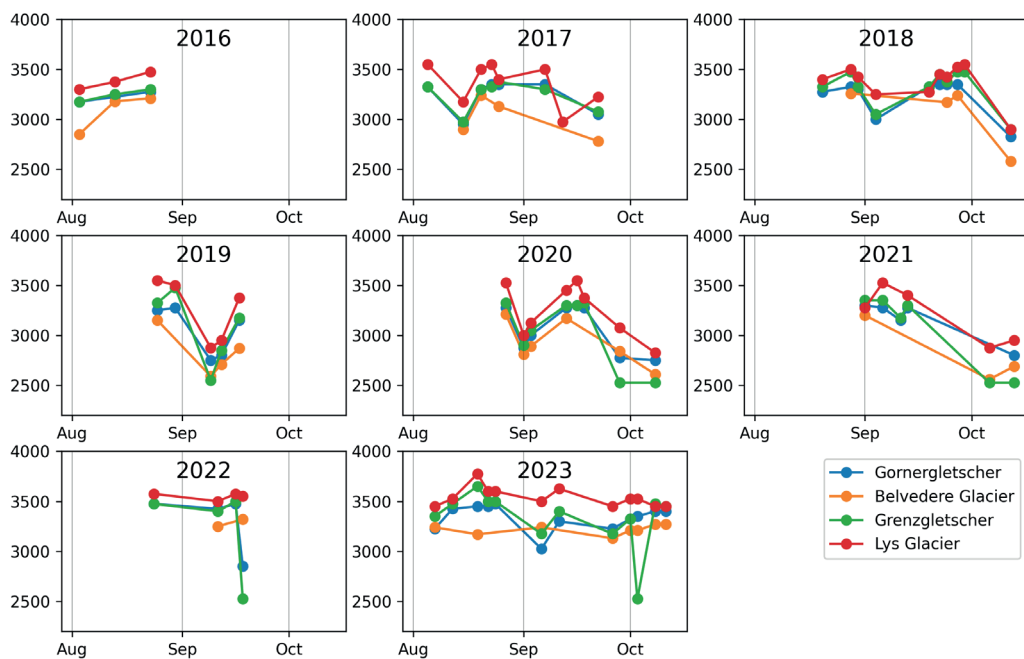


Fig. 5 Snow line elevations derived for the four studied glaciers for the end of the ablation period (August to mid-October) in the period 2016–2023. Note that all the y-axes have the same range of values.

vicinity and related similarities in climate conditions in terms of temperature and precipitation.

The time series for Belvedere Glacier has the least number of observations as many values were discarded due to the cloudiness which often gathers along the main ridge of Monte Rosa’s summits. Due to the steepness of the east face, the snow line can be easily covered either by a cloud or its shadow. An example of such an image affected by sparse cloudiness is shown in Fig. 6. Lys and Gornergletscher are surprisingly similar considering they are separated by the main ridge of the Pennine Alps which acts as a major climate divide.

The selection of maxima in the SLA time series for each year and glacier resulted in an estimate of the ELA of the glacier in the period 2016–2023 (Tab. 2). The ELA for all four glaciers showed an increasing trend (Fig. 7 and Tab. 2). Lys Glacier has the highest mean ELA of 3571 m a.s.l. which is indeed due to the southern orientation. It has a high trend in ELA which is 27 m/y for the studied period.

The lowest mean ELA was determined for Belvedere Glacier. It is at 3230 m a.s.l. which is 340 m lower compared to Lys Glacier. The ELA of Belvedere passes high in the east face of the Monte Rosa and follows the lower edge of the Signal Glacier which is a large

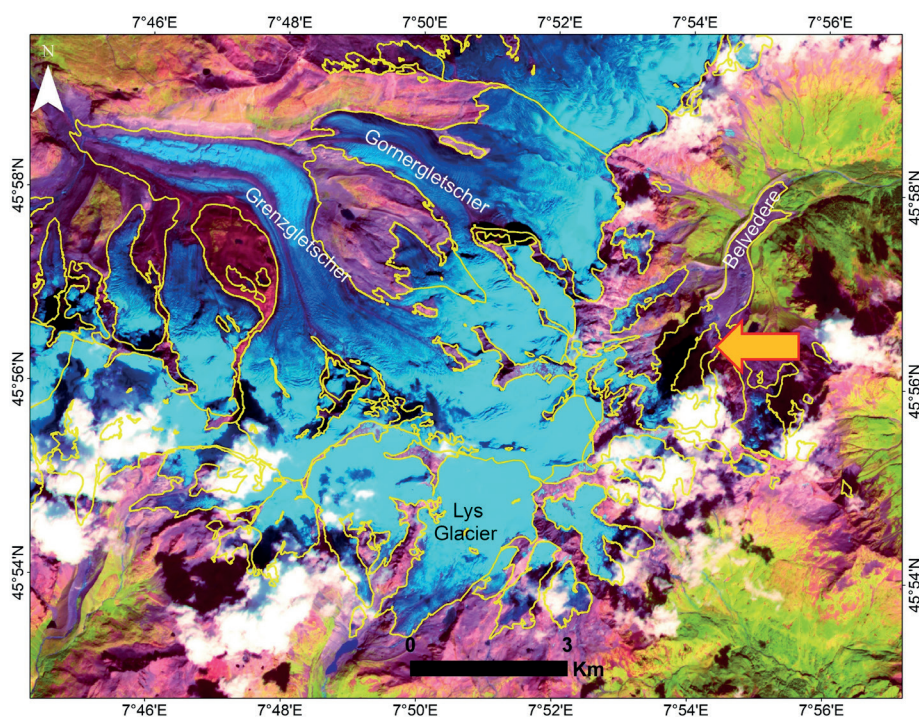


Fig. 6 A typical situation of cloud shadow (marked by an arrow) on Belvedere Glacier as shown on a false-colour Sentinel-2 image, with RGB displaying B11-B8-B4 (SWIR-NIR-R), from 24 August 2023. Clouds are in white, snow and ice in cyan and blue respectively, and the debris cover in purple colour.

Tab. 2 Values of ELA (m a.s.l.) for the period 2016–2023 for the four studied glaciers and the increase in the ELA per year derived by linear regression.

Glacier	2016	2017	2018	2019	2020	2021	2022	2023	mean	Trend in ELA (m/y)
Gornergletscher	3280	3370	3360	3280	3300	3300	3490	3490	3360	22.7
Belvedere	3210	3240	3260	3150	3210	3200	3320	3270	3230	8.3
Grenzgletscher	3310	3330	3490	3480	3330	3350	3510	3660	3430	33.1
Lys	3470	3550	3560	3550	3550	3520	3580	3790	3570	27.0

hanging glacier with a connection to the main flow of Belvedere. This altitude is influenced by a synergy of many local factors such as slope leading to avalanching, concavity and shadowing. An accumulation of snow drifted from the NW can also be an important influencing factor here. Belvedere Glacier has the lowest trend in ELA reaching only 8.3 m/y.

Although both Gornergletscher and Grenzgletscher have a western orientation and are on the north from the main ridge of the Pennine Alps, fluctuations of their ELAs differ. For Grenzgletscher a shift to a higher altitude occurred in 2018 and 2019, as it can be seen in Fig. 7, whereas ELA of Gornergletscher was almost stable between 2017 and 2018 and decreased in 2019 similarly to Belvedere Glacier (Fig. 7). The higher ELA of Grenzgletscher compared to Gornergletscher might be due to the shadowing effect of Lyskamm which is a high ridge between Gornergletscher and Lys Glacier or due to a higher accumulation caused by wind drift.

5. Discussion

Our results reveal a large variation of ELA both in time and space. This points to the fact that the general deglaciation, under the influence of climate change, is modified by very local morphological and climatic conditions. The mean ELAs for the four glaciers span the range 3230–3570 m a.s.l., with the lowest and highest values standing for Belvedere Glacier and Lys Glacier respectively. This elevation span of 340 m reveals a large variation in ELA over a relatively short distance. For the Himalaya-Karakoram region, Racoviteanu et al. (2019) report a gradient in ELA of 8 m

per 1 km in the Hunza area with a strong gradient in precipitation while the ELA gradient in Trishuli area was 13 m per 1 km on the transition of dry Tibetan Plateau. This points out a strong influence of precipitation on ELA in general. The variation of ELA at Monte Rosa, however, represents the influence of local conditions complying with the concept of effective ELA rather than an overall spatial trend. Similarly, for the nearby Allalingletscher and Schwarzberggletscher the difference in ELA of 200 m was reported by Huss et al. (2015). A higher amount of winter accumulation due to the closeness to the main weather divide was proposed to explain the difference. A larger difference of even 420 m was reported between Allalingletscher and Claridengletscher by the same authors, this time however, the distance between the glaciers was 120 km. Variations in ELA in the order of hundreds of metres over a trajectory crossing the major climate divides could be seen in the results by Racoviteanu et al. (2019) as well. The relation of these differences to local terrain and climate variations is consistent with findings of Rabatel et al. (2013).

Both the SLA fluctuations and ELA and its trend of Belvedere Glacier were surprisingly similar to the three other glaciers. Larger differences might have been expected considering the very different properties of Belvedere Glacier compared with the other three glaciers considering the possible shift of ELA for a debris-covered glacier for hundreds of metres reported by Securo et al. (2024) for a small debris-covered glacier in the Dolomites in the eastern Alps.

The fluctuations of ELA can partially be explained by the climate variables shown in Fig. 8. The general

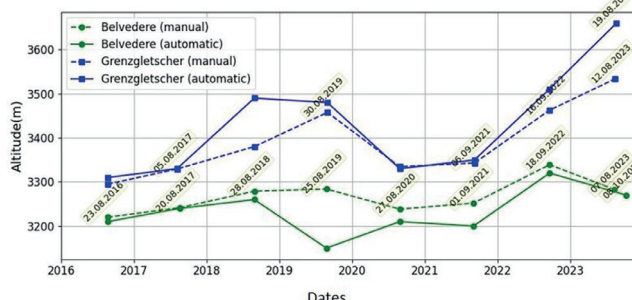
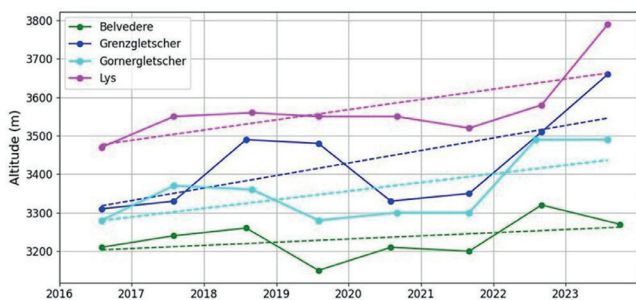


Fig. 7 Changes in ELA for the four studied glaciers and the linear trends showing the increase in ELA for all of them (left). The manually derived ELA from Sentinel-2 images for Belvedere Glacier and Grenzgletscher are compared to the automatically derived ones (right).

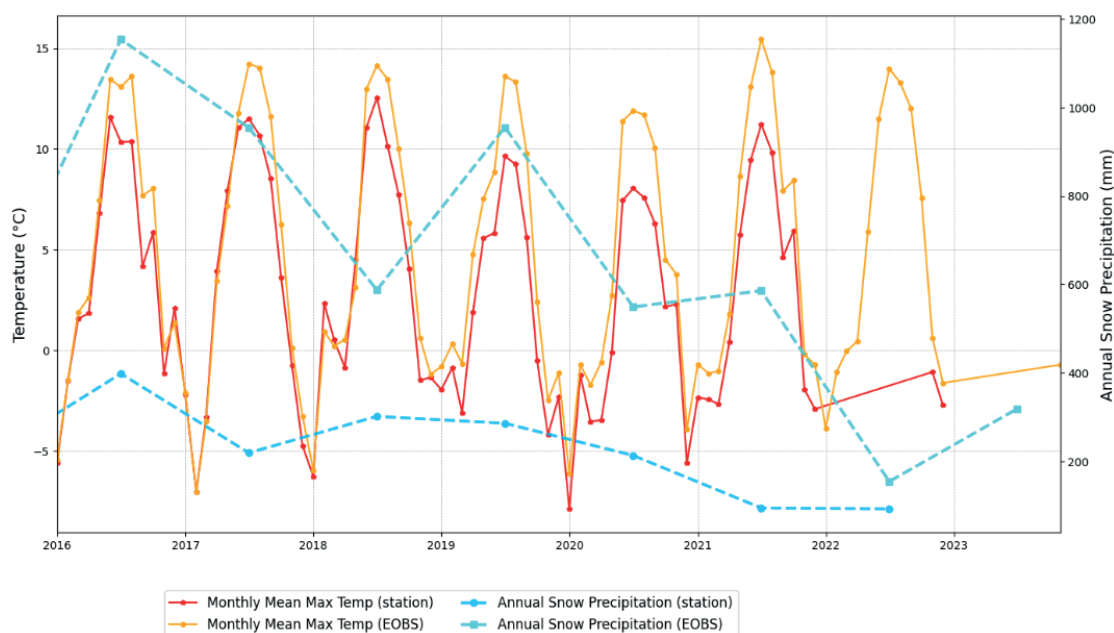


Fig. 8 The mean annual and mean summer temperature, total annual precipitation, and snow precipitation (precipitation with daily mean temp < 0 °C in the period October–June) in the area based on weather station Passo del Monte Moro (2820 m a.s.l., installed in 1988 and operated by *Agenzia Regionale per la Protezione Ambientale*) and on E-OBS ensemble gridded dataset (0.1-degree resolution).

increase in ELA corresponds to the increase in the mean summer temperature from both E-OBS and station data which is in accordance with the findings of Davaze et al (2020) for the Alps in the period 2000–2016. In our studied period, Europe was affected by summer heatwaves in 2018, 2019, 2022, and 2023 (Lhotka and Kyselý 2024). However, the heatwave years 2018 and 2019 coincide with an increase in ELA only for Grenzgletscher while the heatwave years 2022 and 2023 are well reflected in ELA as a clear increase for all four glaciers. Apart from 2021 the heatwave are not clearly reflected in monthly temperatures from both the EOBS and the station. The overall decreasing trend in solid precipitation corresponds to the increase in ELA in the studied period. This precipitation decrease is probably the reason behind the high rates of ELA increase which exceed the rates found by other authors for the Alps (see below). A more detailed analysis of the influence of precipitation on ELA is hindered by inconsistency between the data from the station and from EOBS. The mean trends of ELA for the four glaciers exceed the results of previous studies. The value of increase of 6.5 m/y derived by Rabatel et al. (2013) for the Western Alps in the period 1984–2010 using remote sensing is close to the one that we derived for the Belvedere Glacier (8.3 m/y) but it is about four times less than for the other three glaciers studied here. The average increase of the environmental ELA in the Alps in the period 1971–2000 determined by Žebre et al. (2021) by a modelling effort, based on climate model simulations, is even less (3.8 m/y).

The positive trend for all four glaciers is mainly due to the high ELA values in 2022 and 2023 (Fig. 7)

which corresponds to the temperature increase which is unfortunately not fully covered by the climate data (Fig. 8). Clearly, the trends largely influenced by a single climate fluctuation cannot represent a general tendency connected to climate but rather show the sensitivity of ELA to climate drivers.

The high temporal acquisition frequency of the Sentinel-2 constellation leads indeed to a better availability of cloud-free scenes at the end of the ablation season compared to the studies using historical Landsat data, for which a systematic shift of ELA due to data availability was reported by Rastner et al. (2019) which, however, did not affect glacier-specific differences. Still, there are large differences in availability of cloud-free Sentinel-2 data in different years, as it can be seen in Fig. 5. For instance, the lack of September images in 2016 might have led to a bias in ELA estimation.

The validation based on manual snowline detection for Belvedere and Grenzgletscher resulted in a good agreement with the automatic approach (Fig. 7). Large differences were found only in 2018 for Grenzgletscher and 2019 for Belvedere Glacier which was due to an enormous patchiness of the snow limits.

6. Conclusions

The ELA was derived for the four major glaciers of the Monte Rosa massif for the last eight years from Sentinel-2 data using a multitemporal approach and percentile of elevation of the snow-covered part of the glaciers. In conclusion, the analysis of equilibrium line altitude (ELA) trends over the past eight years for

the major glaciers of the Monte Rosa massif reveals consistent increasing trends with slight variations across the glaciers. However, attributing these ELA changes solely to climate change cannot be concluded, given the relatively short duration of the study period. Instead, these variations may be linked to climate oscillations, highlighting the importance of considering natural climate variability in interpreting glacier dynamics.

The trend and temporal pattern for Belvedere glacier was surprisingly similar to the other three keeping in mind the avalanching, steep slope inclination and challenging morphology of the slope with shadows and variations in illumination. Despite the challenges posed by the complex terrain and varying illumination conditions, the trend for the Belvedere glacier could be discerned without problems, underscoring the robustness of the methodology employed.

In moving forward, continued monitoring of ELA trends, coupled with longer-term observational records and complementary data sources, will be essential for disentangling the complex interplay of climate variability and anthropogenic climate change in shaping glacier dynamics.

Acknowledgements

We used the Copernicus DEM, GLO-30 dataset (<https://doi.org/10.5270/ESA-c5d3d65>). We acknowledge the E-OBS dataset from the EU-FP6 project UERRA (<https://www.uerra.eu>), the Copernicus Climate Change Service, and the data providers in the ECA&D project (<https://www.ecad.eu>). Climate data from the Passo del Monte Moro station were provided by ARPA (Agenzia Regionale per la Protezione Ambientale Piemonte). This work was supported by the Cooperatio project 255-207023032 of the Ministry of Education, Youth and Sports of the Czech Republic, the 4EU+ grant number 4EU+/23/F4/19 and Charles University Grant Agency project (GAUK project no. 208223) awarded to Pragma Mehrishi. We are grateful to Dr. Andrea De Zordi from Provincia del Verbano-Cusio-Ossola for her support of our field visits.

References

- Ahlmann, H. W. S. (1924): Le niveau de glaciation comme fonction de l'accumulation d'humidité sous forme solide: Méthode pour le calcul de l'humidité condensée dans la haute montagne et pour l'étude de la fréquence des glaciers. *Geografiska Annaler* 6(3–4), 223–272, <https://doi.org/10.1080/20014422.1924.11881098>.
- Auer, I., Böhm, R., Jurkovic, A., Lipa, W., Orlik, A., Potzmann, R., Schöner, W., Ungersböck, M., Matulla, C., Briffa, K., Jones, P., Efthymiadis, D., Brunetti, M., Nanni, T., Maugeri, M., Mercalli, L., Mestre, O., Moisselin, J.-M., Begert, M., Müller-Westermeier, G., Kveton, V., Bochnicek, O., Stastny, P., Lapin, M., Szalai, S., Szentimrey, T., Cegnar, T., Dolinar, M., Gajic-Capka, M., Zaninovic, K., Majstorovic, Z., Nieplova, E. (2007): HISTALP – historical instrumental climatological surface time series of the Greater Alpine Region. *International Journal of Climatology: A Journal of the Royal Meteorological Society* 27(1), 17–46, <https://doi.org/10.1002/joc.1377>.
- Barcaza, G., Aniya, M., Matsumoto, T., Aoki, T. (2009): Satellite derived equilibrium lines in Northern Patagonia Icefield, Chile, and their implications to glacier variations. *Arctic Antarctic and Alpine Research* 41, 174–182, <https://doi.org/10.1657/1938-4246-41.2.174>.
- Benn, D. I., Lehmkühl, F. (2000): Mass balance and equilibrium-line altitudes of glaciers in high-mountain environments. *Quaternary International* 65–66, 15–29, [https://doi.org/10.1016/S1040-6182\(99\)00034-8](https://doi.org/10.1016/S1040-6182(99)00034-8).
- Berthier, E., Arnaud, Y., Baratoux, D., Vincent, C., Rémy, F. (2004): Recent rapid thinning of the “Mer de Glace” glacier derived from satellite optical images. *Geophysical Research Letters* 31(17), <https://doi.org/10.1029/2004GL020706>.
- Bloomberg, L. P. (2023): Alpine Heat Wave Pushes Freezing Level Above Europe’s Glaciers, SWI swissinfo.ch. Available online: <https://www.swissinfo.ch/eng/alpine-heat-wave-pushes-freezing-level-above-europe-s-glaciers/48752620> (accessed on 5. 12. 2023).
- Braithwaite, R. J. (1984): Can the mass balance of a glacier be estimated from its equilibrium-line altitude? *Journal of Glaciology* 30(106), 364–368, <https://doi.org/10.3189/S0022143000006237>.
- Braithwaite, R. J. (1984): Calculation of degree-days for glacier-climate research. *Z. Gletscherkd. Glazialgeol* 20, 1–20.
- Braithwaite, R. J., Raper, S. C. B. (2009): Estimating equilibrium-line altitude (ELA) from glacier inventory data. *Annals of Glaciology* 50(53), 127–132, <https://doi.org/10.3189/172756410790595930>.
- Brückner, E. (1886): Die hohen Tauern und ihre Eisbedeckung, eine orometrische Studie. *Z. Deutscher und Österreichischer Alpenverein* 17, 163–187.
- Brun, F., Berthier, E., Wagnon, P., Kääh, A., Treichler, D. (2017): A spatially resolved estimate of High Mountain Asia glacier mass balances from 2000 to 2016. *Nature Geoscience* 10(9), 668–673, <https://doi.org/10.1038/ngeo2999>.
- Cornes, R. C., van der Schrier, G., van den Besselaar, E. J., Jones, P. D. (2018): An ensemble version of the E-OBS temperature and precipitation data sets. *Journal of Geophysical Research: Atmospheres* 123(17), 9391–9409, <https://doi.org/10.1029/2017JD028200>.
- Davaze, L., Rabatel, A., Dufour, A., Hugonnet, R., Arnaud, Y. (2020): Region-wide annual glacier surface mass balance for the European Alps from 2000 to 2016. *Frontiers in Earth Science* 8:149, <https://doi.org/10.3389/feart.2020.00149>.
- Demuth, M., Pietroniro, A. (1999): Inferring glacier mass balance using RADARSAT: results from Peyto Glacier, Canada. *Geografiska Annaler: Series A, Physical Geography* 81(4), 521–540, <https://doi.org/10.1111/1468-0459.00081>.
- Diolaiuti, G. A., Vezzola, L. C., Senese, A., D’Agata, C., Fugazza, D., Leonelli, G., Pelfini, M. (2016): Recent changes of the ablation tongue and glacier foreland at the Lys Glacier (Italian Alps).

- Drusch, M., Del Bello, U., Carlier, S., Colin, O., Fernandez, V., Gascon, F., Hoersch, B., Isola, C., Laberinti, P., Martimort, P., Meygret, A., Spoto, F., Sy, O., Marchese, F., Bargellini, P. (2012): Sentinel-2: ESA's optical high-resolution mission for GMES operational services. *Remote sensing of Environment* 120, 25–36, <https://doi.org/10.1016/j.rse.2011.11.026>.
- Echelmeyer, K. A., Harrison, W. D., Larsen, C. F., Sapiano, J., Mitchell, J. E., De Mallie, J., Rabus, B., Adalgeirsdóttir, G., Sombardier, L. (1996): Airborne surface profiling of glaciers: a case-study in Alaska. *Journal of Glaciology* 42(142), 538–547, <https://doi.org/10.3189/S002214300000352X>.
- Gardelle, J., Berthier, E., Arnaud, Y. (2012): Impact of resolution and radar penetration on glacier elevation changes computed from DEM differencing. *Journal of Glaciology* 58, 419–422, <https://doi.org/10.3189/2012JG11J175>.
- Gross, G., Kerschner, H., Patzelt, G. (1977): Methodische Untersuchungen über die Schneegrenze in alpinen Gletschergebieten. *Z. Gletscherkd. Glazialgeol* 12(2), 223–251.
- Hall, D. K., Riggs, G. A. (2010): Normalized-difference snow index (NDSI). *Encyclopedia of snow, ice and glaciers*, https://doi.org/10.1007/978-90-481-2642-2_376.
- Hoinkes, H. (1970): Methoden und Möglichkeiten von Massenhaushaltsstudien auf Gletschern: Ergebnisse der Messreihe Hintereisferner (Ötztaler Alpen) 1953–1968. *Z. Gletscherkd. Glazialgeol* 6 (1–2), 37–90.
- Huss, M., Bauder, A., Werder, M., Funk, M., Hock, R. (2007): Glacier-dammed lake outburst events of Gornersee, Switzerland. *Journal of Glaciology* 53(181), 189–200, <https://doi.org/10.3189/172756507782202784>.
- Huss, M., Sold, L., Hoelzle, M., Stokvis, M., Salzmann, N., Farinotti, D., Zemp, M. (2013): Towards remote monitoring of sub-seasonal glacier mass balance. *Annals of Glaciology* 54(63), 75–83, <https://doi.org/10.3189/2013AoG63A427>.
- Kääb, A., Huggel, C., Barbero, S., Chiarle, M., Cordola, M., Epifani, F., Haerberli, W., Mortara, G., Semino, P., Tamburini, A., Viazzo, G. (2004): Glacier hazards at Belvedere Glacier and the Monte Rosa East Face, Italian Alps: processes and mitigation. 1, 67–78.
- Kerschner, H., Ivy-Ochs, S. (2008): Palaeoclimate from glaciers: Examples from the Eastern Alps during the Alpine Lateglacial and early Holocene. *Global and Planetary Change* 60(1–2), 58–71, <https://doi.org/10.1016/j.gloplacha.2006.07.034>.
- Lhotka, O., Kyselý, J. (2024): Three-dimensional analysis reveals diverse heat wave types in Europe. *Communications Earth & Environment* 5(1), 323, <https://doi.org/10.1038/s43247-024-01497-2>.
- Liboutry, L. (1965): *Traité de glaciologie*. Tome II: Glaciers, variations du climat, sols gelés, Paris, Masson et Cie.
- Loewe, F. (1971): Considerations of the origin of the Quaternary ice-sheet in North America. *Arctic, Antarctic and Alpine Research* 3(4), 331–344, <https://doi.org/10.1080/00040851.1971.12003623>.
- Loibl, D., Richter, N., Grünberg, I. (2022): Remote sensing-derived time series of transient snowline altitudes for High Mountain Asia 1986–2021 (preprint), <https://doi.org/10.31223/X5WH2D>.
- Lukas, S., Bradwell, T. (2010): Reconstruction of a Lateglacial (Younger Dryas) mountain ice field in Sutherland, north-western Scotland, and its paleoclimatic implications. *Journal of Quaternary Science: Published for the Quaternary Research Association* 25(4), 567–580, <https://doi.org/10.1002/jqs.1376>.
- Main-Knorn, M., Pflug, B., Louis, J., Debaecker, V., Müller-Wilm, U., Gascon, F. (2017): Sen2Cor for sentinel 2. *Proc. SPIE 10427. Image and Signal Processing for Remote Sensing XXIII* (4 October 2017), <https://doi.org/10.1117/12.2278218>.
- Maisch, M. (2000): The long-term signal of climate change in the Swiss Alps: Glacier retreat since the end of the Little Ice Age and future ice decay scenarios. *Geografia fisica e dinamica quaternaria* 23(2), 139–151.
- Mathieu, R., Chinn, T., Fitzharris, B. (2009): Detecting the equilibrium-line altitudes of New Zealand glaciers using ASTER satellite images. *New Zealand Journal of Geology and Geophysics* 52(3), 209–222, <https://doi.org/10.1080/00288300909509887>.
- Meier, M. F. (1962): Proposed definitions for glacier mass budget terms. *Journal of Glaciology* 4(33), 252–263, <https://doi.org/10.3189/S0022143000027544>.
- Neckel, N., Kropáček, J., Bolch, T., Hochschild, V. (2014): Glacier mass changes on the Tibetan Plateau 2003–2009 derived from ICESat laser altimetry measurements. *Environmental Research Letters* 9(1): 014009, <https://doi.org/10.1088/1748-9326/9/1/014009>.
- Østrem, G. (1975): ERTS data in glaciology – an effort to monitor glacier mass balance from satellite imagery. *Journal of Glaciology* 15(73), 403–415, <https://doi.org/10.3189/S0022143000034511>.
- Pandey, A., Kropáček, J. (2023): Rapid formation and drainage of a new glacial lake in the Monte Rosa Massif, Swiss Alps, as observed on Sentinel-2 imagery. *Annals of Glaciology*, 1–3, <https://doi.org/10.1017/aog.2023.19>.
- Pellitero, R., Rea, B. R., Spagnolo, M., Bakke, J., Hughes, P., Ivy-Ochs, S., Lukas, S., Ribolini, A. (2015): A GIS tool for automatic calculation of glacier equilibrium-line altitudes. *Computers & Geosciences* 82, 55–62, <https://doi.org/10.1016/j.cageo.2015.05.005>.
- Rabatel, A., Dedieu, J. P., Vincent, C. (2005): Using remote-sensing data to determine equilibrium-line altitude and mass-balance time series: validation on three French glaciers, 1994–2002. *Journal of Glaciology* 51(175), 539–546, <https://doi.org/10.3189/172756505781829106>.
- Rabatel, A., Dedieu, J. P., Thibert, E., Letréguilly, A., Vincent, C. (2008): 25 years (1981–2005) of equilibrium-line altitude and mass-balance reconstruction on Glacier Blanc, French Alps, using remote-sensing methods and meteorological data. *Journal of Glaciology* 54(185), 307–314, <https://doi.org/10.3189/002214308784886063>.
- Rabatel, A., Bermejo, A., Loarte, E., Soruco, A., Gomez, J., Leonardini, G., Vincent, C., Sicart, J. E. (2012): Can the snowline be used as an indicator of the equilibrium line and mass balance for glaciers in the outer tropics? *Journal of Glaciology* 58(212), 1027–1036, <https://doi.org/10.3189/2012JG12J027>.
- Rabatel, A., Letréguilly, A., Dedieu, J. P., Eckert, N. (2013): Changes in glacier equilibrium-line altitude in the western Alps from 1984 to 2010: evaluation by remote sensing and modeling of the morpho-topographic and climate controls. *The Cryosphere* 7(5), 1455–1471, <https://doi.org/10.5194/tc-7-1455-2013>.

- Racoviteanu, A. E., Rittger, K., Armstrong, R. (2019): An automated approach for estimating snowline altitudes in the Karakoram and eastern Himalaya from remote sensing. *Frontiers in Earth Science* 7: 220, <https://doi.org/10.3389/feart.2019.00220>.
- Rastner, P., Prinz, R., Notarnicola, C., Nicholson, L., Sailer, R., Schwaizer, G., Paul, F. (2019): On the automated mapping of snow cover on glaciers and calculation of snow line altitudes from multi-temporal Landsat data. *Remote Sensing* 11(12): 1410, <https://doi.org/10.3390/rs11121410>.
- Rettig, L., Lukas, S., Huss, M. (2023): Implications of a rapidly thinning ice margin for annual moraine formation at Gornergletscher, Switzerland. *Quaternary Science Reviews* 308: 108085, <https://doi.org/10.1016/j.quascirev.2023.108085>.
- RGI 7.0 Consortium (2023): Randolph Glacier Inventory – A Dataset of Global Glacier Outlines, Version 7.0. Boulder, Colorado USA. NSIDC: National Snow and Ice Data Center, <https://doi.org/10.5067/f6jmovy5navz>.
- Richter, E. (1885): Beobachtungen an den Gletschern der Ostalpen. II. Die Gletscher der Ötztaler Gruppe im Jahre 1883. *Zeitschrift des Deutschen und Österreichischen Alpenvereins* 16, 54–65.
- Rizzi, C., Finizio, A., Maggi, V., Villa, S. (2019): Spatial-temporal analysis and risk characterisation of pesticides in Alpine glacial streams. *Environmental pollution* 248, 659–666, <https://doi.org/10.1016/j.envpol.2019.02.067>.
- Ryser, C., Lüthi, M., Blindow, N., Suckro, S., Funk, M., Bauder, A. (2013): Cold ice in the ablation zone: Its relation to glacier hydrology and ice water content. *Journal of Geophysical Research: Earth Surface* 118(2), 693–705, <https://doi.org/10.1029/2012JF002526>.
- Securo, A., Del Gobbo, C., Rettig, L., Pillon, S., De Luca, A., Fontana, D., Fasil, E. B., Colucci, R. R. (2024): A glacier in transition: Surface elevation change, ELA and geomorphic evolution of a very small glacier in the Dolomites (SE Alps). *Geomorphology* 444: 108956, <https://doi.org/10.1016/j.geomorph.2023.108956>.
- Six, D., Vincent, C. (2014): Sensitivity of mass balance and equilibrium-line altitude to climate change in the French Alps. *Journal of Glaciology* 60(223), 867–878, <https://doi.org/10.3189/2014JG14J014>.
- Smiraglia, C., Maggi, V., Novo, A., Rossi, G., Johnston, P. (2000): Preliminary results of two ice core drillings on Monte Rosa (Colle Gnifetti and Colle del Lys), Italian Alps. *Geografia Fisica Dinamica Quaternaria* 23, 165–172.
- Spagnolo, M., Ribolini, A. (2019): Glacier extent and climate in the Maritime Alps during the Younger Dryas. *Palaeogeography, Palaeoclimatology, Palaeoecology* 536: 109400, <https://doi.org/10.1016/j.palaeo.2019.109400>.
- Truffer, M., Käab, A., Harrison, W. D., Osipova, G. B., Nosenko, G. A., Espizua, L., Gilbert, A., Fischer, L., Huggel, C., Craw Burns P. A., Lai, A. W. (2021): Glacier surges. In *Snow and ice-related hazards, risks, and disasters (Second Edition)*, 417–466, <https://doi.org/10.1016/B978-0-12-817129-5.00003-2>.
- Valovcin, F. R. (1976): Snow/cloud discrimination (No. 349). Meteorology Division, Air Force Geophysics.
- Villa, S., Negrelli, C., Maggi, V., Finizio, A., Vighi, M. (2006): Analysis of a firn core for assessing POP seasonal accumulation on an Alpine glacier. *Ecotoxicology and Environmental Safety* 63(1), 17–24, <https://doi.org/10.1016/j.ecoenv.2005.05.006>.
- Žebre, M., Colucci, R. R., Giorgi, F., Glasser, N. F., Racoviteanu, A. E., Del Gobbo, C. (2021): 200 years of equilibrium-line altitude variability across the European Alps (1901–2100). *Climate Dynamics* 56, 1183–1201, <https://doi.org/10.1007/s00382-020-05525-7>.
- Zeller, H. R. (1893): Die Schneegrenze im Triftgebiet. *Jahrb. Geogr. Ges. Bern* 11, 198–225.
- Zemp, M., Hoelzle, M., Haeberli, W. (2007): Distributed modelling of the regional climatic equilibrium line altitude of glaciers in the European Alps. *Global and Planetary Change* 56(1–2), 83–100, <https://doi.org/10.1016/j.gloplacha.2006.07.002>.

Exploring the potential of historical images for the investigation of glacier changes: the case of Belvedere Glacier, Italian Alps

Jan Kropáček^{1,*}, Marcus Nüsser^{2,3}, Susanne Schmidt²

¹ Charles University, Faculty of Science, Department of Physical Geography and Geoecology, Czechia

² Heidelberg University, South Asia Institute, Department of Geography, Germany

³ Heidelberg University, Heidelberg Centre for the Environment, Germany

* Corresponding author: kropacja@natur.cuni.cz

ABSTRACT

Historical images dispersed in various archives can be instrumental in documenting processes connected to glacier changes in mountains. A series of more than 29 engravings and photographs of the Monte Rosa east face have been found covering the period since 1789. Some images were produced by a combination of photography and engraving, a common approach before practical techniques for printing halftone images were introduced. Using a repeat photography approach, the present study documents the changes in the extent and debris cover of the Belvedere Glacier. Based on visual comparison of images, it appears that the debris cover of the lower part of the glacier developed mainly during the period of the 1860s–1880s. Furthermore, the image series documents the evolution of the terminus both in terms of elevation and shape, as well as a breach in lateral moraine which could be dated back to the end of the 19th century, well before the reported glacier lake outburst flood in 1904.

KEYWORDS

historical landscape images; graphical techniques; repeat photography, extent of glaciation; Monte Rosa

Received: 19 March 2024

Accepted: 10 September 2024

Published online: 5 November 2024

Kropáček, J., Nüsser, M., Schmidt, S. (2024): Exploring the potential of historical images for the investigation of glacier changes: the case of Belvedere Glacier, Italian Alps. *AUC Geographica* 59(2), 240–254

<https://doi.org/10.14712/23361980.2024.16>

© 2024 The Authors. This is an open-access article distributed under the terms of the Creative Commons Attribution License (<http://creativecommons.org/licenses/by/4.0>).

1. Introduction

Historical landscape drawings, paintings, and photographs of high mountain environments make up a visual record and provide valuable information, especially for the reconstruction of glacier changes (Steiner et al. 2008; Zumbühl and Nussbaumer 2018; Nüsser and Schmidt 2021a). Using various techniques over the last centuries, such pictorial materials were created for various purposes including landscape visualization and cartographic representation, as well as for promoting tourism and aspirations in visual arts.

While scientific attention focused on high mountains, especially the European Alps, towards the end of the 18th century, graphical techniques allowed reproduction by printing using established techniques such as copper plates and aquatint or lithography invented in 1798 (Hopkinson 2017). These early landscape images of the Alps were produced along with a growing interest in the geology and physics of glaciers among European geoscientists. The evolution of photography and photomechanical printing techniques in the second half of the 19th century overlapped with the first efforts to map glaciers in terms of their extent and their changes in the period following the Little Ice Age (LIA). These early scientific studies inaugurated a “glacier fever” and growing interest in glaciers began to spread worldwide (Nüsser and Baghel 2014).

The first sketch maps with a distinct focus on glaciers were compiled by Louis Agassiz, Johann von Charpentier, and James David Forbes in the western Alps (Hattersley-Smith 1966). Detailed glacier maps were produced by the brothers Adolf and Hermann Schlagintweit for different regions in the Alps (Schlagintweit and Schlagintweit 1850, 1854) and by Friedrich Simony for the Dachstein Massif in the eastern Alps in the 1840s (Vukovic and Fischer 2022). In the second half of the 19th century, Sebastian and Richard Finsterwalder introduced systematic and more accurate surveying of glaciers using terrestrial photogrammetry for topographical and glaciological mapping purposes (Finsterwalder 1897; Brunner and Welsch 2002). Historical glacier photographs allowed for bi- and multitemporal comparisons with replicates taken from viewpoints identical to the earlier ones, using repeat photography as a method for detailed change detection (Kull 2005; Nüsser 2001). Especially panoramic images taken from exposed viewpoints form a valuable basis for replication. Repeat photography provides longer temporal coverage than aerial photographs and satellite images (Trimble 2008). Furthermore, the method can be instrumental in debunking environmental myths and can point out the complexity of processes often described in an oversimplified or biased manner (Nüsser 2000; Nyssen 2009; Kropáček 2019). The contemporary or replicate photograph can also be replaced by an image

simulated in a 3D viewer of very high-resolution satellite data available in Google Earth. Especially in cases of difficult accessibility of the camera point due to various reasons, including political or administrative restrictions, as well as difficult terrain, bad weather conditions, or frequent cloudiness, this is a valuable option (Kropáček 2019).

In the specific context of glacier research, multi-temporal repeat photography has been used to document changes in the Nanga Parbat Massif (northwestern Himalaya) since the 1930s (Schmidt and Nüsser 2009; Nüsser and Schmidt 2021a,b), Bara Shigri Glacier in the Western Himalayas (Chand et al. 2017) since the 1860s and in the Khumbu region (Central Himalaya) since the 1950s (Byers 2007). For the European Alps, studies were conducted to visualize the impact of climate change on glacier retreat (Zängl and Hamberger 2004) and to investigate glacier fluctuations in the western Alps during the 19th century (Zumbühl et al. 2008). For the case of Belvedere, Käab et al. (2004) repeated a set of photographs from the 1980s and 1990s to document the deglaciation of the east face of Monte Rosa, the volume changes of the lower part of Belvedere Glacier during the surge-type event in 2001–2002 and associated changes of Effimero Lake, which was formed and drained in connection to this event. Hundreds of repeat photographs of retreating glaciers were acquired in high mountains of four continents in the framework of a project called ‘On the Trail of the Glaciers’ for research and popularization purposes (<https://onthetrailoftheglaciers.com/>).

This article aims to meet three objectives.

1. To review techniques used to produce images of glaciated high mountain environments.
2. To recover largely neglected visual materials depicting the Belvedere Glacier and the east face of Monte Rosa.
3. To assess the potential of historical graphics and photographs for investigating a glacier under four focal themes (the extent of glaciation, the extent of debris cover, the evolution of the terminus, the evolution of a breach of the lateral moraine).

2. Basic characteristics of Belvedere Glacier

The heavily debris-covered Belvedere Glacier (formerly referred to as Macugnaga Glacier) (Fig. 1), located in the Valle Anzasca in the Piedmont, Italy, is one of the rare surge-type glaciers in the Alps (Truffer et al. 2021). The glacier covers an area of about 4.53 km² according to the New Italian Glacier Inventory (Smiraglia and Diolaiuti 2015) and is largely fed by snow and ice avalanches from the Monte Rosa east face, being the most prominent rock face in the Alps. The two lobes of Belvedere reach below the tree line to approximately 1840 m a.s.l., divided by a larch forest

(*Larix decidua*). In many aspects, such as debris coverage, snout position below the tree line, and bilobation, Belvedere Glacier is similar to Miage Glacier in the Mont Blanc Massif (Stefaniak et al. 2021; Bollati et al. 2013).

The historical phases of glacier advance and retreat in the Monte Rosa Massif were outlined by Monterin (1922). There were two advancing phases towards the end of the LIA, one ending in 1826 and the second between 1842 and 1859, interleaved by a retreating phase. Two more advancing phases occurred in the second half of the 19th century (1878–1893) and the first half of the 20th century (1912–1922). In the case of Belvedere Glacier, the later advance appeared to be larger than in the phase 1878–1893 as is evident by the crossing of the 1880s moraines, however, the moraines from the phase 1842–1859 were not reached (Monterin 1926). Further advancing periods can be figured out from the records of the Italian Glaciological Committee and for instance from the study by Diolaiuti et al. (2003). There was an advance at the end of the 1960s and some minor advances in the period 1986–2000 which were followed by an advance connected to the surge-type event in 2001–2002. This was followed by a strong retreat. The measurements for the period 1974–1985 which was the time of the general advance of Alpine glaciers are unfortunately missing. Since the LIA, the glacier has retreated by more than 800 m (WGMS 2024).

The upper catchment of the Belvedere Glacier has been the source of numerous natural hazards including glacial lake outburst floods (GLOF) and

enormous rock and ice avalanches over the last decades. A series of three GLOFs originating from the Locce Lake, dammed by the terminal moraine of the former tributary North delle Locce Glacier occurred in 1970, 1978, and 1979 (Kääb et al. 2004). These floods further incised a breach in the lateral moraine (near the seasonal settlement Alpe Pedriola), which was formed during an earlier outburst flood in 1904 (Mazza 1998). The short-lived Effimero Lake was formed in 2002 and 2003 due to a surge-like event in 2001–2002 (Haeberli et al. 2002; Kääb et al. 2004). The lake reached a volume of $3 \times 10^6 \text{ m}^3$ and its level had to be lowered by pumping in 2002 to prevent an outburst (Tamburini and Mortara 2005). However, a non-destructive outburst flood occurred from this lake in 2003.

Caused by the massive ice loss, various rock and ice avalanches of different sizes have been documented. For example, one rock avalanche ($1.2 \times 10^6 \text{ m}^3$) considered to be among the largest rock avalanches in the Alps detached from the Monte Rosa east face at an elevation of 3580–3820 m a.s.l. in August 2005 (Tamburini et al. 2013; Fischer et al. 2013). Another large slope failure occurred in September 2010 in the upper basin of Northern Locce Glacier, which reached a volume of $0.1 \times 10^6 \text{ m}^3$ (Fischer et al. 2013; Paranunzio et al. 2016).

3. Materials and methods

The search for useful images was started in Google browser using the following keywords: 'Monte Rosa', 'Belvedere glacier', 'Macugnaga glacier' to specify the location and 'engraving', 'aquatint', 'old photography', 'Daguerreotype', 'photo-xylograph' etc. for the technique. Various language variants were tried which appeared to be useful, for instance, the search using the term 'Mont Rose' resulted in further discovery of historical material. The search revealed several archives, which were used for further investigations.

The following archives were searched online or contacted directly:

1. Documentation Center CAISiDoc of the Italian Alpine Club (CAI) in Torino, Italy
2. Archive of Eidgenössische Technische Hochschule (ETH) in Zurich, Switzerland
3. Fondazione Vittorio Sella in Biella, Italy
4. Archive of the University of Lausanne, Switzerland
5. Bavarian State Library (BSB) in Munich, Germany

Websites of various auction houses and vendors of antique prints and drawings such as Pettinaroli and Abebooks were explored in the next step. Amongst the further explored sources, the Web page of the mountaineering club CAI Varallo, Italy can be named.

The images were relocated using Google Earth. An accurate overlap of closer and further topographical

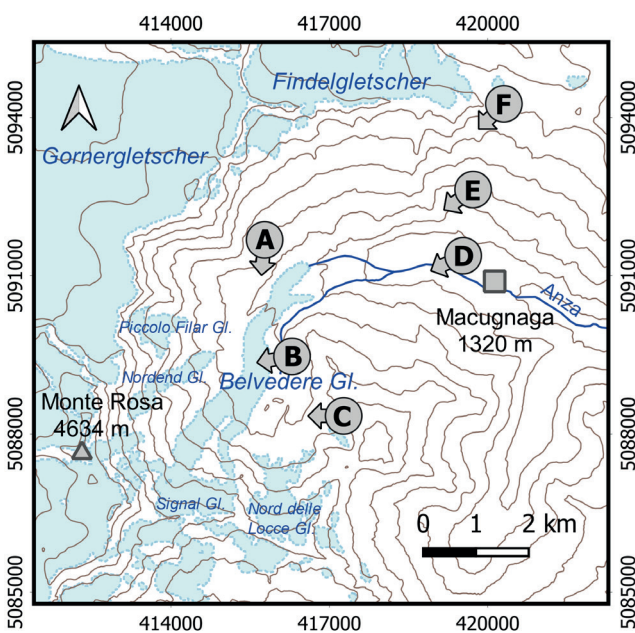


Fig. 1 Map of the eastern part of the Monte Rosa Massif showing the approximate positions of the viewpoints from which most of the images of the east face were taken: A: a point above Alpe Jazzi, B: Alpe Pedriola, C: Punta Battisti, D: Macugnaga, E: slope below Monte Moro and F: Monte Moro Pass.

features was aimed at. In some cases, the correction of wrongly given viewpoints could be done. Furthermore, based on the relocation, it was revealed that some images were taken from airplanes. The identified viewpoints were used for the preparation of simulation images considering the same view azimuth and elevation angle. Images from approximately the same viewpoints were collated into bi- or multitemporal collections and used for visual image interpretation based on experiences from repeat photography. In addition, some historical photographs were repeated during a field survey in August 2021 and July 2024.

Images showing the glacier terminus were used to estimate its elevational position to get an insight into the glacier's response to climate fluctuations. They were compared with images in Google Earth simulating the view from the same vantage point. To facilitate the elevation reading, contours with a spacing of 50 m were superimposed over the simulated images. The contours were generated from a digital elevation model (DEM) based on airborne laser scanning technique. The model with a grid spacing of 5 m, acquired in 2009–2011 and referred to as DEM 5, was received from *Geoportale Piemonte*, which is a map portal of the region. The expected accuracy of the elevation reading was on the order of tens of meters, which led us to the selection of contour interval of 50 m.

4. Image record of the Monte Rosa east face

Due to its prominence, Monte Rosa is visible from long distances both from the Po plain and exposed viewpoints from the north. It has a long record of visual materials, many of which have been produced by scientists, artists, and mountain photographers from various European countries.

4.1 Engravings

The east side of Monte Rosa has already been visited by pioneers, scientists, and explorers at the end of the 18th century, including Horace Bénédict de Saussure, who travelled to Monte Rosa accompanied by his son Theodore in 1787. They crossed the Belvedere Glacier during their ascent of Pizzo Bianco, from where they carried out a trigonometric measurement of the elevation of Monte Rosa. Theodore authored the sketch, which was elaborated into the probably first engraving showing the Monte Rosa east face (de Saussure 1779–1796; de Saussure et al. 1989). However, this image does not show the glacier snout, and most of the east face is covered by a ridge due to the distant viewpoint.

Another early image of Monte Rosa east face is titled *Ansicht des Monte Rosa von Macugnaga aus*, in the book published by the Austrian army officer Franz Ludwig von Welden (Fig. 10 a) who was in charge of the topographical survey of Piedmonte in 1821 (von



Fig. 2 Engraving by J. T. Willmore from 1845 shows the tongue of the Belvedere Glacier reaching far down into the valley at the beginning of the last advancing phase during the LIA (viewpoint D in Fig. 1).

Welden and Welden 1824). Some illustrations in the book – probably also the Monte Rosa east face – were drawn using the *camera lucida* technique, as given on some of the image frames. This technique was invented in the early 19th century and is based on a prism attached to the drawing pan onto which the landscape of interest is projected and can be sketched.

Another painting of the Monte Rosa east face from 1829 was produced by G. Lory using aquatint, a technique that allows the reproduction of grey tones and colours and was introduced in the second half of the 18th century (Tab. 1). A steel engraving showing a view of Monte Rosa and the Belvedere Glacier from Macugnaga was published by J. T. Willmore in 1845 (Fig. 2). It is not known whether a mechanic-optical tool was used to ensure an accurate geometry of these two images.

In 1851, A. Schlagintweit visited the Monte Rosa Massif to investigate the physical geography and geology of the area. In this context, they produced rich material including a topographical map and a landscape panorama of the Belvedere Glacier (A. Schlagintweit and H. Schlagintweit 1854) (Fig. 7).

4.2 Transition between engraving and photography

Shortly after the invention of photography in the mid-19th century, it gradually became an established method of documentation in mountain research (Milner 1946). However, the use of photographs in printed media remained limited due to the lack of a suitable reproduction method for halftone images (Bridson 1987). Therefore, photographs were used as a base for traditional methods of image reproduction rather than direct printing. In the case of photo-xylography, for example, the image was manually engraved on a cross-grain wooden block using the photograph as a template (Levin 1980). As this technique is partially a manual process, the quality of the representation depends on the attitude and style of the engraver.



Fig. 3 Photo-xylograph of the Monte Rosa east face from 1884 by Duruy as an example of a mixed technique, in which the photograph is used as a template for manual engraving (viewpoint F).

One of the first photo-xylographs of Monte Rosa was produced by V. Duruy in 1884 based on a photograph by M. E. Lamy, published in ‘The New Universal Geography’ by Reclus (1876–1894) (Fig. 3). Only seven years later, another photo-xylograph of the Belvedere Glacier was authored by Edward Whymper (1891), a British explorer, illustrator, and the first who summited the Matterhorn in 1869.

The halftone reproduction process of photography was not introduced until the early 1880s with the invention of photolithography, which was capable of rather grainy reproductions (Sealy 2016). Another image of Monte Rosa east face taken from the Monte Moro Pass in 1860 is authored by Étienne Eugène Cicéri, a French painter and engraver. This image, denoted as a ‘lithograph’, is, in reality, a photolithograph. It is a part of Cicéri’s album *La Suisse et la Savoie* based on photographs by Frédéric Martens taken between 1859 and 1865 (Savale 1994).

A decisive move towards a high quality in halftone reproduction was the introduction of a commercially viable form of photogravure, invented by Karel Klíč in 1878 (Mustalish 1997). This technique, in which a copper plate was etched after its sensitive gelatine coating was exposed and then partially chemically removed, allowed the detailed reproduction of photographs in halftone.

4.3 Photography

From a glaciological point of view, the advent of photography represents a major step towards objectifying reality. Photographs can be taken as most accurate materials in terms of shapes and tonal variations of ice fields, glaciers, debris and snow cover, rocks and vegetation. The beginning of mountain photography can be dated to the decade following the invention of the daguerreotype in 1839, the first practical, albeit technically demanding, photographic process (Jacobson 2015). One of the first photographs

showing a glacier-covered mountain in the Alps was a daguerreotype of the Matterhorn, just 17 km west of Monte Rosa, taken in August 1849 by John Hobbs on behalf of the British scientist, writer and art critic John Ruskin, who himself had taken a series of daguerreotypes in the Alps in the 1840s (von Brevern 2009). Further early photographs of the Alps taken by Camille Bernabé and Gustave Dardel in 1849 and 1850 can be seen in the *Collection de 28 daguerréotypes représentant les plus anciennes reproductions héliographiques des Alpes* in the online archive Viatimages hosted by the University of Lausanne, Switzerland (Viatimages 2024).

In the 1850s, the daguerreotype gave way to the wet collodion process, in which glass plates were coated with a sensitive emulsion in a dark tent immediately before exposure. The invention of gelatine emulsion dry plate process in the 1880s brought an increased portability and simplification of mountain photography (Osterman 2013). Adopting the techniques, Bisson brothers from Paris took panoramas from the summit of Mont Blanc using 44 × 54 cm plates and equipment carried by 25 porters and guides (Milner 1946). They also took a number of high-quality photographs of mountain sceneries including glaciers in the Savoyan Alps during the expedition by Napoleon III in 1860, celebrating the annexation of the area by France (Frangne 2010). Some of their photographs such as the panoramas of the Glacier du Géant, the Aiguilles de Chamonix, and of Mont Blanc were used by the French geologist and orographer Daniel Dollfus-Ausset (Frangne 2010).

The first photograph of Monte Rosa east face was probably taken by the French photographer Aimé Civiale (Tab. 1) from Monte Moro Pass between 1859 and 1868, however, the exact date is unknown. This was a part of his monumental effort in which he took more than 40 full panoramas (360 degrees) from medium-altitude summits in the Alps in the period 1859–1868. One of these panoramas was taken from Bella Tola (3023 m a.s.l.) close to Sierre in Switzerland, approximately 37 km from Monte Rosa. The complete panorama was covered by 14 overlapping photographs each exposure taking between twelve and fifteen minutes. He used the technique of dry wax paper negatives and he travelled with 250 kg of photographic equipment. His aim was to produce valuable photographs for geologists and physical geographers, rather than commercial or personal memoirs (Civiale 1882; von Brevern 2009).

The second photograph of Monte Rosa’s east face from Monte Moro was taken between 1870 and 1880 by Eugène Lamy, the owner of a well-established photographic studio in Paris. This was followed by a photograph taken by the French alpinist Gabriel Loppé, a member of the British Camera Club. He began to devote himself to photography in the 1880s when his career as a painter of the Alps was already fully developed. Furthermore, Monte Rosa did not escape the

Tab. 1 List of images of the Monte Rosa east face. The positions of viewpoints are shown in Fig. 1 and are marked by letters as follows: A: viewpoint above Alpe Jazzi, B: Alpe Pedriola, C: summit of Punta Battisti, and D: Monte Moro Pass. The images which are oblique aerial photographs are marked by “AP” followed by the closest viewpoint in brackets. The names of the engravers, if known, are given after the slash. Some of the sources are given as abbreviations: M&T 2009 – Mortara and Tamburini (2009); BnF – Bibliothèque nationale de France; BSB – Bayerische Staatsbibliothek; JMFP – John Mitchell Fine Paintings, London; MPV – Museo del Paesaggio Verbania; ÖNB – Österreichische Nationalbibliothek; PPR – Period Paper or Roberts – University of Toronto; CAISiDoc – Sistema Documentario dei beni culturali del Club Alpino Italiano; ETH – Eidgenössische Technische Hochschule Zürich.

Id	Autor	Date	Type	Colour/BW	Viewpoint	Figure	Source	Viewpoint
1	Saussure, Theodore	1789	engraving	BW/colour	D	–	Viatimages	Macugnaga
2	Escher, Hans Konrad	1797	coloured ink drawing	coloured	D	–	M&T 2009	Macugnaga
3	Welden, Franz Ludwig	1824	engraving	BW	D	10	ÖNB	Pecetto Superiore
4	Birmann, Samuel	1825	drawing	coloured	A	–	M&T 2009	Alpe Jazzi
5	Lory, Gabriel/ Falkeisen	1829	acquatint	coloured	E	11	Pettinaroli	Macugnaga – Passo MM
6	Buhlmann, Johann Rudolf	1835	engraving	coloured	E	–	M&T 2009	Macugnaga – Passo MM
7	Cuvillier, A.	1840	litograph	coloured	E	11	Pettinaroli	Macugnaga – MM Pass
8	Willmore, J.T.	1845	steel engraving	BW	D	2	Pettinaroli	Macugnaga
9	Schlagintweit, A./ Loeillot, W.	1851	lithograph	colored	A	7	BSB	Alpe Jazzi
10	Civiale, Aimé/ Chardon, C.	1859–1868	photogravure	BW	F	4	BnF	Monte Moro Pass
11	Martens/Ciceri, Eugene	1862	photolithograph	coloured	F	–	Pettinaroli	Monte Moro Pass
12	Rüdisühli, Jakob Lorenz	1870	acquatint	BW	F	–	AbeBooks	Monte Moro Pass
13	Lamy, Eugene	1870–1880	photography	BX	F	–	CAISiDoc	Monte Moro Pass
14	Lamy, M.E./Duru, Victor	1884	photoxylograph	BW	F	3	PPR	Monte Moro Pass
15	Ashton, Federico	1887	oil on canvas	colour	D	10	MPV	Macugnaga
16	Loppé, Gabriel	1880s	photography	BW	A	6	JMFP	above Alpe Jazzi
17	Carnagbi/Doyen	1889	litography	BW	C	13	Pettinaroli	below Punta Battisti
18	Whymper, Edward	1891	xylography	coloured	F	–	Pettinaroli	Monte Moro Pass
19	Zandonati, A.	1893	photograph	BW	D	10	CAISiDoc	Macugnaga
20	Sella, Vittorio	1895	photograph	BW	F	5	Fondazione Sella	Monte Moro Pass
21	McLeish, Donald	before 1913	photograph	BW	F	–	Media Storehouse	Monte Moro Pass
22	Mittelholzer, Walter	1919	photograph	BW	AP (C)	8	BSB	airplane
23	Monterin, Umberto	1920	photograph	BW	C	–	M&T 2009	west from Punta Battisti
24	unknown	1923	postcard	BW	F	4	–	Monte Moro Pass
25	Sella, Vittorio	1930s	photograph	BW	F	–	Fondazione Sella	Monte Moro Pass
26	Hielscher, Kurt	1930s	photograph	BW	B	–	ETH archive	Alpe Pedriola
27	Fantin, Mario	1953	photograph	BW	AP (C)	8	CAISiDoc	airplane?
28	Fantin, Mario	1950–1960	photograph	BW	AP (E)	9	CAISiDoc	airplane, close to P. Battisti
29	Vespa, Marco	2007	photograph	colour	F	5	Wikipedia	Monte Moro Pass

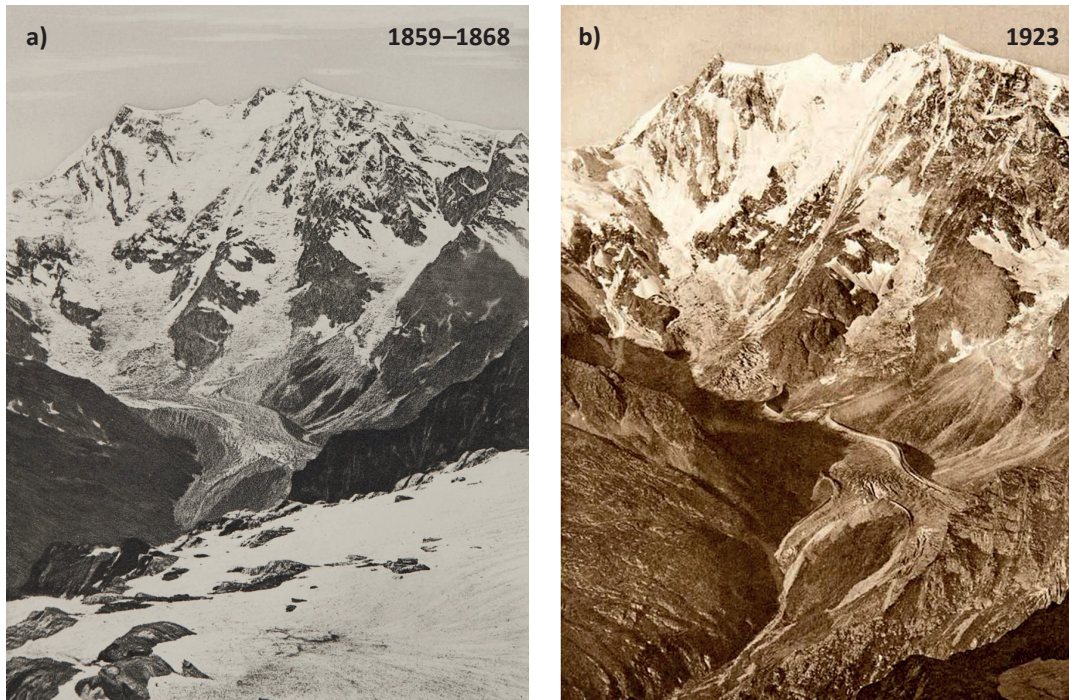


Fig. 4 Photograph by A. Civiale reproduced by photogravure from 1859–1868 (a) and a postcard from 1923 (b) taken from almost the same spot at Monte Moro Pass (2850 m a.s.l., viewpoint F).

attention of the prominent mountain photographer Vittorio Sella, who was born in Biella, at a distance of 45 km south of Monte Rosa. During his career, he photographed glaciers and mountains in the Alps, Caucasus, and Karakoram often from high and exposed viewpoints. He took photographs of Monte Rosa east face from Monte Moro Pass in 1895 and the 1930s. Donald McLeish, a British reportage photographer took a snapshot of the classical view from Monte Moro Pass, which was published in a book by Gibbs (1910).

In 1919, Walter Mittelholzer, a Swiss aviation pioneer, took probably the first aerial photograph of the Monte Rosa Massif (Garimoldi 2005). Other high-quality photographs of the east face were taken by the Italian mountaineer and photographer Mario Fantin in 1953. He was a founder of the documentation centre of mountaineering CISDAE (Centro italiano studio e documentazione alpinismo extraeuropeo) in 1967, now located in Torino, Italy.

5. Results

The results are presented in four focal themes: the extent of glacier-covered area, the extent of debris cover, the evolution of the terminus, and the evolution of a breach of the lateral moraine.

5.1 Focal theme 1: Extent of glacier-covered area of the Monte Rosa east face

For the first photograph of the Monte Rosa east face by Aimé Civiale only a rough date of acquisition

between 1859 and 1868 is known, which represents the second decade after the LIA (Fig. 4 a). It can be assumed that the image was taken during mid-summer as the mountain slopes and rock cliffs are snow-free and the shadows indicate high solar elevation. The photograph also shows that Nordend Glacier was still connected to the Belvedere Glacier and the Piccolo Fillar Glacier was still reaching its LIA terminal moraine. The second image is a postcard from 1923, taken by an unknown photographer about 60 years after Civiale (Fig. 4 b). It shows the ice extent after the phase of advance of glaciers during the time of the First World War (Monterin 1926), when glaciological measurements ceased. The second image has a different foreground, but the view of the Monte Rosa east face with heavy crevassed ice in the lower part is almost identical to the first one. The picture was probably taken in September as the shadows are longer and the seasonal snow cover is still minimal. The connection between Nordend and Belvedere glaciers lacks texture and remains unclear. The ice extent is similar in both pictures and the largest differences are caused by seasonal snow cover.

The third example of the Monte Rosa east face is taken by Vittorio Sella from a viewpoint at Monte Moro Pass in the 1930s (Fig. 5 a). A drastic retreat and volume loss of the hanging glaciers can be detected as well as an increase of debris cover in the transition zone between the hanging glaciers and the Belvedere Glacier. These changes are evident also in the comparison of the 1880 and 2017 images (Fig. 6).

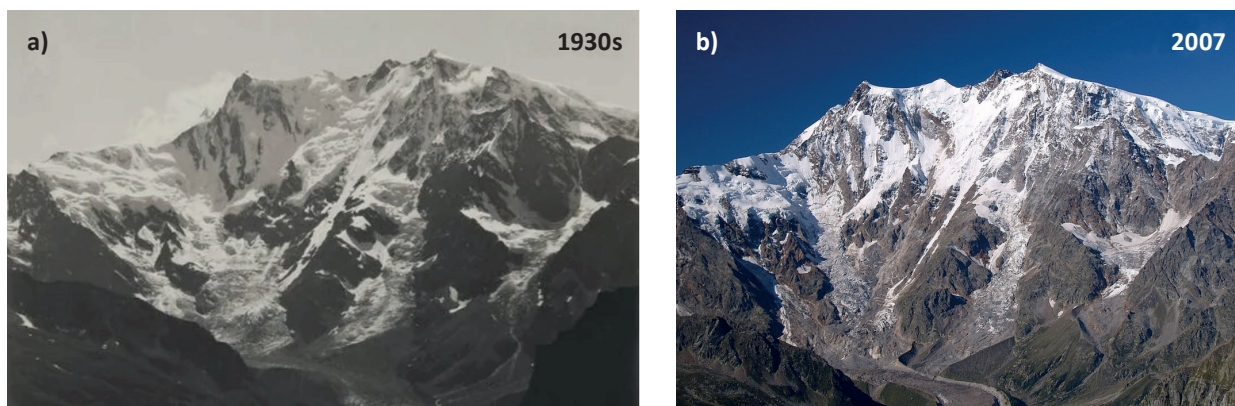


Fig. 5 An almost identical view as Fig. 4 (viewpoint F) taken by V. Sella in the 1930s (photo detail) and by M. Vespa on 9 September 2007 (photo detail).

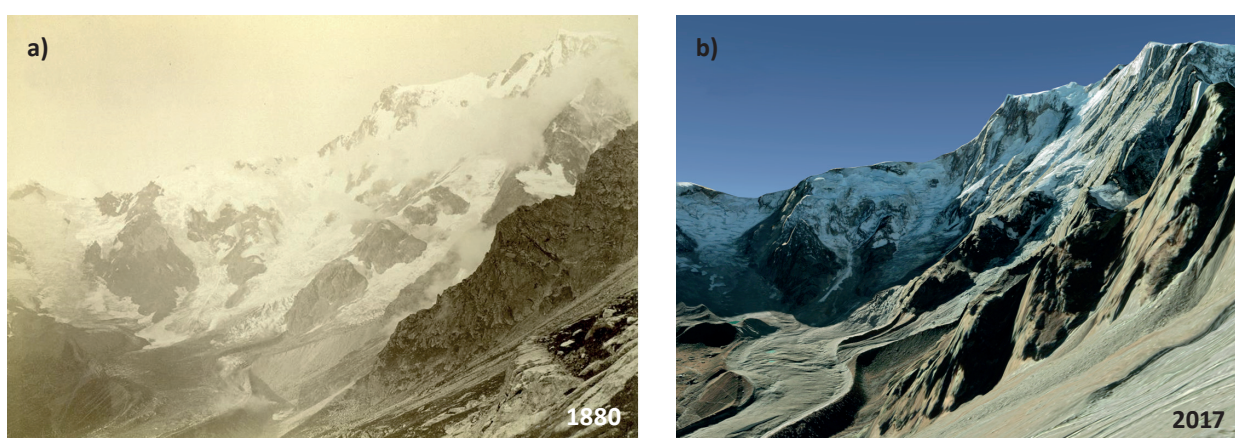


Fig. 6 A heliogravure based on the photograph by G. Loppé from the 1880s (a) and a simulated image in Google Earth (viewpoint E). The image by G. Loppé is courtesy of John Mitchell Fine Paintings, London.

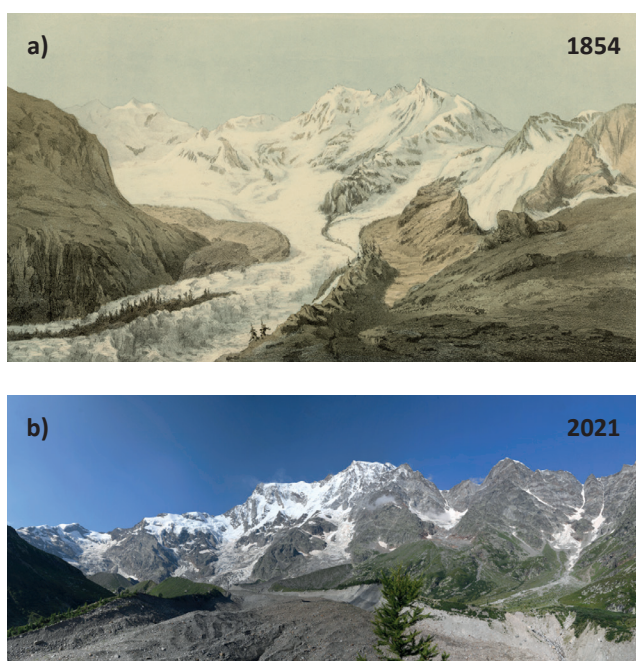


Fig. 7 The lithograph based on a historical drawing of Belvedere Glacier by A. Schlagintweit published in 1854 (a) with the original caption: *Ansicht des Monte Rosa und des Macugnagagletschers (Schlagintweit and Schlagintweit 1854)*. The recent photograph was taken by M. Nüsser on 12 August 2021 (b).

5.2 Focal theme 2: Extent of debris cover

Historical photographs as well as paintings are useful to analyse gradual changes of debris cover on glaciers.

The 1845 steel engraving by J. T. Willmore (Fig. 2) shows a clean-ice glacier tongue. Likewise, in the painting and explanatory sheet by A. Schlagintweit from 1851 (Schlagintweit and Schlagintweit 1854), the Belvedere Glacier appears to be debris-free (Fig. 7). Also their topographical sketch map of the glacier (published in *Atlas zu den neuen Untersuchungen über die physicalische Geographie und die Geologie der Alpen* 1854) indicates that the tongue was only partly debris-covered along the margins, medial moraines and at the lower terminus. A slight increase of debris cover can be seen in A. Civiale’s photograph (Fig. 4 a), where only the central glacier line appears to be debris-free. Accordingly, the glacier was described as debris-covered at least close to the two terminal lobes by the priest and geologist A. Stoppani who visited the glacier in 1870 and 1876 (Mortara et al. 2009). The increase of debris cover can also be traced in the photographs from the end of the 19th century (Fig. 4–6), a process that continues until the

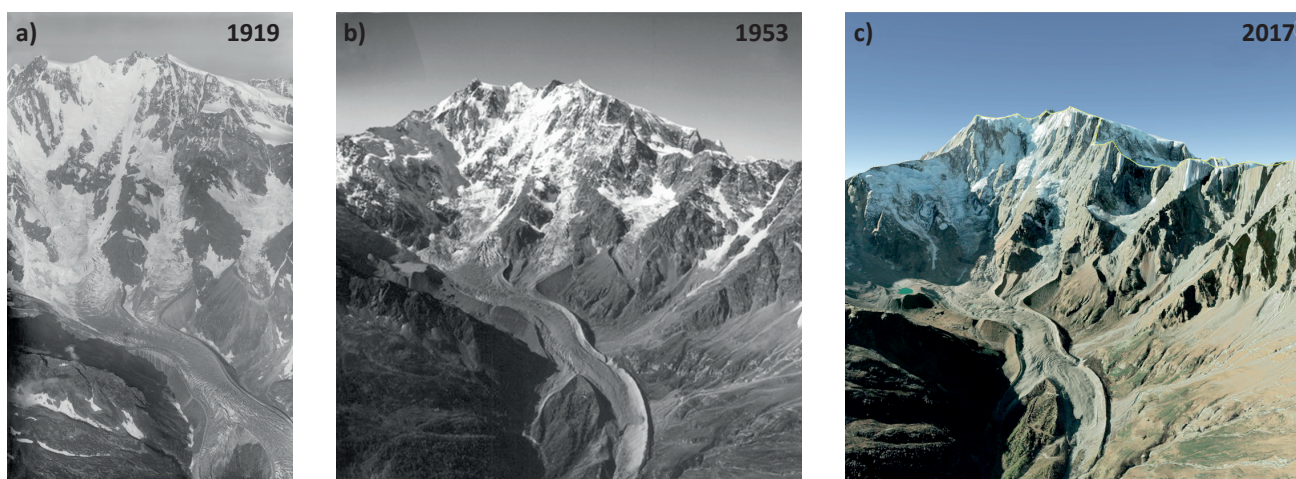


Fig. 8 Comparison of oblique aerial photographs taken by W. Mittelholzer in 1919 (a), and by M. Fantin from 1953 (b), and a simulated image in Google Earth (c). The relocation of the viewpoint indicates that the photograph by M. Fantin was also taken from an airplane.

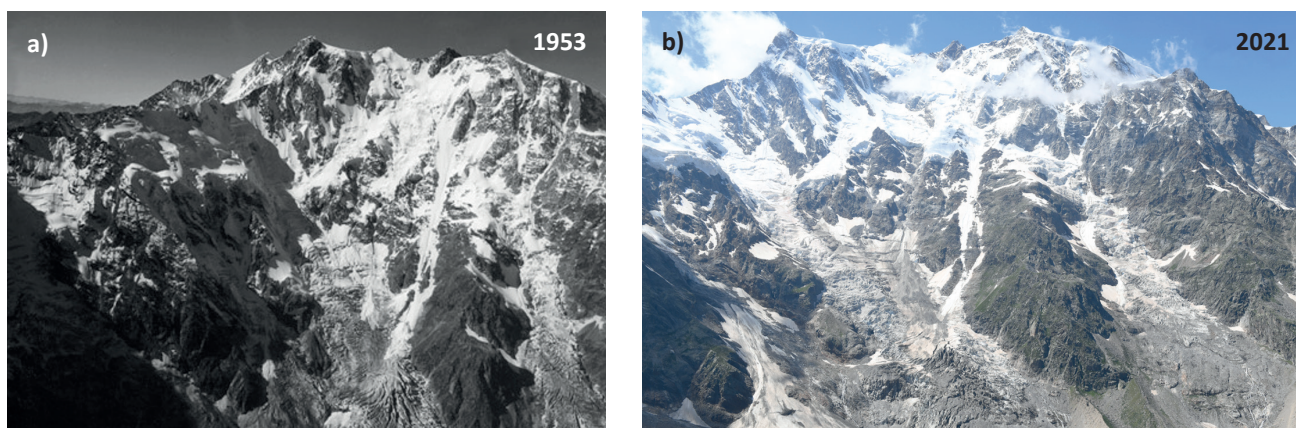


Fig. 9 Comparison of a photograph of Monte Rosa east face taken by M. Fantin (aerial photograph in 1953) (a) and a photograph taken by M. Nüsser from the Punta Battisti (viewpoint C) at 2754 m a.s.l. on 11 August 2021 (b).

present day (Fig. 7 b). This multitemporal image comparison suggests that the debris cover of the glacier tongue gradually developed after the LIA.

An upward shift of the upper limit of debris cover and an increase of the debris cover thickness become obvious when comparing the oblique aerial photographs taken by W. Mittelholzer in 1919 and M. Fantin in 1953 (Fig. 8). Another pair of photographs taken by M. Fantin in 1953 and M. Nüsser in 2021 (Fig. 9) shows the debris on the lower part of the east face. The picture from 2021 indicates significantly more snow and rock avalanche tracks, which means that more debris has recently been transported onto the glacier than 70 years before.

5.3 Focal theme 3: Evolution of the terminus

The evolution of the terminus can be traced on several historical images. The engraving by F. Welden in 1824 (Fig. 10 a) based on the ‘camera lucida’ technique shows a realistic geometry which becomes evident by a comparison with contemporary a photograph (Fig. 10 b). Some features such as trees and the glacier

outlet are not shown at realistic scales but rather in a schematic style. The orographic right lobe of the terminus, which probably developed due to a breach of the lateral moraine, is present in the image but absent on the map in Welden’s book, likely due to generalization. Welden’s image suggests that the right lobe developed before 1824. Another image from a similar viewpoint with a high geometrical accuracy is an oil painting by the Milanese painter Federico Ashton from 1887 (Fig. 10 c). It features highly realistic shapes of the glaciers Nordend and Piccolo Fillar. The glacier outlet of the left lobe is located in a higher position than in Welden’s image. A triangular area on the slope between the two lobes is free of trees which is also shown in the photograph taken by A. Zandonati in 1893 (Fig. 10 d). The triangular area is very similar in size and shape, which is further evidence of the high fidelity of Ashton’s painting.

The absence of forest in this triangular area can be attributed to the outburst flood in 1868 described by A. Stoppani. This is supported by the account of the pastor of Macugnaga who eye-witnessed the event. He mentioned that about a hundred large larches had been



Fig. 10 Engraving from the book by Welden from 1824 showing the Monte Rosa east face from a viewpoint close to the hamlet of Pecetto Superiore (viewpoint D), a part of Macugnaga (a), the same view as a simulated image in Google Earth (b), subset from the oil painting by Federico Ashton from 1887 (c), and a photograph taken by A. Zandonati in 1893 (d).

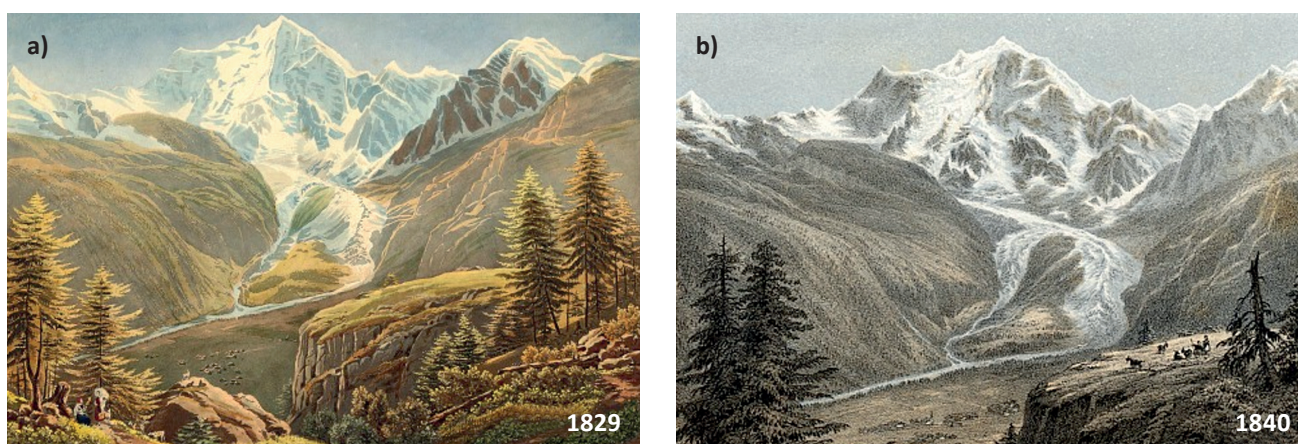


Fig. 11 Two strikingly similar images show the terminus from viewpoint E towards the end of the LIA. An aquatint titled “Mont Rosa” by G. Lory was published in 1829 (a) and a lithography by A. Cuviller: “Le Mont Rose – Vue de la Valle de Macugnana” from 1840 (b).

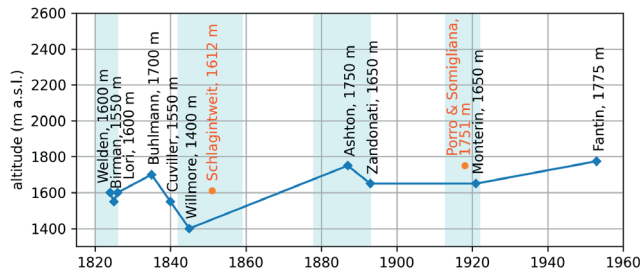


Fig. 12 Elevation changes of the terminus derived from the images. For the dates of the images, see the text and Tab. 1. The light blue stripes represent the periods of glacier advance for Belvedere after Monterin (1922). Orange dots represent field measurements of terminus elevation.

swept by a burst of the lateral moraine in this location following a blockage of the outflow from the glacier outlet for several hours (Mortara and Tamburini 2009).

The evolution of the terminus can also be traced in two landscape paintings from viewpoint E located on the slope between Macugnaga and Monte Moro Pass from 1829 and 1840. The first painting by G. Lory shows the glacier between the two last advancing phases of the LIA (Fig. 11 a), while the second painting by A. Cuviller corresponds to the beginning of the last advancing phase of the LIA (Fig. 11 b). Comparing the geometry and ice-related features of the mountains in the background and the glacier terminus indicates a high degree of realism.

While on the 1840 image, two clearly separated lobes can be recognised (Fig. 11 b), the 1829 image shows a whitish triangle similarly to the photograph taken by A. Zandonati in 1893 (Fig. 10 d). Apart from the outburst flood in 1868, this slope was affected by the extension of a third ice lobe during glacier fluctuations in 1896 and the 1920s (Mortara and Tamburini 2009). The third lobe is also present in a map from the 1920s (Monterin 1922) and did not exist anymore at least since the 1950s (Fig. 8 b). The 1829 image suggests the third lobe might have existed already during

the LIA long before the advancing period 1878–1893 which can also be detected in the painting by S. Birmann from 1835 (Tab. 1) (Mortara and Tamburini 2009).

The elevation changes of the left lobe terminus (Fig. 12) are well in line with the general pattern of glacier advances/retreats as outlined by Monterin (1922), which in turn reflect the climate fluctuations since the last phase of LIA. The low terminus elevation in the images by Welden (1824), Birman (1825), and Lori (1826) corresponds to one of the glacier advance periods in the Monte Rosa Massif reaching a maximum in 1826 (Monterin 1922). The oscillation in the terminus elevation for 50 m between 1824–1825 and 1825–1826 likely does not reflect the real changes in elevation but rather the accuracy of the method. Another glacier advance phase at the very end of LIA is captured in the images by Cuviller (1840) and Willmore (1845) with the lowest terminus elevation reaching 1400 m a.s.l.

Both the images by Ashton (1887) and Zandonati (1893) were taken during the glacier advancing phase 1878–1893, while the photograph by Monterin (1921) falls into the following glacier advance period in 1912–1921 (Monterin 1926). In 1918 the increase of the glacier mass even reached the crests of the lateral moraines as reported by Porro and Somigliana (1919). The image by Fantin (1953) was taken during the retreating period of Belvedere Glacier (Diolaiuti et al. 2003). Except for the 1835 image by Buhmann, all images until the 1920s correspond to glacier advance periods. Buhmann's image is responsible for the peak on the curve between two glacier advance periods during LIA, while the peak caused by Ashton's image is due to the lack of images covering the adjacent glacier retreat periods.

5.4 Focal theme 4: The evolution of a breach of the lateral moraine at Alpe Pedriola

The lithography from 1889 by Doyen (Fig. 13) shows a small breach in the right lateral moraine of the



Fig. 13 The east face of Monte Rosa as seen from the pasture hut of Alpe Pedriola (viewpoint E) shows a breach of the lateral moraine on the lithography by Doyen based on a photograph by Carnagbi from 1889 (a) and a photograph by M. Nüsser from 31 July 2024 (b). The breach is below on the right.

Belvedere Glacier. This breach was caused by the 1904 GLOF, in which the flood wave first followed the inner side of the lateral moraine, then breached it, and flowed along the ablation valley at the outer side of the moraine. The breach was further incised by a series of GLOFs originating from Locce Lake in 1970, 1978, and 1979. The small incision on the Doyean's lithography evidences that the breach is much older than 1904 than presumed.

6. Discussion

A large collection of multitemporal visual material, including engravings, paintings, and photographs, documents changes of Belvedere Glacier and the Monte Rosa east face over the last two centuries. This historical material provides evidence on glacier changes since the end of the LIA. The images also provide valuable evidence of the changes in debris cover and document the evolution of the terminus area shaped by a rather complex interplay of ice retreats and advances, formation of the third lobe and GLOF events.

In the presented study, we attempted to assemble and evaluate a long visual record of landscape changes based on images created for various purposes. For such studies, the growing availability of historical landscape images, in particular via online access to various archives, is highly beneficial (Kropáček et al. 2019). The presented and discussed images were produced by various techniques. The oldest engravings and paintings have accurate geometrical frameworks suggesting the utilization of graphical tools such as *camera lucida* as in the case of Welden's image. The accuracy of the painting by F. Ashton reveals a more realistic approach in landscape painting, common for the second half of the 19th century. The common denominator of the images, which were acquired independently of each other are the vantage points which are restricted to a few locations, often in the vicinity to exposed viewpoints with relatively easy access. Surprisingly none of the images shows Belvedere Glacier from the bifurcation point of the lobes – the Belvedere viewpoint.

The image record proved useful for documentation of the evolution of particular features, such as the breach of the left lateral moraine and left terminal lobe. Furthermore, the images allowed us to compile the elevations of its termini similarly as exemplified for instance by Zumbühl and Nussbaumer (2018) for the Lower Grindelwald Glacier and the Mer de Glace. The accuracy of the elevations can be compared to two historical ground measurements. The first measured elevation of the terminus position can be found in a map by the Schlagintweit brothers from 1851 as 1612 m (4960 feet). This can be compared with altitudes based on the engravings by Willmore from 1845 and Cuviller from 1840, which are 1550 and 1400 m a.s.l., thus showing differences of 62 m and

212 m, respectively. While the first difference can be explained by the expected error of the method, the second difference probably indicates an exaggeration of glacier extent in the image by Willmore.

The terminus elevation of 1700 m a.s.l. estimated from the photograph by Monterin from 1921 can be compared with the altitude of 1751 m a.s.l. measured by Porro and Somigliana in 1918 (Monterin 1922). The difference of 51 m could be explained by the inaccuracy in historical image interpretation. However, for this period (1918–1921) glacier advance was reported leading to the terminus elevation decrease of 53 m (Monterin 1922), which almost exactly corresponds to the difference. These comparisons and the experience with the work with the images lead us to the accuracy estimation of the approach to be around 50 m, while higher accuracy can be expected in the case of photographs compared to engravings.

In general, comparisons of photographs need to consider differences in illumination, shadows and snow cover (Nüsser 2001). Especially in our case study, the exact extent of ice on steep slopes of the Monte Rosa east face is biased by seasonal snow cover. It appeared, that graphical techniques and photographs cannot be strictly separated as in some materials, these techniques were combined (Zumbühl et al. 2018), which may explain some inconsistencies.

7. Conclusions

Based on an extensive search in various archives, we found 29 historical images of Monte Rosa's east face and the Belvedere Glacier. They provide a valuable visual record dating back to the end of the 18th century, greatly extending the observation period covered by aerial photography and satellite imagery. As the viewpoints of the images are restricted to a few spots, we could build bi- and multitemporal series of repeat images. The historical images could be complemented by contemporary photographs or by simulated images prepared in Google Earth. These visual records allowed us to investigate the glacier changes since the LIA. We could document the evolution of debris cover, changes at the terminus, and the appearance of the breach of the right lateral moraine further shaped by a series of outburst floods. From the images by A. Schlagintweit (1854), A. Civiale (1859–1868), and G. Loppé (the 1880s) it appeared that the debris cover of the lower part of the glacier developed mainly between the 1860s and 1880s, in the period following the LIA.

The analysis of the terminal part of Belvedere Glacier showed that the slope between the two terminal lobes was affected by the ice movement already towards the end of the LIA and a third lobe likely already existed, similarly to 1896 and the 1920s, as seen in the aquatint by G. Lory (1829). Seven graphics and three photographs were used to analyse the

changes in the terminus elevation. Although most of these images fall by coincidence in periods of glacier advance, they document well the general glacier retreat since the end of the LIA. Furthermore, the photolithograph by Doyen/Carnaghi evidenced that the breach of the lateral moraine used by the floods in 1904 and the 1970s existed long before 1904 as previously assumed. All the listed materials not only document the glacier changes and related processes of the study site but also reflect the evolution of graphical techniques used by mountain explorers over the last two centuries.

Acknowledgements

For the access to visual material and the permission to use material for this publication, we would like to thank the Documentation Center – Museo Nazionale della Montagna – CAI Turin; the digital archive of Eidgenössische Technische Hochschule (ETH) Zurich for the photograph by W. Mittenholzer (ETH-Bibliothek Zürich, Bildarchiv/Stiftung Luftbild Schweiz / Fotograf: Mittenholzer, Walter / LBS_MH01-002036 / Public Domain Mark; <http://doi.org/10.3932/ethz-a-000342754>), Bibliothèque nationale de France (BnF), Österreichische Nationalbibliothek, the Bayerische Staatsbibliothek (BSB) Munich and Museo del Paesaggio Verbania. We also gratefully acknowledge the permissions for the publication of visual materials by Fondazione Sella, Biella; F. Petinarolli sas, Milano; John Mitchell Fine Paintings, London. We acknowledge the Geoportale Piemonte for providing the DEM 5. This work was supported by the Cooperatio project 255-207023032 of the Ministry of Education, Youth and Sports of the Czech Republic. The research was funded by the 4EU+ grant number 4EU+/23/F4/19. We are grateful to Dr. Andrea De Zordi from Provincia del Verbano-Cusio-Ossola for her support of our field visits.

References

- Bollati, I., Smiraglia, C., Pelfini, M. (2013): Assessment and selection of geomorphosites and trails in the Miage Glacier Area (Western Italian Alps). *Environmental Management* 51, 951–967, <https://doi.org/10.1007/s00267-012-9995-2>.
- von Brevern, J. (2009): Counting on the unexpected: Aimé Civiale's mountain photography. *Science in Context* 22(3), 409–437, <https://doi.org/10.1017/S026988970999007X>.
- Bridson, G. D. (1989): From xylography to holography: five centuries of natural history illustration. *Archives of Natural History* 16(2), 121–141, <https://doi.org/10.3366/anh.1989.16.2.121>.
- Brunner, K., Welsch, W. (2002): High-mountain cartography of the German and the Austrian Alpine Clubs. *ISPRS Journal of Photogrammetry and Remote Sensing* 57(1–2), 126–133, [https://doi.org/10.1016/S0924-2716\(02\)00108-9](https://doi.org/10.1016/S0924-2716(02)00108-9).
- Byers, A. C. (1987): An assessment of landscape change in the Khumbu region of Nepal using repeat photography. *Mountain Research and Development* 7(1), 77–81, <https://doi.org/10.2307/3673327>.
- Byers, A. C. (2007): An assessment of contemporary glacier fluctuations in Nepal's Khumbu Himal using repeat photography. *Himalayan Journal of Science* 4(6), 21–26, <https://doi.org/10.3126/hjs.v4i6.979>.
- Byers, A. C. (2017): A qualitative assessment of contemporary glacier loss in the Cordillera Blanca, Peru, using repeat photography. *Revista de Glaciares y Ecosistemas de Montaña* 2, 10–10.
- Cerney, D. L. (2010): The use of repeat photography in contemporary geomorphic studies: an evolving approach to understanding landscape change. *Geography Compass* 4(9), 1339–1357, <https://doi.org/10.1111/j.1749-8198.2010.00376.x>.
- Chand, P., Sharma, M. C., Bhambri, R., Sangewar, C. V., Juyal, N. (2017): Reconstructing the pattern of the Bara Shigri Glacier fluctuation since the end of the Little Ice Age, Chandra valley, north-western Himalaya. *Progress in Physical Geography* 41(5), 643–675, <https://doi.org/10.1177/0309133317728017>.
- Chen, H., Yin, K., Wang, H., Zhong, S., Wu, N., Shi, F., Zhu, D., Zhu, Q., Wang, W., Ma, Z., Fang, X., Li, W., Zhao, P., Peng, C. (2011): Detecting one-hundred-year environmental changes in western China using seven-year repeat photography. *PLOS ONE* 6(9): e25008, <https://doi.org/10.1371/journal.pone.0025008>.
- Civiale, A. (1882): *Les Alpes: au point de vue de la géographie physique et de la géologie: voyages photographiques dans le Dauphiné, la Savoie, le Nord de l'Italie, la Suisse et le Tyrol* (Vol. 1). J. Rothschild.
- Davis, T. (1989): Photography and landscape studies. *Landscape Journal* 8(1), 1–12, <https://doi.org/10.3368/lj.8.1.1>
- Diolaiuti, G., D'Agata, C., and Smiraglia, C. (2003): Belvedere Glacier, Monte Rosa, Italian Alps: Tongue Thickness and Volume Variations in the Second Half of the 20th Century. *Arctic, Antarctic, and Alpine Research* 35(2), 255–263, [https://doi.org/10.1657/1523-0430\(2003\)035\[0255:BGMRIA\]2.0.CO;2](https://doi.org/10.1657/1523-0430(2003)035[0255:BGMRIA]2.0.CO;2).
- Finsterwalder, S. (1897): *Der Vernagtferner – Seine Geschichte und seine Vermessung in den Jahren 1888 und 1889*. Wissenschaftliche Ergänzungshefte des Deutschen und Österreichischen Alpenvereins 1(1), 1–95.
- Fischer, L., Huggel, C., Käab, A., and Haeblerli, W. (2013): Slope failures and erosion rates on a glacierized high-mountain face under climatic changes. *Earth Surface Processes and Landforms* 38(8), 836–846, <https://doi.org/10.1002/esp.3355>.
- Frangne, P. H. (2010): The Dehiscent Image. Théophile Gautier and the Mountain Photographs of the Brothers Bisson. *Études photographiques* 25, 210–242, <https://journals.openedition.org/etudesphotographiques/3062>.
- Gibbs, P. (1910): *The Wonders of the World*. Hutchinson & Co. London.
- Gnifetti, G. (1858): *Nozioni topografiche del Monte Rosa ed ascensioni su di esso*. Crotti.
- Garimoldi, G. (2005): *Immagini di montagna e immagini d'alpinismo. Memoria e ricerca: rivista di storia contemporanea*. Fascicolo 19, 1000–1021.

- Haeberli, W., Käab, A., Paul, F., Chiarle, M., Mortara, G., Mazza, A., Deline, P., Richardson, S. (2002): A surge-type movement at Ghiacciaio del Belvedere and a developing slope instability in the east face of Monte Rosa, Macugnaga, Italian Alps. *Norsk Geografisk Tidsskrift* 56(2), 104–111, <https://doi.org/10.1080/002919502760056422>.
- Hattersley-Smith, G. (1966): The symposium on glacier mapping. *Canadian Journal of Earth Sciences*, 3(6), 737–741, <https://doi.org/10.1139/e66-055>.
- Hopkinson, M. (2017): Book Review: *The Print before Photography. An Introduction to European Printmaking 1550–1820* by Anthony Griffiths. *The British Art Journal* 17(3), 92–94.
- Jacobson, K. (2015): John Ruskin's Lost Daguerreotypes. *Daguerreotype Journal* 2(3), 8–19.
- Käab, A., Huggel, C., Haeberli, W., Cordola, M., Barbero, S., Mortara, G., Semino, P., Tamburini, A., Viazzo, G. (2004): Glacier hazards at Belvedere Glacier and the Monte Rosa east face, Italian Alps: processes and mitigation, *Internationales Symposium Interpraevent 2004 – Riva/Trient*.
- Kull, C. A. (2005): Historical landscape repeat photography as a tool for land use change research. *Norsk Geografisk Tidsskrift-Norwegian Journal of Geography* 59(4), 253–268, <https://doi.org/10.1080/00291950500375443>.
- Kropáček, J. (2019): Erosion dynamics in the southern Tibetan Plateau at a century time scale from historical photographs. *Journal of Arid Environments* 161, 47–54, <https://doi.org/10.1016/j.jaridenv.2018.10.005>.
- Kropáček, J., Vařilová, Z., Nyssen, J. (2019): Historical aerial and terrestrial photographs for the investigation of mass movement dynamics in the Ethiopian Highlands. *Land Degradation & Development* 30(5), 483–493, <https://doi.org/10.1002/ldr.3220>.
- Levin, J. A. E. (1980): *The golden age of illustration: popular art in American magazines, 1850–1925*. University of Pennsylvania.
- Mazza, A. (2000): Some results of recent investigations on Ghiacciaio del Belvedere (Anzasca valley, western Alps) taking into account the glacier mechanics. *Geografia Fisica e Dinamica Quaternaria* 23(7), 59–71, <https://www.jstor.org/stable/1552378>.
- Milner, C. D. (1946): Focal Press, London
- Monterin, U. (1922): Il Ghiacciaio di Macugnaga dal 1870 al 1922. *Bollettino del Comitato Glaciologico Italiano* 5, 12–40.
- Monterin, U. (1926): La fine della fase progressiva e l'inizio della nuova fase di ritiro dei ghiacciai italiani nel Monte Rosa 1922–1925. *Zeitschrift für Gletscherkunde* 15(1), 31–54.
- Mortara, G., Tamburini, A. (2009): Il ghiacciaio del Belvedere e l'emergenza del Lago Effimero, Regione Piemonte. *Società Meteorologica Subalpina*.
- Mustalish, R. A. (1997): The development of photomechanical printing processes in the late 19th century. *Topics in photographic preservation* 7, 73–87.
- Nüsser, M. (2000): Change and persistence: contemporary landscape transformation in the Nanga Parbat region, northern Pakistan. *Mountain Research and Development* 20(4), 348–355, [https://doi.org/10.1659/0276-4741\(2000\)020\[0348:CAPCLT\]2.0.CO;2](https://doi.org/10.1659/0276-4741(2000)020[0348:CAPCLT]2.0.CO;2).
- Nüsser, M. (2001): Understanding cultural landscape transformation: A re-photographic survey in Chitral, eastern Hindukush, Pakistan. *Landscape and Urban Planning* 57(3–4), 241–255, [https://doi.org/10.1016/S0169-2046\(01\)00207-9](https://doi.org/10.1016/S0169-2046(01)00207-9).
- Nüsser, M., Baghel, R. (2014): The emergence of the cryoscape: Contested narratives of Himalayan glacier dynamics and climate change. In: Schuler B. (ed.): *Environmental and climate change in South and Southeast Asia: How are local cultures coping?* Leiden, Boston: Brill (Climate and Culture 2), 138–156, https://doi.org/10.1163/9789004273221_007.
- Nüsser, M., Schmidt, S. (2021a): Assessing glacier changes in the Nanga Parbat region using a multitemporal photographic dataset. *Data in Brief* 37: 107178, <https://doi.org/10.1016/j.dib.2021.107178>.
- Nüsser, M., Schmidt, S. (2021b): Glacier changes on the Nanga Parbat 1856–2020: A multi-source retrospective analysis. *Science of The Total Environment* 785: 147321, <https://doi.org/10.1016/j.scitotenv.2021.147321>.
- Nyssen, J., Haile, M., Naudts, J., Munro, N., Poesen, J., Moeyersons, J., Frankl, A., Deckers, J., Pankhurst, R. (2009): Desertification? Northern Ethiopia re-photographed after 140 years. *Science of The Total Environment* 407(8), 2749–2755, <https://doi.org/10.1016/j.scitotenv.2008.12.016>.
- Osterman, M. (2013): The technical evolution of photography in the 19th century. *The Concise Focal Encyclopedia of Photography*, 5–16, <https://doi.org/10.1016/B978-0-240-80998-4.50008-6>.
- Paranunzio, R., Laio, F., Chiarle, M., Nigrelli, G., Guzzetti, F. (2016): Climate anomalies associated with the occurrence of rockfalls at high-elevation in the Italian Alps. *Natural Hazards and Earth System Sciences* 16(9), 2085–2106, <https://doi.org/10.5194/nhess-16-2085-2016>.
- Porro F, Somigliana, C. (1919): Ghiacciaio do Macugnaga. *Bollettino del Comitato Glaciologico Italiano* 3, 187–189.
- Reclus, E. (1876–1894): *The universal geography: earth and its habitants*. Southern Europe (Greece, Turkey in Europe, Rumania, Servia, Italy, Spain and Portugal), Vol. 2., London: J. S. Virtue & Co.
- de Saussure, H. B., Zanzi, L., Martinoni, R., Rainaldi, G., Martinoni, R. (1989): *Viaggi intorno al Monte Rosa*. Fondazione Arch. Enrico Monti.
- de Saussure, H. B. (1779–1796): *Voyages dans les Alpes*, Neuchâtel, Vol. 4.
- Savale, C. (1994): Les campagnes photographiques de Martens en Suisse et en Savoie. *Histoire de l'art* 25(1), 67–77, <https://doi.org/10.3406/hista.1994.2600>.
- Schlagintweit H. and Schlagintweit A. (1850): *Untersuchungen über die physicalische Geographie der Alpen in ihren Beziehungen zu den Phaenomenen der Gletscher, zur Geologie, Meteorologie und Pflanzengeographie*. Leipzig.
- Schlagintweit A. and Schlagintweit H. (1854): *Neue Untersuchungen über die physicalische Geographie und die Geologie der Alpen*. Leipzig.
- Schmidt, S., Nüsser, M. (2009): Fluctuations of Raikot Glacier during the last 70 Years: A case study from the Nanga Parbat Massif, northern Pakistan. *Journal of Glaciology* 55(194), 949–959, <https://doi.org/10.3189/002214309790794878>.
- Schulze, S. (2021): Seen from above: Wilhelm Halffter's photographs of 1854, depicting the terrain models of Hermann and Adolph Schlagintweit. In *Hybrid*

- Photography, Routledge, 41-56, <https://doi.org/10.4324/9781003157854>.
- Sealy, P. (2016): After a photograph, before photography (takes command). *The Journal of Architecture* 21(6), 911–937, <https://doi.org/10.1080/13602365.2016.1220970>.
- Smiraglia, C., Diolaiuti G., eds. (2015): *The New Italian Glacier Inventory*. EvK2CNR, Bergamo, <https://sites.unimi.it/glaciol/index.php/it/catasto-dei-ghiacciai-italiani/>.
- Stefaniak, A. M., Robson, B. A., Cook, S. J., Clutterbuck, B., Midgley, N. G., Labadz, J. C. (2021): Mass balance and surface evolution of the debris-covered Miage Glacier, 1990–2018. *Geomorphology* 373: 107474, <https://doi.org/10.1016/j.geomorph.2020.107474>.
- Steiner, D., Zumbühl, H. J., Bauder, A. (2008): A scientific view based on pictorial sources. In: Orlove B, Wiegandt E and Luckman B, eds. *Darkening peaks: glacier retreat, science, and society*, Berkeley: University of California Press, 83–99, <https://doi.org/10.1002/jqs.1213>.
- Tamburini, A., Mortara, G. (2005): The case of the Effimero lake at Monte Rosa (Italian Western Alps). *Studies, field surveys, monitoring*. Proc. 10th ERB Conference Progress in surface and subsurface water studies at plot and small basin scale (Turin, 13-17 October 2004), Torino, <http://www.cnr.it/prodotto/i/88695>.
- Tamburini, A., Villa, F., Fischer, L., Hungr, O., Chiarle, M., Mortara, G. (2013): Slope instabilities in high-mountain rock walls. Recent events on the Monte Rosa east face (Macugnaga, NW Italy). In: Margottini, C., Canuti, P., Sassa, K. (eds) *Landslide Science and Practice*. Springer, Berlin, Heidelberg, https://doi.org/10.1007/978-3-642-31310-3_44.
- Trimble, S. W. (2008): The use of historical data and artifacts in geomorphology. *Progress in Physical Geography* 32(1), 3–29, <https://doi.org/10.1177/0309133308089495>.
- Truffer, M., Käab, A., Harrison, W. D., Osipova, G. B., Nosenko, G. A., Espzua, L., Gilbert, A., Fischer, L., Huggel, C., Craw Burns, P. A., Lai, A. W. (2021): Glacier surges. In: Haeberli, W. and Whiteman, C. (eds.). *Snow and Ice-Related Hazards, Risks, and Disasters*. Elsevier, 417–466, <https://doi.org/10.1016/B978-0-12-817129-5.00003-2>.
- Vukovic, M., Fischer, A. (2022): The Camera as a Tool in Geography: Parallels between Friedrich Simony's Pictures of the Dachstein and the Use of Photographic Images in Geography Today. *Umění/Art* 70(3), <https://doi.org/10.54759/ART-2022-0305>.
- Viatimages (2024): Available online: <https://www2.unil.ch/viatimages/index.php?lang=fr&projet=viatimages&#/ouvrage-221> (accessed on 4.6.2024).
- von Welden, F. L. F., Welden, L. (1824): *Der Monte-Rosa: eine topographische und naturhistorische Skizze, nebst einem Anhang der von Herrn Zumstein gemachten Reisen zur Ersteigung seiner Gipfel*. C. Gerold.
- WGMS (World Glacier Monitoring Service, 2024): *Fluctuations of Glaciers Browser*. Available online: <https://experience.arcgis.com/experience/836c66d14c8b410f940355056ddb1bf8?org=uzh> (accessed on 14.02.2024).
- Zängl, W., Hamberger, S. (2004): *Gletscher im Treibhaus*. Tecklenborg, Steinfurt.
- Zumbühl, H. J., Nussbaumer, S. U. (2018): Little Ice Age glacier history of the Central and Western Alps from pictorial documents. *Cuadernos de Investigación Geográfica* 44(1), 115–136, <https://doi.org/10.18172/cig.3363>.
- Zumbühl, H. J., Steiner, D., Nussbaumer, S. U. (2008): 19th century glacier representations and fluctuations in the central and western European Alps: An interdisciplinary approach. *Global and Planetary Change* 60(1–2), 42–57, <https://doi.org/10.1016/j.gloplacha.2006.08.005>.
- Zumstein, J. (2020): *Cinque viaggi alle vette del Monte Rosa (1819–1822)* editor Crivellaro, P., Zeisciu, Alagna Valsesia.

What do trees reveal about the sliding of the lateral moraine of the Belvedere Glacier (western Italian Alps)?

Irene Maria Bollati^{1,*}, Roberto Sergio Azzoni¹, Anna Tagliaferri¹, Gianluca Tronti¹, Manuela Pelfini¹, Vít Vilímek², Lukáš Brodský³

¹ University of Milan, Earth Sciences Department, "A. Desio", Italy

² Charles University, Faculty of Science, Department of Physical Geography and Geoecology, Czechia

³ Charles University, Faculty of Science, Department of Applied Geoinformatics and Cartography, Czechia

* Corresponding author: irene.bollati@unimi.it

ABSTRACT

The debris-covered Belvedere Glacier is an iconic place for investigating glacier dynamics and geomorphological processes typical of high mountain environments. Moreover, being located in an area highly suited to tourism, glacial and geomorphological hazards can evolve into risk scenarios. Particular attention has been paid during this research to the surge-type event that occurred at the beginning of the 21st century, and to the recent sliding of a lateral moraine nearby the chairlift station. Tree sampling was performed (19 trees on the lateral moraine; 10 undisturbed trees), and the results were compared with morphometric measurements on orthophotos of different years. Besides sampling trunks, the six available exposed roots (13 samples) from a tree located along the sliding niche were sampled to identify the exposure time. Morphometric measurements of the touristic trail dislocation indicate a sliding rate of 1.87 m/y – 1.98 m/y (2018–2023), while the regression rate of the sliding niche is 1.70 m/y (2021–2023). The age of trees along the trench is variable (14–49 years), as is the signal of compression wood, enhancing differentially the passage of the surge wave and the subsequent glacier downwasting. The beginning of root exposure occurred between 2017 and 2019, before the effective evidence of large fractures in the ground. Moreover, the roots show traumatic resin ducts in the period between 2020 and 2022, confirming the tree disturbance. In conclusion, the investigated events are recorded differentially in the sampled trees, especially in roots, anticipating the actual commencement of ground failure. A multidisciplinary approach, including remote sensing, field survey, and dendrogeomorphological analysis is essential to define the dynamics of complex systems.

KEYWORDS

dendrogeomorphology; paraglacial dynamics; surge-type event; moraine sliding; Belvedere Glacier

Received: 3 April 2024

Accepted: 2 September 2024

Published online: 14 October 2024

Bollati, I. M., Azzoni, R. S., Tagliaferri, A., Tronti, G., Pelfini, M., Vilímek, V., Brodský, L. (2024): What do trees reveal about the sliding of the lateral moraine of the Belvedere Glacier (western Italian Alps)? *AUC Geographica* 59(2), 255–271 <https://doi.org/10.14712/23361980.2024.14>

© 2024 The Authors. This is an open-access article distributed under the terms of the Creative Commons Attribution License (<http://creativecommons.org/licenses/by/4.0>).

1. Introduction

The debris-covered Belvedere Glacier, located on the eastern side of Monte Rosa (Western Italian Alps) (Fig. 1a), is an iconic area in the European Alps. Together with the Miage Glacier, another peculiar debris-covered glacier located in the Mont Blanc Massif (Italian side) (Bollati et al. 2015), it represents one of the most deeply studied glacial areas in the Italian Alps. The glacier has an extensive debris coverage, which is not so common in the European Alps, and a very peculiar morphology, similar to the Miage Glacier, with the glacial snout divided into two lobes. It presents a complex response to climate change, marked by altered surface ablation rates and spatial patterns of mass loss, as generally observed in debris-covered glaciers in other mountain ranges (e.g., Benn et al. 2012). Since debris coverage can reduce the ablation rate when it exceeds a critical thickness (e.g., Nakawo et al. 1999; Fyffe et al. 2014; Mehta et al. 2023), the Belvedere Glacier maintains its front at relatively low elevations (approximately 1800–1900 m a.s.l.), below the tree line. On the contrary, Belvedere tributary glaciers, not covered by debris, are undergoing a fast retreat in line with the overall trend in the European (Paul et al. 2020) and Italian Alps (Smiraglia and Diolaiuti 2015). Even if this trend may vary depending on the glacier types, since valley glaciers are found to be less sensitive to air temperature and precipitation (Serandrei-Barbero et al. 2022), this trend is leading to the separation of Belvedere from the tributary glaciers.

Despite the snout of the Belvedere Glacier remaining at relatively low elevations, constant in-situ monitoring (Mortara et al. 2023) and recent photogrammetric studies provide evidence of downwasting, gradual glacier retreat, and morphological modifications (Ioli et al. 2023; Brodský et al. 2024, in this issue).

The scientific interest derives from the different kind of processes (glacial, gravity-, and water-related) potentially generating hazards in the area (Mortara et al. 2017). For instance, the Glacier Lake Outburst Floods (GLOFs) from Lake Locce (1970, 1978, and the most recent one in 1979; Mortara and Tamburini 2009; Käab et al. 2004) posed serious issues, since they affected localities in the municipality of Macugnaga (i.e., the destruction of the lower chairlift station and the sudden increase of solid and liquid discharges along the Anza River). As a response to these events, several investigations and interventions to mitigate the risk scenarios were planned in the area (VAW 1983, 1985). Considering the 21st century in more detail, the most relevant geomorphological processes related to the Belvedere Glacier and its surrounding areas, interfering in some way with the glacier dynamic and also generating hazards downvalley, were: a surge-type event, characterized by glacier changes between 1999 and 2003, and reaching the

acme between 2000–2002 (Mazza 2003; Käab et al. 2004); the formation and evolution of an ephemeral lake (Lake Effimero; Fig. 1a) whose GLOF is a potential threat to Macugnaga village; significant rock falls and avalanches (2005, 2007) sometimes also accompanied by ice (Fig. 1a); the Castelfranco debris flow that recently hit the glacier area in August 2023 (Fig. 1a); and, finally, the continuous sliding of lateral moraines (Fig. 1a).

Most of these processes may be classified as paraglacial-type processes i.e., according to Church & Ryder (1972) "... non-glacial processes that are directly conditioned by glaciation". They refer both to "proglacial processes, and to those occurring around and within the margins of a former glacier that are the direct result of the former presence of ice". Balantyne (2002) classified a series of paraglacial-type processes, among which there is the debuttressing of lateral rocky and debris slopes along glacial valleys, favoring rock falls and avalanches, and landsliding in general. The latter is a process continuously affecting the Belvedere area (Mortara et al. 2023), especially since the end of the Little Ice Age (14th century CE – 1850–1860 CE; Ivy-Ochs et al. 2009), but it became more significant after the sudden exhaustion of the 2000–2002 surge-type event, as the support offered by the huge ice volume disappeared quite rapidly.

Since the snout of the Belvedere Glacier is located below the tree line, the moraines bordering the central-lower part of the glacier, including the one undergoing sliding, are colonized by broadleaves and coniferous trees of different species. Among them, larches (*Larix decidua* Mill.) are pioneer species also colonizing unstable surfaces and constituting an early step in the renewal of the ecological series.

In the literature, dendrochronological analyses, based on tree rings, have been performed on larch and coniferous species in high altitude environments to detect climatic signals (e.g., Leonelli et al. 2016), or to reconstruct geomorphological disturbances in different geomorphological contexts, such as landslides (e.g., Fantucci 1997; Guida et al. 2008; Tichavský et al. 2019), debris flows (e.g., Garavaglia et al. 2009; Bollati et al. 2018), or snow avalanches (Garavaglia and Pelfini 2011; Bollati et al. 2018; Favillier et al. 2023), as well as in glacial contexts for detecting glacier fluctuations, mass balance, surface instability (e.g., Pelfini 1999; Richter et al. 2004; Leonelli et al. 2008; Leonelli and Pelfini 2013), and also proglacial stream activity (e.g., Pelfini et al. 2007; Garavaglia et al. 2010).

Several morphological (micro and macro) indicators in tree rings (i.e., growth anomalies, compression wood, eccentricity index, traumatic resin ducts; Pelfini et al. 2007; Stoffel and Bollschweiler 2007) are used to reconstruct such dynamics. Their reliability may vary accordingly; for instance, to the type of process and to morphological features of the sites (de Bouchard d'Aubeterre et al. 2019). Moreover, when

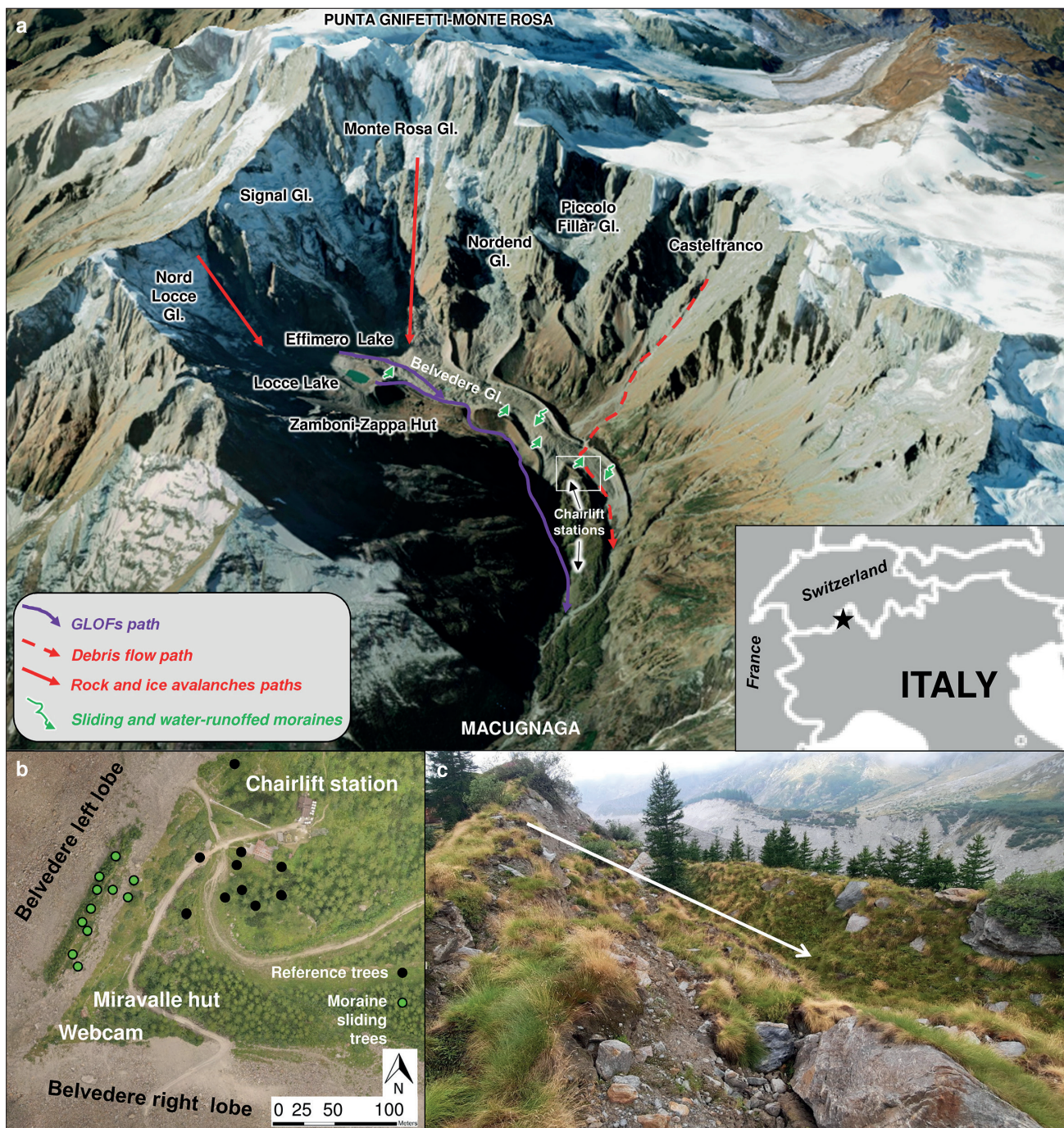


Fig. 1 The head of the Belvedere Glacier hydrographic basin on a Google Earth 3D image with the white square indicating the study area and referring to Fig. 1b, c, and the path of the most significant geomorphic processes affecting the area (a); the tree sampling distribution on the orthophotos, created in 2023 using a drone flight (b), and an image of a trench related to moraine sliding (c).

tree roots are exposed along erosion surface, they may also be used to date the sediment removal and to calculate average erosion rates (e.g., Stoffel et al. 2013; Bollati et al. 2016).

Concerning dendroglaciological analyses in the Italian Alps in more detail, and firstly considering the case of a debris-free glacier, Pelfini (1999) detailed the advance of the Grande di Verra Glacier (Aosta Valley, Italian Alps) as far as the Little Ice Age (14th century CE – 1850–1860 CE; Ivy-Ochs et al. 2009), as well as the retreat phases, through the analysis of

tree ring width anomalies. On the other hand, the glacial dynamic of a debris-covered glacier is even more particular. The position of the debris-covered glacier snout remains quite constant despite the mass transferring through kinematic waves crossing the glacier as far as the snout, the crevasses or the ice cliffs, where the mass wasting is greatest. In the case of the Miage glacier (Aosta Valley, Italian Alps), for instance, there is a proper forest growing on the glacier debris coverage, and the analyses of tree rings enabled the passage of a kinematic wave in 1980s to be detected,

differentially on its two lobes (i.e., 5-years delay; Pelfini et al. 2007; 2012).

In both these cases, the data extracted from the tree cores provided information at an annual resolution, which may be further discussed in comparison with data from remote sensing analyses (e.g., velocity of the glacier flow, surface topographic change), based on aerial images and digital elevation models with different space and time resolution (e.g., Azzoni et al. 2023).

In this work, the aim was to analyze in detail the response of the lateral moraine of the Belvedere Glacier nearby the chairlift station to the pressure it underwent during the surge-type event, to the ongoing relaxation due to glacier downwasting (e.g., paraglacial debuitressing, sensu Ballantyne 2002), and to water runoff affecting the moraine's inner flank. To achieve this, the traditional tree ring indicators and dendrogeomorphological investigations were used and compared with field observations, and morphometric data from remote sensing analyses.

2. Study area

The Belvedere Glacier is one of the most famous debris-covered glaciers in the European Alps, renowned for its debris coverage and its location just below the base of the east side of Monte Rosa, the highest European alpine wall. It is located at the head of the Anzasca Valley (Western Italian Alps), on the border with Switzerland (Fig. 1). The debris coverage is fed by ice and snow avalanches, and rock falls, frequently originating from the eastern face of Monte Rosa (Giordan et al. 2022). The Belvedere Glacier is hence featured by an elevated sediment coverage (i.e., Monterin 1923, Mazza 1998; Haerberli et al. 2002). The forest surrounding, but also connected with the glacier environment, is formed by European larch (*Larix decidua* Mill.), Norway spruce (*Picea abies* Karst), and other alpine species such as birch (*Betula pendula*) and green alder (*Alnus alnobetula*) in wetter areas. Above the climatic tree line, located at 2215 m a.s.l. (Tampucci et al. 2017), open environments prevail, characterized by extensive rocky surfaces, scree, moraines, and remnants of acidic substrates from glaciers where alpine scrub or scrubland comprise primarily of green alder, and rhododendron (*Rhododendron ferrugineum*). The vegetation growing on the Belvedere Glacier is distinct, as exists in a colder environment compared to the surroundings. It hosts unique assemblages of cold-adapted plant species, which remain unaffected by glaciological variations within debris-covered glaciers (Tampucci et al. 2017). This characteristic makes it a potential warm-stage refuge for cold-adapted species (Caccianiga et al. 2011). Compared to similar environments (i.e., the Miage Glacier, Pelfini et al. 2007; 2012), the

vegetation and trees on its surface have considerably younger ages, up to 5–6 years old.

Vegetation has to cohabit within a highly dynamic environment. Indeed, despite the seemingly stable position of its front, composed of two distinct lobes (left and right in this work; see Fig. 1), the Belvedere Glacier is undergoing dramatic changes, particularly in terms of glacier thickness (e.g., Ioli et al. 2021; De Gaetani et al. 2021; Ioli et al. 2023; Mortara et al. 2023).

Moreover, after the separation from of the Nordend Glacier and the Nord Locce Glacier, the Belvedere Glacier is now solely fed by the very steep Monte Rosa Glacier. However, this connection may also be compromised in the near future due to global warming if glacier retreat continues.

Several authors have estimated the losses and gains of Belvedere ice volumes since the middle of the 20th century using topographic maps, digital elevation models, and punctual measurements through ice stakes. Tab. 1 provides a summary of the main results in the literature of the ice volume variations, and the ice flow velocities are also included.

An important event that occurred in the study area, attracting the attention of several scientists, was the surge-type event (i.e., kinematic wave), that, considering all the possible evidences, was observed in the 1999–2003 timeframe (Kääb et al. 2004). Details are provided in section 2.1. De Gaetani et al. (2021) calculated an acceleration of ice thickness (and volume) reduction during the period between 2001 and 2009, during and after the end of this surge-type event based on five surveys conducted on the glacier between 1977 and 2019. In particular, during the 2009–2019 the volume loss propagated towards the glacier snout, which began in 2001 from higher elevations. In total, a loss of 54 million m³ of ice was calculated by the authors during the 1977–2019 time interval.

When, then, the moraine under investigation began to collapse (2015–2020), Ioli et al. (2021) measured an ice loss rate of between 2 and 3.5 million m³/y, lower than the values calculated immediately after the surge, but detecting an active downwasting nevertheless.

Mortara et al. (2023) calculated the punctual ablation between 2010 and 2023 testifying to a variable annual surface lowering of between 270 and 430 cm with maximum values in 2015. They also recorded a decrease in velocity during the 1987–2023 time interval, interpreted as the slowing down of the ice mass transfer from the accumulation to ablation zone favoring the glacier snout retreat. Again, in terms of velocity, Ioli et al. (2021) found variable values in the different areas of the glacier. In normal periods, the data in the literature report a velocity of between 2 and 43 m/y, while during the surge-type event it reached values of 100–200 m/y (Tab. 1; Kääb et al. 2005; Ioli et al. 2021).

Tab. 1 Summary of the main measurements of ice volume and surface velocity variations present in literature.

Time interval	Author	Volume (million m ³)	Rate (million m ³ /y)	Note
1957–1991	Diolaiuti et al. (2003)	+22.7	0.69	
1983–1985	Roethlisberger et al. (1985)		+1.50	
1977–1991	De Gaetani et al. (2021)	+10.06	+0.72	
1991–2001		+10.61	+1.06	Before surge
1977–2001		+20.66	+0.72	Before surge
2001–2009		–47.78	–5.97	During surge and after
2009–2019		–27.16	–2.72	Before the moraine collapse
1977–2019		–54.28		
2015–2020	Ioli et al. (2021)		2.0–3.5	Before and during the moraine collapse
Time interval	Author	Surface velocity (m/y)		Note
1995–1999	Kääb et al. (2005)	32–43		
2001		100–200		
2015–2020	Ioli et al. (2021)	17–22		Central portion
2015–2020		2–7		Accumulation zone and glacier snout

After the surge-type event a total retreat of the glacier snout of 300-m was measured by Mortara et al. (2023). The glacier snout morphological modifications were also measured by Ioli et al. (2023) through an innovative photogrammetric technique, indicating an average glacier retreat rate of 2.7 m in one month (July–August 2022), and an ice volume loss of approximately $14 \times 10^3 \text{ m}^3$.

In this historical framework of the Belvedere Glacier, two events are considered for the present study, both affecting the area below the tree line, in a period overlapping with the tree chronologies: the surge-type event between 2000 and 2002, and the moraine collapse at the chairlift station and near the Miravalle hut and in subsequent years, highlighted by ground failures in 2019. These events are described in detail in the following sections.

2.1 The surge-type event

The surge-type event with first evidences in 1999, reached the acme during the summer of the year 2000 till the late spring of 2002, exhausting in 2003 (Mazza 2003; Kääb et al. 2004). The deep morphological changes affecting the glacier made this event quite unique in the European Alps. The three main features of this event, described by Mortara et al. (2023), are: i) the increase in superficial velocity, ii) the intense crevassing of the glacier tongue, and iii) the local increase in the volume and thickness (up to 20 m; Kääb et al. 2004). This allowed the ice to overwhelm the Little Ice Age moraines, especially on the right side, near the Zamboni-Zappa hut, and filling the breach in the moraine generated during the previous Lake Locce GLOFs (Mortara and Tamburini 2009). During the surge-type event, indeed, a glacial mass transformation and transfer occurred: the glacier terminus moved downvalley for 40 m. The measured

velocity was 100–200 m/y (Kääb et al. 2005) compared to the normal 20–30 m/y (Mortara and Tamburini 2009). According to Haeberli et al. (2002), in the summer of 2000, the Monte Rosa glacier flowing into the Belvedere accelerated its flow, as testified by several crevasses, and induced compression and deformation on the Belvedere ice mass. Evident new moraines are now the past witnesses of this surge-type event, especially along the right moraine, and the right side of the left lobe, downvalley in regard to the lobe separation. Haeberli et al. (2002) underlined how this process may have triggered potential hazards for the infrastructure in the area, and also downvalley, if pressurized water came out, for instance from an ephemeral lake formed during the surge-type event. For this reason, it was observed and monitored in detail to set specific rescue strategies with the local authorities (VAW 1983, 1985).

After the event, the dramatic ice downwasting induced a generalized instability along the lateral moraines, leading to their subsequent degradation, and collapse and hazards related to the surge-type event have continued some years after the end of the event.

2.2 Sliding of the lateral moraine at the Miravalle hut

After the exhaustion of the surge-type event, the Little Ice Age degradation of the lateral moraines, for the paraglacial debuttressing and water runoff on the inner flank of the moraine no longer covered by ice, induced sliding and genesis of pseudo-badlands morphology (Curry and Ballantyne 1999; Klimeš et al. 2016; Bollati et al. 2017).

The greater effects of the decrease in ice thickness after the surge-type event were recorded along the up-valley portion of the right lateral moraine (Mortara et al. 2023). Along the other moraines, the instability

is also still ongoing, which is matter of concern due to the tourist and alpinist trails along the moraines (Tamburini et al. 2019; Mortara et al. 2023). For instance, in the summer of 2023, the local authorities attempted to reconstruct the trail to Zamboni-Zappa hut through intense excavation on the moraine and regularization of the glacier surface of the right glacier lobe. The aim was to create a larger path also usable by excavators. However, this track underwent rapid degradation (within two months), especially on the unstable portion descending the inner flank of the left moraine of the right lobe and crossing the glacier.

Nearby the chairlift station, used by skiers in winter and mountaineers in summer, the right moraine of the left lobe, the object of interest for this study (see Fig. 1), has been affected by large fractures since 2019. This process is decreasing the trail stability along the moraine ridge, which is not walkable

anymore and has been moved to the external flank of the moraine. In addition, the Meteo Live VCO webcam, located at the lobe divide, undergoing destabilization, eventually fell in May 2024, as a consequence of heavy rains probably combined with snow melting (see Fig. 2). During the second half of July 2019, when the fracture was detected, Tamburini et al. (2019) calculated a glacier surface lowering of approximately 46 cm (4.6 cm/day). During the period between 2015 and 2020, the rate of ice volume loss was estimated to be 2.0–3.5 million m³/year (Ioli et al. 2021). The investigated moraine is located in sector S3, one of the three sectors identified by Ioli et al. (2023). This low relief sector is particularly stressed: the glacier splits in two different lobes, the authors detect a velocity of approximately 2–7 m/y, and the crevassed area up valley from the glacier division features a very high variability of surface velocity.



Fig. 2 Examples of trees in the unstable portion of the right moraine of the left lobe of the Belvedere Glacier (a), and a view of the sliding moraine from the opposite side of the glacier, as well as from the Meteo Live VCO webcam, lost in May 2024.

As the collapsing moraine is at a lower elevation than the tree line, it is colonized by coniferous and broadleaves species, as described in detail previously. Fig. 2a and 2b provide examples of trees along the sliding niche, which are investigated in this study as potential data loggers for tracking sliding movements. The aim is to detect the reliability of trees in understanding, with annual resolution, when the movement effectively began and whether it corresponded to the opening of the fracture in 2019. Fig. 2 shows the sliding moraine from the opposite side of the glacier (c) and the extensional trench visible from the Meteo Live VCO webcam, unfortunately now lost (d). The trench is also well visible in Figure 1 (c), and on the orthophoto from the Unmanned Aerial Vehicle (UAV) flights performed in August 2023 (Fig. 1b).

3. Material and methods

3.1 Geomorphological mapping and morphometric measurements

Mapping of geomorphological features was performed in detail nearby the sliding moraine, to survey the main geomorphic signs of the sliding. The mapping was included in the ongoing broader geomorphological mapping activity covering the entire Belvedere Glacier area. The landforms were classified according to their genetic processes (e.g., gravity, glacial) and particular attention was paid to morphodynamic conditions because of their potential relation to hazard scenarios (Bollati et al. 2024). In addition, landforms deriving from human activity were also mapped. The manmade elements, such as the remodeled surfaces, the chairlift infrastructure, and the old

tourist trail along the moraine ridge, leaving evident signs on the landscape, were also considered.

Morphometric measurements were performed to quantify the sliding and the retreat of the niche (Fig. 3). The tourist trail not involved in the sliding (T1), and the one that ran along the moraine ridge, and that was lost (T2), were useful for estimating the surface displacement. Two different features were measured to quantitatively assess the displacement using the orthophotos from 2018 (the last year before the appearance of the field evidence, AGEA orthophoto, average resolution 0.30 m) 2021 (AGEA orthophoto, average resolution 0.30 m), and 2023 (year of the drone survey in the area, 0.05 m):

- *Sliding of the moraine ridge* using two features:
 - i) tourist trail displacement calculated as the distance between the location of trail T2a on the 2018 orthophoto, T2b on the 2021 orthophoto, and T2c on the 2023 orthophoto (Fig. 3);
 - ii) difference between the distance between trail T1, which was not affected by instability (Fig. 3), and the tree canopy on the moraine ridge before (2018 orthophoto) and during the sliding (2021 and 2023 orthophotos). The linearity of elements used for measurement in the i-method provided more accurate data with an error related to the resolution of the image (variable between 0.05–0.3 m, i.e., orthophoto resolution). In the second case (ii-method), the measurements were based on tree canopies growing on the moraine ridge, and their detection on the orthophotos from 2018 and 2021 was quite challenging. A greater specimen or particular clusters of trees were considered, since they were more easily detectable on the images. Nevertheless, these measurements are considered not in an absolute sense but as a confirmation of the i-measurements.

- *Regression of the sliding niche*: calculated as the distance between the position of the sliding niche

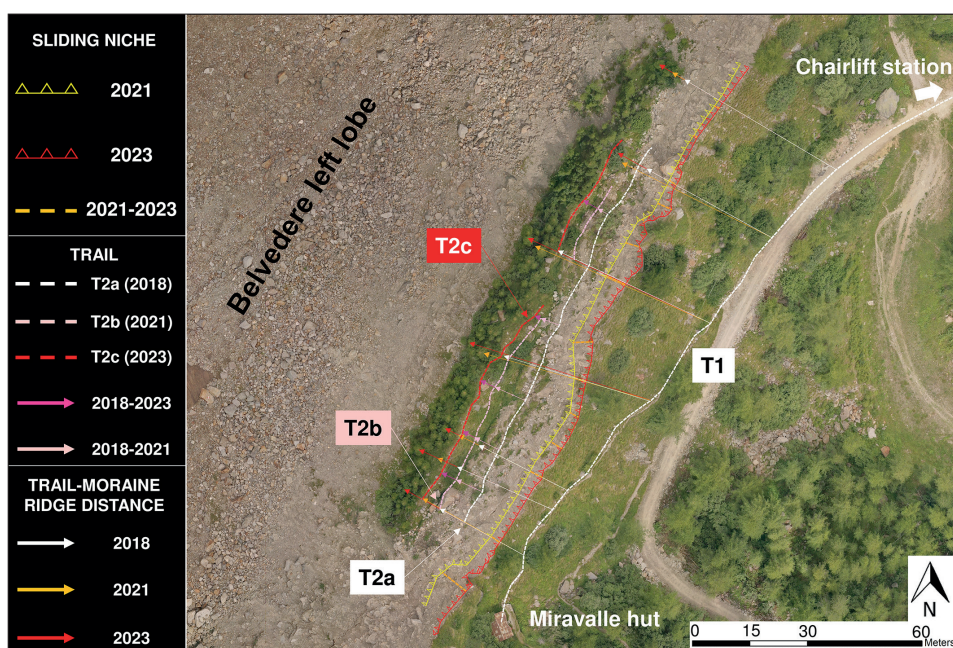


Fig. 3 Displacement measurements along the sliding moraine. The trail and the moraine ridge displacement are indicated (different colored arrows), as well as the regression of the sliding niche (orange dashed line) considering the orthophoto from 2018–2021 by AGEA; and 2023 resulting from the UAV flight performed in August 2023. The latter is also the background of the image.

on the 2021 orthophoto and the 2023 orthophoto (Fig. 3).

In addition to the displacement, average rates of sliding and retreat were calculated for the different time intervals. Two rates were calculated: one considering the year of the last orthophoto available before the sliding (2018), and another considering the year of ground fracture observation (2019) reported in the literature (Mortara et al. 2023).

3.2 Dendrogeomorphological analyses

Field sampling was performed in 2021 and 2022 (Fig. 4b, c) in order to collect samples from trees and exposed roots mostly stressed by the processes of sliding. Fig. 1 (b) shows the location of the sampled trees for dendrogeomorphological analyses. It should be noted that some tree positions taken with the GPS represent a cluster of trees due to GPS error (approximately 3 m).

Samples from tree trunks were taken using a Pressler increment borer. The cores extracted from the trunks were collected in most cases at the standard height of the trunk of 1.30 m (chest height), but because the sample locations were quite unstable, and in some cases very hard to access, the samples were sometimes taken nearby the base of the trunk, also to obtain the longest chronology as possible. Nevertheless, the aim of the analysis was not to date the germination of the trees or the surface stabilization and relative colonization by trees; hence, the minimum age of trees was only considered, and no corrections were made based on the sampling height. In total 19 trees growing along the lateral moraine (48 cores) in the newly formed trench, and 10 trees (20 cores) in an undisturbed area were sampled for a total of 68 cores analyzed. The tree chronologies and ring features of reference trees were compared with those of disturbed trees to detect the possible differences in relation to active geomorphic processes.

Moreover, disks were cut from the available six exposed roots (13 samples) from one of the trees (No. 6) located along the sliding niche, to determine when the effective exposure began. The changes in the tree root micromorphology, from the production of root-type wood to trunk-type wood, were used to detect the exposure year. Root exposure is also useful for estimating the average erosion rate over the exposure period. This may be calculated as the ratio between the thickness of the removed sediment and the time interval since the exposure (e.g., Hupp and Carey 1991 Pelfini and Santilli 2006; Stoffel et al. 2013; Bollati et al. 2016). A significant uncertainty may be introduced during this calculation (Bodouque et al. 2015), especially in complex contexts of an exposure of this type. Hence, in this specific case, we decided not to measure the erosion rate through the removed sediment thickness, but to focus on the different years of exposure obtained from roots,

comparing them with the calculated values through morphometric techniques using orthophotos (see Section 3.1).

After preparing the tree cores and root disks, the ring widths were measured (accuracy of 0.01 mm) using the LINTAB and TSAP systems (Rinn 1996) and image analysis using WinDENDRO software (Régent Instruments Inc. 2001). The cross dating of the dendrochronological series was performed visually with TSAP, considering the Gleichläufigkeit (GLK), the Cross Date Index (CDI) and the Generalized Level of Significance (GLS) coefficients, to establish the date of each individual annual ring. GLK (Eckstein and Bauch 1969) compares the similarity between two growth curves based on the concordance and discordance of curves' tendency, while GSL, depicts the significance of the GLK value, and CDI represents the synthesis of the similarity tests (GLK, GSL) conducted between the curves (Schmidt 1987). The detrending of the tree growth curves for the autocorrelation removal was performed with the Arstan software (Cook 1985), and after this phase, the cross-dating was checked again. The growth disturbances in the tree cores were finally analyzed (i.e., compression wood, growth anomalies, traumatic resin ducts). Since consideration of the percentage of trees affected by disturbance is influenced by the number of trees present in a specific year, according to the age of the trees, the time frame considered for the analysis began in 1997, i.e., when at least 50% of the trees were present.

The following disturbance indicators were selected for the analysis:

i) *Growth anomaly index* (e.g., Pelfini et al. 2007; Bollati et al. 2016): it is useful for analyzing abrupt growth changes (i.e., release and suppression) and it is based on the yearly percentage growth variation with respect to the mean of the four previous years. The growth anomaly index was calculated after detrending and autocorrelation removal. For the plotting, specific threshold values for growth suppression in trees (Negative Anomaly Index – NAI), potentially related to suffering, were then considered, with thresholds of 40% and 70% for negative anomalies (as adopted by Pelfini et al. 2007), while specific thresholds for positive growth anomalies were not distinguished. The NAIs were calculated for both disturbed and reference trees to determine which NAIs may be related to the local conditions of geomorphic disturbance or to a more general disturbance according to the considered species. In NAI investigation, it is important to consider in particular the climate effect. The growth of European larch above 1400 m a.s.l. is driven positively by high summer temperatures, warm autumn temperatures, and abundant July precipitation, also considering favorable microclimatic conditions (Saulnier et al. 2019). If the anomalies are common between trees in disturbed and reference clusters, the anomaly may be related to unfavorable climate conditions

or other regional impacts (e.g., insect attack; Vejputsková and Jaroslav 2006). The NAI, especially the positive values, were also considered for raw growth curves of roots since after exposure a growth release is usually found (Pelfini and Santilli 2006; Bollati et al. 2016). For the growth anomaly calculation, the analysis extends from 1997 to 2021, since 2022 was not in all the cases a complete ring.

ii) *Compression wood (CW)* (Timell 1986): it is a particular, denser kind of wood, being a response to mechanical stress. The space–time distribution of CW among the trees along the trench and sliding moraine ridge, and sliding niche, was assessed through the occurrence on the tree cores. Also, a compression-type wood may appear in roots after exposure (Pelfini and Santilli 2006). For the compression wood analysis, as opposed to the NAI analysis, which ended in 2021, the year 2022 was also considered, even if not completed,

as the CW could be visually detected and it may indicate the continuation of the disturbance.

iii) *Traumatic resin ducts (TRDs)* (e.g., Bollschweiler et al. 2008): these appear as a continuous row of resin ducts in earlywood or latewood, and they are considered indicators of the tree undergoing trauma. TRDs, often associated to scars, may show when the plant needs a greater support of resin, during very intense stress, and they may also appear in roots (Cruickshank et al. 2006). The disturbance may be caused by geomorphic events (e.g., debris flows or snow avalanches, Bollschweiler et al. 2008) but also by fires and insect attacks (Cruickshank et al. 2006).

The investigation of tree ring anomalies focused on finding a possible relation to the main glaciological events (surge-type event and moraine sliding) that occurred in the timeframe when the moraine tree and root chronologies overlap.

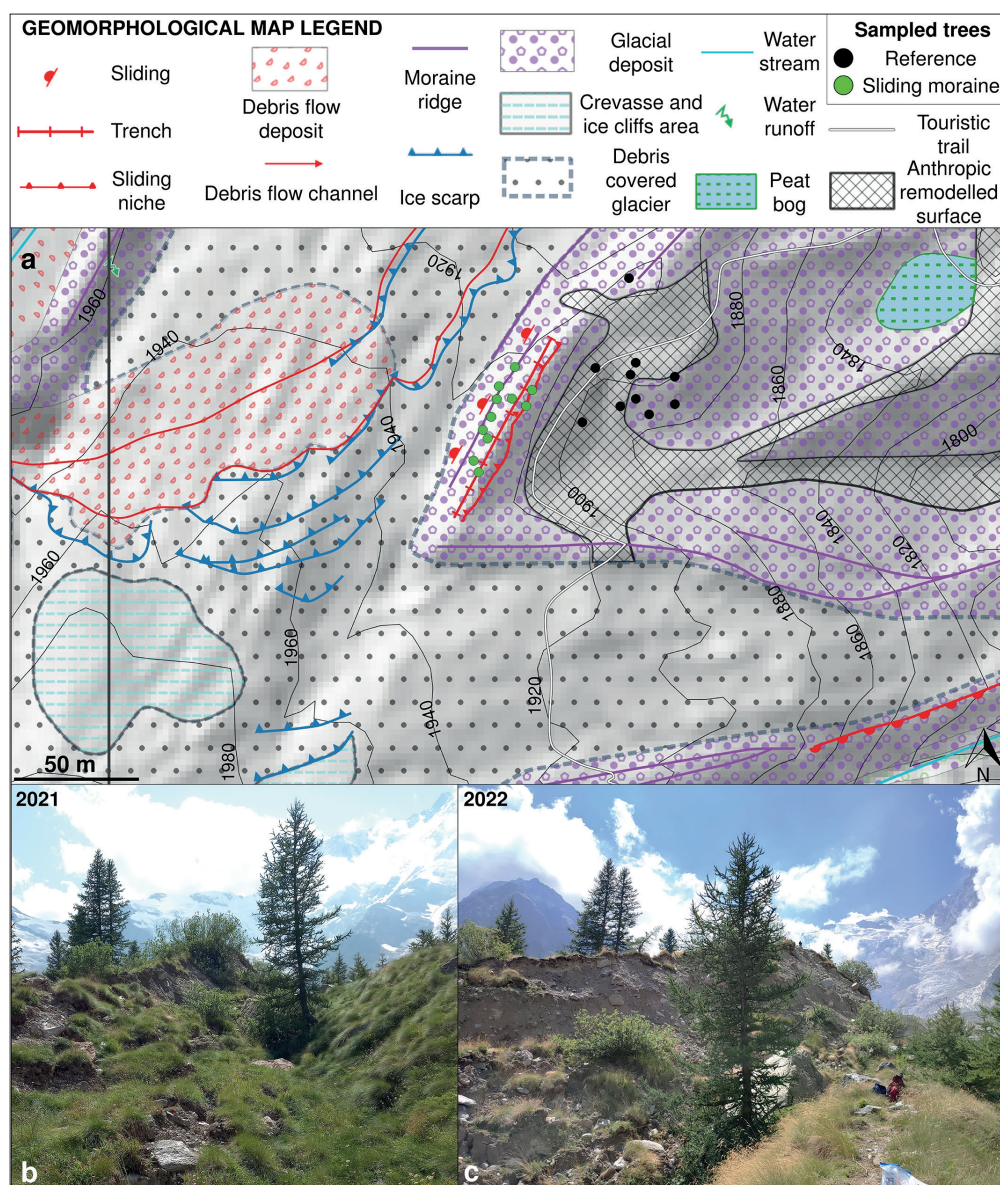


Fig. 4 Geomorphological map showing the location of the sampled trees on the right lateral moraine of the left lobe (a), and the trench in the timeframe 2021 (b) – 2022 (c).

4. Results and discussion

4.1 Geomorphological mapping and morphometric measurements

Fig. 4 (c) shows the geomorphological map with the sampled trees located in the area of the sliding moraine. The moraine ridge has moved towards the glacier debris-covered surface, favoring the opening of a trench. Moreover, the sliding niche is undergoing regressive erosion. The intensity of erosion is not homogeneous along the niche (Fig. 3). Tab. 2 shows the values measured for the time interval between 2018 and 2023 with the error estimated according to the orthophoto resolution. The considered timeframe begins one year before the fracture opening during the field survey in 2019 (2018, available orthophoto) reported in the literature (Mortara et al. 2023).

The average displacement rates related to the sliding of the moraine are comparable, within the error related to orthophoto resolution, both using the trail displacement (1.98 m/y, since 2018, or 2.47 m/y, since 2019; Tab. 2) and the tree canopies growing along the sliding moraine ridge (1.87 m/y, since 2018, or 2.34 m/y; Tab. 2). The average values for the time interval between 2021 and 2023 (1.78 m/y for the trail; 1.96 m/y for the moraine ridge; Tab. 1) are also comparable, within the error related to orthophoto resolution, with the sliding niche retreat rate in the same period (1.70 m/y; Tab. 1). During the analyzed time interval comparing the available orthophotos (2018–2023) the rates are quite constant. However, if we consider the year in which ground fracturing was surveyed on the field (i.e. 2019) for the rate calculation, a slowing-down of the sliding from the period between 2019 and 2021 (3.17 m/y for the trail; 2.72 m/y for

Tab. 2 Values of displacement and the related rates affecting the moraine sliding area. The (*) rates are calculated considering the year of displacement (2019) in relation to ground evidence (Mortara et al. 2023).

Process	Indicator	2018–2021 (m) (± 0.3 m)	2021–2023 (m) (± 0.3 m)	2018–2023 (m) (± 0.3 m)
Sliding	Trail displacement	2.96	4.27	7.22
		5.18	1.66	6.84
		8.68	4.17	12.85
		7.36	3.44	10.79
		7.52	4.22	11.74
	Average	6.34	3.55	9.89
	Rate	2.11 (3.17*)	1.78	1.98 (2.47*)
	Moraine ridge displacement	5.24	5.3	10.54
		5.60	5.32	10.92
		5.88	3.92	9.8
5.17		4.35	9.52	
5.96		2.52	8.47	
6.48		2.11	8.58	
Average	5.43	3.92	9.35	
Rate	1.81 (2.72*)	1.96	1.87 (2.34*)	
Regressive erosion	Sliding niche displacement		5.41	
			5.25	
			2.55	
			3.46	
			3.5	
			2.75	
			7.92	
			2.97	
			3.83	
			1.04	
			4.03	
			2.26	
			1.05	
		1.51		
Average		3.40		
Rate		1.70		

the moraine ridge) to the period between 2021 and 2023 (1.78 m/y for the trail; 1.96 m/y for the moraine ridge) may be hypothesized. These data are discussed in relation to the tree and, especially, root information.

4.2 Dendrogeomorphological analyses

Tree cores

Fig. 5 shows the hillshade built from the 2023 DSM (Digital Surface Model), which highlights the presence of the trench. In the background, the minimum age of sampled trees is plotted. The oldest trees were present at least from the middle of the 1970s. These data agree with the orthophotos reconstruction (Fig. 6) where the trees were absent in 1951 and began to appear in 1989, when three trees had already germinated (Nos. 1, 5, and 6). In the 1990s, seven additional trees were present at least (Nos. 2, 14–19), while other nine tree ages indicated their presence from the 2000s (Nos. 3, 4, 7–9, 10, 12, and 13). The youngest are trees No. 8 and 11, less than 20 years old. The distribution of age is hence quite random in the moraine area, despite the fact that oldest trees (Nos. 1, 5, and 6) are located along the current erosion scarp.

Supplementary File A includes the evolution of the area through orthophotos since 1951, with the current position of trees plotted, and specific symbols to show their germination through time (i.e., minimum age).

The analysis of tree ring width anomalies (NAI) and of the CW in tree cores is summarized in Fig. 6,

where the percentage of trees affected by NAI (for reference chronology and sliding moraine trees) and compression wood (only for the sliding moraine) are depicted, also indicating the number of trees growing in each year on the moraine area. The figure shows the timing of the most important glacial events interfering with the moraine, i.e., the surge-type event (the wider timeframe in which evidence is indicated in the literature; 1999–2003; Kääb et al. 2004) and the sliding (considering the field evidence from 2019; Mortara et al. 2023). In the first case, the moraine trees show a more intense NAI compared to the reference chronology, not so much during the event itself, but immediately after, in the years between 2003 and 2004 (30% of the trees with NAI < -40%). Even if two years of disturbance may be few to be considered a reliable response to a disturbing event, potentially this anomaly may be put in relation to the ground destabilization following the glacier downwasting. Indeed, the surge may have potentially affected the trees both during the event by the push provoked by the glacier overwhelming the moraine, or after the event, under debutting conditions. The reference chronology, on the other side, shows a more intense NAI only in 2004 (approximately 55% of the trees with NAI < -40%). Anyway, the less intense NAI in 2004 in the sliding moraine trees may be related to the NAI calculation itself, which considered the average of the previous four years. Since the NAI began in 2003, the disturbance may have been smoothed.

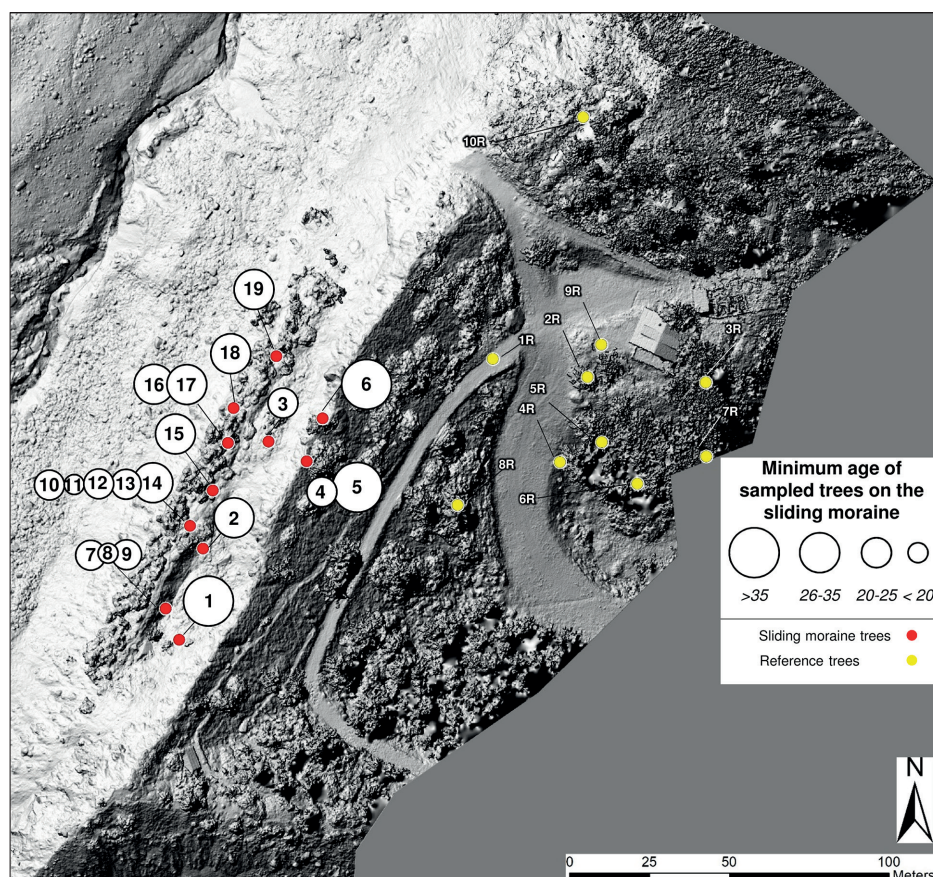


Fig. 5 Distribution of the minimum ages of sampled trees plotted on the 2023 Hillshade – Digital Surface Model from the UAV flight performed in August 2023 (resolution 0.05 m) (Brodský et al. 2024, in this issue), showing the trench in the sliding moraine.

Considering the meteorological conditions 2004 was not an extreme year neither in terms of temperature, nor drought conditions, hence they could not be considered as a potential influencer on tree ring growth. Later on, at the beginning of the sliding in 2019, the NAI does not prove to be a discriminant indicator between the reference chronology and sliding trees.

Concerning CW, the temporal distribution in relation to the number of trees is reported in Figure 6, and the spatio-temporal distribution of the compression wood for the timeframe 1997–2022 is presented in Supplementary File B. Compression wood is clearly present in the moraine tree rings since 2001, slightly after the beginning of the surge-type event. The increase during and after the surge is evident, and in some years particularly intensifying, probably due to the general relaxation of the inner flank of the moraine parallel to the glacier downwasting. Other information retrieved is the absence of specific spatial sub-clusters of trees featured by CW at different moments or with different intensities. Considering the sliding period from 2018 to 2019, different behavior may be expected between the trees on the niche, above the erosion scarp, and those located on the landslide body, as detected in other cases (e.g.,

Bollati et al. 2016). In this case, no significant distinction occurs, as the disturbance is distributed in the area quite homogeneously. Concerning climate and its direct relation with the sliding, and hence its indirect relation with tree growth, heavy and/or prolonged rains, as well as snow melting during very snowy years, may trigger sliding and water-runoff (Manconi and Giordan 2015). The CW peak recorded in 2009 may be related to the greater quantity of snow available until the late spring of 2009 and the intense related snow melting, destabilizing the moraine. The moraine flank relaxation finally evolved in 2019 in the form of ground fracturing and sliding (Mortara et al. 2023). In 2018, in particular, a slight peak is visible one year before the ground fracturing (Fig. 7; Supplementary File B). It is worth considering that some of the trees have maintained a relatively stable position, moving together with the moraine. This may have caused the apparent decrease in CW during the last period, with the trees being in a new and relative stable position during the sliding. As a final observation, no significant occurrences of TRDs were found in the tree cores, indicating that during the surge period, the glacier probably did not mechanically impact the trees on this moraine as occurred on other moraines (Mortara and Tamburini 2009).

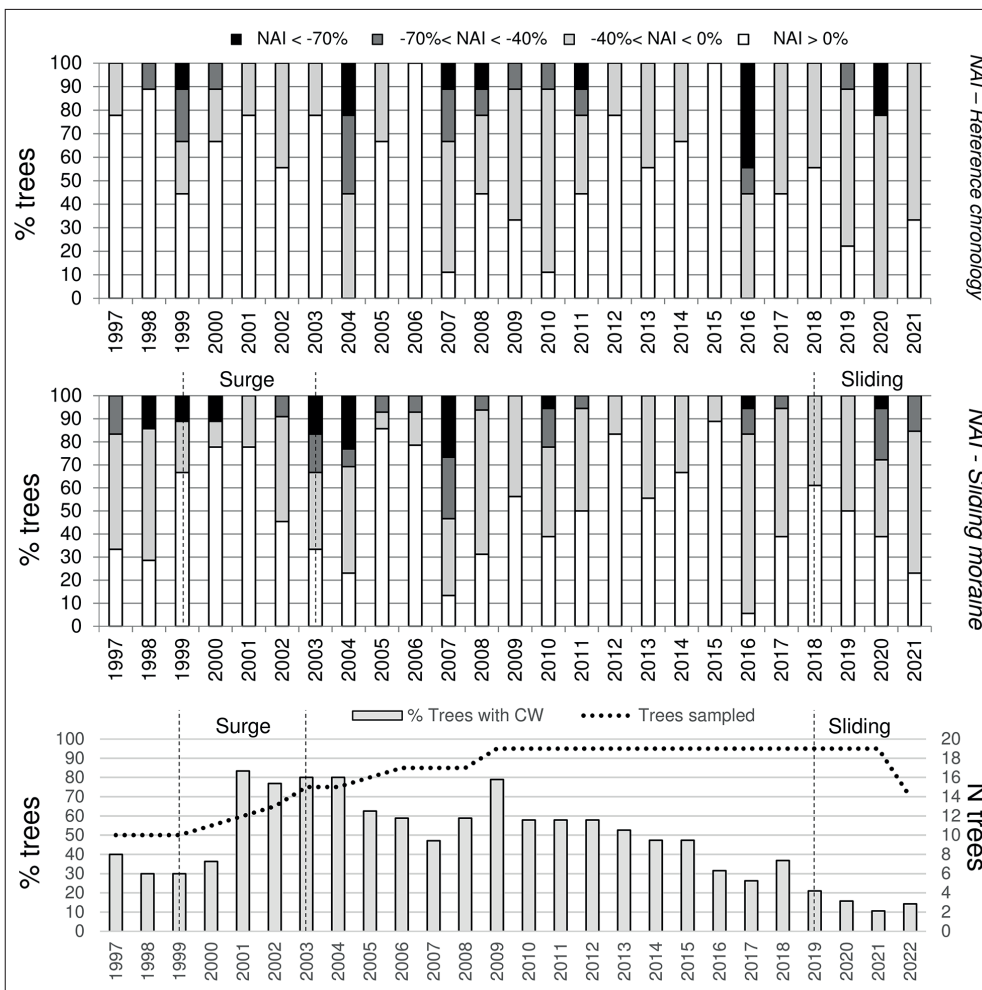


Fig. 6 Negative anomaly index (NAI) for the reference (first graph) and sliding (second graph) tree chronologies, and compression wood for sliding trees (third graph). The data are plotted since 1997, when at least 50% of the trees were present.

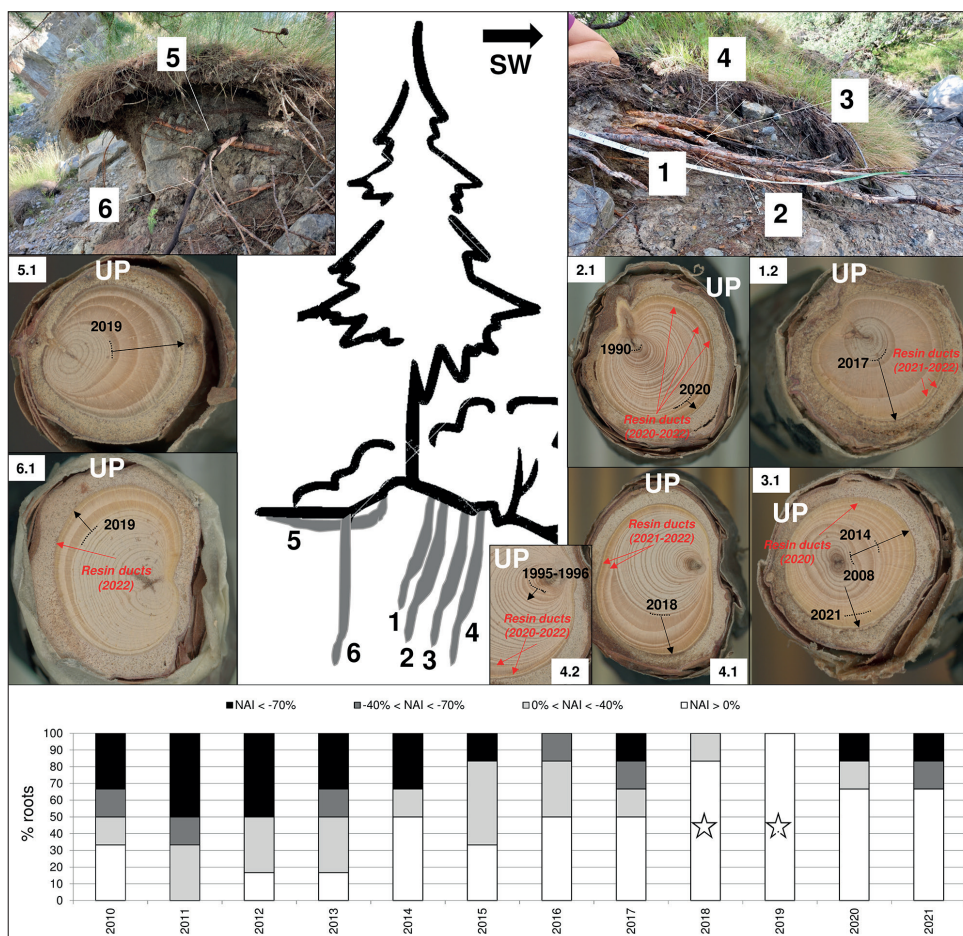


Fig. 7 Tree No. 6 and its sampled roots (1 to 6). Disks from some of the root samples indicating the main features (exposure year, traumatic resin ducts) as identified under the microscope. The graph below plots the NAI resulting for the timeframe between 2010 and 2021 with the white stars indicating the growth release in relation to the moraine sliding.

Root exposure

Along the detachment niche, despite some trees still being located in precarious positions, only one tree (No. 6 in fig. 5) showed roots suitable for sampling.

The main aim of the analysis was to detect the exposure year. Fig. 7 shows the root sections together with their position in the sampling field of tree No. 6.

The roots are concordant in showing an abrupt release in ring width in these last seven years, also testified by the NAI (white stars). Despite the field evidence of trenching along the moraine in 2019, one root shows an abrupt release in 2017 (root No. 1.2, Fig. 7), with the majority of roots showing an evident growth release in the period between 2018 and 2019 (e.g., Nos. 1 and 4), with a total positive growth anomaly (100% of the roots) in 2019, continuing, even if less intensely, to-date. This may be put in relation also with the peak of compression wood in the trunk cores in 2018 (Fig. 6). In two cases (root Nos. 2, and 4), a small peak in the 1990s was also identified, and in one of them (root No. 2) also in the second half of the 2000s, with an evident peak in 2009. As mentioned before 2009 was a year with an intense snow melting, potentially favoring local superficial denudation. Finally, very clear TRDs in the period between 2020 and 2021 in almost all the roots testify to disturbance.

4.3 Integration of geomorphic feature survey, morphometric measurements, and dendrogeomorphological data

According to De Gaetani et al. (2021), the period when the downwasting occurred in the glacier snout area, including the investigated moraine, is between 2009 and 2019. Nevertheless, the trees (trunk and roots) indicate instability conditions that, even if with different degree of intensity and spatio-temporal distribution, are uninterrupted since the surge-type event (2000–2002) to-date. Considering the dendrogeomorphological data of the roots and trunk cores, and the year 2018 as the first year with dendrogeomorphological signs of ground destabilization along the moraine, the average displacement rates of the trail calculated through morphometric techniques for the time interval between 2018 and 2023 seem to be the most realistic: 1.87–1.98 m/y (Tab. 2).

This would exclude the hypothesized slow-down of rates beginning in 2019 and previously discussed in Section 4.1. In this case, the temporal trend using 2018 for the trail (2.11 m/y to 1.78 m/y; Tab. 2), and for the moraine ridge (1.81 m/y to 1.96 m/y; Tab. 2) is discordant. Unfortunately, due to the continuous vegetation coverage and the unfavorable shadows, the orthophoto from 2018 could not be used to confirm these data.

The results from the tree analyses, field surveys, and morphometric measurements, if combined, may provide a more reliable time constraint, and consequently, movement rates to geomorphic processes. The limitation of remote sensing may be the time interval between the release of orthophoto or satellite images and their resolution, the presence of vegetation coverage or illumination and shadows, masking the geomorphic evidence (e.g., ground fracturing), while trees provide a yearly/seasonal time resolution. The remote sensing limitation, has recently been solved by the widespread use of UAV technology, allowing for very high-resolution acquisitions on demand within very short time intervals according to the type of events affecting an area, with the most adequate light conditions. The limitation of field surveys may be related to underground conditions that may not always produce sudden morphological effects at the topographic surface, but they may do earlier on trees and root systems. In this case, trees may reveal something already occurring below the surface (the roots are in the ground), while surface effects are not yet visible. However, in this specific case, the limit of dendrogeomorphology rely in the not-always clear signal in terms of NAI and CW, and, mainly, in the number of trees available for coring (trunks and roots). Concerning roots, specifically, since the data come in this case from only one tree specimen, the data obtained through the root exposure, even if very useful at punctual scale, could not be considered representative of the erosive regression along the whole detachment niche, as testified by the different values obtained along it from the morphometric measurements (Tab. 2).

5. Concluding remarks

Since a portion of the Belvedere Glacier is located below the tree line, it serves as a compelling study case for investigating glacier dynamics through a multidisciplinary approach, including morphometry, geomorphological survey and mapping, and dendrogeomorphological analyses. Besides the debris coverage providing a form of ecologic support role towards organisms, as highlighted in the literature, the glacial dynamic affects the vegetation growing on glacial depositional landforms such as the lateral moraine. This study has enabled the detection of signals in tree rings (growth anomalies, compression wood) and root rings (growth release and traumatic resin ducts), even if it was not always easy to disentangle. Nevertheless, information about the timing of glacial and geomorphological events affecting the right moraine of the left lobe of the glacier has been retrieved and discussed. The oldest trees were present at least from the middle of the 1970s, and, considering the surge-type event, they record the peak of disturbance in terms of NAI in the period between 2003 and 2004, slightly

after the acme of the surge-type event. Compression wood indicates disturbance since 2001, slightly after the beginning of the surge-type event, and prosecuting also in the following years, even if diminishing. The trench opening in the ground, surveyed in the literature in 2019, is preceded by a slight peak in compression wood already present in 2018. These data are also confirmed by the roots that show in one case an abrupt release in 2017, with the majority of growth release in the period between 2018 and 2019, continuing, even if less intensely, to-date. Moreover, roots show in these last years a disturbance in the form of very evident TRDs. Finally, the average displacement rates along the moraine calculated for the time interval between 2018 and 2023 are 1.87–1.98 m/y, while the regression rate of the sliding niche was also calculated to be 1.70 m/y (2021–2023).

To conclude, considering the limits of all the techniques applied, the integration of different techniques and a multidisciplinary approach are essential for delineating the dynamic features of a complex geomorphological and glaciological context like the Belvedere Glacier environment. Discussing these dynamics is relevant not only for the glacier site but it may provide information for managing hazard scenarios also affecting downvalley areas.

Acknowledgements

The project was funded in the aim of the 4EU+ European University Alliance, with the Mini grants afforded to Charles University in Prague (*Multidisciplinary approaches to assess the evolution of glacial and periglacial areas in the Alps under climate change conditions; Remote Sensing of the Cryosphere Dynamics under the Influence of Climate Change: a 4EU+ Project to investigate the evolving glacial environment*), grant number 4EU+/23/F4/19. The work was also partly supported by the Italian Ministry for Universities and Research (MUR) through the projects “Dipartimenti di Eccellenza 2018–22” (*Le Geoscienze per la società: risorse e loro evoluzione*) and “Dipartimenti di Eccellenza 2023–27” and (*Le Georisorse per la transizione ecologica e lo sviluppo territoriale*) and through the PRIN (Progetto di Ricerca di Rilevante Interesse Nazionale) (GEOTRes – Geoheritage threatening and resilience: mapping the impact of geomorphic and human processes in sensitive morphoclimatic environments); by University of Milan through the Sostegno alla ricerca Project 2021 (*Indicatori geomorfologici e geopedologici per ricostruire l'evoluzione delle aree di recente deglaciazione*; grant number PSR2021_RAZZONI) and 2022 (*Evoluzione dei processi geomorfologici e degli impatti sul ciclo idrologico in contesti sensibili al cambiamento climatico*; grant number PSR2022_RAZZONI). The Authors would like to thank the Province of Verbano-Cusio-Ossola for the permit of UAV and dendrogeomorphological surveys

(dr. Andrea De Zordi, Settore III – Assetto del Territorio Georisorse e Tutela Faunistica, Servizio Rete Natura 2000 e Forestazione).

References

- Azzoni, R. S., Franzetti, A., Fontaneto, D., Zullini, A., Ambrosini, R. (2015): Nematodes and rotifers on two Alpine debris-covered glaciers. *Italian Journal of Zoology* 82(4), 616–623, <https://doi.org/10.1080/11250003.2015.1080312>.
- Azzoni, R. S., Pelfini, M., Zerboni, A. (2023): Estimating the evolution of a Post-Little Ice Age deglaciated Alpine Valley through the DEM of Difference (DoD). *Remote Sensing* 15(12), 3190, <https://doi.org/10.3390/rs15123190>.
- Ballantyne, C. K. (2002): Paraglacial geomorphology. *Quaternary Science Reviews* 21(18–19), 1935–2017, [https://doi.org/10.1016/S0277-3791\(02\)00005-7](https://doi.org/10.1016/S0277-3791(02)00005-7).
- Benn, D. I., Bolch, T., Hands, K., Gulley, J., Luckman, A., Nicholson, L. I., Quincey D., Thompson T., Toumi R., Wiseman, S. (2012): Response of debris-covered glaciers in the Mount Everest region to recent warming, and implications for outburst flood hazards. *Earth-Science Reviews* 114(1–2), 156–174, <https://doi.org/10.1016/j.earscirev.2012.03.008>.
- Bodoque, J. M., Ballesteros-Cánovas, J. A., Lucía, A., Díez-Herrero, A., Martín-Duque, J. F. (2015): Source of error and uncertainty in sheet erosion rates estimated from dendrogeomorphology. *Earth Surface Processes and Landforms* 40, 1146–1157, <https://doi.org/10.1002/esp.3701>.
- Bodoque, J. M., Ballesteros-Cánovas, J. A., Lucía, A., Díez-Herrero, A., Martín-Duque, J. F. (2015): Source of error and uncertainty in sheet erosion rates estimated from dendrogeomorphology. *Earth Surface Processes and Landforms* 40(9), 1146–1157, <https://doi.org/10.1002/esp.3701>.
- Bollati, I., Leonelli, G., Vezzola, L., Pelfini, M. (2015): The role of Ecological Value in Geomorphosite assessment for the Debris-Covered Miage Glacier (Western Italian Alps) based on a review of 2.5 centuries of scientific study. *Geoheritage* 7, 119–135, <https://doi.org/10.1007/s12371-014-0111-2>.
- Bollati, I. M., Pellegrini, M., Reynard, E., Pelfini, M. (2017): Water driven processes and landforms evolution rates in mountain geomorphosites: examples from Swiss Alps. *Catena* 158, 321–339, <https://doi.org/10.1016/j.catena.2017.07.013>.
- Bollati, I. M., Crosa Lenz, B., Golzio, A., Masseroli, A. (2018): Tree rings as ecological indicator of geomorphic activity in geoheritage studies. *Ecological indicators* 93, 899–916, <https://doi.org/10.1016/j.ecolind.2018.05.053>.
- Bollati, I. M., Masseroli, A., Mortara, G., Pelfini, M., Trombino, L. (2019): Alpine gullies system evolution: erosion drivers and control factors. Two examples from the western Italian Alps. *Geomorphology* 327, 248–263, <https://doi.org/10.1016/j.geomorph.2018.10.025>.
- Bollati, I. M., Viani, C., Masseroli, A., Mortara, G., Testa, B., Tronti, G., Pelfini M., Reynard, E. (2023): Geodiversity of proglacial areas and implications for geosystem services: A review. *Geomorphology* 421, 108517, <https://doi.org/10.1016/j.geomorph.2022.108517>.
- Bollati, I. M., Cavalli, M., Masseroli, A., Viani, C., Moraschina, F., Pelfini, M. (2024): Thematic mapping for sediment cascade analysis in small mountain catchments – The case of the Buscagna valley (Lepontine Alps). *Geomorphology* 446, 109001, <https://doi.org/10.1016/j.geomorph.2023.109001>.
- Bollschweiler, M., Stoffel, M., Schneuwly, D. M., Bourqui, K. (2008): Traumatic resin ducts in *Larix decidua* stems impacted by debris flows. *Tree physiology* 28(2), 255–263, <https://doi.org/10.1093/treephys/28.2.255>.
- Caccianiga, M., Andreis, C., Diolaiuti, G., D’Agata, C., Mihalcea, C., Smiraglia, C. (2011): Alpine debris-covered glaciers as a habitat for plant life. *The Holocene* 21(6), 1011–1020, <https://doi.org/10.1177/0959683611400219>.
- Chiarle, M., Iannotti, S., Mortara, G., Deline, P. (2007): Recent debris flow occurrences associated with glaciers in the Alps. *Global and Planetary Change* 56(1–2), 123–136, <https://doi.org/10.1016/j.gloplacha.2006.07.003>.
- Church, M., Ryder, J. M. (1972): Paraglacial sedimentation: a consideration of fluvial processes conditioned by glaciation. *Geological Society of America Bulletin* 83(10), 3059–3072, [https://doi.org/10.1130/0016-7606\(1972\)83\[3059:PSACOF\]2.0.CO;2](https://doi.org/10.1130/0016-7606(1972)83[3059:PSACOF]2.0.CO;2).
- Cook, E. R. (1985): A time series approach to tree-ring standardization. PhD thesis, University of Arizona.
- Cruickshank, M. G., Lejour, D., Morrison, D. J. (2006): Traumatic resin canals as markers of infection events in Douglas-fir roots infected with *Armillaria* root disease. *Forest Pathology* 36(5), 372–384, <https://doi.org/10.1111/j.1439-0329.2006.00469.x>.
- Curry, A. M., Ballantyne, C. K. (1999): Paraglacial modification of glacial sediment. *Geografiska Annaler, Series A: Physical Geography* 81(3), 409–419, <https://doi.org/10.1111/j.0435-3676.1999.00070.x>.
- De Bouchard d’Aubeterre, G., Favillier, A., Mainieri, R., Saez, J. L., Eckert, N., Saulnier, M., Peiry, J. L., Stoffel, M., Corona, C. (2019): Tree-ring reconstruction of snow avalanche activity: Does avalanche path selection matter? *Science of the Total Environment* 684, 496–508, <https://doi.org/10.1016/j.scitotenv.2019.05.194>.
- De Gaetani, C. I., Ioli, F., Pinto, L. (2021): Aerial and UAV Images for Photogrammetric Analysis of Belvedere Glacier Evolution in the Period 1977–2019. *Remote Sensing* 13(18), 3787, <https://doi.org/10.3390/rs13183787>.
- Diolaiuti, G., D’Agata, C., Smiraglia, C. (2003): Belvedere Glacier, Monte Rosa, Italian Alps: Tongue Thickness and Volume Variations in the Second Half of the 20th Century. *Arctic Antarctic Alpine Research* 35, 255–263, [https://doi.org/10.1657/1523-0430\(2003\)035\[0255:BGMRIA\]2.0.CO;2](https://doi.org/10.1657/1523-0430(2003)035[0255:BGMRIA]2.0.CO;2).
- Eckstein, D., Bauch, J. (1986): Beitrag zur Rationalisierung eines dendrochronologischen Verfahrens und zur Analyse seiner Aussagesicherheit. *Forstwiss. Centralblatt* 88, 230–250, <https://doi.org/10.1007/BF02741777>.
- Fantucci, R. (1997): La dendrogeomorfologia nello studio della dinamica dei versanti: alcune recenti applicazioni in Italia. *Geologia tecnica e ambientale* 2/97, 21–31.
- Favillier, A., Guillet, S., Lopez-Saez, J., Giacona, F., Eckert, N., Zenhäusern, G., Peiry, J. L., Stoffel, M., Corona, C. (2023): Identifying and interpreting regional signals in tree-ring based reconstructions of snow avalanche activity in the Goms valley (Swiss Alps). *Quaternary Science Reviews*

- 307: 108063, <https://doi.org/10.1016/j.quascirev.2023.108063>.
- Fyffe, C. L., Reid, T. D., Brock, B. W., Kirkbride, M. P., Diolaiuti, G., Smiraglia, C., Diotri, F. (2014): A distributed energy-balance melt model of an alpine debris-covered glacier. *Journal of Glaciology* 60(221), 587–602, <https://doi.org/10.3189/2014JG13148>.
- Garavaglia, V., Pelfini, M., Bini, A., Arzuffi, L., Bozzoni, M. (2009): Recent evolution of debris-flow fans in the Central Swiss Alps and associated risk assessment: two examples in Roseg Valley. *Physical Geography* 30(2), 105–129, <https://doi.org/10.2747/0272-3646.30.2.105>.
- Garavaglia, V., Pelfini, M., Motta, E. (2010): Glacier stream activity in the proglacial area of an Italian debris-covered glacier: an application of dendroglaciology. *Geografia Fisica e Dinamica Quaternaria* 33(1), 2010, 15–24.
- Garavaglia, V., Pelfini, M. (2011): The role of border areas for dendrochronological investigations on catastrophic snow avalanches: a case study from the Italian Alps. *Catena* 87(2), 209–215, <https://doi.org/10.1016/j.catena.2011.06.006>.
- Giordan, D., Lanteri, L., Fioraso, G., Bormioli, D., Luino, F., Turconi, L., Chiarle, M., Mortara, G., Tamburini, A. (2022): Itinerario 2.3. Frane in alta quota: il Ghiacciaio del Belvedere e la parete Est del Monte Rosa. In: Calcaterra, D., Cencetti, C., Meisina, C., Revellino, P., Frane d'Italia. Associazione Italiana Geologia Applicata Ambientale. Luciano Ed., pp. 81–84.
- Gray, M., Gordon, J. E., Brown, E. J. (2013): Geodiversity and the ecosystem approach: the contribution of geoscience in delivering integrated environmental management. *Proceedings of the Geologists' Association* 124(4), 659–673, <https://doi.org/10.1016/j.pgeola.2013.01.003>.
- Guida, D., Pelfini, M., Santilli, M. (2008): Geomorphological and dendrochronological analyses of a complex landslide in the Southern Apennines. *Geografiska Annaler: Series A, Physical Geography* 90(3), 211–226, <https://doi.org/10.1111/j.1468-0459.2008.340.x>.
- Haeblerli, W., Kääb, A., Paul, F., Chiarle, M., Mortara, G., Mazza, A., Deline, P., Richardson, S. (2002). A surge-type movement at Ghiacciaio del Belvedere and a developing slope instability in the east face of Monte Rosa, Macugnaga, Italian Alps. *Norsk Geografisk Tidsskrift – Norwegian Journal of Geography* 56(2), 104–111, <https://doi.org/10.1080/002919502760056422>.
- Hupp, C., Carey, W. P. (1990): Dendrogeomorphic approach to estimating slope retreat. *Geology* 18, 658–661, [https://doi.org/10.1130/0091-7613\(1990\)018%3C0658:DATESR%3E2.3.CO;2](https://doi.org/10.1130/0091-7613(1990)018%3C0658:DATESR%3E2.3.CO;2).
- Ioli, F., Bianchi, A., Cina, A., De Michele, C., Maschio, P., Passoni, D., Pinto, L. (2021): Mid-term monitoring of glacier's variations with UAVs: The example of the Belvedere Glacier. *Remote Sensing* 14(1), 28, <https://doi.org/10.3390/rs14010028>.
- Ioli, F., Bruno, E., Calzolari, D., Galbiati, M., Mannocchi, A., Manzoni, P., Martini, M., Bianchi, A., Cina, A., De Michele, C., Pinto, L. (2023): A replicable open-source multi-camera system for low-cost 4D glacier monitoring. *International Archives of the Photogrammetry, Remote Sensing and Spatial Information Sciences (ISPRS Archives)*, XLVIII-M-1-2023, 137–144, <https://doi.org/10.5194/isprs-archives-XLVIII-M-1-2023-137-2023>.
- Ivy-Ochs, S., Kerschner, H., Maisch, M., Christl, M., Kubik, P. W., Schlüchter, C. (2009): Latest Pleistocene and Holocene glacier variations in the European Alps. *Quaternary Science Reviews* 28(21–22), 2137–2149, <https://doi.org/10.1016/j.quascirev.2009.03.009>.
- Kääb, A., Huggel, C., Barbero, S., Chiarle, M., Cordola, M., Epifani, F., Haebelri, W., Mortara, G., Semino, P., Tamburini, A., Viazzo, G. (2004) Glacier hazards at Belvedere Glacier and the Monte Rosa East Face, Italian Alps: processes and mitigation. *INTERPRAEVENT 2004–RIVA/TRIENT*, pp. 67–78.
- Kääb, A., Huggel, C., Fischer, L., Guex, S., Paul, F., Roer, I., Salzmann, N., Schläfli, S., Schmutz, K., Schneider, D., Strozzi, T., Weidmann, Y. (2005): Remote sensing of glacier-and permafrost-related hazards in high mountains: An overview. *Natural Hazard Earth Systems* 5, 527–554, <https://doi.org/10.5194/nhess-5-527-2005>.
- Klimeš, J., Novotný, J., Novotná, I., Jordán de Urries, B., Vilímek, V., Emmer, A., Strozzi, T., Kusák, M., Rapre, A. C., Hartvich, F., Frey, H. (2016): Landslides in moraines as triggers of glacial lake outburst floods: example from Palcacocha Lake (Cordillera Blanca, Peru). *Landslides* 13(6), 1461–1477, <https://doi.org/10.1007/s10346-016-0724-4>.
- Leonelli, G., Pelfini, M., Cherubini, P. (2008): Exploring the potential of tree-ring chronologies from the Trafoi Valley (Central Italian Alps) to reconstruct glacier mass balance. *Boreas* 37, 169–198, <https://doi.org/10.1111/j.1502-3885.2007.00010.x>.
- Leonelli, G., Pelfini, M. (2013): Past surface instability of Miage debris-covered glacier tongue (Mont Blanc Massif, Italy): a decadal-scale tree-ring-based reconstruction. *Boreas* 42, 613–622, <https://doi.org/10.1111/j.1502-3885.2012.00291.x>.
- Leonelli, G., Coppola, A., Baroni, C., Salvatore, M. C., Maugeri, M., Brunetti, M., Pelfini, M. (2016): Multispecies dendroclimatic reconstructions of summer temperature in the European Alps enhanced by trees highly sensitive to temperature. *Climatic Change* 137, 275–291, <https://doi.org/10.1007/s10584-016-1658-5>.
- Manconi, A., Giordan, D. (2015): Landslide early warning based on failure forecast models: the example of the Mt. de La Saxe rockslide, northern Italy, *Natural Hazards and Earth System Science* 15(7), 1639–1644, <https://doi.org/10.5194/nhess-15-1639-2015>.
- Mazza, A. (1998): Evolution and dynamics of Ghiacciaio Nord delle Locce (Valle Anzasca, Western Alps) from 1854 to the present. *Geografia Fisica e Dinamica Quaternaria* 21, 233–243.
- Mazza, A. (2003): The kinematics wave theory: a possible application to “Ghiacciaio del Belvedere” (Valle Anzasca, Italian Alps). Preliminary hypothesis. *Terra glacialis* 6, 23–36.
- Mehta, M., Kumar, V., Kunmar, P., Sain, K. (2023): Response of the Thick and Thin Debris-Covered Glaciers between 1971 and 2019 in Ladakh Himalaya, India – A Case Study from Pensilungpa and Durung-Drung Glaciers. *Sustainability* 15(5): 4267, <https://doi.org/10.3390/su15054267>.
- Monterin, U. (1923): Il Ghiacciaio di Macugnaga dal 1870 al 1922. *Bollettino del Comitato Glaciologico Italiano* 5, 12–40.
- Mortara, G., Chiarle, M., Tamburini, A., Mercalli, L., Cat Berro, D. (2023): a vent'anni dal Lago Effimero (Ghiacciaio del Belvedere, Monte Rosa): eredità di un evento emblematico per le Alpi. *Nimbus* 90, 26–41.

- Mortara, G., Carton, A., Chiarle, M., Tamburini, A. (2017). Ai piedi della parete più alta delle Alpi. In: Società Geologica Italiana, Itinerari glaciologici nella Alpi Italiane – Il ghiacciaio del Belvedere al Monte Rosa. Guide Geologiche Regionali 12 193–214.
- Mourey, J., Ravanel, L., Lambiel, C. (2022): Climate change related processes affecting mountaineering itineraries, mapping and application to the Valais Alps (Switzerland). *Geografiska Annaler: Series A, Physical Geography* 104(2), 109–126, <https://doi.org/10.1080/04353676.2022.2064651>.
- Nakawo, M., Yabuki, H., Sakai, A. (1999): Characteristics of Khumbu Glacier, Nepal Himalaya: recent change in the debris-covered area. *Annals of Glaciology* 28, 118–122, <https://doi.org/10.3189/172756499781821788>.
- Paleari, M. (2014) Evoluzione delle pareti alpine di alta montagna ed effetti sull'approccio alpinistico: l'esempio dell'alta Valle Anzasca, Parete Est del Monte Rosa, Italia. Unpublished thesis.
- Paul, F., Rastner, P., Azzoni, R. S., Diolaiuti, G., Fugazza, D., Le Bris, R., Nemeč, J., Rabatel, A., Ramusovic, M., Schwaizer, G., Smiraglia, C. (2020): Glacier shrinkage in the Alps continues unabated as revealed by a new glacier inventory from Sentinel-2. *Earth System Science Data* 12(3), 1805–1821, <https://doi.org/10.5194/essd-12-1805-2020>.
- Pelfini, M. (1999): Dendrogeomorphological study of glacier fluctuations in the Italian Alps during the Little Ice Age. *Annals of Glaciology* 28, 123–128, <https://doi.org/10.3189/172756499781821634>.
- Pelfini, M., Santilli, M. (2006): Dendrogeomorphological analyses on exposed roots along two mountain hiking trails in the Central Italian Alps. *Geografiska Annaler, Series A: Physical Geography* 88(3), 223–236, <https://doi.org/10.1111/j.1468-0459.2006.00297.x>.
- Pelfini, M., Santilli, M., Leonelli, G., Bozzoni, M. (2007): Investigating surface movements of debris-covered Miage glacier, Western Italian Alps, using dendroglaciological analysis. *Journal of Glaciology* 53(180), 141–152, <https://doi.org/10.3189/172756507781833839>.
- Pelfini, M., Diolaiuti, G., Leonelli, G., Bozzoni, M., Bressan, N., Briosch, D., Riccardi, A. (2012): The influence of glacier surface processes on the short-term evolution of supraglacial tree vegetation: The case study of the Miage Glacier, Italian Alps. *The Holocene* 22(8), 847–857, <https://doi.org/10.1177/0959683611434222>.
- Richter, M., Fickert, T., Gruninger, F. (2004): Pflanzen auf schuttbedeckten Gletschern – wandernde Kuriositäten. *Geoko [Bensheim]* 25(3/4), 225–256.
- Schmidt, B. (1987): Ein dendrochronologischer Befund zum Bau der Stadtmauer der Colonia Ulpia Traiana. *Bonner Jahrbuch* 187.
- Serandrei-Barbero, R., Donnici, S., Zecchetto, S. (2022). Past and future behavior of the valley glaciers in the Italian Alps. *Frontiers in Earth Science* 10, 972601, <https://doi.org/10.3389/feart.2022.972601>.
- Smiraglia, C., Diolaiuti, G. A. (2015): The New Italian Glacier Inventory; Ev-K2-CNR: Bergamo, Italy. Available online <https://sites.unimi.it/glaciol/index.php/en/italian-glacier-inventory> (accessed on 20. 2. 2024).
- Stoffel, M., Bollschweiler, M. (2008): Tree-ring analysis in natural hazards research—an overview. *Natural Hazards and Earth System Sciences* 8(2), 187–202, <https://doi.org/10.5194/nhess-8-187-2008>.
- Stoffel, M., Corona, C., Ballesteros-Cánovas, J. A., Bodoque, J. M. (2013): Dating and quantification of erosion processes based on exposed roots. *Earth-Science Reviews* 123, 18–34, <https://doi.org/10.1016/j.earscirev.2013.04.002>.
- Tamburini, A., Chiarle, M., Mortara, G. (2019): Il collasso delle morene del Ghiacciaio del Belvedere. www.nimbus.it/ghiacciai/2019/190816_BelvedereCollassoMorene.htm.
- Tampucci, D., Azzoni, R. S., Boracchi, P., Citterio, C., Compostella, C., Diolaiuti, G., Isaia, M., Marano, G., Smiraglia, C., Gobbi, M., Caccianiga, M. (2017): Debris-covered glaciers as habitat for plant and arthropod species: Environmental framework and colonization patterns. *Ecological Complexity* 32(Part A), 42–52, <https://doi.org/10.1016/j.ecocom.2017.09.004>.
- Tichavský, R., Kluzová, O., Šilhán, K. (2019): Differences between the responses of European larch (*Larix decidua* Mill.) and Norway spruce (*Picea abies* (L.) Karst) to landslide activity based on dendrogeomorphic and dendrometric data. *Geomorphology* 330, 57–68, <https://doi.org/10.1016/j.geomorph.2019.01.013>.
- VAW (Versuchsanstalt für Wasserbau, Hydrologie und Glaziologie, ETH Zürich) (1983–1985): Ricerche glaciologiche al Lago delle Locce, Macugnaga, Italia; Studi sul comportamento del Ghiacciaio del Belvedere, Macugnaga, Italia; Valutazione dei rischi glaciali nella Regione Macugnaga/Monte Rosa, Relazioni Nr. 97.2, 97.3, 97.4 per La Comunità Montana della Valle Anzasca.
- Vejpustková, M., Holuša, J. (2006): Impact of defoliation caused by the sawfly *Cephalcia lariciphila* (Hymenoptera: Pamphilidae) on radial growth of larch (*Larix decidua* Mill.). *European Journal of Forest Research* 125, 391–396, <https://doi.org/10.1007/s10342-006-0112-z>.

Application of the Schmidt hammer in the relative-age dating of rockfall deposits in the Belvedere Glacier Valley

Jan Bařka^{1,*}, Roberto Sergio Azzoni², Vít Vilímek¹

¹ Charles University, Faculty of Science, Department of Physical Geography and Geoecology, Czechia

² University of Milan, Earth Science Department, "A. Desio", Italy

* Corresponding author: jan.batka@natur.cuni.cz

ABSTRACT

The Schmidt hammer is a cost-effective tool for both relative- and absolute-age dating of rocks (the latter in connection with previously absolutely dated surfaces). Its application in high-mountain environments is particularly favoured due to the abundance of dating material and the small size of the dating tool compared to other options. The use of the Schmidt hammer on rock types with macroscopic crystals is not recommended due to the varying weathering rates of different minerals. However, in harsh alpine conditions, there is often no other choice. We applied the Schmidt hammer in the relative dating of boulders in the Belvedere Glacier valley (Italian Alps) with orthogneiss and paragneiss being the dominant rock types (both consisting of macroscopic minerals). For the first time in the Schmidt hammer-related studies, we prepared a chart for the objective inclination correction of the data. The correction for aspect was also performed. The results suggest the successful applicability of the Schmidt hammer even under the unfavourable circumstances.

KEYWORDS

Schmidt hammer; relative dating; rockfalls; weathering; Belvedere Glacier

Received: 19 April 2024

Accepted: 28 November 2024

Published online: 16 December 2024

Bařka, J., Azzoni, R. S., Vilímek, V. (2024): Application of the Schmidt hammer in the relative-age dating of rockfall deposits in the Belvedere Glacier Valley. *AUC Geographica* 59(2), 272–281

<https://doi.org/10.14712/23361980.2024.25>

© 2024 The Authors. This is an open-access article distributed under the terms of the Creative Commons Attribution License (<http://creativecommons.org/licenses/by/4.0>).

1. Introduction

The Schmidt hammer was originally developed for non-destructive testing of the strength of concrete by the Swiss engineer, Ernst Schmidt, whose goal was to measure the deterioration rate of concrete structures over time (Schmidt 1950). It consists of a spring-loaded piston and a plunger, which is pressed against the surface. Thereby, the piston is released and its impact onto the plunger transfers the energy to the material (Aydin 2015). A certain part of the energy is transformed into heat, sound, and surface deformation, the rest is recovered forcing the piston to rebound (Goudie 2006). The amount of recovered energy depends on the hardness of the material and is measured as a percentage of the maximum stretch length of the spring before release, the so-called R value (Aydin 2015).

The potential of this new instrument for environmental science was first exploited by Yaalon and Singer (1974) and Day and Goudie (1977) in the assessment of rock hardness. Matthews and Shakesby (1984) and Betts and Latta (2000) conducted pivotal studies of the use of the Schmidt hammer in relative- and numerical-age dating, respectively. The new technique steadily gained attention and found its application in the dating of various geomorphological events and landforms (fully summarised by Matthews and Winkler 2022): bedrock and moraine ridges formed during the Late Pleistocene deglaciation and Younger Dryas (Longhi et al. 2024; Longhi and Guglielmin 2020; Tomkins et al. 2018, 2016; Engel et al. 2011), paraglacial rockfalls and alluvial fans (McEwen et al. 2020; Scotti et al. 2017), rock glaciers and other periglacial landforms (Marr et al. 2022; Nesje et al. 2021), coastal landscapes (Sjöberg and Broadbent 1991), fluvial terraces (Stahl et al. 2013), and slope movements in tropical and temperate environments (Burda et al. 2018; Klimeš et al. 2009). The strong supremacy of glacial or permafrost environment-related research has an obvious reason, i.e., the abundance of dating material.

Contrary to the above, the studies of the weathering itself that use the Schmidt hammer show larger diversity, as reviewed by Goudie (2006). The possible applications include karstic forms (Haryono and Day 2004), tafoni and shore platforms (Stephenson and Kirk 2000; Matsukura and Matsuoka 1996), development of inselbergs (Pye et al. 1986), weathering-based rock classification (Karpuz and Paşamehmetoğlu 1997), temporal changes of weathering rates (White et al. 1998; Sjöberg and Broadbent 1991), and the relation between aspect and weathering rates (Waragai 1999).

Application of the Schmidt hammer for numerical-age dating requires a set of pre-dated control points for the calculation of calibration curves between the R value and absolute age. Commonly, a few control points are dated using terrestrial cosmogenic nuclide dating. The bulk of the surface

exposure-ages are then determined with calibrated R values as the high cost of the nuclide technique prevents its more extensive application (Matthews and Winkler 2022). When only relative ages are needed, the considerably cheaper Schmidt hammer proves to be a robust dating tool (Shakesby 2006). The constraints of the technique include its sensitiveness to moisture content, and influence of surface texture, as well as rock inhomogeneity, on the results (Goudie 2006). However, the study of high mountain environments often offers only macroscopically inhomogeneous rocks, such as orthogneiss. Should they be a priori precluded from Schmidt hammer studies or is there any potential for reliable relative data?

Our aim was to apply the Schmidt hammer for relative age dating of orthogneiss and paragneiss boulders in the Belvedere Glacier valley (the Italian Alps). The inspected blocks of complex glacial and periglacial origin span temporally from rather fresh supraglacial samples to more weathered ones partly buried in the flat sedimentary plain neighbouring the glacier. We created a systematic chart for the inclination corrections, the first one ever published and based on the findings by Basu and Aydin (2004). Lastly, we examine the plausibility of the results and discuss them in a broader geomorphological context.

2. Study area

The Belvedere Glacier is a valley glacier located at the foot of the northeastern (i.e., Italian) face of the well-known Monte Rosa (4634 m a.s.l.). It is fed by frequent snow and ice avalanches from the surrounding steep hanging glaciers. The altitudinal range of the debris-covered tongue reaches approximately 400 m stretching from about 1800 to 2200 m a.s.l. (Fig. 1). The glacier occupies the orographic left (western) part of a broader valley carved during the Pleistocene glaciations with its left lateral moraine partially leaning against a valley side. The right lateral moraine neighbours a moraine-dammed lake named Lago delle Locce in the uppermost section, overlooks an almost flat plain littered with boulders in the central part (Fig. 5), and in the lower section steeply descends into a gorge of the stream that drains the eastern portion of the catchment. The valley runs in a north-south direction and turns to the northeast near the head of the gorge. It takes another 45° turn towards the east some 650 metres downstream, at the point where the Belvedere Glaciers splits into two lobes. Both lobes terminate well above the mountainous village of Macugnaga.

The valley is significantly shaped by snow and ice avalanches that feed the glacier and often deposit fresh rock debris on its surface. Fresh taluses on the valley sides suggest the activity of rockfalls related to the structural changes of steep rock faces caused by thawing permafrost. Moraine lobes accumulated during

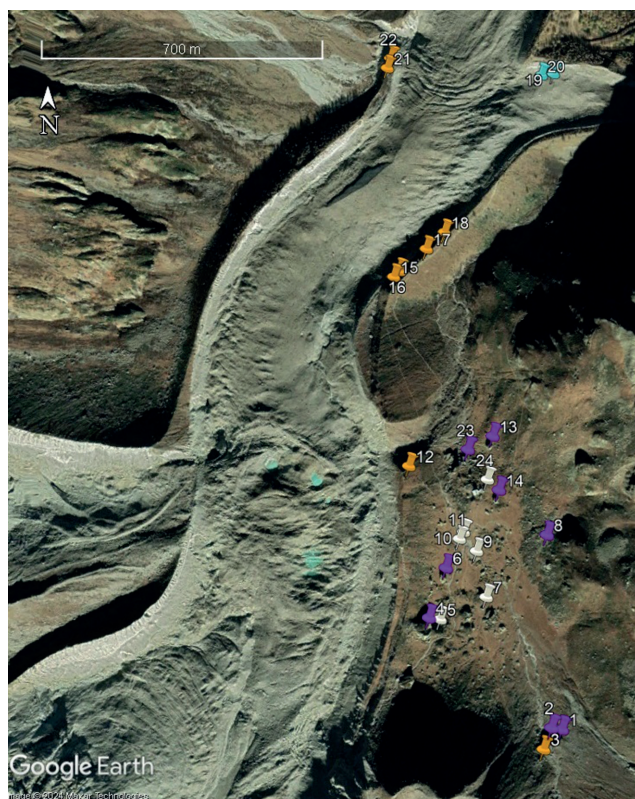


Fig. 1 Location of the sampled boulders within the Belvedere Glacier valley; boulders on the surface in violet; partly buried boulders in white; boulders in moraine in orange; supraglacial boulders in blue.

the Little Ice Age witnessed steady glacier retreat during the last century with the occasional formation of several moraine-dammed lakes. The largest one, the Lago delle Locce, was the source of a significant glacial flood event in 1978, and therefore was an object of remedial works in the 1980s (Haeberli and Epifani 1986). The Belvedere Glacier experienced an unexpected surge event in 2001–2003 (Kääb et al. 2004), whereafter it underwent a continuous downwasting. The glacial flood and surge events formed several over spills of the right lateral moraine and a significant V-shaped breach with outwash accumulations at the head of the gorge. The debuitting of the moraine slopes caused by the lowering of the Belvedere Glacier surface is demonstrated by numerous small slides and the fresh surface of the inner moraine slopes.

The geology of the Monte Rosa east face is characterized by layers of two different lithologies: orthogneiss and paragneiss. The two lithologies stem from the crystalline of the Penninic Monte Rosa nappe. The composition of orthogneiss varies considerably throughout the Monte Rosa east face but the predominant constituent minerals are always quartz, K-feldspar, plagioclase, muscovite and biotite. Paragneiss contains either biotite or muscovite as a main part, often combined as well, and garnet, quartz and feldspar as a minor part. The paragneiss shows a pronounced parallel texture (schistosity) with varying formation from schist to gneiss (Fisher et al. 2006).

3. Methods

3.1 Data collection

The readings were gathered during three cloudy but dry days in August 2022 (9th–11th) and 2023 (1st–2nd). A standard Proceq N-type Schmidt hammer (Proceq SA N-34) was operated by three alternating researchers generally following standard recommendations (e.g., Aydin 2015; Day and Goudie 1977). Each measurement was made perpendicular to the surface while avoiding sharp edges, cracks, fissures, weathering rinds, and visibly exfoliating slabs. In several cases, exfoliating flakes hidden under the boulder surface were indicated after impact by a typical sound resembling a machine gun. The locations with the least microtopography were selected, the task being hindered by the heterogeneous nature of the orthogneiss. Preferably, the surfaces covered in lichens were avoided despite the difficulty of the task as these thrive in the cold humid climate of the Belvedere Glacier valley.

The mineralogical structure of the boulder surface was largely obscured by the severe effects of weathering. Therefore, a bias may have arisen from repeated measurements of harder (or softer) minerals of the heterogeneous orthogneiss. To compensate for this, three measurements, all of which were taken from locations typically a few centimetres apart from each other, were averaged. This means that each reading is an average rock hardness value of a small area on the boulder's surface. The neighbouring readings were usually distanced at least 10 centimetres. The record of each reading contains the boulder-related information (location, position, rock type, size) and the aspect and inclination of the small area from which it was taken (Tab. 1).

3.2 Correction for the impact angle

As the Schmidt hammer measures the rebound of the piston after the impact, gravity may facilitate (impact on overhanging surfaces) or hinder (impact on sloping or flat surfaces) the rebound. The largest and zero effect of gravity is recorded after impacts in the vertical and horizontal direction, respectively. The original correction chart for the impact angle was designed by the manufacturer for measurements of concrete hardness and was corrected by Basu and Aydin (2004) for field rock hardness measurements. However, both the manufacturer and the later study only provide a correction graph plotting the original against the corrected values without precise equations. The corrections are therefore made through visual interpretation (Fig. 2).

The corrections are calculated relatively to the horizontal impact. The two lower curves in the graph for negative impact angles -45° and -90° represent the situation when gravity “helps” the piston to rebound

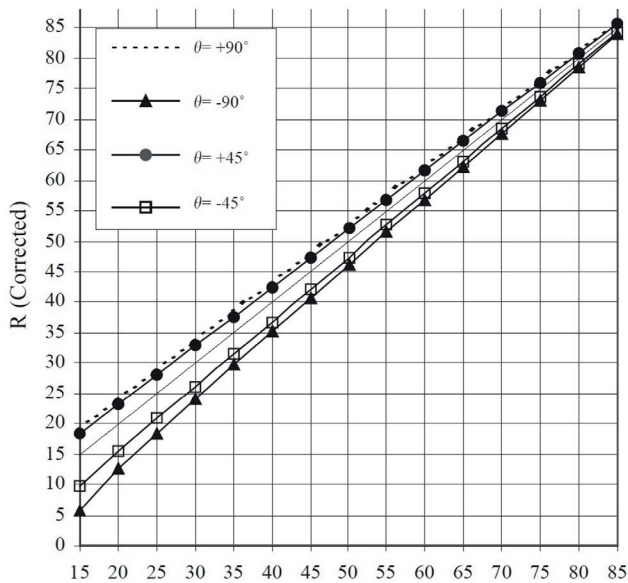


Fig. 2 Correction chart for inclination (Basu and Aydin 2004).

after the impact from below (overhanging surfaces). The recorded values are therefore higher than in the case of a horizontal impact and must be lowered back afterwards. The dependence of correction size on the original impact angle is obviously non-linear, which furthermore hinders the application of impact-angle corrections. In order to ensure homogeneous corrections for strictly integer R values, a set of thresholds was created for each recorded impact angle (Tab. 2).

3.3 Correction for aspect

The north-south orientation of the Belvedere Glacier valley controls the orographic wind direction. The combination of prevailing north or south winds predisposes higher weathering rates on the boulder sides facing the respective directions. The particular settings of most boulders did not allow for readings from all eight aspects, and often not even the basic four directions. Altogether, the boulder sides facing

Tab. 1 Characteristics of the sampled boulders; please note that the coloured categories of position are the same as in Fig. 1 and are retained in the following figures.

Boulder	Latitude (N)	Longitude (E)	Position	Rock type	Size (m)	Readings (n)
No. 1	45°56'49.76"	7°55'15.61"	on the surface	orthogneiss	10 × 15 × 15	50
No. 2	45°56'49.90"	7°55'14.30"	on the surface	orthogneiss	10 × 15 × 10	49
No. 3	45°56'48.21"	7°55'13.40"	moraine	orthogneiss	3 × 5 × 5	30
No. 4	45°56'59.36"	7°54'58.62"	on the surface	orthogneiss	15 × 25 × 30	38
No. 5	45°56'59.21"	7°55'00.00"	partly buried	orthogneiss	15 × 43 × 26	63
No. 6	45°57'03.68"	7°55'00.62"	on the surface	orthogneiss	13 × 16 × 10	40
No. 7	45°57'01.07"	7°55'05.74"	partly buried	orthogneiss	10 × 11 × 11	49
No. 8	45°57'06.61"	7°55'13.51"	on the surface	orthogneiss	2.5 × 4.5 × 4	41
No. 9	45°57'05.14"	7°55'04.45"	partly buried	orthogneiss	8 × 13 × 7	51
No. 10	45°57'06.84"	7°55'02.74"	partly buried	orthogneiss	12 × 10 × 8	50
No. 11	45°57'06.22"	7°55'02.23"	partly buried	orthogneiss	7 × 13 × 6	45
No. 12	45°57'12.74"	7°54'55.98"	moraine	orthogneiss	2 × 6 × 4	40
No. 13	45°57'15.34"	7°55'06.25"	on the surface	orthogneiss	12 × 18 × 12	42
No. 14	45°57'10.55"	7°55'07.25"	on the surface	orthogneiss	11 × 12 × 11	46
No. 15	45°57'29.76"	7°54'53.24"	moraine	paragneiss	4 × 6 × 4	41
No. 16	45°57'30.29"	7°54'53.93"	moraine	paragneiss	3 × 4 × 2.5	41
No. 17	45°57'32.36"	7°54'57.36"	moraine	paragneiss	6 × 3 × 3	47
No. 18	45°57'33.93"	7°54'59.67"	moraine	paragneiss	4 × 2 × 2	41
No. 19	45°57'49.20"	7°55'13.53"	supraglacial	paragneiss	6 × 3 × 1.5	40
No. 20	45°57'49.03"	7°55'11.92"	supraglacial	orthogneiss	4 × 4 × 2	41
No. 21	45°57'49.31"	7°54'51.68"	moraine	paragneiss	9 × 6 × 3	33
No. 22	45°57'50.26"	7°54'52.07"	moraine	paragneiss	10 × 8 × 6	31
No. 23	45°57'14.14"	7°55'03.08"	on the surface	orthogneiss	3 × 2 × 1	35
No. 24	45°57'11.48"	7°55'05.72"	partly buried	orthogneiss	2 × 1 × 2	30



Fig. 3 Examples of boulders from all positional categories; A – boulder No. 2 located on surface; B – partly buried boulder No. 7; C – morainic boulder No. 17; D – supraglacial boulder No. 19.

the easterly directions were inspected most often. A combination of the above stated results in a potential aspect bias for most of the inspected boulders. To correct for the aspect, the deviation from the boulder average was calculated for each reading. Subsequently, the mean deviations for all eight aspects were obtained and these eight values served as the aspect corrections.

4. Results

Altogether, 1015 readings were collected from 24 boulders in two field campaigns (boulders No. 1–20 in 2022, and 21–24 in 2023). The number of readings per boulder ranged from 30 to 63, being randomly distributed among the accessible sides of each boulder. The boulders were split into four categories based on their location as seemed fit for the geomorphological interpretation. Fourteen boulders were located on the valley floor outside the moraine ridges, either partly buried within the plain or on its surface. Two blocks rested directly on the glacier surface (right lateral lobe), and eight were part of the lateral moraines of the Locce Glacier and the Belvedere

Glacier (Fig. 1 and Fig. 3, Tab. 1). The two supraglacial and eight morainic boulders were presumed not to be rock avalanche-sourced and were included for comparison with the two first groups.

4.1 Uncorrected data

The average R values for each boulder calculated from the raw data are shown in Fig. 4A. The values span between 34 and 58, the vast majority of boulders fitting into the interval 40–55. The two boulders with extreme average R values were the only two located on the glacier surface. The second largest inhomogeneity of R values is among the morainic boulders (41–56.1), while the boulders positioned on the surface of the plain and those partly buried have considerably higher levels of homogeneity in R values (45.2–53.8 and 42.8–46.7, respectively).

The boulders partly buried within the plain tend to have lower R values than the boulders on the plain's surface. As lower R values mean a relatively older age, these data suggest two stages of boulder deposition. The obvious source of large boulders is the surrounding high rockwalls of the Monte Rosa massif. In prolonged periods of positive mass balance, the surface

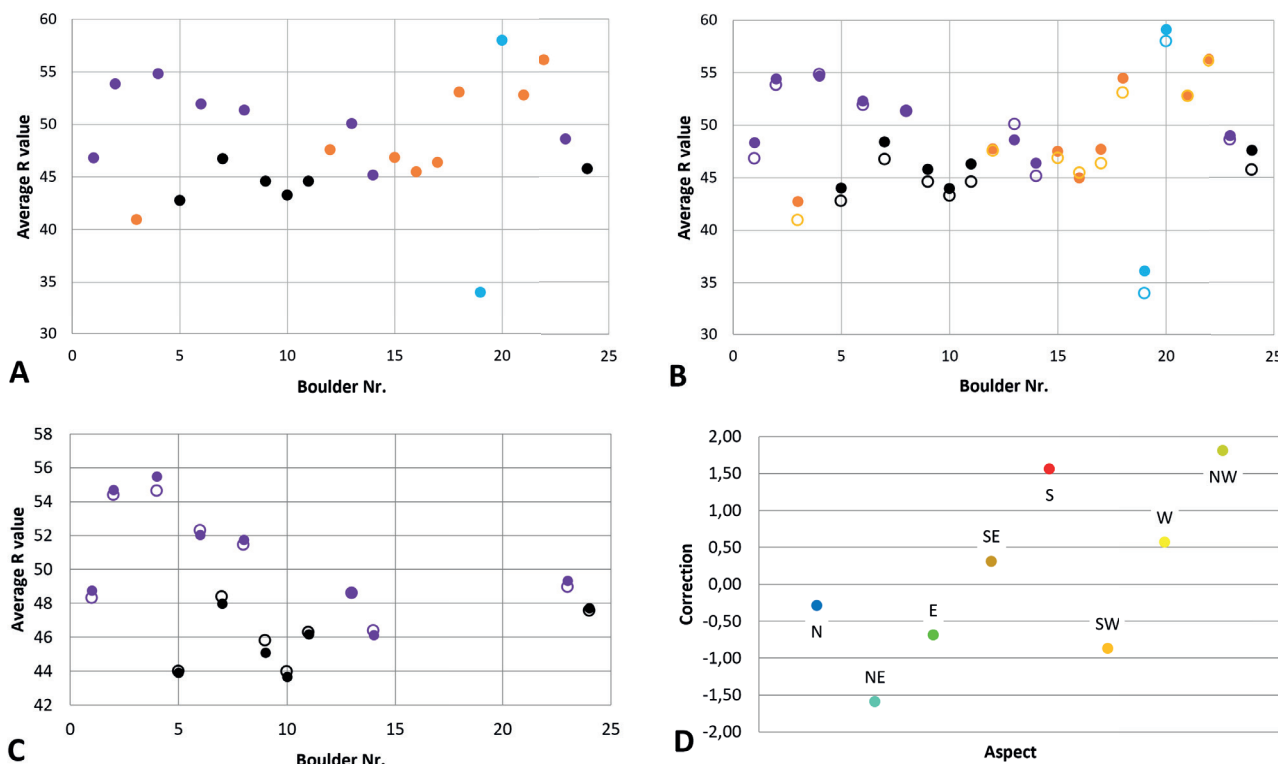


Fig. 4 Average R values of the sampled boulders; A – raw data; B – comparison of data before (hollow circles) and after the correction for inclination (filled circles); C – data before and after the correction for aspect (hollow and filled circles, respectively); D – calculated corrections for each aspect; colours in A–C correspond to the previous figures, colours in D correspond to Fig. 6.

of the Belvedere Glacier used to be well above current lateral moraine ridges. The rockfalls originating in the steep mountain faces could simply run over the glacier tongue and terminate between its right lateral moraine and the valley slopes.

4.2 Data corrected for inclination

The objective correction for the inclination of the boulder face created based on Basu and Aydin (2004) is presented in Tab. 2. The intervals for both the R values and impact angle are approximate; nonetheless, they are applied on the dataset. The raw data were divided into groups based on the inclination of the boulder face. For each group of inclinations (rows), the original R values define the correction that is found in the head of the respective column.

The correction for the surface inclination (Fig. 4B) slightly increased most of the average boulder R values (overall average change +1.1 per boulder) with only few exceptions (boulders No. 8, 14, and 16). The original scatter of values in the boulder positional categories, as well as the difference between partly buried boulders and those on the plain’s surface were preserved. The generally positive compensation ensues from the absence of large overhanging surfaces that require negative compensations.

4.3 Data corrected for aspect

The very high scatter of R values in the morainic boulders and the two located directly on the glacier surface resulted in their exclusion from the final correction step, i.e., the compensation for the surface

Tab. 2 The inclination correction table; each cell gives the interval of R values corresponding to the respective combination of the impact angle and ensuing correction value.

Impact angle	Corrections					Impact angle	Corrections					
	4+	3+	2+	1+	0+		0-	1-	2-	3-	4-	5-
0–10°	32–	33–52	53+	x	x	100°	61+	60–	x	x	x	x
20–30°	x	29–44	45+	x	x	110°	x	40+	39–	x	x	x
40–50°	x	34–	35+	x	x	120°	x	65+	35–64	34–	x	x
55–60°	x	27–	28–54	55+	x	135°	x	x	55+	32–54	31–	x
70–75°	x	x	25–45	46+	x	150°	x	x	x	47+	33–46	32–
80°	x	x	x	54–	55+	160°	x	x	x	51+	36–50	35–

orientation. In addition, the prevailing wind directions may very well be obscured by the complex history of these boulders due to previous glacier transport and the unknown duration of their aspect to weathering. Therefore, only the boulders from the plain (on the surface and partly buried) were considered in the analysis of the orientation-related differences in R values. As there were only orthogneiss boulders in this subset, the aspect analysis should not be biased by lithology differences.

The most weathered boulder surfaces were oriented towards the south and northwest, whereas the most sheltered faces were oriented towards the northeast (resulting in positive and negative corrections, respectively, in Fig. 4D). However, there proved to be no distinct pattern, which would correspond to the north-south valley orientation.

Despite the uneven distribution of readings among the eight basic aspects, the corrections only slightly altered the average boulder R values (Fig. 4C). The calculated average change per boulder was negligible (+0.03).

5. Discussion

5.1 Geomorphological interpretation

Schmidt hammer readings from gneiss show higher dispersion due to the macroscopic properties of this rock type (Goudie 2006). The boulders of the Belvedere Glacier valley give average R values similar to the results listed by Goudie (2006) as the occasional impacts of crystals of stronger and weaker mineral disappeared in the most of the average data. The differentiation among the four boulder position categories showed to be very important. The boulders located directly on the glacier surface and on the lateral moraine ridges had a higher diversity in their average R values. This confirms their more complex history compared to the rock avalanche-sourced boulders of the surface of the plain due to the dynamicity of

the supraglacial debris cover, and the activity of the proximal moraine sides. Both processes commonly allow for the appearance of rather fresh boulder surfaces with unknown previous evolution. Apparently, despite the neighbouring location of the boulders on the right glacier lobe (both No. 19 and 20), they must have experienced very different factors, one being strongly weathered and one still very fresh. The difference in lithology may be a contributing factor as well (No. 19 paragneiss whereas No. 20 orthogneiss). There were less differences among the boulders positioned on moraines, as the moraines were stable for tens of years before the onset of slope instabilities that unravelled the interior of the moraine ridges.

Higher homogeneity of average R values among the boulders positioned on the surface and partly buried as opposed to the supraglacial and morainic blocks supports a common origin of the two former groups. Rock avalanches from the surrounding high rockwalls represent the most probable source. Further differentiation between the boulders positioned on the surface of the plain (Fig. 5) and those partly buried (both groups consist strictly of orthogneiss boulders) should follow a simple rule. The boulders positioned on the surface should be younger and therefore give generally higher R values. This proved to be true for all boulders except one (No. 14, Fig. 4C), which would fit perfectly into the other positional category. Such misinterpretation is possible, as the only indication is the angle of the boulder sides at the surface. Even though its sides are apparently rounded at ground level, the central portion of boulder No. 14 may be protruding downwards into the plain.

The lithological disparity between orthogneiss and paragneiss are known to ensue in different weathering rates reflected in the R values (Longhi et al. 2024). This may be a contributing factor for the discrepancy between the two supraglacial boulders (No. 19 and No. 20) as suggested before. The same potential bias is inherent in most of the correction stages. However, the geomorphological interpretation regarding the

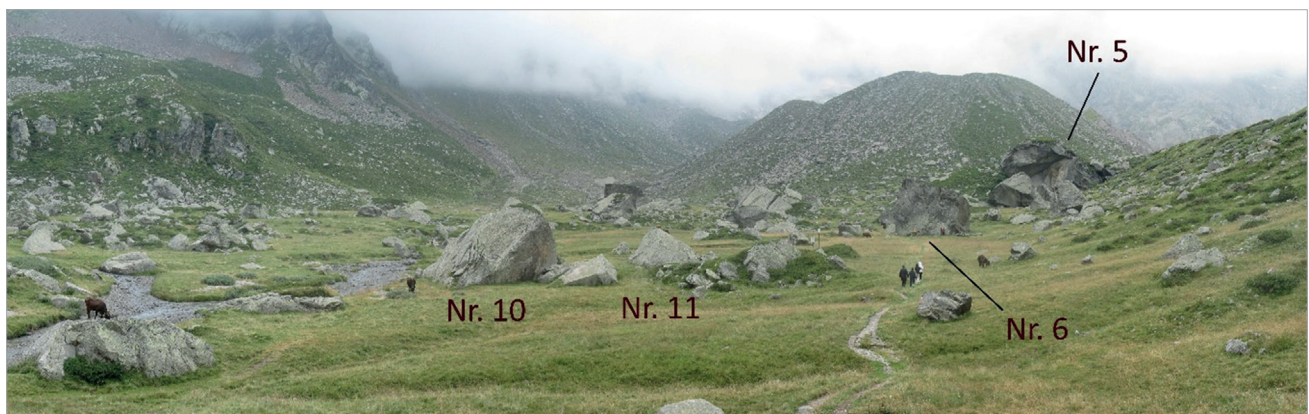


Fig. 5 The flat plain littered exclusively with orthogneiss boulders of varying deposition age (view towards the terminal moraine of the Locce Glacier where the Locce Lake is present); IDs of several block indicated.

source of the boulders of the plain was not affected as they were all orthogneiss boulders.

5.2 Significance of Corrections

The correction table (Tab. 2) created based on the findings by Basu and Aydin (2004) proved to be a suitable alternative to the classical graphical representation of the correction for the impact angle. As the majority of the readings were taken from surfaces inclined by about 90° and lower, the overall positive compensation was correctly in place. The correction may be viewed as redundant since it meant no significant change in the average R values, but this is not the case. It is unlikely for the boulders partly buried in the plain to have overhanging faces, as opposed to those positioned on the surface. Indeed, the corrected values for all the partly buried boulders were higher than the uncorrected values (meaning average inclination angles lower than 90°). However, some of the boulders on the surface (boulders No. 4 and 13) had a negative change due to the correction for the impact angle.

Similarly, the correction for the aspect did not bring significant changes. It seems that the uneven distribution of the accessible boulder faces among the basic directions was not uneven enough to cause a meaningful bias. The principle of similar representation of all aspects may not be as important as we thought, but then again, this is only one location with a specific orographic setting.

5.3 Aspect analysis

The south-north orographic setting of the upper portion of the Belvedere Glacier valley should ensue in the prevalence of northern and southern winds. This means that the boulder sides facing north and south should be more weathered as they experience higher changes in temperature and humidity. As the southern sides are shielded by the Monte Rosa massif, the most weathered boulder faces should be those oriented towards the north. On the other hand, the boulder sides facing west and east should be less weathered.

The highest positive compensation of boulder sides oriented towards the northwest and south (1.81 and 1.56, respectively) confirms this hypothesis. However, the lowest weathered sides facing north-east (negative compensation of -1.59) undermines it, as do the data from the western and eastern boulder sides. The faces oriented towards the west were significantly more weathered than the opposite sides, even though the compensations differ less (0.57 for the west and -0.69 for the east). In addition, the boulder sides facing north showed an average level of weathering (a compensation of only 0.31).

The data preclude even the back-up hypothesis of the level of weathering gradually decreasing from one aspect to the opposite one. Nevertheless, there

still may be a logical explanation. The plain with the boulders is significantly closer to the eastern flank of the valley as the western half of the valley is occupied by the glacier tongue and both lateral moraines. The boulder sides facing east should therefore be more sheltered than the faces oriented towards the west. This is corroborated by less weathered northeastern and eastern boulder sides.

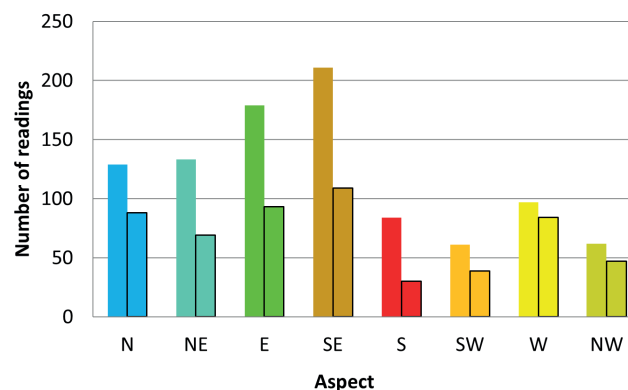


Fig. 6 Number of readings per aspect showing both all readings and those used for the aspect correction (unframed and framed columns, respectively).

The lowest number of readings suitable for the aspect analysis was obtained from the boulder sides facing south and southwest (both $n < 40$ in Fig. 6). Consequently, the average R values for each of these aspects were calculated based on the readings from three boulders. It is therefore possible that only more (or less) weathered faces may have been used. The resulting inaccuracy may be large. Nevertheless, this could not serve as an explanation to the conspicuous differences between the northwestern and northeastern aspects. Systematic misjudgement of aspects involving all the boulders may have been introduced as well. However, considering the high number of readings (each reading being an average of three values), such a systematic bias is not probable, and it should still leave the pattern of aspects intact, albeit distorted, and that is not the case.

6. Conclusions

The Schmidt hammer was applied to achieve the relative age dating of boulders in the Belvedere Glacier valley. A mixed set of 24 orthogneiss and paragneiss boulders of complex glacial and periglacial origin was sampled and split into four groups based on their location (boulders on the glacier, on the moraine, on the surface of the plain, and those partly buried within the plain). The raw data were corrected for the inclination angle and aspect. The results suggest an unpredictable history of the boulders located on the moraine and glacier surface. These exhibit large differences in

average R values between boulders of the same group. The majority of sampled blocks (58.3%) were located on the plain and their higher homogeneity of R values supports their common origin in rock avalanches from the surrounding rockwalls. The boulders partly buried within the plain are generally more weathered than those positioned on the surface (with comparable lithology) and are therefore older. There is only one exception in the case of boulder No. 14, which may have been misplaced in the wrong group (its base may be much lower in the centre than observed at the sides).

The corrections refined the data in a sense as the original overlap between the two groups of boulders of the plain was larger. No dramatic change in the results occurred but the sign of the correction usually varied boulder to boulder, so it proved to be relevant. For the first time, a table of objective inclination corrections was created based on Basu and Aydin (2004). It proved very useful as reading the correction from the scaling chart of limited size had been odious. The final analysis of aspect-related weathering differences showed no clear pattern. The most weathered seem to be boulder sides facing south and northwest, while the least weathered are the boulder faces oriented towards the northeast. The possible explanations include shielding by high relief and the potential bias introduced by the low number of boulders with sides of certain aspects (south and northwest).

The Schmidt hammer proved to be useful even in an environment with a complex geomorphological history and unsuitable rock types with macroscopic crystals. The precision of the results may probably increase with a larger set of sampled boulders. However, the Schmidt hammer technique is known to be sensitive to the moisture content of the rock surface. The high mountain environment offers only a limited period of dry conditions before the weather deteriorates. A potential next step may be a combination of a higher number of sampled boulders and several surfaces with known absolute dating, even though this may prove to be costly. The absolute dating would be especially useful for geomorphological mapping.

Acknowledgements

Both field campaigns were funded by the Project GAUK No. 258522 of the Charles University Grant Agency.

The Authors would like to thank the Province of Verbano-Cusio-Ossola for the permit of UAV and dendrogeomorphological surveys (dr. Andrea De Zordi, Settore III – Assetto del Territorio Georisorse e Tutela Faunistica, Servizio Rete Natura 2000 e Forestazione). The authors' gratitude belongs particularly to two anonymous reviewers and to the editors of *AUC Geographica*.

References

- Aydin, A. (2015): ISRM Suggested Method for Determination of the Schmidt Hammer Rebound hardness: Revised Version. R. Ulusay (ed.) *The ISRM Suggested Methods for Rock Characterization, Testing and Monitoring: 2007–2014*. Springer, <https://doi.org/10.1007/978-3-319-07713-0>.
- Basu, A., Aydin, A. (2004): A method for normalization of Schmidt hammer rebound values. *International Journal of Rock Mechanics and Mining Sciences* 41(7), 1211–1214, <https://doi.org/10.1016/j.ijrmms.2004.05.001>.
- Betts, M. W., Latta, M. A. (2000): Rock surface hardness as an indication of exposure age: an archaeological application of the Schmidt hammer. *Archeometry* 42(1), 209–223, <https://doi.org/10.1111/j.1475-4754.2000.tb00877.x>.
- Burda, J., Veselý, M., Řehoř, M., Vilímek, V. (2018): Reconstruction of a large runout landslide in the Krušné hory Mts. (Czech Republic). *Landslides* 15, 423–437, <https://doi.org/10.1007/s10346-017-0881-0>.
- Day, M. J., Goudie, A. S. (1977): Field assessment of rock hardness using the Schmidt test hammer. *British Geomorphological Research Group Technical Bulletin* 18, 19–29.
- Engel, Z., Traczyk, A., Braucher, R., Woronko, B., Křížek, M. (2011): Use of ¹⁰Be exposure ages and Schmidt hammer data for correlation of moraines in the Krkonoše Mountains, Poland/Czech Republic. *Zeitschrift für Geomorphologie* 55(2), 175–196, <https://doi.org/10.1127/0372-8854/2011/0055-0036>.
- Fisher, L., Käab, A., Huggel, C., Noetzi, J. (2006): Geology, glacier retreat and permafrost degradation as controlling factors of slope instabilities in high-mountain rock wall: the Monte Rosa east face. *Natural Hazard Earth System Sciences* 6(5), 761–772, <https://doi.org/10.5194/nhess-6-761-2006>.
- Goudie, A. S. (2006): The Schmidt Hammer in geomorphological research. *Progress in Physical Geography: Earth and Environment* 30(6), 703–718, <https://doi.org/10.1177/0309133306071954>.
- Haerberli, W., Epifani, F. (1986): Mapping the Distribution of Buried Glacier Ice – An Example from Lago Delle Locce, Monte Rosa, Italian Alps. *Annals of Glaciology* 8, 78–81, <https://doi.org/10.3189/S026030550000118X>.
- Haryono, E., Day, M. (2004): Landform differentiation within the Gunung Kidul Kegelkarst, Java, Indonesia. *Journal of Cave and Karst Studies* 66(2), 62–69.
- Käab, A., Huggel, C., Barbero, S., Chiarle, M., Cordola, M., Epifani, F., Haerberli, W., Mortara, G., Semino, P., Tamburini, P., Viazzo, G. (2004): Glacier hazards at Belvedere Glacier and the Monte Rosa east face, Italian Alps: processes and mitigation. *Internationales Symposium Interpraevent 2004 – Riva/Trient*.
- Karpuz, C., Paşamehmetoğlu, A. G. (1997): Field characterisation of weathered Ankara andesites. *Engineering Geology* 46(1), 1–17, [https://doi.org/10.1016/S0013-7952\(96\)00002-6](https://doi.org/10.1016/S0013-7952(96)00002-6).
- Klimeš, J., Vilímek, V., Omelka, M. (2009): Implications of geomorphological research for recent and prehistoric avalanches and related hazards at Huascarán, Peru. *Natural Hazards* 50, 193–209, <https://doi.org/10.1007/s11069-008-9330-7>.

- Longhi, A., Guglielmin, M. (2020): Reconstruction of the glacial history after the Last Glacial Maximum in the Italian Central Alps using Schmidt's hammer *R*-values and crystallinity ratio indices of soils. *Quaternary International* 558, 19–27, <https://doi.org/10.1016/j.quaint.2020.08.045>.
- Longhi, A., Morgan, D., Guglielmin, M. (2024): Reconstruction of rock avalanche history in Val Viola, (Upper Valtellina, Italian Central Alps) through ¹⁰Be exposure ages, Schmidt Hammer *R* values, and surface roughness. *Landslides* 21, 949–962, <https://doi.org/10.1007/s10346-024-02210-2>.
- Marr, P., Winkler, S., Dahl, S. O., Löffler, J. (2022): Age, origin and palaeoclimatic implications of peri- and paraglacial boulder-dominated landforms in Rondane, South Norway. *Geomorphology* 408: 108251, <https://doi.org/10.1016/j.geomorph.2022.108251>.
- Matsukura, Y., Matsuoka, N. (1996): The effect of rock properties on rates of tafoni growth in coastal environments. *Zeitschrift für Geomorphologie* 106, 57–72, <https://doi.org/10.1127/0372-8854/2007/0051S-0115>.
- Matthews, J. A., Shakesby, D. A. (1984): The status of the “Little Ice Age” in southern Norway: relative-age dating of Neoglacial moraines with Schmidt hammer and lichenometry. *Boreas* 13(3), 333–346, <https://doi.org/10.1111/j.1502-3885.1984.tb01128.x>.
- Matthews, J. A., Winkler, S. (2022): Schmidt-hammer exposure-age dating – a review of principles and practice. *Earth-Science Reviews* 230, 104038, <https://doi.org/10.1016/j.earscirev.2022.104038>.
- McEwen, L. J., Matthews, J. A., Owen, G. (2020): Development of a Holocene glacier-fed composite alluvial fan based on surface exposure-age dating techniques: the Illåe fan, Jotunheimen, Norway. *Geomorphology* 363: 107200, <https://doi.org/10.1016/j.geomorph.2020.107200>.
- Nesje, A., Matthews, J. A., Linge, H., Bredal, M., Wilson, P., Winkler, S. (2021): New evidence for active talus-foot rock glaciers at Øyberget, southern Norway, and their development during the Holocene. *The Holocene* 31(11–12), 1786–1796, <https://doi.org/10.1177/09596836211033226>.
- Pye, K., Goudie, A. S., Watson, A. (1986): Petrological influence on differential weathering and inselberg development in the Kora area of central Kenya. *Earth Surface Processes and Landforms* 11(1), 41–52, <https://doi.org/10.1002/esp.3290110106>.
- Schmidt, E. (1950): Der Beton-Prüfhammer. *Schweizerische Bauzeitung* 68(28), 378–379.
- Scotti, R., Brardinoni, F., Crosta, G. B., Cola, G., Mair, V. (2017): Time constraints for post-LGM landscape response to deglaciation in Val Viola, Central Italian Alps. *Quaternary Science Reviews* 177, 10–33, <https://doi.org/10.1016/j.quascirev.2017.10.011>.
- Shakesby, R. A., Matthews, J. A., Owen, G. (2006): The Schmidt hammer as a relative-age dating tool and its potential for calibrated-age dating in Holocene glaciated environments. *Quaternary Science Reviews* 25, 2846–2867, <https://doi.org/10.1016/j.quascirev.2006.07.011>.
- Sjöberg, R., Broadbent, N. (1991): Measurement and calibration of weathering, using the Schmidt Hammer, on wave washed moraines on the Upper Norrland coast, Sweden. *Earth Surface Processes and Landforms* 16(1), 57–64, <https://doi.org/10.1002/esp.3290160107>.
- Stahl, T., Winkler, S., Quigley, M., Bebbington, M., Duffy, B., Duke, D. (2013): Schmidt hammer exposure-age dating (SHD) of late Quaternary fluvial terraces in New Zealand. *Earth Surface Processes and Landforms* 38(15), 1838–1850, <https://doi.org/10.1002/esp.3427>.
- Tomkins, M. D., Dortch, J. M., Hughes, P. D. (2016): Schmidt hammer exposure dating (SHED), establishment and implications for the retreat of the last British Ice. *Quaternary Geochronology* 33, 46–60, <https://doi.org/10.1016/j.quageo.2016.02.002>.
- Tomkins, M. D., Dortch, J. M., Hughes, P. D., Huck, J. J., Stimson, A. G., Delmas, M., Calvet, M., Pallàs, R. (2018): Rapid age assessment of glacial landforms in the Pyrenees using Schmidt hammer exposure dating (SHED). *Quaternary Research* 90(1), 26–37, <https://doi.org/10.1017/qua.2018.12>.
- Waragai, T. (1999): Weathering processes on rock surfaces in the Hunza Valley, Karakoram, North Pakistan. *Zeitschrift für Geomorphologie, Supplementband* 119, 119–136.
- White, K., Bryant, R., Drake, N. (1998): Techniques for measuring rock weathering: application to a dated fan segment sequence in southern Tunisia. *Earth Surface Processes and Landforms* 23(11), 1031–1043, [https://doi.org/10.1002/\(SICI\)1096-9837\(199811\)23:11<3C1031::AID-ESP919%3E3.0.CO;2-G](https://doi.org/10.1002/(SICI)1096-9837(199811)23:11<3C1031::AID-ESP919%3E3.0.CO;2-G).
- Yaalon, D. H., Singer, S. (1974): Vertical variation in strength and porosity of calcrete (Nari) chalk, Shefela, Israel and interpretation of its origin. *Journal of Sedimentary Research* 44, 1016–1023, <https://doi.org/10.1306/212F6C17-2B24-11D7-8648000102C1865D>.

Interpretation of the glacial lake outburst floods database in relation to climatic conditions in different world regions

Matouš Kovanda*

Charles University, Faculty of Science, Department of Physical Geography and Geoecology, Czechia

* Corresponding author: kovandama@natur.cuni.cz

ABSTRACT

This article investigates the response of glacial lake outburst floods (GLOFs) to climatic conditions since the beginning of the 20th century and during individual seasons based on the data from the publicly available online database recording past GLOFs worldwide. All recorded GLOFs were classified into the regions of Alaska, Western Canada and USA, Central Andes, Southern Andes, Iceland, Scandinavia, Alps, Caucasus, Tian Shan, Central Asia I (west), Central Asia II (east), and New Zealand. In each of these regions, the influence of temperature and precipitation on the frequency of glacial flood occurrences was investigated. It was established that GLOFs occur mainly during the summer months and air temperature is their main triggering factor. Since the frequency of GLOFs is influenced by both temperature and precipitation, a gradual increase in the frequency of GLOFs is expected because of global warming, although the relative importance of each factor will vary across regions.

KEYWORDS

glacial lake outburst floods; climate change; air temperature; precipitation

Received: 2 May 2024

Accepted: 26 July 2024

Published online: 18 September 2024

Kovanda, M. (2024): Interpretation of the glacial lake outburst floods database in relation to climatic conditions in different world regions. *AUC Geographica* 59(2), 282–293

<https://doi.org/10.14712/23361980.2024.12>

© 2024 The Author. This is an open-access article distributed under the terms of the Creative Commons Attribution License (<http://creativecommons.org/licenses/by/4.0>).

1. Introduction

Glacial lake outburst flood (GLOF) is the term used for the sudden release of water from any type of glacial lake (dammed most commonly by ice, bedrock, or moraine), regardless of its cause (Clague and Evans 2000; Iturrizaga 2011). Many of these glacial lakes are dammed by unconsolidated glacial deposits forming unstable dams, whose destruction and subsequent GLOF can be triggered by a variety of mechanisms. It may involve, for example, the sudden entry of a large volume of material into the lake (such as landslides, rockfalls, or avalanches), the inflow of a large volume of water from a higher-altitude lake (Richardson and Reynolds 2000; Liu et al. 2013), or intense rainfall leading to dam degradation and lake overtopping (Worni et al. 2012). This paper examines how changing climatic conditions affect the frequency of GLOFs.

In the past, GLOFs have claimed thousands of lives in single incidents and caused severe damage to infrastructure. Because of their far-reaching destructive potential, they pose a significant hazard in many high-altitude areas around the world (Vuichard and Zimmermann 1987; Chowdhury et al. 2021). Vilímek et al. (2014) state that due to continuous deglaciation (glacier retreat), GLOFs will pose a more serious problem in the future. Due to the rapidly changing natural environment, the formation of new lakes in dynamic high mountain environments will continue (Emmer et al. 2016b; Chowdhury et al. 2022). Since a complete understanding of the process is crucial for hazard assessment, emphasis should be placed on the description of all basic parameters of the sudden water release from the lakes. In this regard, a global database of GLOFs may help to provide a better insight into the issue and help prevent further disasters.

Catastrophic events of sudden releases of water from glacial lakes have been reported in many regions across continents (Sattar et al. 2021) and tend to be monitored by regional or global databases. In order to best describe the behaviour of GLOFs in relation to climatic conditions, data describing local air temperatures (NASA 2020) and precipitation totals (Meteo-blue 2023) were processed in this work. Furthermore, relevant data available in the global database of GLOFs (Veh et al. 2022) were processed. Since such a database seeks to analyse all known GLOFs, the GLOFs in this paper are divided into several groups based on their occurrence (Chapter 2). The main objective of this paper was to characterise the behaviour of GLOFs in each of the studied regions and analyse climate-related triggering factors. Furthermore, differences or similarities between the regions were identified.

2. Analysed database of GLOFs

The analysed GLOFs database records glacial floods across continents (Veh et al. 2022). Besides the global

database, there are regional databases that focus on areas with a higher incidence of GLOFs. Such databases often contain detailed information characterising each known glacial flood, allowing the user to develop an understanding of the behaviour of GLOFs in a particular location. For example, the one created by Emmer et al. (2022) focusing on historical GLOFs in the tropical Andes may be considered as a regional database, where 160 GLOFs from the Little Ice Age to the present are analysed. It is also worth mentioning the regional database recording historical GLOFs in the territory of High Mountain Asia, which documents 697 GLOFs that occurred between 1833 and 2022 (ICIMOD 2022). Information from regional databases carries the potential to create a unified global database, which is the aim of many researchers striving to establish a comprehensive and accessible data resource. The authors of the constructed and analysed databases are also worth mentioning (Veh et al. 2022). Other researchers also dedicate themselves to creating such informational environments (Emmer et al. 2016a), or specialize in building specific global databases, such as the one focused on monitoring GLOFs from moraine-dammed lakes (Harrison et al. 2018).

The data in the analysed database (Veh et al. 2022) were publicly available online as of 10 June 2021 (version 1.0). However, the database is continuously enriched with new data and therefore regular updates are made. In this paper, the database version 2.0., created on 1 March 2022, is analysed. This version is currently out of date. By updating the database to version 3.0 (17 November 2022), it was enriched with new parameters describing GLOFs including those recorded in Greenland. After the update to version 3.0, the database contained a total of 3151 GLOFs occurring between the years of 850 and 2022 (Lützow et al. 2023). The latest update to version 4.0 took place on 4 March 2024, and the database then contained records of 4664 GLOFs.

Within the analysed global database, all GLOFs entries include associated characteristic metadata. The database contains 51 parameters that are detected for each GLOF (Veh et al. 2022). The basic parameters, with the least amount of missing data, are mainly region, major RGI region, mountain range region, country, glacier, RGI glacier ID, RGI glacier area, lake name, lake type, longitude, latitude, river, date, and outburst mechanism. For the purpose of analysis, only the selected parameters shown in Fig. 1 were used in this paper.

The authors constantly add to the database and enrich it with data describing GLOFs. Data from 769 different sources have been used to enrich the database (Lützow et al. 2023), including analyses of flow gauges, satellite and aerial imagery, stratigraphy, tree rings, reports from local authorities, news media, workshop reports, social media accounts, and unpublished papers (Veh et al. 2022). All information

Major RGI region	Lake type	Longitude	Latitude	Date	Min. date	Max. date	Outburst mechanism
All	All	All	All				All
Southern Andes	ice	-73.256578	-47.28773	1922			subglacial
Southern Andes	ice	-73.256578	-47.28773	1923			subglacial
Southern Andes	ice	-73.256578	-47.28773	1924			subglacial
Southern Andes	ice	-73.256578	-47.28773	1925			subglacial
Southern Andes	ice	-69.98	-33.1199999999999	1926			
Southern Andes	ice	-73.256578	-47.28773	1926			subglacial
Southern Andes	ice	-73.256578	-47.28773	1927			subglacial
Southern Andes	ice	-73.256578	-47.28773	1928			subglacial
Southern Andes	ice	-73.256578	-47.28773	1929			subglacial
Southern Andes	ice	-73.9599999999999	-49.03		1929	1945	
Southern Andes	ice	-73.256578	-47.28773	1930			subglacial
Southern Andes	ice	-73.256578	-47.28773	1931			subglacial
Southern Andes	ice	-73.256578	-47.28773	1932			subglacial
Low Latitudes	moraine	-76.9379	-10.2333	1932-03-14			breach

Fig. 1 Parameters taken from the GLOFs database (Veh et al. 2022).

collected in the database relates to historical GLOFs. In the paper, these GLOFs are divided into the following regions based on their occurrence: Alaska (the Kenai Mountains, the Chugach Mountains, the Wrangell Mountains, the Saint Elias Mountains and the northern part of the Coast Mountains), Western Canada and USA (the southern part of the Coast Mountains, the northern part of the Rocky Mountains, the Cascade Mountains and the Sierra Nevada Mountains), Central Andes (territory of the states of Peru and Bolivia), Southern Andes (territory of the states of Chile and Argentina), Iceland, Scandinavia (territory of the states of Norway and Sweden), Alps, Caucasus, Tian Shan, Central Asia I (west) (Hindu Kush, Karakoram, western and central Himalayas west of the Gandak River), Central Asia II (east) (eastern and central Himalayas east of the Gandak River, the southeastern part of the Tibetan Plateau and the Hengduan Mountains).

The database contains a large amount of data on past GLOFs, through which it is possible to get at least a basic idea of their behaviour and thereby determine their likely subsequent development. Such a useful database should be continuously updated with new data and parameters that allow for a more accurate characterisation of GLOFs. A disadvantage of the database is the small amount of information recorded on the causes of GLOFs. A more comprehensive analysis of these triggers would significantly enhance our understanding of GLOF behaviour and improve risk prediction. The unavailability of such information in the database may be explained by the fact that there are many triggering mechanisms that can often only be detected by direct observation of the lake at the time of glacial flood formation (Singh et al. 2011). However, despite these limitations, there is sufficient data for each region to define glacial lake behaviour in the region with greater precision through analysis.

3. Methods

In this paper, regions with recorded occurrences of GLOFs were analysed (Chapter 2). This study analyses 2939 GLOFs from 707 glacial lakes occurring between 850 and 2022 within these regions. To characterise each GLOF, suitable parameters describing each event were selected from the database (Veh et al. 2022) (Fig. 1). One of these parameters is the 'major RGI region', which provides information about the geographic area where the GLOF occurred. Another parameter is 'lake type', which carries information about the type of material damming the glacial lake. In addition to the geographical coordinates of the analysed glacial lake's occurrence, it was subsequently possible, using the 'date', 'min. date', and 'max. date' parameters, to obtain information about the precise or approximate year and month when the GLOF event occurred. Furthermore, using the 'outburst mechanism' parameter, it was possible to determine whether the lake dam was somehow compromised in connection with a massive water discharge or if it simply overflowed.

In order to identify the relationship between the occurrence of GLOFs and climatic conditions, data on temperature, precipitation and glacial lake elevation were collected in the study regions in addition to the parameters already mentioned. Due to the lack of data in the database, the elevation of each lake was collected using the Google Earth web application (Google 2022). Lake elevation data helped select a climate model that best represents the study area.

Furthermore, using NASA (2020), the average air temperature at 2 meters above the ground was determined, which was measured by a station located in the analysed region (Fig. 2). The values were calculated as the average of the measured temperatures for each year in the period of interest (1900–2019), with each average divided into 10-year intervals in the form of

From: To: Dataset: Update Stations: 1199



Fig. 2 Stations measuring air temperature between 1900 and 2019 (NASA 2020).

1900–1909, 1910–1919, and 2010–2019. Since temperature data in specific areas were obtained for the purpose of comparing them with GLOF development, data on events from 1899 and earlier were not analysed. This is due to the larger amount of missing data, without which the selected region cannot be objectively assessed in terms of glacial flood frequency. Although data for 2020–2022 are available in the database, it is very likely that there will be a larger amount of missing data on GLOFs in this dataset that have not yet been included in the database. For this reason, the relationship between GLOF occurrence and temperature trends is not established for 2020–2022.

To compare the dependence of GLOFs on total precipitation and temperatures for individual months, climate models available from Meteoblue 2022 were used (Fig. 3). Data were extracted from climate diagrams, representing average total precipitation and

daily maximum and minimum temperatures for individual months between 1985 and 2022. A climate diagram was selected for each analysed geographical area based on the following two criteria: firstly, there must be a higher number of recorded GLOFs in the vicinity of the location, and secondly, the location must fall within an elevation range where the frequency of GLOFs is highest.

Using the acquired data of the above-mentioned parameters, several graphical outputs were generated. Tab. 1 presents the changes in GLOF frequency from 1900 to 2019. The table also includes regional warming rates and data showing the relationship between local air temperatures (NASA 2020) and global air temperatures (EPI 2015; NOAA 2022). The ‘Trend in the number of GLOFs’ parameter indicates if there is an increasing (+) or decreasing (–) trend in GLOF occurrences over time. In the case of an uneven occurrence, the GLOF frequency is marked with +/-.

Average temperatures and total precipitation

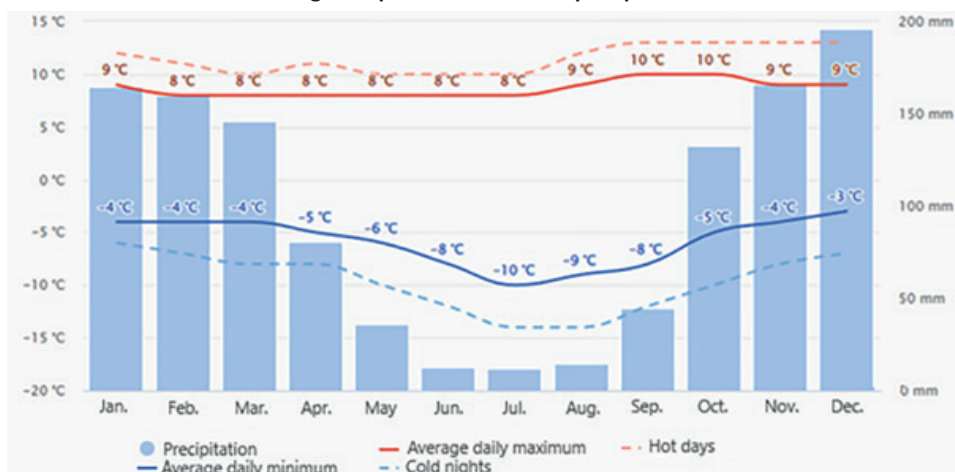


Fig. 3 Climate model of the Cordillera Blanca at 4568 m a.s.l. used for the analysis, Central Andes (Meteoblue 2022).

Tab. 1 Changes in air temperatures and frequencies of GLOFs between 1900 and 2019 in the monitored regions (EPI 2015; NOAA 2022; Veh et al. 2022).

Analysed region	Trend in the number of GLOFs	Measurement start	Warming [°C]	Pearson correlation coefficient
Alaska	+	1920	1.61	0.90
Western Canada and USA	–	1900	0.85	0.78
Central Andes	+	1950	1.33	0.83
Southern Andes	+	1930	0.98	0.94
Iceland	+	1900	1.05	0.61
Scandinavia	+	1900	1.42	0.79
Alps	+	1900	2.49	0.98
Caucasus	+/-	1940	2.12	0.87
Tian Shan	–	1900	1.78	0.75
Central Asia I (west)	+	1900	1.38	0.71
Central Asia II (east)	+	1900	1.85	0.98
New Zealand	+/-	1910	1.17	0.76
Globally	+	1900	1.05	1.00

This trend is evident from the dates of glacial floods recorded in the GLOFs database. The ‘Measurement start’ parameter indicates the year continuous 2-meter air temperature data began for each analysis area. For more than half of the analysed regions, these data have been recorded by stations since 1900. The least available continuous air temperature data are in the Central Andes region, where measurements by the station have been recorded only since 1950. The ‘Warming [°C]’ parameter shows the difference in average air temperature measured by stations in the analysed regions over a certain period of time. The value is expressed as the difference between the averaged air temperature over the decade when the measurements started (‘Measurement start’) and the averaged air temperature over the years 2010–2019. The ‘Pearson correlation coefficient’ analysis is used to show the relationship between local (i.e., station data) and global temperature changes.

Tab. 2 compares the dependence of GLOF occurrences on temperature and precipitation throughout the year. Data on air temperature and total precipitation for individual months in each region are extracted from climate model diagrams (Meteoblue 2022) that accurately depict the specific region. The value for the ‘Air temperature correlation coefficient’ parameter indicates the relationship between the frequency of GLOFs and the average maximum air temperature for each month of the year using Pearson’s correlation coefficient. The value for the ‘Precipitation correlation coefficient’ parameter indicates the relationship between the frequency of GLOFs and the total precipitation for each month of the year also using Pearson’s correlation coefficient. The ‘Annual maximum air temperature [°C]’ parameter shows the average monthly temperature maximum during the year. Based on the values given for this parameter, it is possible to determine whether only snow precipitation or also

Tab. 2 Dependence of GLOF occurrence on temperature and precipitation (Meteoblue 2022; Veh et al. 2022).

Analysed region	Air temperature correlation coefficient	Precipitation correlation coefficient	Annual maximum air temperature [°C]	Range of annual air temperature [°C]
Alaska	0.82	0.38	–2 to +15	17
Western Canada and USA	0.77	–0.50	–5 to +15	20
Central Andes	–0.32 (–0.16)	0.34 (0.65)	+8 to +10	2
Southern Andes	0.88	0.36	–2 to +4	6
Iceland	0.83	–0.51	–2 to +11	13
Scandinavia	0.85	–0.48	–6 to +13	19
Alps	0.85	0.72	–7 to +11	18
Caucasus	0.63	0.09	–12 to +10	22
Tian Shan	0.75	0.67	–12 to +9	21
Central Asia I (west)	0.93	0.77	–13 to +11	24
Central Asia II (east)	0.82	0.93	–2 to +12	14
New Zealand	0.66	0.30	–1 to +11	12

rain precipitation occurs during the year at the altitude where GLOFs predominantly occur. The 'Range of annual air temperature [°C]' parameter gives the range of the average maximum air temperature over the year.

Fig. 7 shows the total number of GLOFs recorded in each month. Global analysis requires considering opposite seasonal temperatures in the hemispheres. To compare regions in different hemispheres, months are represented by Roman numerals I–XII. For the regions on the Northern Hemisphere, I–XII corresponds to January–December, while for the regions on the Southern Hemisphere (Central Andes, Southern Andes, New Zealand), I–XII corresponds to July–June. Along with the total number of GLOFs, the graph includes curves for 1900 and 2019. These curves show how much warmer each month is than the annual global mean air temperature (NASA 2022).

4. Results

4.1 Changes in the frequency of GLOFs over the observed period 1900–2019

In all the analysed regions, the occurrence rate of GLOFs changes over time (Tab. 1). The results presented in the table show that for almost all regions the number of GLOFs increases progressively. Exceptions include the Western Canada and USA, and Tian Shan regions, where GLOF occurrences are decreasing. This decrease may be due to the complete disappearance of glaciers (Zoback and Grollmund 2001), which stops the supply of meltwater to glacial lakes (Singh et al. 2011). Another reason may be the reinforcing of dams by humans, which may lead to the prevention of water spilling out of potentially dangerous lakes. Extensive dam reinforcement, particularly in Western Canada and the USA (Fig. 4), may have significantly reduced GLOF occurrences. An uneven occurrence of GLOFs was observed in the Caucasus and New Zealand regions between 1900 and 2019. In

both of these regions, glacial floods occur only rarely (17 cases of GLOFs were recorded in the database for each region) and no trend in possible increases or decreases in their frequency can be observed due to the small amount of data. The overall comparison of all analysed regions globally indicates an increasing frequency of GLOFs.

Within the start of measurement parameter, five regions had the start of continuous air temperature data measurement after 1900. Because warming was not calculated here as the difference between the decades 1900–1909 and 2010–2019, these regions cannot be reliably compared with regions where data are available from 1900 onwards.

Globally, there has been a warming of 1.05 °C between the decades 1900–1909 and 2010–2019. In all the analysed regions, there is a warming trend during the observed time period, with only three of them having a warming value in the table less than the mentioned 1.05 °C. For the South Andes region, the warming value is 0.98 °C. However, this value results from the temperature difference between the decades 1930–1939 and 2010–2019, so it is likely that the warming is faster here than the global trend. The fastest warming is recorded in the Alps, where it warmed by 2.49 °C over the time period. A similar increase may occur in the Caucasus region, where it warmed by 2.12 °C between the decades 1940–1949 and 2010–2019.

The results for the correlation coefficient indicate that the relationship between the change in air temperature and global temperature varies in different regions. The smallest value of the correlation coefficient was measured in Iceland, where there was a continuous cooling between 1950 and 1989, contrary to the global temperature. In contrast, a very high correlation coefficient value was measured in the Alps and Central Asia II (east) regions. In all the regions, Pearson's correlation coefficient is no less than 0.6. Therefore, it may be assumed that due to ongoing global warming, there will also be warming in all the monitored areas.

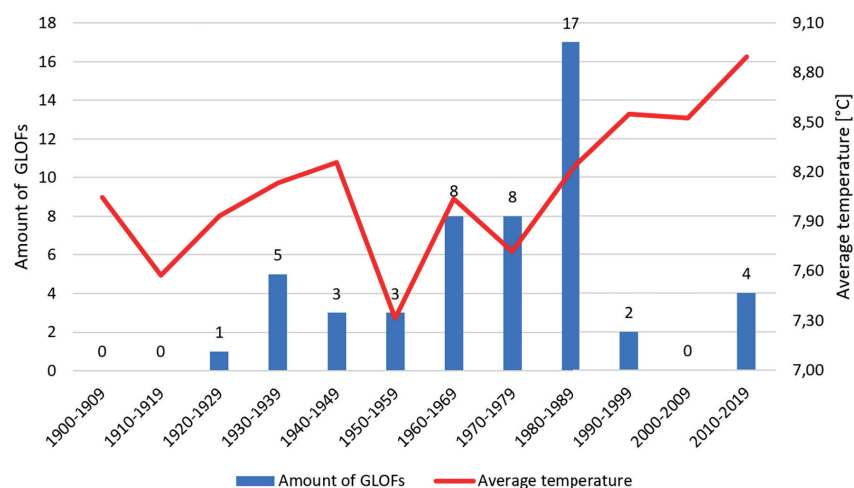


Fig. 4 Number of GLOFs in individual decades, and changes in average temperature in the Western Canada and USA region (NASA 2020; Veh et al. 2022).

4.2 Dependency of GLOF occurrences on temperature and precipitation throughout the year

In most regions, the resulting positive value of the air temperature correlation coefficient is high, and the increasing number of GLOFs correlates with rising air temperature (Tab. 2). The Caucasus and New Zealand regions show a lower value of the air temperature correlation coefficient compared to the other regions. It is likely that the correlation inaccurately represents the true degree of dependence due to the small number of GLOFs recorded. Since the correlation is high in all the regions that have an annual air temperature range greater than or equal to 6 °C, a higher correlation may be expected in the Caucasus and New Zealand regions.

The lowest dependence on the quantity of GLOFs with air temperature is observed in the Central Andes region, where the correlation value is also the only negative one. This area is located closest to the equator, and the annual range of the average maximum air temperature is only 2 °C (Fig. 3). The almost constant air temperature throughout the year has a negligible impact on the distribution of GLOFs during the year. An earthquake occurred in the area in May 1970 (Lliboutry et al. 1977), which triggered five GLOFs (Fig. 5). In Tab. 2, the values in parentheses provides the correlation value without considering these five cases. Similarly, the values in parentheses for the precipitation correlation coefficient parameter is affected.

Unlike the previous parameter, the value of the Precipitation correlation coefficient is highly variable. For regions where GLOFs occur mainly in the warmest part of the year, negative values of the Precipitation correlation coefficient indicate the highest precipitation mainly in the cooler part of the year. On the other hand, positive values of this correlation coefficient indicate a predominance of precipitation in the warmer season.

In regions where the frequency of GLOFs is conditioned by air temperature and precipitation occurs

predominantly in the warmer part of the year (meaning both correlation coefficients have positive and high values), there are likely to be numerous landslides that may contribute to glacial flooding. The combination of high temperatures and intense precipitation is the cause of landslide formation (Emmer et al. 2014). Areas with favourable conditions for landslide formation include the Alps, Tian Shan, Central Asia I (west), and Central Asia II (east).

The region where mass movements significantly contribute to the occurrence of GLOFs is the Central Andes (Emmer et al. 2014), located closest to the equator. Due to the consistently positive average daily temperature maximum in elevations where GLOFs predominantly occur (Fig. 3), the distribution of the GLOF frequency throughout the year is primarily influenced by precipitation. The dependence on precipitation is confirmed by the value of the precipitation correlation coefficient. If the five GLOFs that were caused by earthquakes, which were created by an earthquake in May 1970 (Fig. 5), are not included in the correlation, the correlation of the frequency of GLOFs with precipitation is 0.65. For instance, the GLOF that occurred on 19 March 2013 was caused by a landslide into Lake Palcacocha in Cordillera Blanca. This landslide was most likely triggered by the saturation of moraine material due to intense rainfall (Klimeš et al. 2016). The landslide created a wave over 8 meters high, which overcame two concrete dams (Ojeda 1974) built as a countermeasure in response to the catastrophic GLOF that took place on 13 December 1941 (Lliboutry et al. 1977; Zapata 2002).

Since slope movements are a major contributor to GLOFs in the Central Andes (Emmer et al. 2014), where GLOFs occur mainly from moraine-dammed lakes (Fig. 6), a similar trend can be observed in the Central Asia II (east) region, where the incidence of moraine-dammed lakes is also high. In contrast, in the Alps, Tian Shan, and Central Asia I (west) regions, potential slope movements contribute less to the formation of GLOFs. This is due to the predominant number of GLOFs formed from glacial-dammed lakes.

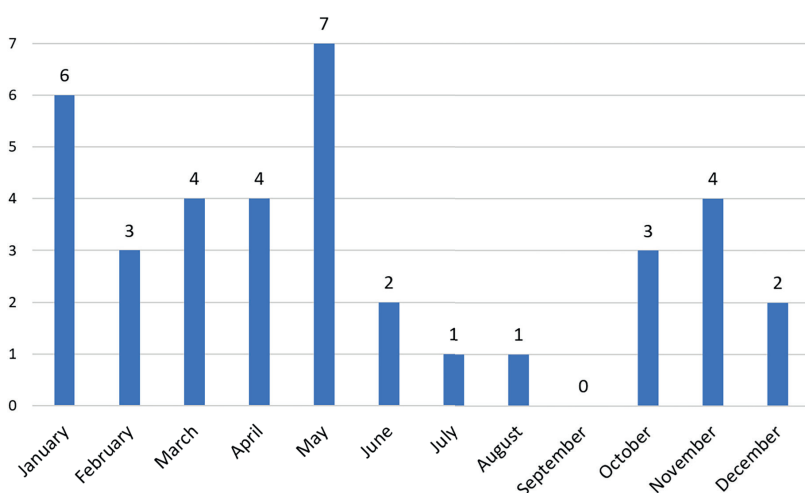


Fig. 5 Number of GLOFs by month in the Central Andes region.



Fig. 6 Lake Palcacocha in the Cordillera Blanca (Peru) is an example of moraine-dammed lake (Photo by V. Vilímek).

In this type of lakes, glacial dam breaching occurs repeatedly. Such events can occur, for example, as a result of cyclic increases in hydrostatic pressure capable of disrupting the integrity of the dam (Whalley 1971; Anderson et al. 2003).

The annual range of the mean maximum air temperature is lowest in the Central Andes and South Andes regions. However, the correlation value between the frequency of GLOFs and air temperature is significantly different in these areas. The high correlation in the Southern Andes results from the fact that air temperatures in certain parts of the year remain below freezing throughout the day. Therefore, during the cold part of the year, the potential causes of GLOFs are muted. In the warmer part of the year with positive daytime temperatures, the likelihood of GLOFs increases significantly. This may be due to, for example, increased slope instability (Emmer et al. 2014) or melting ice and snow increasing the likelihood of GLOFs due to glacial lake water filling (Jain et al. 2012). Conversely, in the Central Andes, average daily maximum temperatures are positive throughout the year, while daily minimums are negative (Fig. 3). The repeated alternation of positive and negative temperatures promotes frost weathering in the region

(Draebing and Krautblatter 2019), making the slopes more susceptible to the occurrence of potential slope movements. Due to relatively constant temperatures throughout the year, GLOFs are initiated during periods of intense precipitation.

4.3 Frequency of recorded GLOFs in individual months

The results presented in Fig. 7 confirm the dependence of GLOF occurrences on air temperature. The majority of GLOFs occur mainly in the warm half of the year (between the IV. and IX. month), where the regions of Alaska, Iceland, Alps, and Tian Shan predominantly contribute to their quantity. Conversely, the fewest cases occur in the cold half of the year (between the X. and III. month), where Iceland has the greatest share in the overall number of recorded GLOFs. Iceland's high GLOF frequency is mainly driven by year-round volcanic activity (Björnsson 1992).

Global air temperature curves indicate an increase of over 1 °C from 1900 to 2019. Due to the correlation between the number of GLOFs and temperature, it is likely that ongoing warming will lead to more frequent GLOFs.

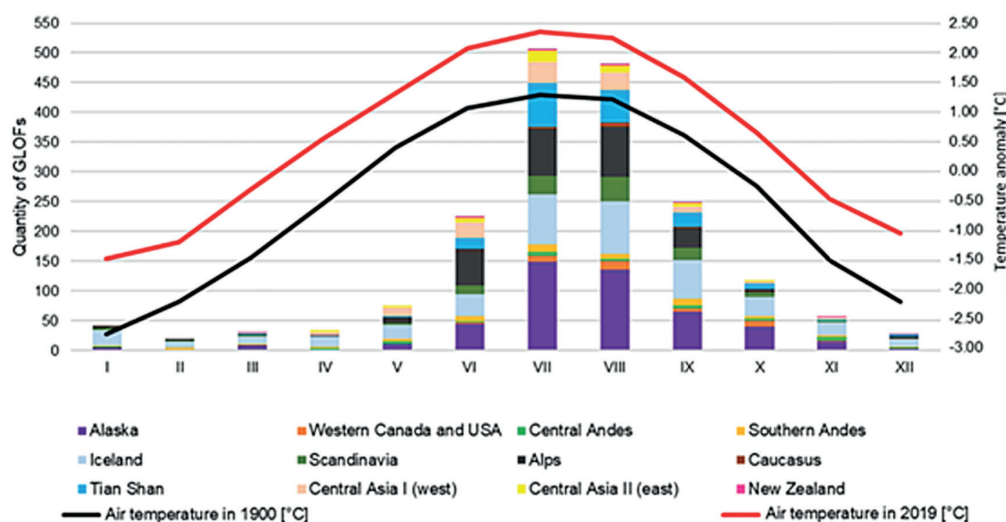


Fig. 7 Monthly Distribution of recorded GLOFs and Air Temperature (NASA 2022; Veh et al. 2022).

5. Discussion

This paper aimed to analyse and compare individual regions based on data available in the GLOFs database (Veh et al. 2022). The discussion focuses on factors contributing to the increased inaccuracies in the processed data, the benefits of the database itself, and the possibilities leading to the reduction in the number of new glacial lake outburst floods.

5.1 Factors affecting the accuracy of the GLOFs database analysis

An analysis of the GLOFs database revealed patterns in GLOF behaviour across various regions. The resulting reliability of the data is different for each of the analysed regions, as each region is affected by different factors that increase their inaccuracy.

Such factors include the inconsistent classification of parameters describing GLOFs across regions. For example, occurrences of GLOFs originating from lakes with a combined type of dam are only listed in the database for the Central Andes. However, it is likely that failures of combined dams also occurred in other areas, where such cases may have been classified as failures of moraine dams or bedrock dams.

The accuracy of the resulting analysis is also determined by the availability of data in each examined area. The availability of historical data tends to be lower in areas that were settled relatively late. The availability of data is also influenced by the amount of conducted research on GLOFs in the analysed areas. For example, the development of GLOFs in the Alps can be traced in the database since the 15th century, while in the Tian Shan Mountain range, the first recorded GLOFs date back to the early 20th century. Due to the uneven level of data availability, the analysis of the GLOFs database (Veh et al. 2022) does not fully accurately portray the rate of increase or decrease of GLOFs in each area.

The accuracy of the analysis is also affected by the overall frequency of recorded GLOFs, where lower numbers reduce the likelihood of reliably characterising individual areas. For example, in the Caucasus and New Zealand regions, the small amount of data makes it impossible to know whether there is an increasing or decreasing trend in the occurrence of new GLOFs.

Another factor affecting the resulting reliability of data in different regions is the use of different research methods. For instance, field research provides detailed data, such as determining the elevation of a lake (Bařka et al. 2020). To determine the elevation of the lakes, the software Google Earth (Google 2022) was used in this paper. The lower quality of the Google Earth digital elevation model (DEM) does not guarantee accurate elevation data. Therefore, field research could be used to measure the exact elevation of glacial lakes (Bařka et al. 2020). In contrast, combining various remote sensing data, like Synthetic Aperture Radar (SAR), Digital Elevation Model (DEM), and optical images, provides a broader view for analysing GLOF processes at a large scale (Yang et al. 2023).

Even with a maximum emphasis on recording individual data, it is not possible for the resulting analysis to fully capture the behaviour of GLOFs within and between areas. The accuracy of the resulting analysis is influenced by the factors mentioned above as well as many other influences operating at the regional or global level. These include, for example, various climatic phenomena and anomalies (Huggel et al. 2020; Gao et al. 2024).

Results that would more accurately represent the behaviour of GLOFs may be achieved for each area by, for example, long-term data collection, the completeness of data describing the events that took place, or a uniform classification of the parameters describing GLOFs. At the same time, it would be possible to increase the accuracy and extend the possibilities of the resulting analysis by identifying new parameters

that are not or barely present in the database. Such parameters may include, for example, the causes of GLOFs, whose more detailed research may help to better understand the issues related to their behaviour.

An increase in the accuracy of future analyses may also be achieved by comparing parameters in the analysed database with parameters in other possible regional or global databases recording past GLOFs. By comparing the parameters with each other, it would be possible to search for possible inaccuracies between the given data and at the same time it would be possible to find new parameters that are not listed in the GLOFs database (Veh et al. 2022).

The advantage of the database is the possibility of long-term and detailed recording of individual data describing GLOFs. To better understand the behaviour of GLOFs, the database should include parameters related to potential changes that may occur at the lake. Among such parameters are particularly: lake water level, lake volume, moraine stability, movement and dynamic of glacier supplying water to the lake, and local climatic conditions. Subsequent analyses of such a database may be particularly beneficial for monitoring the development of GLOFs in various regions where they may pose certain risks.

The disadvantage of the analysis of the GLOFs database itself, apart from the above mentioned factors affecting its accuracy, is the inability to compare absolute values with each other due to the unequal size of the studied regions. For better comparability, it is necessary to compare the analysed data in relative terms among the examined regions.

5.2 Implementation of possible countermeasures

The results of the analysis of the GLOFs database (Veh et al. 2022) suggest a worldwide increasing trend of new cases of GLOFs. Since potential floods can threaten local populations and infrastructure, implementing appropriate countermeasures can reduce the occurrence of new GLOFs.

In the Cordillera Blanca, there has been extensive construction of various types of countermeasures to prevent (or mitigate) flooding at dangerous glacial lakes (Emmer et al. 2016). The construction was initiated in the 1940s (Broggi 1942) as a response to catastrophic GLOFs (e.g., Lake Palcacocha on 13 December 1941; Klimeš et al. 2016). Countermeasures in the Cordillera Blanca include Open cuts, Artificial dams, Tunnels and their combinations (Emmer et al. 2016).

Open cuts involve creating a channel through the moraine dam. This technique aims to lower and/or fix the lake level, thereby managing the volume of water stored in the lake. Lake Arhueycocha is an example of a lake where this approach has been implemented (Emmer et al. 2016).

Artificial dams are typically constructed with concrete or stone walls with earthen fill, often exceeding 10 meters in height. These more substantial structures

are implemented solely in moraine-dammed lakes of the Cordillera Blanca, frequently used in combination with open cuts for enhanced risk mitigation (Emmer et al. 2016). Lake Palcacocha (Fig. 6) serves as an example of this approach (Ojeda 1974). Reinforcing dams at potentially hazardous lakes is a proven effective measure. Dam reinforcement is evident in the Western Canada and USA region, where there was a significant decline in the number of GLOFs in the 1990s (Fig. 4).

Tunnels represent another approach for managing glacial lake levels. They can be used to either lower the water level (increasing the dam's freeboard, the buffer zone between water and the dam crest) or maintain the current level. However, constructing tunnels in remote, high-altitude regions exceeding 4,500 meters above sea level presents significant technological and financial challenges. This is reflected in the limited number of tunnels implemented in the Cordillera Blanca glacial lakes, with only five documented cases (e.g., Lake Parón) (Emmer et al. 2016).

Similar countermeasures may be appropriate to implement in other areas where, according to the analysis of the GLOFs database (Veh et al. 2022), there is a significant increase in GLOFs. To effectively minimize the potential for GLOF events, it is essential to prioritize the development and implementation of early warning systems, enhance community preparedness programs, and actively pursue climate change mitigation strategies. As each potential GLOF poses a different level of danger, the potential risks for each glacial lake need to be properly assessed. Based on the hazard classification of individual lakes, the subsequent introduction of possible countermeasures should primarily focus on the locations presenting the greatest risk.

6. Conclusion

Based on data available in the GLOFs database (Veh et al. 2022), a total of 2939 GLOFs were analysed, with most occurring after the end of the 19th century. The mentioned GLOFs originate from 707 glacial lakes, which were divided into several regions based on their location (Chapter 2).

In all analysed regions, there has been a warming trend between 1900 and 2019. The slowest warming occurred in the Western Canada and USA region, while the most significant warming was observed in the Alps. In addition to the temperature increase, most regions also show a continuously rising trend in the occurrence of new GLOFs. The opposite trend is observed in the Tian Shan Mountains and Western Canada and USA, where the downward trend is probably caused by the reinforcing of dams at potentially dangerous lakes. The future trend in the frequency of GLOFs in the Caucasus and New Zealand regions is unknown. This is primarily because there is a very

limited amount of available data, making it unreliable to determine future developments accurately.

During the year, the highest occurrence of GLOFs is observed mainly in the summer months, when increased melting has the largest share in the formation of GLOFs. In areas with glacial-dammed lakes, glacial flooding is primarily caused by positive temperatures causing ice and snow to melt, which can subsequently fill glacial lakes with water. Conversely, in regions dominated by moraine-dammed and bedrock-dammed lakes, precipitation heavily influences GLOFs frequency, which is most pronounced in the Central Andes. In such areas, GLOFs during dry periods are rare and are more commonly associated with rainy seasons when precipitation can lead to numerous landslides (Emmer et al. 2014). Climate is not the only factor influencing GLOFs. In Iceland, for example, volcanism is a major factor in the year-round occurrence of GLOFs, especially of the jökulhlaup type (a type of glacial flood connected with subglacial lakes in the neovolcanic zones (Björnsson 1988)). Another factor may be the earthquake that caused five glacial floods in the Central Andes in 1970.

As climate change accelerates glacial melt, the threat of GLOFs is rising dramatically. To prevent future occurrences of GLOFs, it is essential to understand their behaviour and response to changing climatic conditions. This knowledge will make it possible to identify hazardous areas and subsequently prevent the occurrence of glacial floods. To minimize the potential for future GLOF events, prioritizing the reinforcement of dams at potentially hazardous lakes is crucial. This strategy should be a top priority in regions like the Alps and Central Asia, where GLOFs are experiencing a rapid increase. Furthermore, ongoing monitoring and research efforts are essential for developing a proactive response to the rapid changes in climate conditions.

The GLOFs database serves as a critical tool for understanding and mitigating the risks associated with these natural disasters. However, to enhance its comprehensiveness and accuracy, there is an urgent need for international cooperation and data sharing, particularly on factors like historical events, ongoing monitoring data, and detailed lake characteristics. Additionally, integrating local community knowledge and experiences is essential for effective risk assessment and mitigation planning.

References

- Anderson, S. P., Walder, J. S., Anderson, R. S., Kraal, E. R., Cunico, M., Fountain, A. G., Trabant, D. C. (2003): Integrated hydrologic and hydrochemical observations of Hidden Creek Lake jökulhlaups, Kennicott Glacier, Alaska. *Journal of Geophysical Research: Earth Surface* 108(F1), 148–227, <https://doi.org/10.1029/2002JF000004>.
- Bat'ka, J., Vilímek, V., Štefanová, E., Cook, S.J., Emmer, A. (2020): Glacial Lake Outburst Floods (GLOFs) in the Cordillera Huayhuash, Peru: Historic Events and Current Susceptibility. *Water* 12(10), 2664, <https://doi.org/10.3390/w12102664>.
- Björnsson, H. (1988): Hydrology of ice caps in volcanic regions. Reykjavik Societas Scientiarum Islandica, University of Iceland. *Polar Record* 1990, 26(157), 132–132, <https://doi.org/10.1017/S0032247400011293>.
- Björnsson, H. (1992): Jökulhlaups in Iceland: prediction, characteristics and simulation. *Annals of Glaciology* 16, 95–106, <https://doi.org/10.3189/1992AoG16-1-95-106>.
- Clague, J. J., Evans, S. G. (2000): A review of catastrophic drainage of moraine-dammed lakes in British Columbia. *Quaternary Science Reviews* A review of catastrophic drainage of moraine-dammed lakes in British Columbia. *Quaternary Science Reviews* 19, 1763–1783, [https://doi.org/10.1016/S0277-3791\(00\)00090-1](https://doi.org/10.1016/S0277-3791(00)00090-1).
- Draebing, D., Krautblatter, M. (2019): The efficacy of frost weathering processes in alpine rockwalls. *Geophysical Research Letters* 46(12), 6516–6524, <https://doi.org/10.1029/2019GL081981>.
- Emmer, A., Vilímek, V., Klimeš, J., Cochachin, A. (2014): Glacier Retreat, Lakes Development and Associated Natural Hazards in Cordillera Blanca, Peru. In: Shan, W., Guo, Y., Wang, F., Marui, H., Strom, A. (eds) *Landslides in Cold Regions in the Context of Climate Change*. Environmental Science and Engineering. Springer, Cham, https://doi.org/10.1007/978-3-319-00867-7_17.
- Emmer, A., Vilímek, V., Huggel, C., Klimeš, J., Schaub, Y. (2016a): Limits and challenges to compiling and developing a database of glacial lake outburst floods. *Landslides* 13, 1579–1584, <https://doi.org/10.1007/s10346-016-0686-6>.
- Emmer, A., Klimeš, J., Mergili, M., Vilímek, V., Cochachin, A. (2016b): 882 lakes of the Cordillera Blanca: An inventory, classification, evolution and assessment of susceptibility to outburst floods. *CATENA* 147, 269–279, <https://doi.org/10.1016/j.catena.2016.07.032>.
- Emmer, A., Wood, J. L., Cook, S. J., Harrison, S., Wilson, R., Diaz-Moreno, A., Reynolds, J. M., Torres, J. C., Yarleque, C., Mergili, M., Jara, H. W., Bennett, G., Caballero, A., Glasser, N. F., Melgarejo, E., Riveros, C., Shannon, S., Turpo, E., Tinoco, T., Torres, L., Garay, D., Villafane, H., Garrido, H., Martinez, C., Apaza, N., Araujo, J., Poma, C. (2022): 160 glacial lake outburst floods (GLOFs) across the Tropical Andes since the Little Ice Age. *Global and Planetary Change* 208: 103722, <https://doi.org/10.1016/j.gloplacha.2021.103722>.
- EPI (2015): Average Global Temperature by Decade, 1880–2014 (Celsius). Available online: https://www.earth-policy.org/data_center/C23 (accessed on 20. 4. 2022).
- Gao, J., Du, J., Bai, Y., Chen, T., Zhuoma, Y. (2024): The Impact of Climate Change on Glacial Lake Outburst Floods, *Water* 16(12), 1–16, <https://doi.org/10.3390/w16121742>.
- GOOGLE (2022): Google Earth. Available online: <https://earth.google.com/web/> (accessed on 14. 4. 2022).
- Harrison, S., Kargel, J. S., Huggel, C., Reynolds, J., Shugar, D. H., Betts, R. A., Emmer, A., Glasser, N., Haritashya, U. K., Klimeš, J., Reinhardt, L., Schaub, Y., Wiltshire, A., Regmi, D., Vilímek, V. (2018): Climate change and the global pattern of moraine-dammed glacial lake outburst floods.

- The Cryosphere 12(4), 1195–1209, <https://doi.org/10.5194/tc-12-1195-2018>.
- Huggel, C., Carey, M., Emmer, A., Frey, H., Walker-Crawford, N., Wallimann-Helmer, I. (2020): Anthropogenic climate change and glacier lake outburst flood risk: Local and global drivers and responsibilities for the case of lake Palcacocha, Peru. *Natural Hazards and Earth System Sciences* 20(8), 2175–2193, <https://doi.org/10.5194/nhess-20-2175-2020>.
- Chowdhury, A., Kroczeck, T., Kumar De, S., Vilímek, V., Chand Sharma, M., Debnath, M. (2021): Glacial Lake Evolution (1962–2018) and Outburst Susceptibility of Gurudongmar Lake Complex in the Tista basin, Sikkim Himalaya (India). *Water* 13(24): 3565, <https://doi.org/10.3390/w13243565>.
- Chowdhury, A., De, S. K., Sharma, M. C., Debnath, M. (2022): Potential glacial lake outburst flood assessment in a changing environment, Chhombu Chhu Watershed, Sikkim Himalaya, India. *Geocarto International* 37(27), 15627–15655, <https://doi.org/10.1080/10106049.2022.2102219>.
- ICIMOD (2022): GLOF database of High Mountain Asia [Data set], ICIMOD, <https://doi.org/10.26066/RDS.1973283>.
- Iturrizaga, L. (2011): Glacier lake outburst floods. In: Singh, V. P., Singh, P., Haritashya, U. K. (eds) *Encyclopedia of Snow, Ice and Glaciers*. Encyclopedia of Earth Sciences Series. Springer, Dordrecht, https://doi.org/10.1007/978-90-481-2642-2_196.
- Jain, S. K., Lohani, A. K., Singh, R. D., Chaudhary, A., Thakural, L. N. (2012): Glacial lakes and glacial lake outburst flood in a Himalayan basin using remote sensing and GIS. *Natural Hazards* 62(3), 887–899, <https://doi.org/10.1007/s11069-012-0120-x>.
- Klimeš, J., Novotný, J., Novotná, I., Jordán de Urríes, B., Vilímek, V., Emmer, A., Strozzi, T., Kusák, M., Cochachin Rapre, A., Hartvich, F., Frey, H. (2016): Landslides in moraines as triggers of glacial lake outburst floods: example from Palcacocha Lake (Cordillera Blanca, Peru). *Landslides* 13, 1461–1477, <https://doi.org/10.1007/s10346-016-0724-4>.
- Liu, J. J., Tang, C., Cheng, Z. L. (2013): The two main mechanisms of Glacier Lake Outburst Flood in Tibet, China. *Journal of Mountain Science* 10(2), 239–248, <https://doi.org/10.1007/s11629-013-2517-8>.
- Liboutry, L., Arnao, B. M., Schneider, B. (1977): Glaciological Problems Set by the Control of Dangerous Lakes in Cordillera Blanca, Peru. III. Study of Moraines and Mass Balances at Safuna. *Journal of Glaciology* 18(79), 275–290, <https://doi.org/10.3189/S0022143000021353>.
- Lützow, N., Veh, G., Korup, O. (2023): A global database of historic glacier lake outburst floods. *Earth System Science Data* 15(7), 2983–3000, <https://doi.org/10.5194/essd-15-2983-2023>.
- Meteoblue (2022): Podnebí (modelované). Available online: https://www.meteoblue.com/cs/počasí/historyclimate/climatemodelled/rocky-mountains_kanada_6126752?fbclid=IwAR2_ZPqkGwZZmex4cd8SEY6oY1GdcZirZiy-rmE_RNgcEMrXRj7W2FBR_9w (accessed on 5. 4. 2022).
- NASA (2020): GISS Surface Temperature Analysis (v4): Station Data. Available online: https://data.giss.nasa.gov/gistemp/station_data_v4_globe/ (accessed on 8. 4. 2022).
- NASA (2022): GISS Surface Temperature Analysis (v4): Analysis Graphs and Plots. Available online: <https://data.giss.nasa.gov/gistemp/graphs/> (accessed on 2. 6. 2022).
- NOAA (2022): Climate at a Glance: Global Time Series. Available online: <https://www.ncei.noaa.gov/access/monitoring/climate-at-a-glance/global/time-series/globe/land/12/3/1850-2023> (accessed on 18. 5. 2022).
- Ojeda, N. (1974): Consolidación laguna Palcacocha, ELECTROPERU S. A., Unidad de glaciología y seguridad de lagunas, Huaráz, Peru.
- Richardson, S. D., Reynolds, J. M. (2000): An overview of glacial hazards in the Himalayas. *Quaternary International* 65–66, 31–47, [https://doi.org/10.1016/S1040-6182\(99\)00035-X](https://doi.org/10.1016/S1040-6182(99)00035-X).
- Sattar, A., Goswami, A., Kulkarni, A. V., Emmer, A., Haritashya, U. K., Allen, S., Frey, H., Huggel, C. (2021): Future Glacial Lake Outburst Flood (GLOF) hazard of the South Lhonak Lake, Sikkim Himalaya. *Geomorphology* 388: 107783, <https://doi.org/10.1016/j.geomorph.2021.107783>.
- Singh, V. P., Singh, P., Haritashya, U. K. (2011): *Encyclopedia of Snow, Ice and Glaciers*, 1st ed.; Springer Science and Business Media, <https://doi.org/10.1007/978-90-481-2642-2>.
- Veh, G., Lützow, N., Kharlamova, V., Petrakov, D., Hugonnet, R., Korup, O. (2022): Glacier Lake Outburst Flood Database V2.0. Available online: <http://glofs.geoecology.uni-potsdam.de/> (accessed on 10. 4. 2022).
- Vilímek, V., Emmer, A., Huggel, C., Schaub, Y., Würmli, S. (2014): Database of glacial lake outburst floods (GLOFs)-IPL project No. 179. *Landslides* 11(1), 161–165, <https://doi.org/10.1007/s10346-013-0448-7>.
- Vuichard, D., Zimmermann, M. (1987): The 1985 Catastrophic Drainage of a Moraine-Dammed Lake, Khumbu Himal, Nepal: Cause and Consequences. *Mountain Research and Development* 7(2), 91–110, <https://doi.org/10.2307/3673305>.
- Whalley, W. B. (1971): Observations of the Drainage of an Ice-Dammed Lake – Strupvatnet, Troms, Norway. *Norsk Geografisk Tidsskrift – Norwegian Journal of Geography* 25(3–4), 165–174, <https://doi.org/10.1080/00291957108551921>.
- Worni, R., Stoffel, M., Huggel, C., Volz, C., Castellor, A., Luckman, B. (2012): Analysis and dynamic modeling of a moraine failure and glacier lake outburst flood at Ventisquero Negro, Patagonian Andes (Argentina). *Journal of Hydrology* 444–445, 134–145, <https://doi.org/10.1016/j.jhydrol.2012.04.013>.
- Yang, L., Lu, Z., Ouyang, C., Zhao, C., Hu, X., Zhang, Q. (2023): Glacial Lake Outburst Flood Monitoring and Modeling through Integrating Multiple Remote Sensing Methods and HEC-RAS. *Remote Sensing* 15(22): 5327, <https://doi.org/10.3390/rs15225327>.
- Zapata, M. (2002): La dinámica glaciaria en lagunas de la Cordillera Blanca (in Spanish). *Acta Montana* 19, 37–60.
- Zoback, M. D., Grollimund, B. (2001): Impact of deglaciation on present-day intraplate seismicity in eastern North America and western Europe. *Comptes Rendus de l'Académie des Sciences – Series IIA – Earth and Planetary Science* 333(1), 23–33, [https://doi.org/10.1016/S1251-8050\(01\)01623-8](https://doi.org/10.1016/S1251-8050(01)01623-8).